

**MODELLING, DESIGN AND IMPLEMENTATION OF D-Q
CONTROL IN SINGLE-PHASE GRID-CONNECTED INVERTERS
FOR PHOTOVOLTAIC SYSTEMS USED IN DOMESTIC
DWELLINGS.**

JASIM FARHOOD SULTANI

PhD

DE MONTFORT UNIVERSITY

2013

This Thesis is submitted in partial fulfilment of the requirements of

De Montfort University for the award of

Doctor of Philosophy

Supervised by

Dr. John A. Gow and Prof. Errol Tez

Faculty of Technology

De Montfort University

Leicester, UK

ABSTRACT

This thesis focuses on the single-phase voltage-source inverter for use in photovoltaic (PV) electricity generating systems in both stand-alone and grid-tied applications.

In many cases, developments in single-phase PV systems have followed developments in three-phase systems. Time-variant systems are more difficult to control than time-invariant systems. Nevertheless, by using suitable transformation techniques, time-variant systems can often be modelled as time-invariant systems. After the transformation, the control signals that are usually time-variant (often varying sinusoidally in time) become time-invariant at the fundamental frequency, and are hence much easier to deal with. With this approach, synchronous rotating frame control techniques have been previously proposed for high performance three-phase inverter applications. The transformation theory cannot be applied directly in single-phase systems without modification, and the d - q components would not be time-invariant in situations where harmonics, resonances or unbalance is present. Single-phase inverter controller designs based on the use of a synchronous rotating reference frame have been proposed, but such designs do not always perform as well as expected. This thesis aims to improve single-phase voltage-source inverters. The main objective is to address, in terms of cost, efficiency, power management and power quality, the problems found with single-phase designs based on a synchronous rotating frame single-phase inverter controller. Consequently, this thesis focuses on a novel controller approach in order to obtain a more reliable and flexible single-phase inverter.

As the first step, this thesis investigates the single-phase inverter switching gate-drive algorithms and develops a form of space-vector pulse-width-modulation (SVPWM) in order to reduce total harmonic distortion. The results of the new SVPWM algorithm demonstrate its superior performance when compared with sinusoidal pulse-width-modulation (SPWM) which is often used with single-phase inverters.

The second step, which is further reviewed and presented in this thesis, is the modelling of the single-phase inverter control based on the synchronous rotating frame. A mathematical analysis is conducted to determine the mechanism of the coupling that exists between the voltage phase and amplitude terms, and a new transformation strategy is proposed based on using the voltage phase as a reference at the Park transformation stages, and the current phase as a reference for the current at the transformation stages. The line-frequency components of the feedback signals are transformed to time-invariant components, thus eliminating the ripple and reducing the computational burden associated with the controller stage. Consequently, the inverter feedback controller stage is designed so that the coupling terms are decoupled within the controller itself. The effectiveness of the techniques proposed in this thesis are demonstrated by simulation using the MATLAB/SIMULINK environment. The proposed technique was also investigated through a practical implementation of the control system using a Digital Signal Processor (DSP) and a single-phase inverter. This practical system was tested up to 1 kW only (limited by the available inverter hardware). Nevertheless, the correlation between the simulation and the practical results is high and this gives confidence that the developed mechanism will allow the 2.5kW goal to be achieved. Practical test cases illustrate the effectiveness of the models. In addition, the comparisons between experimental and simulation results permit the system's behaviour and performance to be accurately evaluated.

With the development of the new controller, small-scale single-phase renewable energy systems will become more useful in the field of power quality management through their ability to separately control the phase and amplitude of the output voltage. Consequently, incorporation of this type of generator within the national electrical distribution network, as distributed generators (DG) at low-voltage level, can assist with power quality management at the consumer side of the grid. In addition, such a generator can also operate in stand-alone mode if the grid becomes unavailable. The third step in this thesis investigates small-scale single-phase renewable energy systems operating as decentralized distributed generators within a local network. This operation is achieved by controlling the inverter side using the quantities measured at the common coupling point between the grid and the inverter, without requiring other extensive communications. Thus, the small-scale single-phase renewable energy distributed generator systems will contain only a local controller at each installation.

ACKNOWLEDGMENTS

I want to thank god (Allah), the most merciful and the most gracious, who gave me patience, strength and help to achieve this scientific research.

First and foremost, I offer my sincerest and deepest gratitude to my supervisor, Dr. John Gow, who has supported me throughout my thesis with his patience; thanks to him for his trust, guidance and support. He also introduced me to this interesting field. Thanks to Dr.Gow again for his valuable supervision throughout the tiring journey of my PhD study.

Very sincere thanks are due to Prof. E. Tez who made every effort to put me on the right track during my PhD study. His constructive notes always resulted in improvements to my work.

My thanks to Dr. K. Vershinin for supporting me along the study period.

I have not enough words to thank my ever first teachers in this life, my parents, who have been inspiring me and pushing me forward all the way. Their prayers and blessings were no doubt the true reason behind any success I have realized in my life.

Finally, I am grateful to all my family members for their kind support, endurance and encouragements, which have given me the energy to carry on and to motivate myself towards crossing the finish line.

List of abbreviations

AC	Alternating current
DC	Direct current
DSP	Digital signal processing
FFT	Fast Fourier transform
IGBT	Insulated gate bipolar transistor
LV	Low-voltage
MPP	Maximum Power Point
MPPT	Maximum Power Point tracking
MOSFET	Metal-oxide-semiconductor field-effect transistor
PWM	Pulse width modulation
PI	Proportional and Integral controller
P-R	Proportional resonant controller
PV	Photovoltaic
SPWM	Sinusoidal pulse width modulation
SVPWM	Space vector pulse width modulation
THD	Total harmonic distortion
DG	Distributed generator

List of symbols

A	Constant
C	Capacitor (F)
f	Frequency (Hz)
f_c	Corner frequency (Hz)
f_s	Sampling frequency (Hz)
f_{sw}	Switching frequency (Hz)
I	Current (A)
I_c	Instantaneous capacitor current (A)
I_o	Instantaneous output current (A)
I_d	Direct - current rotating frame component (A)
I_q	Quadrature- current rotating frame component (A)
$I_{d\text{-ref}} \text{ or } i_d^*$	Direct- current rotating frame component reference (A)
$I_{q\text{-ref}} \text{ or } i_q^*$	Quadrature - current rotating frame component reference (A)
I_{sc}	Short circuit current (A)
I_{cd}	Instantaneous capacitor direct current component in synchronous rotating frame (A)
I_{cq}	Instantaneous capacitor quadrant current component in synchronous rotating frame (A)
L	Inductor (H)
m	Modulation index
M	Droop function coefficient
N	Droop function coefficient
P	Active power (Watt)
Q	Reactive power (VAr)
r_c	Capacitor parasitic resistance (ohm)
r_L	Inductor parasitic resistance (ohm)
S	Apparent power (VA)
$S1, S2$	Switching transistors
T_s	Sampling period (sec)
T_{sw}	Switching period (sec)
V	Instantaneous Voltage (V)
$V_d \text{ and } V_q$	Direct and quadrant voltage rotating frame components (V)
V_g	Grid voltage magnitude (V)
V_i	Inverter no-load voltage amplitude (V)
V_o	Generator no-load voltage amplitude (V)
V_{oc}	Open circuit voltage (V)
$\mathbf{V}^2 - \mathbf{V}^4$	Vectors
$\mathbf{V}^1 - \mathbf{V}^3$	Zero Vectors

ω	Frequency (rad/sec)
ω_0	Generator no-load frequency (rad/sec)
ω_g	Grid frequency (rad/sec)
ω_i	Inverter no-load frequency (rad/sec)
π	Constant =22/7
ϕ	Power angle
θ	Angle
θ_z	Impedance angle
Z	Impedance magnitude (ohm)

Contents

1 Chapter 1.....	12
1.1 Introduction	12
1.2 Solar Cell in Brief	13
1.3 Solar Cell Equivalent Circuit	15
1.4 A Maximum Power Point Tracker (MPPT)	18
1.5 PV System Power Conditioning Units	20
1.6 Current Developments and How This Research Enhances Them.....	21
1.7 Choice of PV System for this Research	22
1.8 Problem Definition and Proposed Solution on the Inverter Side:	23
1.9 Research Program	24
1.10 Thesis Structure.....	26
2 Chapter 2.....	29
2.1 Introduction	29
2.2 Standard Permits for PV System.....	29
2.3 Inverter-Side Control.....	30
2.3.1 Inverter Circuit	31
2.3.2 Modulation strategy.....	34
2.4 Methods for Inverter Current Control	34
2.4.1 Linear Regulator Based Method.....	35
2.4.2 Hysteresis Control Method.....	37
2.4.3 The Peak Current Control Method	39
2.4.4 Proportional-Resonant current controller.....	40
2.4.5 Synchronous Rotating Frame Controller.....	42
2.5 Decentralized Power Supply	42
2.5.1 Grid-Side Control.....	44
2.6 Design Consideration in This Study.....	46
2.6.1 Carrier Frequency Selection.....	46
2.6.2 Filter Parameter Design.....	47
2.6.3 LC Filter Calculations	50
3 Chapter 3.....	52
3.1 Introduction	52
3.2 General Description of Pulse Width Modulation Techniques.....	53
3.3 PWM Classification	54

3.4	Hysteresis Current Controllers	55
3.5	Sinusoidal PWM	56
3.6	SVPWM Technique:	57
3.7	Space Vector Concept	58
3.8	The Basic Principle of SVPWM	59
3.9	Software Implementation of Single-Phase SVPWM	60
3.9.1	Boundary and Separation Planes.....	61
3.9.2	Switching Sequences.....	62
3.9.3	Time Duration	63
3.9.4	Bipolar SVPWM	63
3.10	Simulation	65
3.11	Harmonics in Electrical System	68
3.12	Summary	73
4	Chapter 4.....	75
4.1	Introduction	75
4.2	Synchronous and Reference Frames in Literature	76
4.3	Synchronous Frame Transformation in three-phase system:	79
4.4	Stationary reference frame Controller in Three-Phase Systems.....	82
4.5	Rotating Reference Frame Control Structure in Three-Phase Systems.....	83
4.6	Overview of the relevant published work for single-phase inverters employing the synchronous rotating frame controller	87
4.7	Summary	91
5	Chapter 5.....	92
5.1	Introduction	92
5.2	Use of the Imaginary Orthogonal Phase in Single-Phase Systems	93
5.3	Modelling of the Single-Phase Inverter in Stationary and Rotating Reference Frames	97
5.3.1	Single-Phase Inverter Model in Stationary Reference Frame	97
5.3.2	Single-Phase Inverter Model in Rotating Reference Frame	101
5.4	Summary	104
6	Chapter 6.....	106
6.1	Introduction	106
6.2	Single-Phase Inverter Controller	106
6.3	Double Feedback Loop Control Strategy	111
6.4	Proposed $d-q$ controller structure	112
6.5	The Stand-Alone Closed-loop Model.....	113

6.6	Transformation stage modification	118
6.7	Validation and operating principles of feedback path.....	120
6.8	Validation of the proposed strategy in stand-alone mode	129
6.9	Step Load Parameter Variation:	131
6.10	FFT analysis	138
6.11	Nonlinear Load Test.....	140
6.12	Quarter Cycle Delay Stage Modification	141
6.13	Grid-tied Inverter mode.....	142
6.14	The Grid-tied Inverter Model.....	143
6.15	Summary	146
7	Chapter 7.....	149
7.1	Introduction	149
7.2	Environmental Characteristics of PV Module.....	150
7.3	PV System Structure	153
7.4	Voltage Balancing across Split Capacitors in a half-bridge Inverter	155
7.5	Inverter Input and Output Instantaneous Power.....	156
7.6	Utility Interfacing Requirements.....	158
7.7	The Revenue from Residential Grid-Tied PV Systems.....	159
7.8	Requirements arising from the PV array interface	160
7.9	DC-Link Capacitor Calculation	160
7.10	Non-Linearity Caused By PV Source	162
7.11	Validation of the PV System Interactive With Utility Grid	165
7.11.1	Grid-Tied Inverter Load Sharing with Constant PV Power	168
7.12	Grid-Tied Inverter Load Sharing with Input Power Dip.....	171
7.13	Summary	175
8	Chapter 8.....	177
8.1	Introduction	177
8.2	Power Network Description	178
8.3	Decentralized Power Management Concept	179
8.4	Impact of Decentralized Distributed Generation on the Network.....	181
8.5	Droop Methodology	183
8.6	Droop Function Methodology in Literature	186
8.7	Voltage Magnitude and Fundamental System Frequency	188
8.8	Solid-State Inverter Droop Behaviours	188
8.9	Proposed Inverter Droop Control Method.....	191

8.10	Simulation Result.....	195
8.11	FFT Analysis.....	201
8.12	Summary	203
9	Chapter 9.....	205
9.1	Introduction	205
9.2	System Hardware Description.....	206
9.3	Power Circuit Devices.....	207
9.4	The Experimental Setup	210
9.5	Stand-Alone Inverter Experimental Setup	211
9.6	Experimental Setup in Grid-Tied Mode	214
9.7	Inverter Harmonic Spectrum Analysis	219
9.8	Summary	222
10	Chapter 10.....	224
10.1	Conclusions	224
10.2	Summary	224
10.3	General Contributions of the Thesis.....	227
10.4	Future Work	229
11	References	230
12	Appendix A:.....	250
13	Appendix B:.....	251
14	Appendix C:.....	258
15	Appendix D:.....	261
16	Appendix E:	265

Chapter 1

INTRODUCTION

1.1 Introduction

Renewable energy is a label given to energy obtained from non-finite resources such as sunlight, wind, tides, hydrogen and geothermal heat, which are renewable (naturally replenished), continuously available and the quantity of which is not affected by human consumption. Renewable energy emerged as a result of a way of generating energy in remote and rural areas.

Remote properties can be a long way from the local electricity substation, with utility companies often charging substantial sums of money for connection to the national grid. A local power system using solar panels or a wind turbine provides an excellent solution to remote power needs, with low running costs and high reliability. Therefore, early renewable energy systems provided electrical power at a remote area, often including remote data monitoring, water pumping, wireless communications and off-grid buildings. Solar cell and wind energy provides excellent solutions for remote power applications, offering reliable, independent sources of electricity.

As a result of increasing environmental concerns, the use of green energy can be seen to benefit the global environment. Wind turbine and solar cell powered systems are becoming more numerous in commercial electric power production applications. From around 1995 [1], industry efforts have focused increasingly on developing and building integrated photovoltaic and power plants for grid-connected applications. This field relies on a variety of manufacturing and installation industries for its development. These

emerging renewable energy technologies, including solar energy, are still undergoing further development.

Solar cells can extract the electrical energy from the sunlight in an elegant way. They produce current when exposed to high levels of light, without moving parts, without noise, and without any pollution (excluding any environmental impact of the solar cell manufacturing process).

The electricity generated by the photovoltaic (PV) systems can be either stored (using batteries) and/or used directly (stand-alone plant) by being fed into a large electricity grid powered by central generating plants (grid-connected or grid-tied plant). It can also be combined with one or many distributed/domestic electricity generators to feed into a small grid (hybrid plant) [2].

This chapter starts with an overview of PV systems in two steps:

1. Description of the solar cell (the first step in the energy conversion process from sunlight to electricity), as well as an explanation of the parameters associated with its performance.
2. Brief descriptions of the PV system units.

Finally, this chapter describes the aim of this research together with the work program used. It also gives a concise overview of the chapters of this thesis.

1.2 Solar Cell in Brief

The solar cell was discovered in 1954 [3, 4] by examining the sensitivity of a properly prepared silicon wafer to sunlight. Among the first applications was that of

powering space satellites. The success of solar cell in space led to commercial applications of photovoltaic technology. The simplest photovoltaic power supply was used with many low power devices such as wrist watches and small calculators [5]. More complicated systems were developed to provide electricity to domestic dwellings.

Solar cells are designed to convert energy from sunlight to electrical energy in a one-step conversion process. This conversion takes place without the use of either chemical reactions or moving parts. Solar cells are essentially semiconductor junctions under illumination. The energy of visible photons is sufficient to excite electrons bound into solids up to higher energy states. Light generates electron-hole pairs on both sides of the junction between the n-type emitter and in the p-type base. The generated electrons (from the base) and holes (from the emitter) diffuse to the junction and are swept away by the electric field [3].

The excited electrons generate a potential difference or electromotive force between the solar cell terminals. The excited electrons quickly relax back to their ground state. However, the photovoltaic device is designed to pull the excited electrons out to feed an external circuit (load), Figure 1.1.

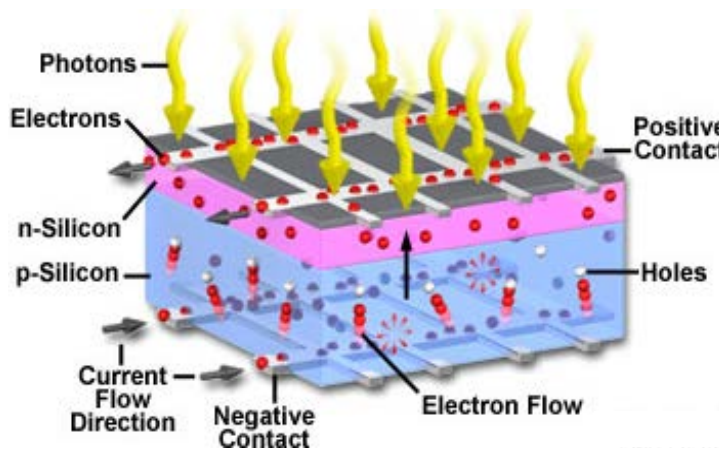


Figure 1.1: Solar cell diagram [6].

The effectiveness of solar cell depends upon the light absorbing materials and the manner of connection to the external circuit. Therefore, the surface is treated in order to reflect as little visible light as possible – thus it appears dark blue or black.

Due to the low-voltage of an individual solar cell (typically 0.5V) [3, 4] several cells are wired in series in the manufacture of a "lamine". The lamine is assembled into a protective weather-proof enclosure, thus composing a photovoltaic module or solar panel. Modules can be strung together into a photovoltaic array. In order to convert the sunlight energy to electrical power in optimum way, the system often consists of multiple components, including the photovoltaic modules, mechanical connections, and electrical power conditioning units, the combination of all these parts are so-called photovoltaic system (PV system).

1.3 Solar Cell Equivalent Circuit

Solar cells have non-linear properties as they are formed from a p-n junction. In order to understand the electronic behaviour of the solar cell, it is useful to create an equivalent circuit based on electrical components whose behaviours are well known. Such an equivalent circuit is shown in Figure 1.2.

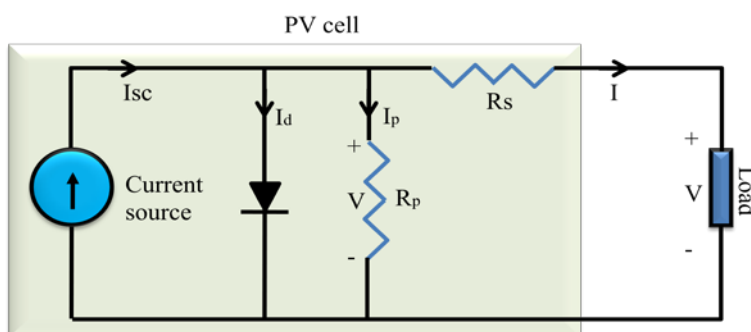


Figure 1.2: Solar cell equivalent circuit.

This equivalent circuit has a current-voltage relationship at its output. In some cases, approximation makes it possible to draw an equivalent circuit of a solar cell in terms of an ideal solar cell represented by a current source in parallel with diode by neglecting the resistances (considering shunt resistance equal to infinity and series resistance equal to zero) [3, 7, 8]. But there is no ideal solar cell in practice.

A mathematical expression for the solar cell equivalent circuit can be obtained from Kirchhoff's current law given by (1.1):

$$I_{sc} = I_d + I_p + I \quad (1.1)$$

where I , I_d and I_p are the cell output current, diode current and the shunt resistance current, respectively. The current through each equivalent circuit element is governed by the voltage across them, so the diode current is given by (1.2).

$$I_d = I_o(e^{qV_d/kT} - 1) \quad (1.2)$$

$$V_d = V + I \cdot R_s \quad (1.3)$$

where I_o is the reverse saturation current of the diode, q is the charge of the electron, k is Boltzmann's constant and T is absolute temperature. At 25°C, the factor $q/kT \approx 0.0259$ volts⁻¹. By substituting equations 1.2 and 1.3 into 1.1 and rearranging the terms, a solar cell characteristic equation can be derived as in (1.4), which relates solar cell parameters to the output voltage and current [3].

$$I = I_{sc} - I_o\left(e^{qV_d/kT} - 1\right) - \frac{V_d}{R_p} \quad (1.4)$$

The solar cell is characterized by its maximum open circuit voltage (V_{oc}) at zero output current and its short circuit current (I_{sc}) at zero output voltage. The cell generates no power in short-circuit or open-circuit. The cell delivers maximum power P_{max} when operating at a point on the characteristic where the $I \cdot V$ product has a maximum value. The (V vs. I) and (V vs. P) curve shapes are shown in Figure 1.3, and the position of the maximum power point represents the largest area of the rectangle.

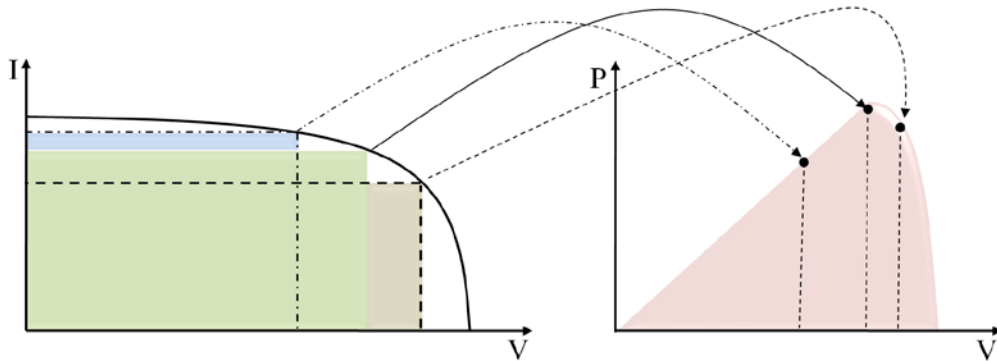


Figure 1.3: Relationships between (I vs. V) curve and (P vs. V) curve.

The efficiency of a solar cell is defined as the power P_{max} supplied by the cell at the maximum power point under standard test conditions, divided by the power of the radiation incident upon it. The most frequent conditions used are: irradiance 100 mW/cm², standard spectrum [3], and temperature 25 °C. The use of this standard irradiance value is particularly convenient since the cell efficiency in percent is then numerically equal to the power output from the cell in mW/cm².

The solar irradiance and cell temperature represent the net effect of variation in the solar cell characteristics. Every given value of solar irradiance and cell temperature will yield a unique cell characteristic.

Temperature (T) affects the characteristic equation via the exponential term. When temperature increases, the magnitude of the exponential term in the characteristic equation

reduces. The value of I_0 is exponentially proportional to temperature. The net effect of increasing temperature is to reduce the open circuit voltage (V_{OC}) linearly. The magnitude of this reduction is inversely proportional to V_{OC} . That is, cells with higher values of V_{OC} suffer smaller reductions in voltage with increasing temperature [3]. The amount of solar cell current I_{sc} increases slightly with increasing temperature because of an increase in the number of thermally generated carriers in the cell. The overall effect of temperature on cell efficiency can be computed using these factors in combination with the characteristic equation, and this also depends on how the cell is made. However, since the change in voltage is much stronger than the change in current, the overall effect on efficiency tends to be similar to that on voltage.

1.4 A Maximum Power Point Tracker (MPPT)

PV generator systems have two major problems [3, 7, 8]:

- The conversion efficiency of electric power generation is very low (e.g. 17%) [3, 4], especially under low irradiation conditions
- The amount of electric power generated by solar arrays changes continuously with weather conditions.

Moreover, the solar cell (V vs. I) characteristic is nonlinear and varies with irradiation and temperature. In general, the Maximum Power Point (MPP) is a unique point on the (V vs. I) as well as on (V vs. P) curve as shown in Figure 1.3. The power delivered by a PV module can be maximized using a maximum power point tracking (MPPT) control system. Such a system consists of a power conditioner to interface the PV output to the load, and a control unit, which drives the power conditioner for extracting the

maximum power from a PV array. As a result, the PV system will operate with maximum efficiency and produce its maximum output power.

PV cells have a single operating point where the values of the current (I) and voltage (V) of the cell result in a maximum power output (MPP). These values correspond to a particular load resistance equal to V/I . The PV cell has a non-linear relationship between current and voltage, and the MPP occurs at the knee of the curve, where the load resistance is equal to the Thevenin equivalent resistance of the cell. In operation, the voltage generated at the PV panel terminals will vary as the Maximum Power Point Tracking (MPPT) automatically adjusts the power taken from the panel, maintaining that power at a maximum for the prevailing conditions. MPPT utilizes a control circuit to search for this point and thus allows the converter circuit to extract the maximum power available from a cell.

The location of the MPP cannot easily be found analytically, but can be located either through numerical models or by search algorithms. Therefore, Maximum Power Point Tracking (MPPT) techniques are needed to maintain the PV array operating point at its MPP. Many MPPT techniques have been proposed in the literature [7-12]:

- The Perturb and Observe methods
- Incremental Conductance methods
- Hill climbing algorithm
- Short circuit current control
- Open circuit voltage control

Maximum power is transferred from a solar panel when the impedance of the load it is driving is optimally matched to its source impedance. In addition, the panel source

impedance also varies as the operating conditions change, and hence more sophisticated PV systems use a maximum power point tracker (MPPT) to optimize the panel's load conditions to its peak power transfer level. In operation, the voltage generated at the PV panel terminals will vary as the MPPT automatically fine-tunes the power taken from the panel, maintaining that power at a maximum for the prevailing conditions.

The MPPT is a high frequency electronic DC-to-DC converter. It takes the DC input from the solar panels, changes it to high frequency AC, and converts it back down to a different DC voltage and current to exactly match the panels to the load. MPPTs operate at relatively high switching frequencies, usually in the range 20-80 kHz [7-13]. The advantage of high frequency circuits is that they can be designed with high-efficiency transformers and small components.

The power output of a solar panel varies significantly with varying load conditions, given constant illumination on the panel's surface. The high efficiency DC-to-DC converter can present an optimal electrical load to a solar panel or array and can produce a voltage suitable for the load. The ideal load for a specific solar panel depends on the solar panel's MPP.

1.5 PV System Power Conditioning Units

Since PV cells generate DC which has to be converted into AC to meet the load frequency and amplitude requirement, the power electronic converters used for this purpose are sometimes collectively referred to as the power conditioning unit. The power conditioning unit plays a key role in the utility interactive PV system. The power conditioning unit is not only responsible for the energy conversion but also for optimizing the energy transfer and for the synchronization and safe transfer of the AC power into the

utility grid. The overall system performance depends heavily on power conditioning unit performance. The output current waveform of the inverter should be of almost perfect sine-wave shape. The modern power conditioner must be totally self-managing and stable in operation. Figure 1.4 shows the typical structure of a PV system unit.

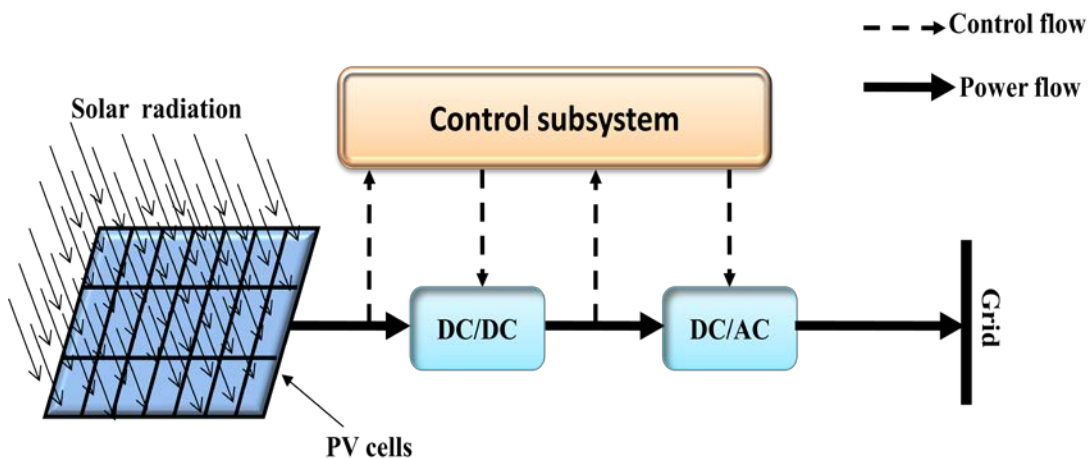


Figure 1.4: Block diagram of a typical solar generator structure.

1.6 Current Developments and How This Research Enhances Them

Solar PV systems cover quite a broad spectrum of system types. For grid-tied PV systems forming part of the approach of employing decentralized distributed generators, PV system characteristics and performance limits allowable for grid-tied applications must be defined. The most important points are [14- 21]:

- Quality of the power injected into the utility.
- Inverter output must be fully synchronized with the utility grid.
- Control of DC-link voltage and control of output amplitude and phase.
- Anti-islanding protection.

Each of these points poses significant challenges in development. Therefore, the PV systems and the controller task have become more and more complex while optimum solutions are sought. It is evident that simulation and simulation models can support systems development in several ways. Furthermore, simulation offers a safety factor in evaluating techniques as well as reducing the necessary development-cycle time.

It is worth stating that high performance three-phase inverters are often implemented using synchronous rotating reference frame (d - q) controllers [22-24]. In many cases, developments in single-phase systems have followed the developments in three-phase systems. Therefore, this thesis proposes a method that harnesses the benefits of synchronous rotating frame control but that can also be employed effectively with the single-phase inverter.

1.7 Choice of PV System for this Research

PV systems can be classified [25] depending on their power rating as below:

1. Large scale systems [26] with output power ranging from hundred kilowatts to megawatts. These usually represent units from a power station generation network.
2. Medium scale systems [27] with output power ranging from ten kilowatts to tens of kilowatts.
3. Small-scale systems [28] with output power less than ten kilowatts.

Usually, this type of PV system is used in domestic dwellings where solar arrays are mounted on the roof of the dwelling.

This thesis describes the development of a PV system for use in individual domestic dwelling applications. The PV system capacity mainly depends on the area available to be covered with solar cells, and this area is limited in the domestic dwellings. Therefore, the decision was taken for this research to focus on small-scale PV systems.

In the presence of sufficient sunlight, the power converters can be designed in such a manner as to provide the dwelling with a modest amount of power should the utility supply fail. In addition, when the energy demand from the dwelling is lower than provided by the PV array, the excess energy can be exported back to the utility. Such conversion systems would be quite small owing to limits on the area of the arrays, and may be constructed as zero-maintenance units requiring no intervention from the owner of the dwelling.

1.8 Problem Definition and Proposed Solution on the Inverter Side:

Fast-tracking and stable current controllers for single-phase inverters are not straightforward. However, a few methods have been proposed in the literature (see Chapter 2). Therefore, the research in this thesis will concentrate on the following points:

1. Developing an efficient converter with low THD. A new single-phase inverter switching gate-drive algorithm will be developed, which will improve efficiency while maintaining low THD.
2. Satisfying the international standards [29] on power quality by the developed controller stage.
3. According to the chosen current-control method, a grid connection controller will be developed. This controller will be capable of injecting active and reactive power (where appropriate) with high power quality into the load or the

grid. A stand-alone control mode will also be taken into account, which will supply high quality power to the load.

4. As the final part of the study, a small-scale individual (decentralized distributed) generator will be developed, and a controller will be designed so as not to require extensive communications between itself and the electricity supply network.

1.9 Research Program

The objective of this research is to build a PV system working in different modes of operation, by means of:

1. Investigating single-phase inverter gate-drive algorithms based on SVPWM (hitherto commonly used with three-phase inverters).
2. Introducing a new control method for a single-phase inverter by utilizing rotating-frame analysis and control design (until recently only used for three-phase converters), i.e. the well-known vector controller [30] or rotating reference frame controller [31]. This research focuses on introducing an additional control method for single-phase half-bridge inverters to give superior dynamic response and system performance even under nonlinear load and no-load. In order to design the control system, the plant and its controller will firstly be described mathematically.
3. Studying the photovoltaic inverter front-end requirements. Subsequently, the inverter performance is to be examined using a DC voltage-source with a variable magnitude and finite (non-zero) source impedance. Accordingly, the requirements for the selection of DC-link capacitors are established and

the optimum capacitance value required is determined. The inverter controller performance is examined under conditions where the DC-link voltage fluctuates.

4. Investigating the effects of incorporating such systems into the utility network as decentralized distributed generators.

Decentralized distributed generators allow generation of smaller amounts of power in a lot of places, rather than a lot of power in one place. This leads to electrical power being generated nearer to the point at which it is consumed. Consequently, this allows more power to travel with lower losses to customers in cities, towns, as well as rural areas. This can make optimal use of small-scale energy generation, as well as allowing the use of the renewable energy sources. Such converters can operate in autonomous mode, can be connected together, or can be used in grid-tied mode.

The present design and implementation practices of electronic circuits and control systems make extensive use of embedded microprocessors and digital signal processors (DSP) in order to facilitate the rapid calculations required when advanced control systems are implemented digitally. One of the requirements for this research program is aimed at optimizing a circuit-based simulation model. A number of powerful component-based electronic simulation systems, such as MATLAB, SPICE and SABER have become available over the recent years. Due to the availability of MATLAB at De Montfort University, it was decided from outset to implement the models in this study by using the MATLAB/SIMULINK program.

The single-phase inverter circuit analysis and controller design is extensively described in this thesis. The proposed controller is developed and verified with the use of

MATLAB/SIMULINK. Furthermore, the proposed prototype is developed as a practical hardware/software implementation and is evaluated in comparison with the simulation results.

1.10 Thesis Structure

Chapter 2: Outlines and provides a review of relevant research literature. This chapter also covers output filter design and inverter switching frequency selection.

Chapter 3: Focuses on investigations appropriate to an improved inverter switching gate-drive algorithm based on space-vector pulse-width modulation (SVPWM) for the single-phase inverter. Results are then compared with those from the more common sinusoidal pulse-width modulation (SPWM).

Chapter 4: Starts with a revision of stationary frame and synchronous rotating frame techniques in literature. Current approaches used in three-phase systems are also evaluated.

The end of this chapter provides an overview of the relevant published work for single-phase inverters employing the synchronous rotating frame controller. This is aimed at understanding the limitations of such existing systems and identifying the direction in which the proposed development should take.

Chapter 5: Focuses on single-phase inverter circuit modelling and analysis based on the synchronous rotating reference frame. The power stage of a single-phase voltage-source inverter based on the synchronous rotating reference frame is described mathematically as a set of differential equations. It is investigated in

order to determine how the transformation method may be employed in controllers for single-phase inverters.

Chapter 6: Describes a single-phase inverter controller with its mathematical model (differential equations) in different modes of operation. A new transformation strategy is proposed in this chapter. The proposed strategy is appropriate to the single-phase inverter controller. This is followed by the development of a complete controller stage. Results of the simulation of this controller using MATLAB/SIMULINK are presented.

Chapter 7: Determines the requirements of the inverter controller when sourced from an MPPT front-end. Accordingly, this chapter describes:

- Establishment of the requirements for the selection of DC-link capacitors and determining the capacitance value required;
- Investigation of the behaviour of the inverter controller taking into account the effects of an MPPT front-end;
- Study of the inverter controller performance under non-linear (PV array) DC source voltage fluctuations.

Chapter 8: Discusses the power distribution network and develops the idea of incorporating a small-scale renewable energy/power supply into the network as a decentralized distributed generator. This chapter then examines the issues of load sharing by controlling the phase and magnitude of the output voltage depending on the quantities measured at the common coupling point between the distributed generator and the network. The approach to load sharing is based on removing the need for exclusive communications between the generator and the network.

Chapter 9: Presents a practical implementation of the PV system. The proposed technique is implemented in physical hardware and is tested in the laboratory, and then a comparison between the practical and simulation results is made. This is to allow accurate investigation of the performance and behaviour of the proposed prototype and the effectiveness of its model. The practical system is tested up to 1 kW only. Nevertheless, the technology used will scale up to easily allow the 2.5kW goal to be achieved.

Chapter 10: Presents the conclusions and the possibilities for future work.

Chapter 2

REVIEW OF PREVIOUS WORK AND DESIGN CONSIDERATIONS

2.1 Introduction

This chapter provides an overview of literature within the proposed research area. The beginning of this section describes the international standards required in the design of a small-scale PV system. Then, the inverter unit, forming the interface between PV arrays and the load and/or grid side, is described. PV system control methods are reviewed, and a new control method is proposed for small-scale PV systems in the grid-tied mode under a decentralized power supply strategy. Consequently, the design considerations such as switching frequency selection and inverter output filter design calculations are also considered in this chapter.

2.2 Standard Permits for PV System

The system proposed in this thesis can be connected to the utility grid. Therefore, there are standards covering the required limits for such aspects as:

- Total Harmonic Distortion (THD).
- DC injection.
- Control and sharing of active and reactive power within grid-tied mode.

Standards and regulations specifically for grid-tied renewable energy exist, such as the IEEE-929 standard [29]. It contains relevant requirements for small-scale PV systems of 10 kW or less. It permits a limit of 5% for the THD in the output current. Furthermore, there is the 4% individual limit specified for each odd harmonic from 3rd to 9th, and a 2%

limit for harmonics from 11th to 15th, with DC injection limited to 0.5% of the rated output current. The European IEC61727 directive [32] requires similar standards for THD and specifies DC injection limits less than 1%.

There are other standards in the world, some with fewer [19] and some more stringent restrictions [29, 32]. The work in this study focuses on meeting the most stringent standards [29] and their requirements. This thesis is not concerned with the design of maximum power tracking systems, but with the DC-AC conversion and the interface to the utilities and loads. Therefore, the DC front-end source including boost converter was initially modelled as a DC voltage-source and later amended to model the characteristics of the output of a maximum power tracking front-end.

2.3 Inverter-Side Control

The use of power electronic converters has enhanced the ability to extract maximum power from PV panels, and to condition the power supplied to the load so as to achieve improved power quality, in addition to meeting the requirements for grid-tied operation. The proposed work is concerned with the control of the power electronics circuitry involved. There are many power electronic converter schemes used for controlling the PV system output power [33-36]. The applied power electronics scheme depends on the electrical generator type, the load supplied by the PV system, and the control topologies used in the system.

The inverter unit represents the core unit in the PV systems for the AC power interfacing purposes. This study will focus on single-phase inverter development particularly in the inverter gate-drive and the controller side. Therefore, it is worthwhile

looking at the components and the functioning of the inverter before starting the development process.

2.3.1 Inverter Circuit

Static (or solid-state) inverters are used in many electrical energy sources requiring a DC-to-AC transformation as well as in power interfacing. In single-phase applications, the full-bridge and half-bridge inverters represent the basic circuit topologies, while multilevel inverters and Z-inverters represent a further development approach retaining the fundamental inverter circuit methodology. Different circuit design approaches address various issues that may be more or less important depending on the way the inverter is intended to be used.

In some cases, the development of the inverter involves changes to the switching gate-drive algorithm e.g. pulse-width modulation (PWM), sinusoidal pulse-width modulation (SPWM), and space-vector pulse-width modulation (SVPWM) [37, 38] in addition to developments of the inverter controller.

The inverter output voltage can be either $+V_{dc}$, $-V_{dc}$ or zero, depending on how the inverter switches are controlled. The inverter controller operates so as to create an AC output voltage by generating an appropriate inverter switching sequence.

The basic circuit of a single-phase half-bridge inverter, which is used for converting a DC voltage to an AC voltage, is shown in Figure 2.1. This type of inverter operates from a positive and a negative DC source and produces AC voltage.

The switching transistor S_1 is driven complementary to switching transistor S_2 . The transistor S_1 conducts during the first sub-interval $0 < t < \delta T_{sw}$ (where T_{sw} is inverter

switching period), while S_2 conducts during the complementary sub-interval $\delta T_{sw} < t < T_{sw}$. The volt-second balance across the inductor is given in (2.1).

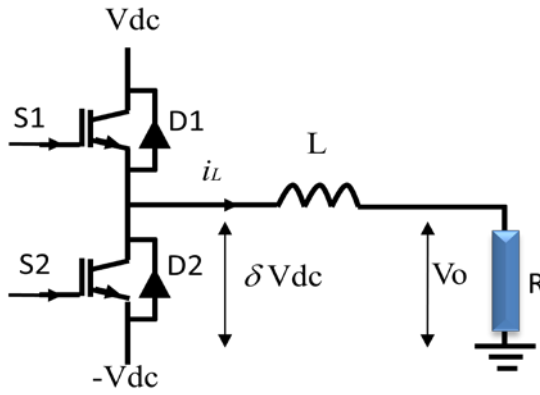


Figure 2.1: Single-phase half-bridge inverter circuit.

$$V_o = \delta V_{dc} - (1 - \delta) V_{dc} \quad (2.1)$$

$$V_o = (2\delta - 1)V_{dc} \quad (2.2)$$

where δ is duty cycle ($0 \leq \delta \leq 1$) and $T_{sw} = t_{on} + t_{off}$. The relationships between switching on/off time (t_{on} , t_{off}) intervals and the switching period T_{sw} are given by

$$t_{on}/T_{sw} = \delta ,$$

$$t_{off}/T_{sw} = 1 - \delta .$$

With an output filter inductor, the inductor current positive slope occurs during δT , and its negative slope during $(1 - \delta)T$. The load current (V_o/R) coincides with the inductor current (i_L) in the equilibrium state.

$$L \frac{di_L}{dt} = V_o - V_{dc}(2\delta - 1) \quad (2.3)$$

Since the load usually contains inductive components [30], the load current will lag the fundamental voltage. Therefore, anti-parallel diodes are connected across each semiconductor switch (D1 and D2 in Figure 2.1) to provide a path for the peak inductive load current when the corresponding switch is turned off.

It can be seen from the half-bridge inverter circuit in Figure 2.1 that the switch in the off state must block a voltage of $2 V_{dc}$. Whenever an inductive load current is interrupted, large voltages can appear across the inductor. If not limited by the circuit design, these are capable of destroying the power switch device if the device is not rated to withstand them. Diodes with a fast reverse recovery characteristic are placed in parallel with every switching device to facilitate commutation of the current depending on the switching states and current direction. Therefore, in the case of an inductive load when the switching transistor S1 is turned on, the voltage applied to the load is equal to $+V_{dc}$. Subsequently, the current i_L through S1 will increase and will supply energy to the load (positive current). But, if the load current i_L is negative, the current will flow back through recovery diode D1 and return energy to the source. A similar process occurs when switching transistor S2 turns on and S1 turns off.

The behaviour of the switching power devices together with the reverse recovery diodes in the half bridge inverter can be described by an ideal 2-position (single-pole double-throw) switch. Notice that both transistor switches on the same leg cannot be in the on-state at the same time, otherwise a short circuit would exist across the DC source, which will destroy the switching devices.

2.3.2 Modulation strategy

The stability and repeatability of inverter performance characteristics are a prerequisite both for reliable PV system performance and for determining parameters in the performance model.

The quality of the inverter output voltage depends on the number (n^{th}) of harmonics and the magnitude of each harmonic that exists in the output voltage. The inverter output quality can be measured by many parameters; the most important ones are the magnitude of individual (n^{th}) harmonics (HF_n), and the total harmonic distortion (THD). Various modulation techniques such as PWM, SPWM and SVPWM are proposed in the literature [30, 37, 38] to increase the quality of inverter output. These techniques are now commonly used for controlling inverter output voltage and current. Some of these techniques are further modified so as to increase the inverter performance and reduce the THD. All these techniques share the same principle of operation, i.e. turning the switch between supply and load on and off at a fast pace (to perform PWM), the frequency of which is referred to as the carrier frequency. Another term associated with PWM is the duty cycle (δ), which represent the percentage ratio of the switch on time (t_{on}) to the full period time (T_{sw}).

2.4 Methods for Inverter Current Control

Control of current is an important issue in power electronic circuits, particularly in DC-to-AC inverters where the objective is to produce a sinusoidal AC output whose magnitude and frequency can both be controlled. The main function of the current controller is that the converter output current should track the applied reference signal with

as low an error as possible. Furthermore, the output voltage should have acceptable transient performance without poor dynamic response, undesirable overshoot or undershoot.

On the other hand, total harmonic distortion should be as low as possible and below the standard threshold values. These objectives of the current control should be delivered with competitive cost and size of the converter. The methods for current control of single-phase inverters are reviewed in the following sections.

2.4.1 Linear Regulator Based Method

The inverter output current is controlled with carrier-based PWM (the so-called carrier-based method [39]). This method has been modified in several studies to reduce the THD of the inverter output current. Among the methods in which the PWM is modified to improve the quality of the current waveform are: the SPWM methods [37, 39], centroid based switching [40], hybrid PWM [41] and random hybrid PWM [42]. Figure 2.2 represents a simplified diagram to describe the carrier-based control method. Proportional+Integral control (PI) has poor performance when tracking a sinusoidal reference due to the steady-state error at frequencies other than DC. Moreover, this controller is not capable of reducing noise in the current signal. This is because the integral term responds to accumulated errors from the past and is less responsive to real (non-noise) and relatively fast alterations in state. Hence, the system tends to be slower to reach the set point and slower to respond to perturbations. As a result, it can cause the present value to overshoot the set point value. One advantage of the carrier-based control method associated with linear regulators is the constant switching frequency operation.

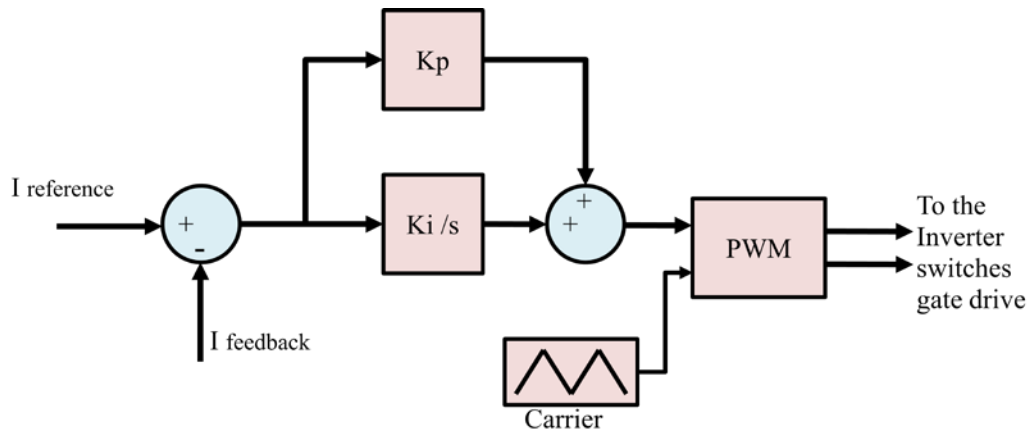


Figure 2.2: Carrier-based current control method.

[43, 44] proposed another modification to the carrier-based method. This is by combining the PI current control transfer function with a sinusoidal transfer function, as shown in Figure 2.3. The resonant frequency brought about by the additional term is equal to the utility frequency. Consequently, the proposed current controller can provide infinite gain at the line fundamental frequency.

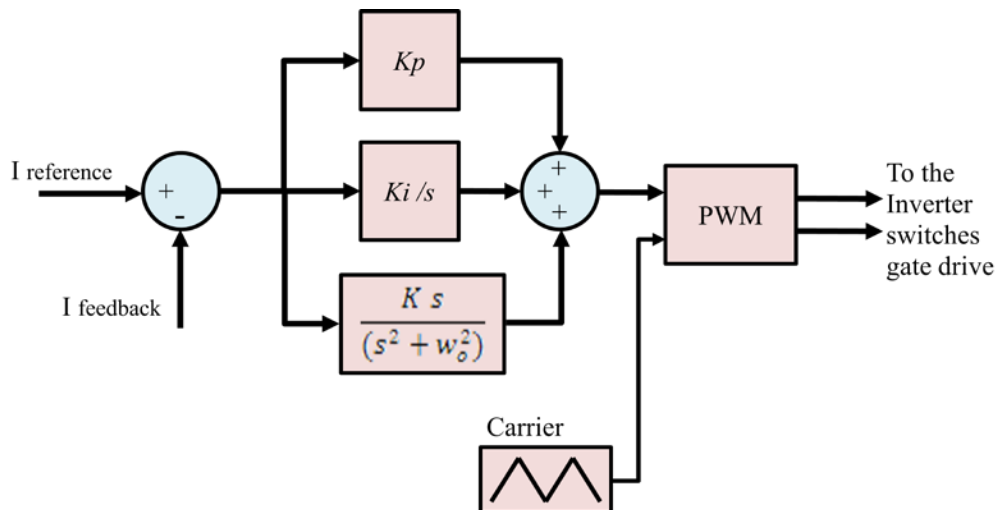


Figure 2.3: Carrier-based controls scheme with sine transfer function.

The disadvantages are that the compensator has a slow response, and it is very sensitive to variations in the fundamental frequency, as well as having a large phase margin around the line frequency [45], which can cause stability problems in the system.

The general drawback of the carrier-based method as compared to other direct current control methods is the poor dynamic response of linear compensators, which causes poor overall transient response.

2.4.2 Hysteresis Control Method

The hysteresis current control method is simple and easy to implement by dedicated hardware and can have acceptable transient performance. This method is considered as direct control since the current is controlled in a hysteresis loop and is based on the switch status. In this method, the inverter output current is forced to follow the current reference. The deviation between reference and output current is limited by the upper and lower band in a hysteresis loop, see Figure 2.4. This also guarantees a peak current limiting capability.

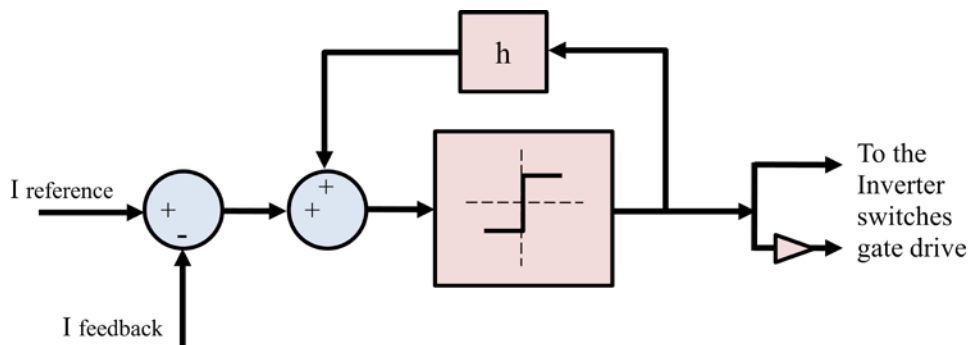


Figure 2.4: Hysteresis current controller scheme.

If the actual output current reaches the upper limit of the hysteresis band, the inverter leg is switched off so that the current decreases to the lower band of hysteresis loop where the inverter leg is once again switched on and the current increases. The sinusoidal wave shape of the reference signal causes variation of the inverter switching frequency and yields current ripple magnitude that varies during one output fundamental period despite the constant width of the hysteresis band. Hence, the current control with a

fixed hysteresis band has the disadvantage that the PWM switching frequency varies because peak-to-peak current ripple is required to be controlled at all points of the fundamental frequency wave [46, 37, 38].

This simple controller has a variable switching frequency and therefore a relatively high THD. The ripple magnitude of the current is proportional to the gap width between the upper and lower band of hysteresis loop. The hysteresis band should be small to reduce the THD in the output current, but this would increase the switching losses. Otherwise, a wider hysteresis band would increase the THD. In many cases the hysteresis band is chosen as a compromise between low losses and low THD.

The controller's bandwidth in controlling the current waveform depends on the parameters of the system. For a more advanced hysteresis current control system, the bandwidth needs to be increased. This can be done by altering the PWM technique so as to modify the hysteresis band in real time as a function of load parameters in order to optimize the PWM performance [47].

In order to keep the switching frequency almost constant, in [47, 48], the hysteresis band was moderated in real time according to the system parameters. It was calculated as a function of the circuit and the load parameters, the reference current slope, and the DC-link voltage. This requires an increased number of wide-bandwidth sensors.

An adaptive hysteresis band was proposed in [49] for current error comparison. The inner adaptive band is calculated off-line in accordance to the currents, voltages, and filter inductances. A comparison with the real time adaptive hysteresis method shows that the adaptive hysteresis band needs fewer sensors and less real-time calculation. On the other hand, it exhibits a greater variation in the PWM switching frequency.

In order to solve the variable switching frequency problem of the hysteresis method, some modified hysteresis methods have been proposed, such as a three-level hysteresis current control strategy [50], as well as a ‘random hysteresis method’ which is based on a random number generated and used to define the upper and the lower bands of the hysteresis controller [51]. These methods deliver an output current with narrow frequency spectrum content. Tolerance and variations in system parameters may affect the performance of the controller. Generally, with hysteresis controllers, there will be a wide bandwidth of harmonics in the inverter output current. Another solution is to use more complicated methods which need more analysis with faster DSPs.

2.4.3 The Peak Current Control Method

The peak current control method is a useful control scheme in power electronics. It is usually implemented with DC-to-DC converters in digital or analogue forms [52-54]. Peak current mode control operates by directly comparing the actual inductor current waveform to the current reference level. It can be described as follows: The peak inductor current control functions by comparing the up-slope of the inductor current (or switch current) to a current level set by the reference value. At a fixed interval in time, the power switching device is turned on. When the instantaneous inductor current reaches the reference value, the switching gate drive turns the power switching device off. This method gives constant switching frequency, Figure 2.5.

This method can produce instability under certain circumstances [55, 56]. Therefore, a compensating saw tooth signal is added to or subtracted from the reference current control signal [57, 58]. The slope of the saw tooth signal is selected to maintain stable operation and to eliminate sub-harmonic oscillation. The peak current mode control

method is inherently unstable at duty ratios exceeding 0.5. In order to reduce the noise, the peak current control can be modified to the average current control with an increased degree of accuracy [52].

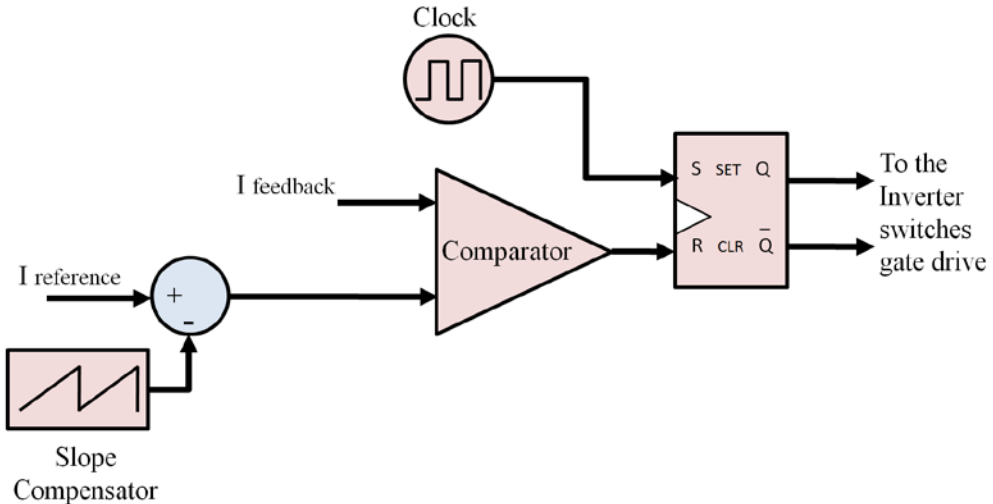


Figure 2.5: Analog peak current mode control scheme.

In solid-state inverter applications, the inductor output current down-slope and up-slope change over a wide range, because the inductor current is tracking the fundamental sinusoidal waveform. Hence, the peak and average current control methods suffer from difficulty of implementation when applied to inverters. Therefore, [58] presents a revised strategy of the current control to include the peak voltage level within a multilevel converter. The algorithm presented makes use of two compensation ramps added to a current reference. When this reference is compared to the load current, it allows the generation of logic signals to form a specific state. This technique increases the complexity of the controller, and the output current suffers from a static error within certain bounds.

2.4.4 Proportional-Resonant current controller

PI controllers are very common in DC-to-DC converters, but this kind of controller has relatively poor performance in inverter applications. This is because the tracking of a

sine wave signal is not as straightforward or direct as the tracking of a DC signal. The reason is the time-variant steady-state error produced when tracking the sinusoidal reference. Furthermore, this controller is unable to reject the noise in the current signal [43].

Therefore, [59] introduced the Proportional-Resonant (PR) current controller. In this approach, the classical PI DC-compensator is transformed into an equivalent AC-compensator having the same frequency response characteristics in the bandwidth of concern.

[60] presents a single-phase grid-connected inverter system with the quasi-PR control scheme, addressing some of the reasons that make PR controllers difficult to implement in reality. Firstly, the infinite gain introduced by a PR controller leads to an infinite quality factor which cannot be achieved in either an analog or a digital system. Secondly, the gain of the PR controller is much reduced at other frequencies and, in itself, it is not adequate to eliminate harmonic influence caused by presence of grid voltage harmonics. However, in case of digital implementation on a low-cost fixed-point DSP, the limited computational power and the limited numerical representation precision can restrict the utilization of this method. Therefore, [61] proposed the filtering approach based on the resonant current controller with selective harmonic compensation to reduce the time-costs associated with a fixed-point DSP.

[62, 63] mention the steady-state errors inherent in the solid-state inverters. The synchronous rotating frame theory can solve this problem in three-phase systems, whereas single-phase systems suffer from shortcomings that arise in the application of this theory. Therefore, PR controllers for current/voltage control are introduced as a solution for grid-

connected converter applications. Advantages exist with the PR controllers, such as the possibility of tuning their individual resonant peaks to the grid frequency for precise fundamental reference tracking and to some low-order harmonic frequencies for selective harmonic compensation, and the possibility of implementing a harmonic reference generator for active filtering of harmonics. The disadvantages are that the compensator is very sensitive to the variation in fundamental frequency, has a low response speed, and stability problems can be caused in the system by a large phase margin around the mains frequency.

2.4.5 Synchronous Rotating Frame Controller

The design of a current-error compensation scheme is critically important especially within grid-tied single-phase inverter applications. Among the previous developments of current controllers and making use of the experience with the three-phase inverter are [64-68], which employs current control strategies based on a separate current controller (current error compensation) and a PWM function that can exploit more advantages in an independently designed overall controller structure [67]. Since the synchronous rotating frame controller was proposed for this study, Chapters 4 and 5 will give more details about this type of controller.

2.5 Decentralized Power Supply

Most power plants are built in a large scale due to a number of economic, safety, logistical, environmental, geographical and geological factors. This is because much of the energy generated is produced by large-scale centralized power plants using fossil fuels,

nuclear power or hydropower. There are number of drawbacks with such centralised systems, including:

- The high level of dependence on non-renewable fuels.
- Environmental impact.
- Transmission and distribution losses.
- Higher cost of the generation plant, transformers, transmission, and distribution network.

In the last two decades, considerable changes occurred in the energy usage patterns of buildings, due in part to widespread utilisation of refrigeration and electric heating in domestic appliances as a result of increasing standards of living. Therefore, distributed generation stations are another approach within the power network to provide further electrical power to the utility. Distributed generation represents a solution to meet the increased demand for power. It reduces the amount of energy lost in transmission because the electricity is generated very near where it is used, perhaps even in the same building group. This also reduces the size and number of power lines that must be constructed. Typical distributed generation exists with the feed-in tariff system and makes use of low maintenance plant, low pollution and high efficiency.

It is known that the rate of growth of electricity demand is on the rise [67]. In addition, energy demand for services is projected to increase considerably due to the increasing level of services in modern economies. A truly secure system would include many different kinds of generating sources that in many cases overlap and provide redundancy. These generators would also be very small-scale so they could be located close to the customer. Rather than building huge transmission lines, a new emphasis would

be placed on power distribution and switching rather than bulk transmission of electricity. Today, the presence of small-scale renewable energy generation technologies has changed the thinking away from large power stations and control, toward the notion that there may be advantages if generation is moved closer to the end user. Therefore, new decentralized power generation has been growing steadily. Modern embedded renewable energy systems such as PV and wind are ideal in this application [9, 10, 16, 36].

There is a gap between actual demand and the level of economic and/or optimal use of the environment. Renewable energy technologies account for only a modest proportion in meeting the world's total commercial energy demand today. For this reason, a number of countries (Australia, Germany, Spain, France) have developed favourable legal frameworks to make it easier for people to invest jointly in grid-connected PV plants, support the PV market, and to disseminate the best investment schemes [69, 70].

2.5.1 Grid-Side Control

This study encourages the idea of incorporating a small-scale renewable energy power supply into domestic dwellings as part of the power network. With this idea, a large number of small-scale decentralized power supplies would be connected to the power network, which may increase the complexity of the power supply control systems. Proper operation in both the grid-connected and the islanding modes requires high performance power flow control and voltage regulation algorithms. Islanding refers to the condition in which a distributed generator continues to power a location even though electrical grid power from the utility is no longer present.

If an existing (stiff) grid is connected only to a large centralized power plant, the voltage at the common coupling point cannot be significantly changed by a small-scale

decentralized power supply. It is specified in [71] that the inverter must not oppose or attempt to regulate the voltage at the point of common coupling (at which point the grid voltage is measured). Inverter's power quality will thus be defined by its output current quality. Indeed, most power networks are three-phase systems. Therefore, distributed resources are connected to the grid via an isolating three-phase transformer to eliminate zero-sequence components in three-phase systems [64].

The work in this study simplifies the inverter-grid load sharing. The inverter side controller uses grid parameters which can be measured at the inverter-grid common coupling point without extensive communications. This is achieved by using the droop function method, which leads to a more efficient usage of small-scale renewable energy sources [72- 76]. In this method, current references are determined from the active and reactive power references resulting from voltage and frequency droop control - controlling the inverter output power by controlling the voltage magnitude and phase shift (the angle between the inverter output voltage and the grid voltages) depending on locally-measured instantaneous information. In this method, the grid parameters at the common coupling points become the reference for all decentralized distributed generators.

The synchronous rotating reference frame controller can be provided with the inverter active and reactive output power control to support the suggested droop strategy. The reactive power is controlled in this method by using the modulation index, while active power is controlled by phase shifting. Chapter 8 gives more details about this strategy.

2.6 Design Consideration in This Study

It is necessary to define the carrier frequency value before choosing the type of the output passive filter and its component values.

2.6.1 Carrier Frequency Selection

In order to reduce the filter component size and also minimize the effect of harmonics, the PWM switching frequency should be as high as possible. However, during the transitions between on and off states of power semiconductor switch devices, both device current and device voltage are non-zero, and considerable power is thus dissipated in the switches. The PWM frequency is restricted by the control unit and the switching device capabilities, e.g. switching rise time and fall time and switching losses. A better switching device should provide a more rapid slope during turn-on and turn-off to avoid a switching overlap (shoot-through) case. For ideal switching elements, rise and fall times should be symmetrical and be small, a trade-off between switching losses and electromagnetic interference.

PWM results in voltage swings at the bridge output from one voltage amplitude extreme to the other. This wide voltage swing takes a lot of filtering to smooth out. Within any PWM smoothing filter, the amplitude of the switching ripple in the output voltage will reduce only by a specific percentage. A good rule for achieving low ripple amplitude levels is to set the PWM frequency to be much higher than the fundamental frequency (10 times high). Today, power switching devices designed for low to medium-power inverters can operate at relatively high frequencies in the tens of kHz range.

On the practical side, microprocessors can have a limited capability due to computational time-speed considerations. Therefore, the computational availability per switching cycle should be determined. The controller, as far as possible, should avoid using mathematical functions that need a lot of iterative calculations. With a control algorithm that needs more time to execute, processes can be affected by computation delay, which can reduce the response times of the system. It should be noted that the same processor may also be required to do other computations (on a time sharing basis) such as protection operations. Hence, this issue is a very practical one for selecting an optimum microprocessor with cost-speed ratio acceptable for the particular application. In the present case, the selected switching frequency is 20 kHz (PWM carrier frequency).

Finally, filtering pulses is not just about the pulse frequency but also about the percentage duty-cycle and how much energy exists in the pulses. The same filter will give different performance (may be better or may be worse) on a high or low duty cycle compared to a 50% duty cycle.

2.6.2 Filter Parameter Design

In a solid-state inverter, the on and off switching states are always opposed in one inverter leg. Hence, either the positive or the negative DC bus voltage is applied to the output. The switched voltage pulses are at a constant switching frequency and contain a wide range of harmonics. The switching noise and high frequency harmonics are usually attenuated by inductors and capacitors, which can be combined in different ways to construct passive filters, such as: L-filter, LC-filter, T-filter, and pi-filter. The low-pass passive filters are applied to solid-state power supplies driving loads that need a clean

sinusoidal waveform. For an adjustable inverter output frequency, the filter must be tuned to a frequency that is above the maximum fundamental frequency.

Generally, low-pass passive filters should be designed to allow the fundamental waveform component to be passed to the output while reducing the passage of the harmonic components. If the inverter is designed to provide power at a fixed frequency, a resonant filter can be used.

Most of the system advantages can be lost if the passive filter elements are not properly designed. To achieve high power quality and low distortion, the power filter should attenuate the harmonics to certain specified levels. A filter which is oversized can unnecessarily add cost, volume, weight, and power loss to the system. The main filter topologies are as follows [77- 78].

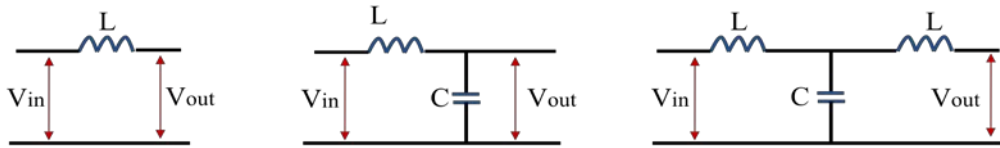


Figure 2.6: Filter configuration circuits.

1. L – Filter: This represents a first order filter giving -20 dB/ decade roll-off into the stop-band. This type of filter achieves only a low level of attenuation of the inverter switching frequency components. Therefore, in order to achieve satisfactory attenuation of the harmonics, the inverter switching frequency has to be much higher than the fundamental frequency.
2. LC – Filter: This represents a second order filter giving -40 dB/ decade attenuation. In this type of filter, a shunt capacitor is present to further attenuate switching frequency components. The shunt capacitor must be selected to produce low reactance at the switching frequency, while

presenting higher impedance within the control frequency range. In the cases where the system uses an isolating transformer at the low-frequency side, the LC filter can satisfy the harmonic limit requirements.

3. LCL – Filter: This represents a third order filter giving -60 dB/ decade attenuation. This type of filter can reduce the harmonic distortion levels at lower switching frequencies. However, it may cause both dynamic and steady-state input current distortion due to resonance.

Since the LC filter yields better performance than the L filter and is less complicated than the LCL filter, the LC filter represents a suitable compromise for the system intended for use in this research. The LC filter can give sufficient output performance with a 20 KHz carrier frequency. The LC-filter with an isolated transformer can satisfy the harmonic limit requirements by a sufficient margin [77].

Cut-off frequency, sometimes also known as break frequency or corner frequency is a boundary in the system frequency response at which energy flowing through the system begins to be reduced (attenuated or reflected) rather than passing through. The attenuation characteristics at the cut off frequency (f_c) is one of the critical factors involved in designing a second order filter. The gain near the cut-off frequency could be very large and amplify the noise at that frequency. The relationship between the filter elements and the cut off frequency of a low-pass filter is given in equation (2.4).

$$f_c = \frac{1}{2\pi\sqrt{LC}} \quad (2.4)$$

The current and voltage harmonic levels are the main requirements of output filter design.

2.6.3 LC Filter Calculations

The bipolar PWM switching type is presented in [78] for LC filter considering the grid-tied power quality issues. Figure 2.7 shows the filter circuit, while equations (2.5) and (2.6) define L and C component values.

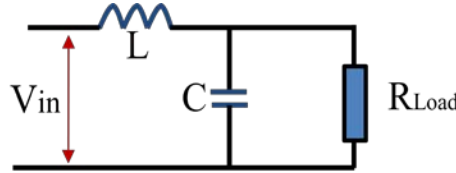


Figure 2.7: LC filter circuits.

$$L = \frac{R_{Load}}{2\pi f_c} \quad (2.5)$$

$$C = \frac{1}{2\pi f_c R_{Load}} \quad (2.6)$$

where R_{Load} is chosen at the lowest output voltage. V_{min} can thus be divided by the highest output current I_{max} , so as to obtain: $R_{Load} = V_{min}/I_{max}$. Equations (2.5) and (2.6) can be used to find the proper filter element values with the following assumptions to simplify filter analysis:

- Inverter input source is ripple free DC source.
- Inverter switching devices are ideal with no parasitics.
- Inductor and capacitor parasitic series resistance are ignored.

The cut-off frequency is selected to be one-sixth of the switching frequency ($f_c = \frac{f_{sw}}{6}$). The inverter output filter parameters are calculated with the cut-off frequency. The L and C calculated values are then approximated to the near available LC component

values. As a result, cut-off frequency $f_c=2371\text{Hz}$. Figure 2.8 is the MATLAB/SIMULINK Bode plot of LC filter with different load values.

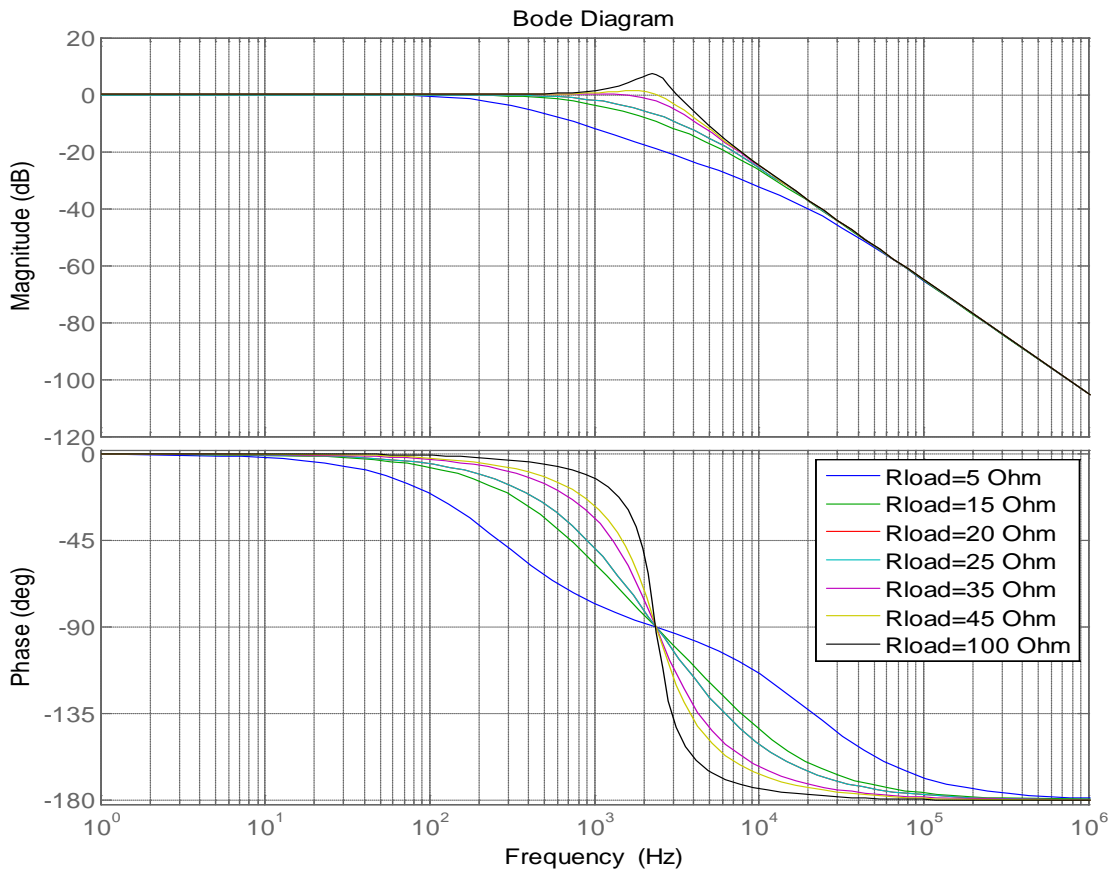


Figure 2.8: LC filter bode-plot.

Chapter 3

SPACE VECTOR PULSE WIDTH MODULATION

3.1 Introduction

This chapter provides an overview of modulation techniques used for generating gate drive signals in solid-state inverter applications. The purpose of modulation is to obtain a variable output having the maximum fundamental component while minimizing switching losses and harmonics. Previous works [37, 38, 79, 80] indicate that careful choice of the PWM strategy can significantly improve the inverter output harmonic spectrum by moving harmonic components to higher frequencies. In addition, Space Vector PWM (SVPWM) strategy is described as preferable to other PWM strategies commonly used with three-phase inverters. It maximizes exploitation of the converter hardware, inherently limiting the effect of an inherent third harmonic injection mechanism [30, 38], and simplifies the control organization. All the PWM techniques have been applied to three-phase inverters as well as single-phase inverters, except SVPWM which has to date not been widely applied to the single-phase inverter.

Therefore, this chapter investigates the use of the SVPWM in the context of the single-phase inverter. The proposed SVPWM algorithm is implemented and simulated using MATLAB/SIMULINK for the control of a single-phase inverter. The results of the proposed SVPWM algorithm show a higher amplitude modulation index compared to that of Sinusoidal PWM (SPWM), as well as a reduction in the output harmonic distortion.

3.2 General Description of Pulse Width Modulation Techniques

Several techniques based on pulse width modulation (PWM) strategies are commonly used today as part of the control of solid-state power supplies. The drawbacks of PWM are that voltage and current ripple levels are dependent upon the duty cycle, switching frequency and properties of the load. With an appropriately high switching frequency and by using an additional passive filter, the PWM output can be smoothed and averaged to limit these effects.

PWM power control systems are easily realizable with semiconductor switches. Little power is dissipated by the switch in either the on or off state. However, during the transitions between the on and off states, both voltage and current are non-zero, and thus considerable power is dissipated in the switches. Nevertheless, the average power dissipation is low compared to the output power being delivered, even when relatively high switching frequencies are used. Modern semiconductor switches such as MOSFETs or insulated gate bipolar transistors (IGBTs) are suitable for use in this application and permit high-efficiency controllers to be built.

Pulse width modulation produces a rectangular periodic pulse train whose duty cycle varies depending on the average value required at the output side, as shown in Figure 3.1.

A typical modulator produces an average output-voltage value equivalent to the reference voltage within each PWM period, in other words the reference voltage is reflected in the fundamental component of the switched pulse pattern. The general aim in all PWM techniques is to create a train of switched pulses which have the same fundamental volt-second average as the target waveform at any instant of time. These

techniques differ in the way of arranging the switching strategy in order to minimize distortion (i.e. unwanted harmonics) and switching losses.

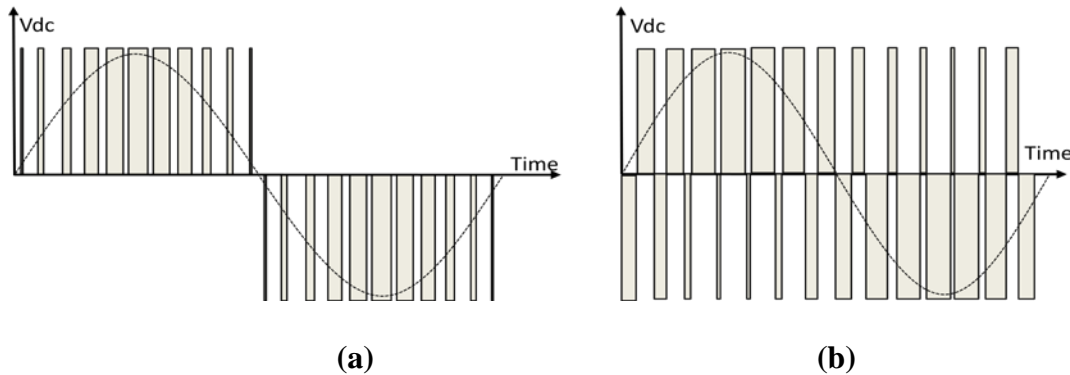


Figure 3.1: (a) Unipolar PWM. (b) Bipolar PWM.

3.3 PWM Classification

Several modulation strategies have been developed [37, 38]. There are many possible PWM techniques proposed in the literature; these differing in concept and/or performance [37, 38, 79]. The important techniques are:

- Hysteresis-band current control PWM.
- Synchronized carrier modulation
- Sinusoidal PWM (SPWM).
- Space vector PWM (SVPWM).

Hysteresis-band PWM and synchronous carrier modulation techniques employ variable switching frequency strategies in which carrier frequency varies with the output waveform [79]. SPWM and SVPWM are fixed (constant) carrier frequency strategies. The fixed frequency strategies share some common features:

- Switched pulse width determination.

- Switched pulse position within the carrier interval.
- Switched pulse sequence across and within the carrier interval.

3.4 Hysteresis Current Controllers

The principle of hysteresis current control is very simple. The current controller controls the load current by forcing it to follow a reference. The switching action of the inverter keeps the current within the hysteresis band. Figure 3.2 shows the principle. When the output current reaches the lower hysteresis limit, the inverter switches its state so as to produce an increasing output current. On the other hand, a decreasing output current is produced when the current reaches the upper hysteresis limit. The hysteresis-controller output voltage waveform is similar to that of bipolar PWM.

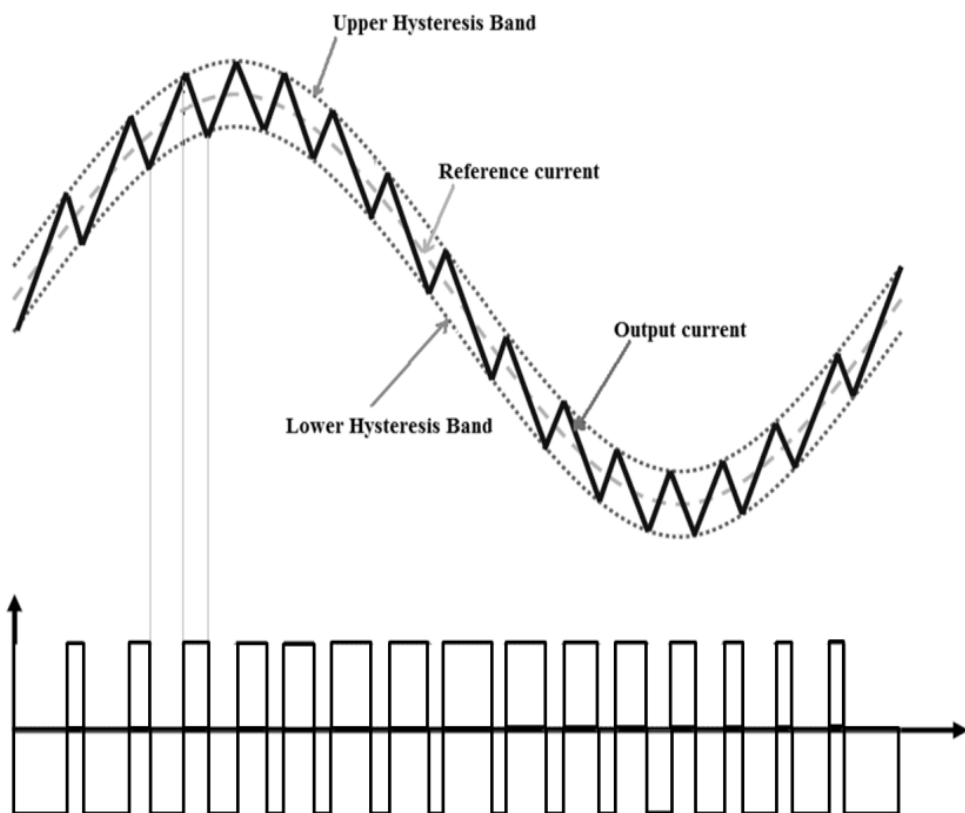


Figure 3.2: Hysteresis current controller PWM.

Hysteresis current controllers have the advantages of simplicity, provision of instantaneous current corrective response (subject to slew rate limitations), and unconditional stability of the system [81]. The drawbacks of this method are that the switching frequency is variable and largely depends on the load parameters that may vary widely. Consequently, the load current harmonic ripple is not optimal [82]. This leads to a wide range of variable switching frequency, causing a wider noise bandwidth.

3.5 Sinusoidal PWM

In this technique, a sinusoidal reference signal (i.e. the modulating signal) is compared with a triangular carrier-wave signal to generate gate pulse signals at the points of intersection between the modulating signal and the carrier signal. Figure 3.3 shows the principle of switching gate signal generation with SPWM [37, 38].

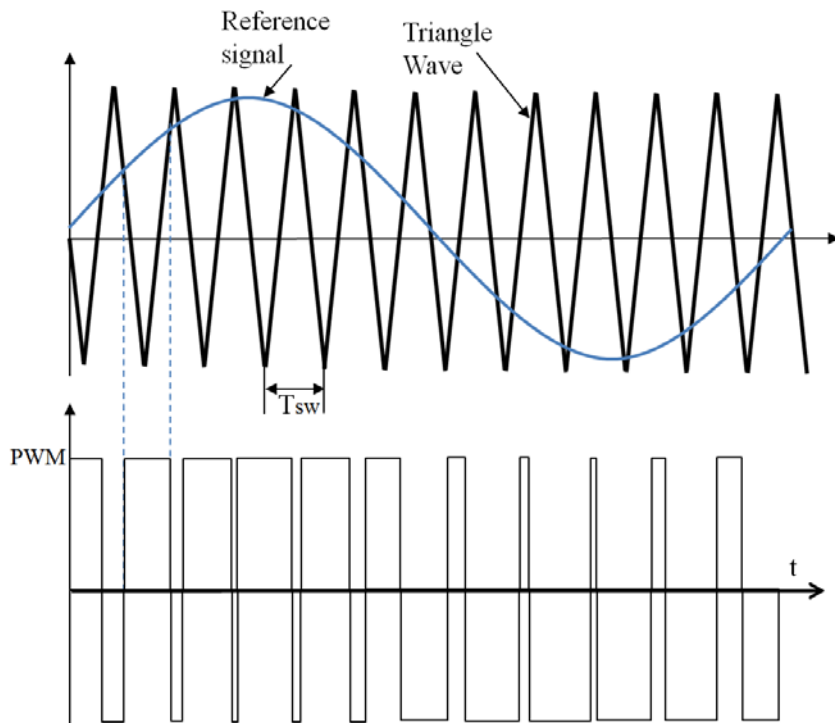


Figure 3.3: Sinusoidal PWM generation.

The modulation index (m) is defined as:

$$m = V_p/V_T \quad (3.1)$$

where V_p is the peak of the modulating wave and V_T is the peak of the carrier wave.

Ideally, the modulation index can be varied between 0 and 1 to give a linear relation between the modulating wave and output wave magnitudes. The inverter basically acts as a linear amplifier with a specific gain between the modulating/reference signal and the output voltage.

The magnitude of the higher harmonics is independent of the carrier frequency. At higher carrier frequencies, the inverter output harmonics will be significantly attenuated by the output filter, and the output voltage and current waveforms become closer to a sinusoid. The selection of carrier frequency depends on the trade-off between the inverter loss and the output waveform quality. Higher carrier frequencies increase inverter switching loss but decrease the output filter cost and size while reducing the output waveform distortion.

3.6 SVPWM Technique:

In recent years, the use of SVPWM has overwhelmed SPWM in three-phase inverter control systems. The former provides for a more efficient use of supply voltage in comparison with other modulation techniques. It appears to be the best technique for three-phase switching power inverters and has become commonplace in three-phase voltage-source inverters. SVPWM can increase the available DC voltage link utilization ratio (modulation index) significantly. SVPWM techniques have been the subject of intensive

research for various different industrial applications in three-phase voltage-source inverters, [83, 84]. The advantages of 3-phase SVPWM are summarized below.

- Its output voltage is higher than regular SPWM for a given DC-link voltage
- Total harmonic distortion (THD) is minimized
- Excellent DC-link voltage utilization is achieved
- The vectors can be arranged to give lower switching losses; or might want to approach a different result, such as center-aligned PWM, edge-aligned PWM, minimal switching [85].
- Gives a greatest variability of arrangement of the zero and non-zero vectors during the PWM period.
- It is easily implemented digitally.

3.7 Space Vector Concept

The space vector concept is derived from the rotating field theory of three-phase induction motors [83]. It refers to a special switching scheme based on the representation of three-phase voltage quantities as two equivalent orthogonal variables in the phasor diagram. These two equivalent orthogonal components can then be represented either in a stationary reference frame or a synchronously rotating frame (rotating at angular speed ω) by using the Clarke and/or Park transformation. The SVPWM technique was developed as a vector approach to three-phase pulse width modulation [83-88].

SVPWM is a digital modulation technique typically implemented in software using a microcontroller or digital signal processor [83-87]. The goal of SVPWM is to generate

the appropriate PWM signals so that the vector quantities (such as voltages or currents) can be represented by time weighting and averaging. This is done by approximating the reference quantity (voltages or currents) instantaneously using a weighted combination of the switching states corresponding to the basic space vectors in the time domain. For a short period of sample time T_s , the average inverter output voltage is the same as the average reference voltage during the sample time, i.e. the amplitude of the fundamental component of the voltage is proportional to the length of the reference vector.

3.8 The Basic Principle of SVPWM

Three-phase SVPWM is implemented by using a transformation from three-phase time-variant quantities to two orthogonal time-invariant quantities. This can be represented as a voltage vector projected onto a two-dimensional vector plane. The basic idea of space vector modulation is to develop the required volt-second product across the output inductor using discrete switching states. The SVPWM can be implemented by the following steps [83, 89].

1. Define the possible switching vectors. For a simplified representation, it is possible to include a coordinate transformation in the output voltage space. This uses a simple mapping to generate gating signals for the inverter. The mapping concept can be used with a variety of schemes.
2. Define the sector planes and determine the location of desired sector for the voltage vector used in the algorithm, where every sector plane is bounded by two or more vectors.
3. Define the boundary planes. Determine whether the given voltage vector can be implemented with the inverter topology.

4. Define the switching sequence. Memory is required to store sequences of switching states. A switching sequence is a set of switching states to be applied in a switching period. The structure of a switching sequence depends on the trajectory of the vector projected onto the mapping unit. This is then used to generate gating signals for the inverter. The switching sequence should minimize switching losses and THD.
5. Determine the time duration. The volt-second on-time calculations can be performed by using geometry mapping which would result in the same on-time equations. At any switching period with a given algorithm map as well as instantaneous modulation parameters, the processing unit will determine the location of the reference vector and identify the switching state. Since a switching state represents a unique combination of “ON” or “OFF” condition for the switches of the inverter, the switching states can therefore be directly applied to generate gating signals.

The three-phase SVPWM principle can conveniently provide an initial point for the development of single-phase SVPWM.

3.9 Software Implementation of Single-Phase SVPWM

The single-phase half-bridge inverter contains two switching elements switched in a complementary manner. Since this 2-switch inverter can generate a single vector, the output voltage vector space can be depicted in a one dimensional space, as shown by the vector at the bottom of Figure 3.4.

In order to provide an output voltage equal to the demanded voltage, the switching strategy combines average adjacent vectors during each switching period (T_{sw}). For this purpose, the nearest possible switching vectors are used.

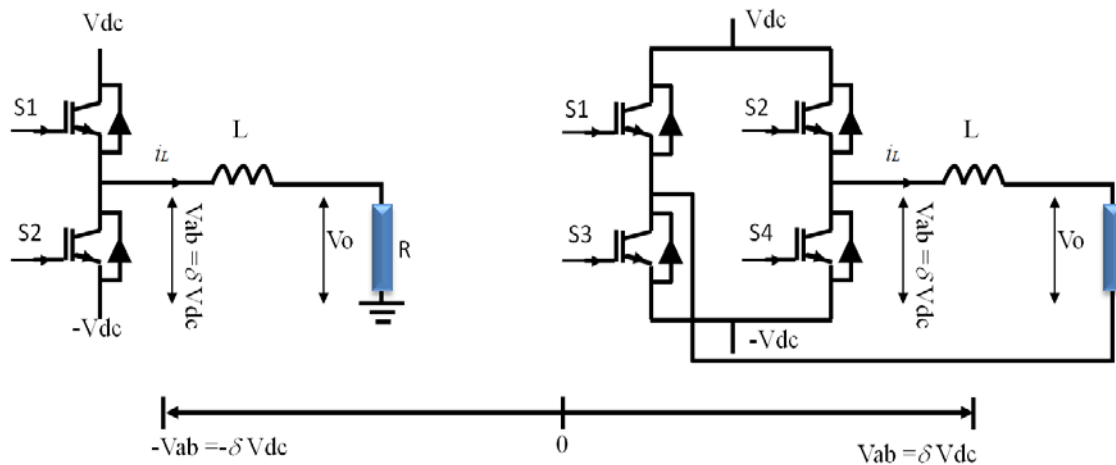


Figure 3.4: Output vector direction of single-phase inverter.

3.9.1 Boundary and Separation Planes

Generally, the instantaneous output voltage of the single-phase inverter (before the filter) v_{ab} can be one of three quantities only ($+V_{dc}$, 0 , $-V_{dc}$). This can be driven by two complementary switching signals and one zero state. Therefore, it is possible to identify two sectors as described in points below.

1. Sector 1, where $v_{ab} > 0$.
2. Sector 2, where $v_{ab} < 0$.
3. Consequently, the separation plane is given by $v_{ab} = 0$.

3.9.2 Switching Sequences

As mentioned previously, the desired switching sequence can be achieved with the nearest adjacent vectors; this will yield smaller output ripples. The possible switching states are represented by two binary numbers which describe the operating state of the inverter switching devices. The vectors V^1 and V^3 shown in Table 3-1 are active vectors, while vectors V^2 and V^4 are zero (or null) vectors. Note that the vector V^4 appears only in the full-bridge, while in the half-bridge inverter the zero vector is represented by V^2 . The switching operation mode can be expressed as in Table 3-1.

Table 3-1: Switching status.

Vector	S1	S2	v_{ab}
V^1	1	0	$+V_{dc}$
V^2	0	0	0
V^3	0	1	$-V_{dc}$
V^4	1	1	0 cannot be valid in the single phase half-bridge inverter

It is necessary to normalize the reference vector length to the base vector. The reference vector magnitude can be limited to V_{dc} by multiplying the reference vector by the coefficient ($1/V_{dc}$) in order to normalize the length of the resultant vector. In SVPWM, the reference voltage vector V_{ref} is constructed from the adjacent vectors of the located sector.

In order to generate the switching pattern, the reference voltage vector is converted to the time-weighted average of adjacent vectors. Therefore, the next step is to compute the duration time of the switching state.

3.9.3 Time Duration

The switching time duration can be computed by applying each switching vector in each switching period (T_{sw}). The time duration in the single-phase inverter can be derived through the two following approaches.

3.9.4 Bipolar SVPWM

Bipolar PWM can be achieved when the switching period (T_{sw}) includes two active vectors in addition to one zero vector. In this case, the vectors can take the following sequence: $V^1 \rightarrow V^2 \rightarrow V^3$, see Figure 3.5.

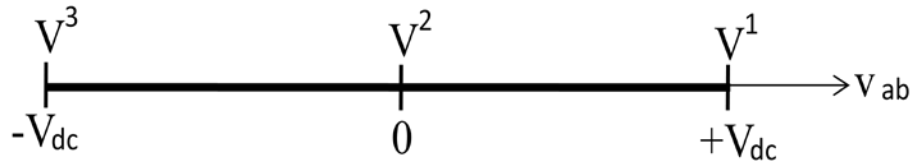


Figure 3.5 Half-bridge single-phase inverter vector sequence.

The above sequence is described mathematically below:

$$\int_0^{T_s} V_{ref} dt = \int_0^{t_1} V^1 dt + \int_{t_1}^{t_2} V^2 dt + \int_{t_2}^{t_3} V^3 dt \quad (3.8)$$

where t_1 , t_2 , and t_3 are the switching transition instants.

As the vectors V^1 and V^3 are active vectors, while V^2 is zero vector, the above equation can be rewritten below:

$$V_{ref} T_{sw} = V^1(t_1 - 0) + V^3(t_3 - t_2) \quad (3.9)$$

where $(t_1 - 0) = \Delta t_a$ is the time duration of vector V^1 and $(t_3 - t_2) = \Delta t_b$ is the time duration of vector V^3 .

$$V_{ref} = \frac{1}{T_{sw}} [V^1(\Delta t_a) + V^3(\Delta t_b)] \quad (3.10)$$

where $\Delta t_a = T_a$ and $\Delta t_b = T_b$, which are the respective time durations for which the switching states corresponding to V^1 and V^3 are applied. However, if we assume that the change in reference voltage V_{ref} is small within T_{sw} , where $T_a + T_b < T_{sw}$, then the residual switching period is reserved for zero vectors. The zero vector time durations (T_o) are given by.

$$T_o = T_{sw} - (T_a + T_b) \quad (3.11)$$

When the output voltage of the half-bridge single-phase inverter approaches zero at 0 and $n\pi$ phase-angles of the reference waveform, $T_a = T_b$, and T_o reaches maximum value. Inverter output voltage at its maximum positive value leads to T_a having a maximum weighting, while T_b and T_o have minimum weighting. (See Figure 3.6, where n is an integer).

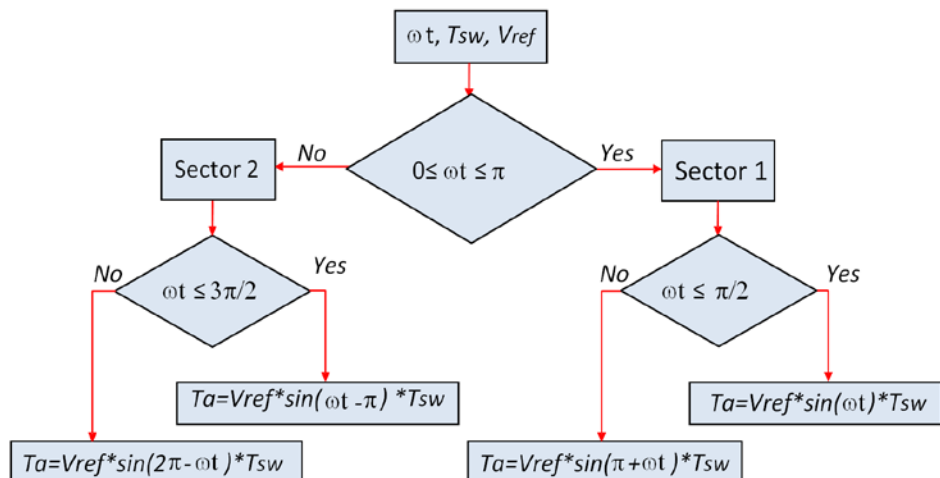


Figure 3.6: Single-phase Bipolar SVPWM flowchart.

3.10 Simulation

A single-phase half-bridge inverter was implemented in MATLAB/SIMULINK using two different modulation techniques. The first circuit uses the SPWM technique, as in Figure 3.7. The second circuit uses SVPWM and is described in Figures 3.8 and 3.9. These two circuits are identical in all other elements and devices (switches, filters, DC input voltage, and loads) and the values of filter elements are those calculated in section 2.3.6, taking into account the parameters listed in Table 3.2. They differ only in the modulation technique implemented in software in each circuit.

Table 3-2: Circuit Parameters.

Rated power	2.5 kW
Nominal input voltage (V_{dc})	370 V
Nominal output voltage (V_{ac})	220 V RMS
Switching frequency (f_{sw})	20 kHz
Fundamental frequency (f)	50 Hz
Filter inductance (L)	3 mH
Inductance resistance (rL)	0.01 Ohm
Filter capacitor (C)	1.5 uF

The switching elements are ideal IGBT antiparallel diode with internal resistance $R_{on} = 1e-3$ Ohms, and Snubber resistance $R_s = 1e5$ Ohms.

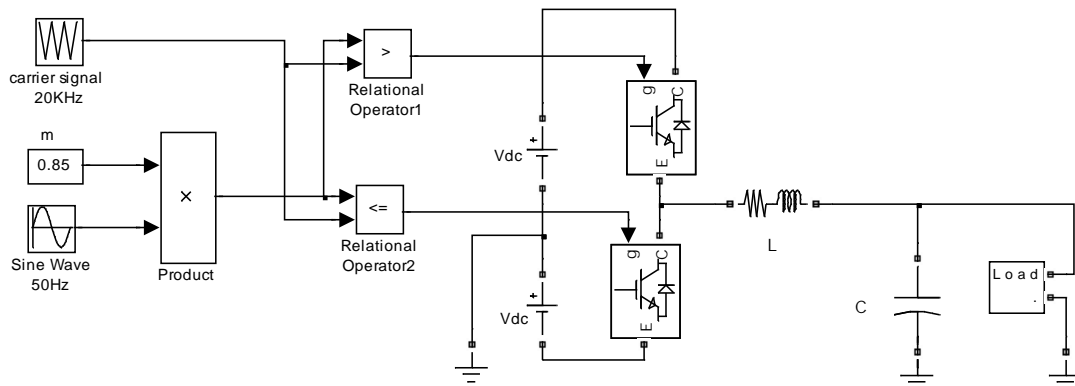


Figure 3.7: Single-phase inverter using SPWM.

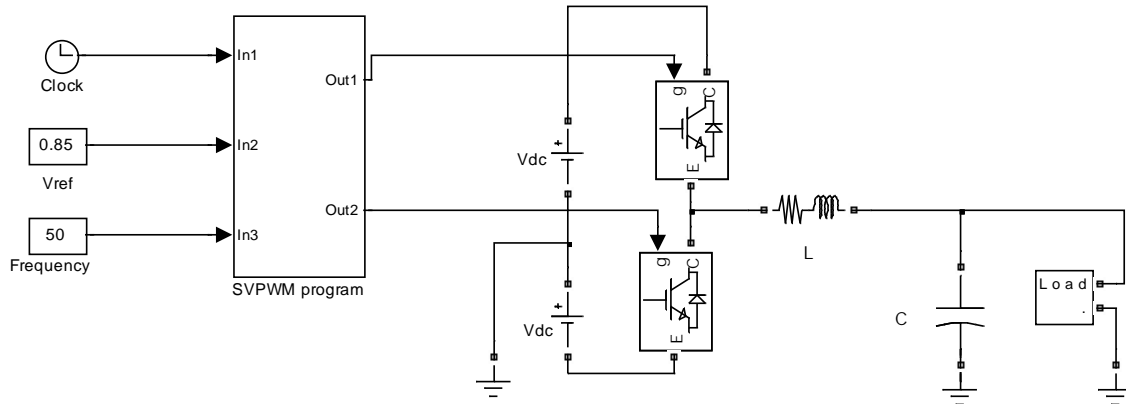


Figure 3.8: Single-phase inverter using SVPWM.

Figure 3.9 shows more details of the SVPWM program block, while the SVPWM program listing can be found in Appendix A. The rounding function block in Figure 3.9 is used for converting scalar output types to vector output types, because the Fcn block produces only scalar output. The ‘floor’ function rounds each element of the input signal to the nearest integer value.

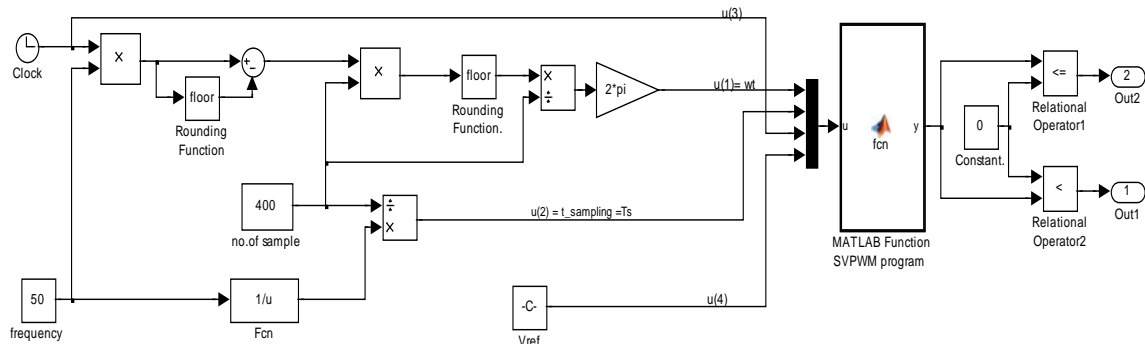


Figure 3.9: Single-phase inverter controller using SVPWM.

The two circuits were simulated with identical loads (2500W, 1000W+500VAr, 1000W, and 500W+500VAr). The results are given below. The (output voltage and current) waveforms produced by the SVPWM and SPWM techniques are shown in Figures 3.10 and 3.11 respectively, each with the same step-wise time-varying load and each with the same modulation index of 0.85.

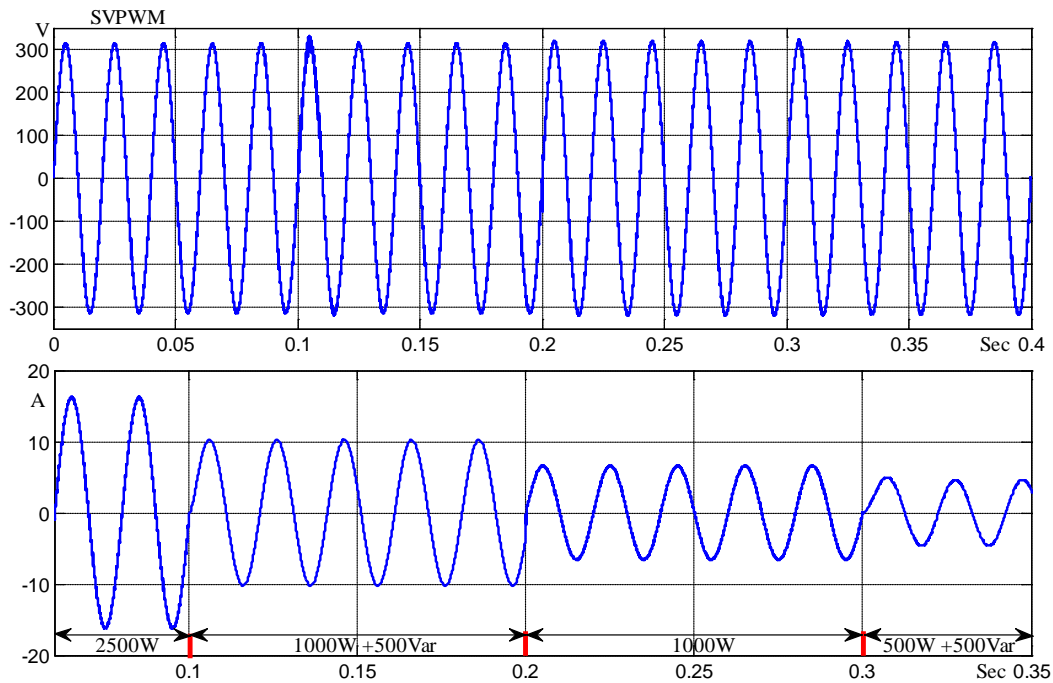


Figure 3.10: SVPWM output voltage and current waveform with different inverter loads.

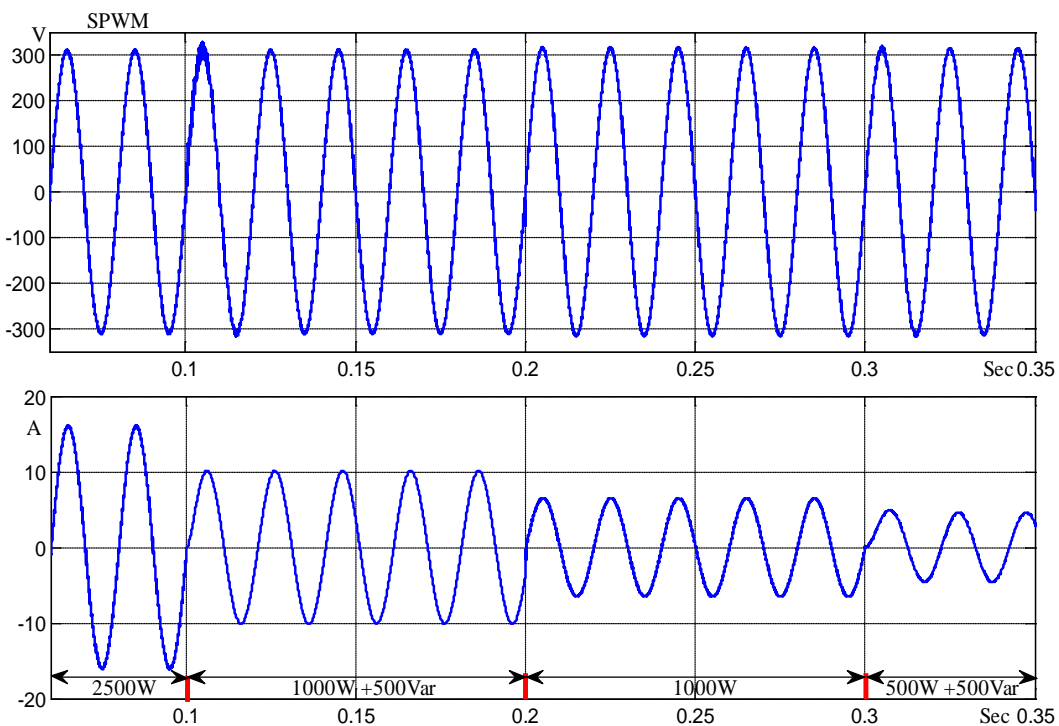


Figure 3.11: SPWM output voltage and current waveform with different inverter loads.

In order to get a deeper knowledge on the new modulation technique, the spectrum of the output voltage and current is analysed in the next section.

3.11 Harmonics in Electrical System

One of the core aspects of power quality is the harmonic content of both voltage and current in the electrical system. Both voltage and current harmonics can be generated on either the source or the load side. Harmonics generated by the load are usually caused by nonlinear operation of devices, including power converters, gas discharge lighting devices, arc-furnaces, etc. Harmonics can cause the overheating of the magnetic cores of transformers and motors. On the other hand, source harmonics are mainly generated by power supplies with non-sinusoidal voltage or current waveforms. Voltage and current harmonics of the source imply power losses, electro-magnetic interference and pulsating torque in AC motor drives. The frequency of each harmonic component is a multiple of the fundamental component.

There are several methods to indicate the quantity of the harmonic content. The most widely used measure is the total harmonic distortion (THD), which is defined in terms of the magnitudes of the harmonics. The THD is mathematically given by:

$$THD = \frac{\sqrt{\sum_{n=2}^{\infty} H_n^2}}{H_1}$$

where H_1 is the magnitude of the fundamental component, H_n are the magnitudes of harmonic components and n is an integer.

Therefore, for deeper comparison between single-phase SPWM and SVPWM, the Fourier spectra for each modulation technique under analysis have been obtained using a fast Fourier transform.

Figure 3.12 shows the SVPWM output voltage FFT spectrum analysis without filtering. The switching frequency (f_{sw}) is present with harmonics are positioned as sidebands at ($f_{sw} \mp 2f$). The frequency component at 50Hz is appearing as a result from higher frequency switching varying pulses width shape. In other word, the frequency component at 50Hz is created by modulating (varying) switching pulse width within the period equal to 0.02 Sec.

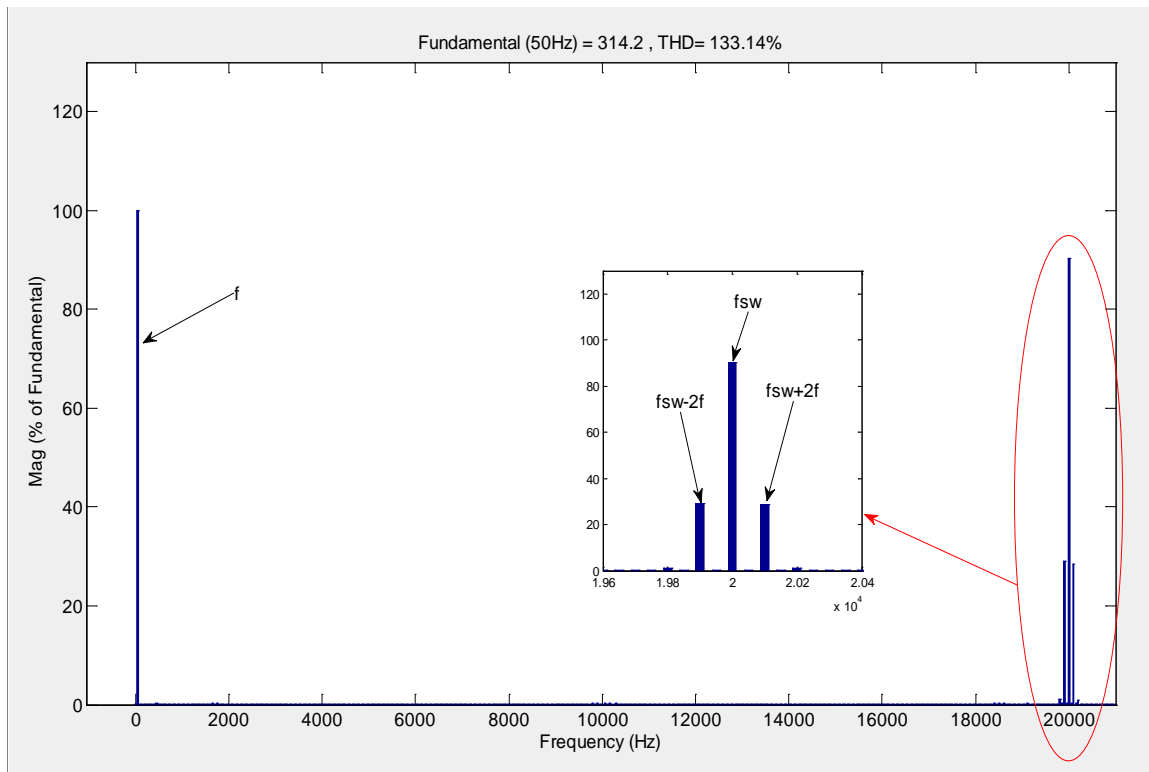


Figure 3.12: Output voltage FFT harmonic analysis before filtering.

FFT spectrum is re-measured after filtering by passive filter (LC filter) (Figure 3.13) [30]. Thus, the switching frequency (f_{sw}) and positioned sidebands at ($f_{sw} \mp 2f$) are reduced to a level dependent upon the passive filter values (LC filter), the 50Hz frequency component is the fundamental frequency. Figures 3.13 and 3.14 shows harmonic distortion (under rated load of 2500Watt) of the SPWM and SVPWM as a function of harmonic frequency and of the fundamental frequency.

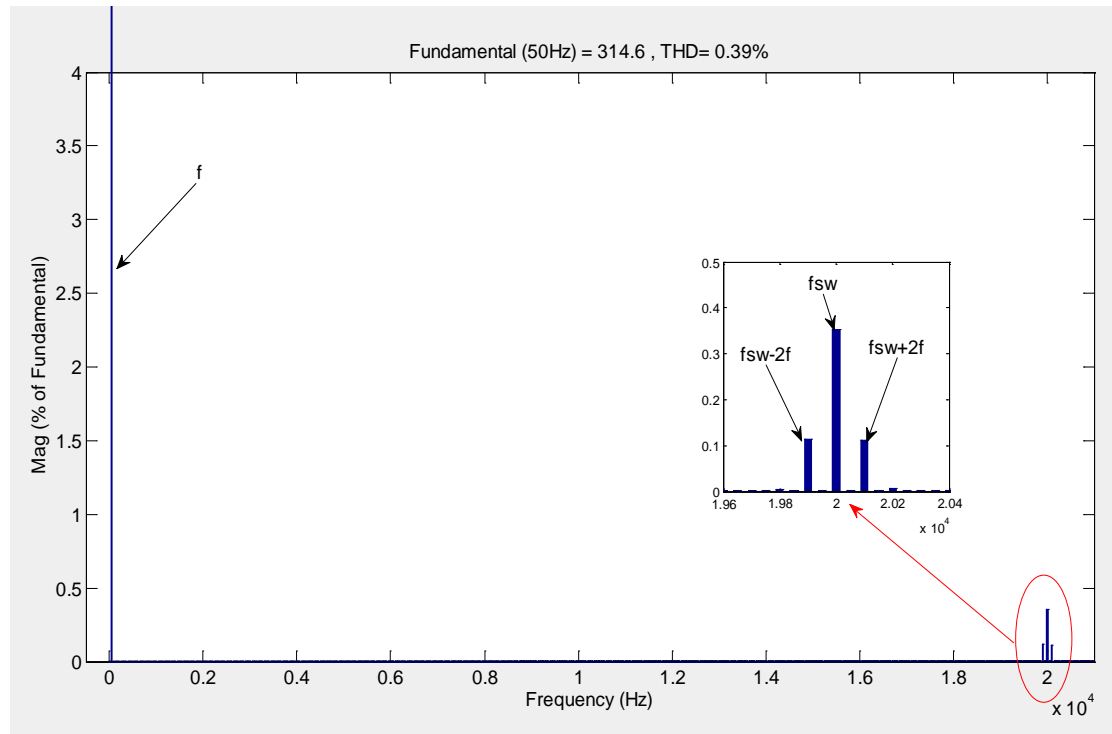


Figure 3.13: SPWM voltage waveform FFT harmonic analysis.

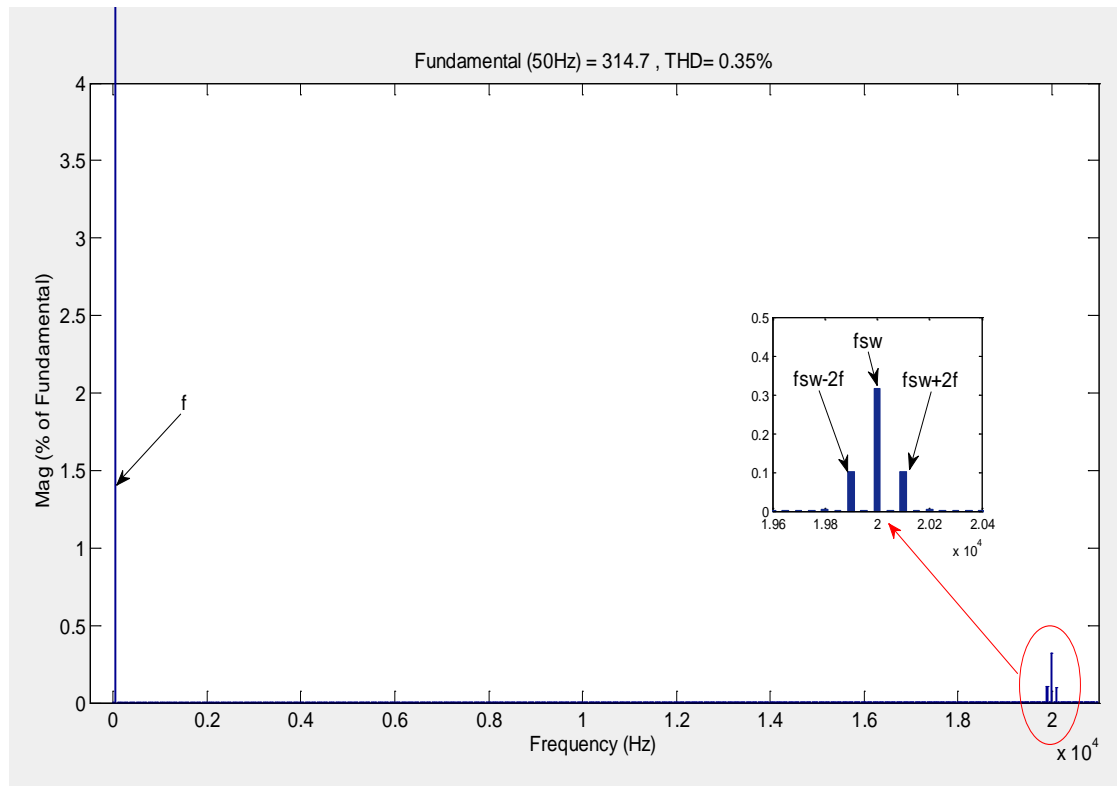


Figure 3.14: SVPWM voltage waveform FFT harmonic analysis.

Note that the switching frequency can be visible by zooming the current and voltage waveforms, Figures 3.15 and 3.16.

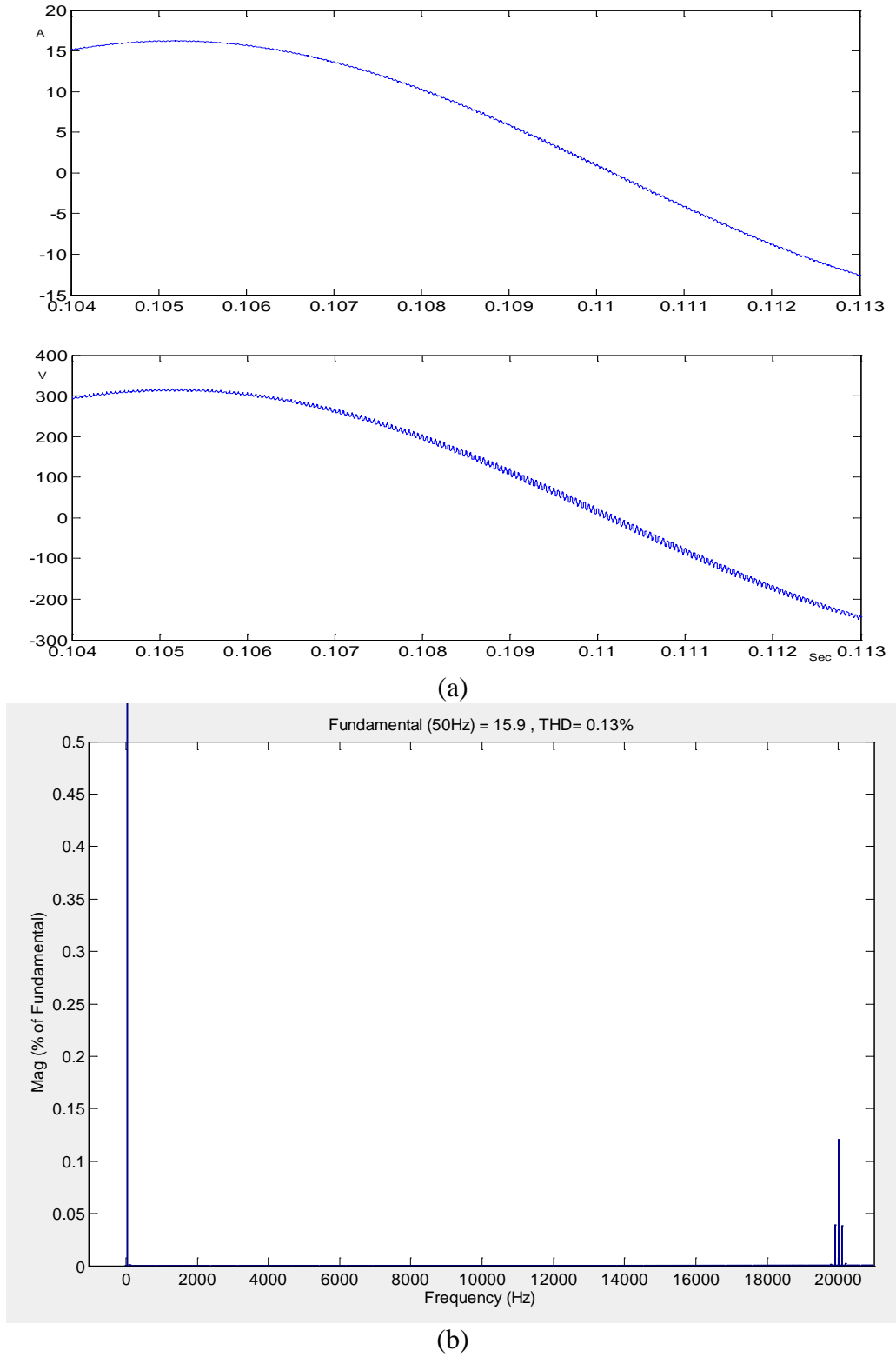
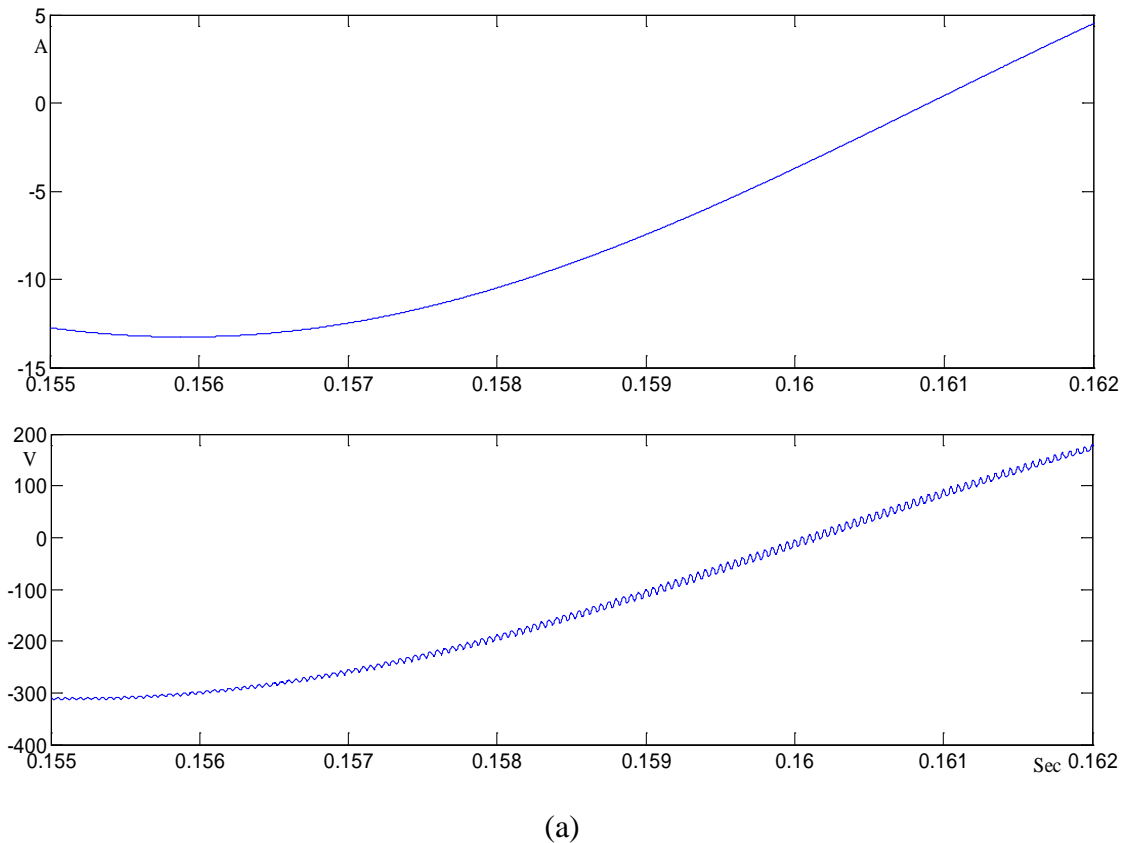
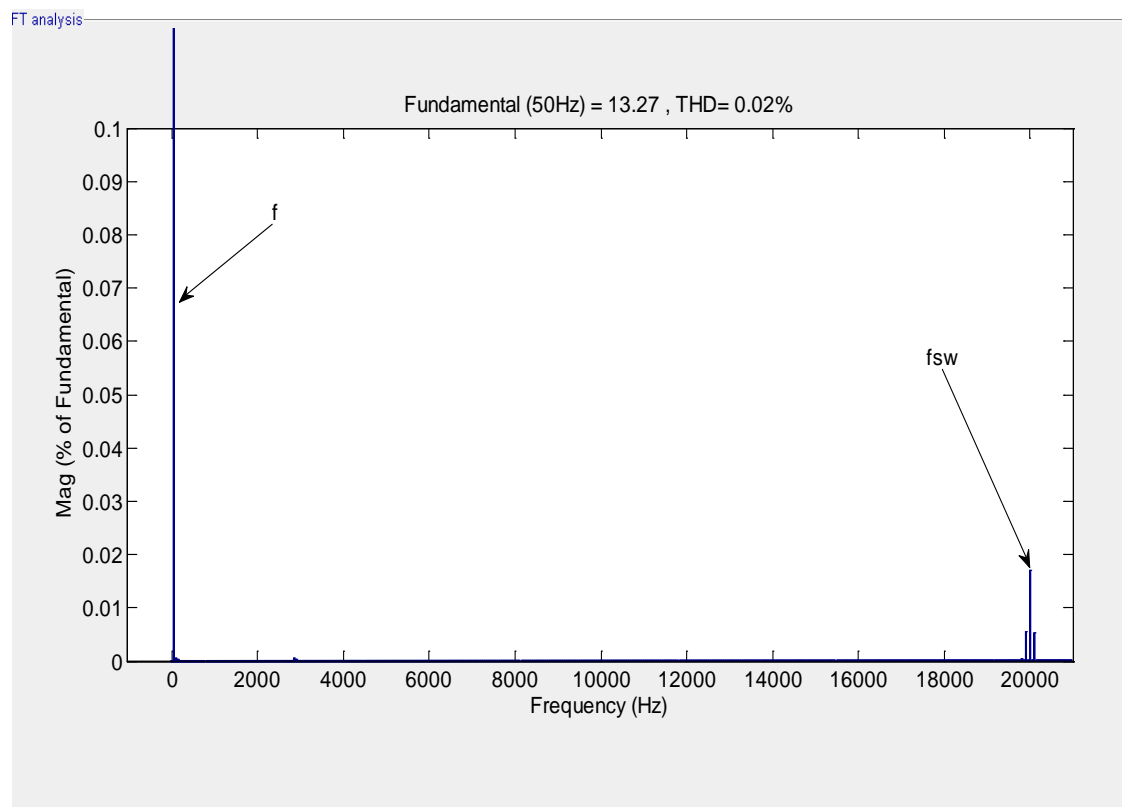


Figure 3.15: (a) SVPWM current and voltage waveforms at 2500W load, (b) SVPWM current waveform FFT harmonic analysis at 2500W load.



(a)



(b)

Figure 3.16: (a) SVPWM current and voltage waveforms at 2000W+500VAr load, (b) FFT harmonic analysis under 2000W+500VAr load.

3.12 Summary

Comparisons between SPWM and SVPWM have been made between different modulation techniques in terms of quality factors. The quality of the modulation strategy can be defined by the generated harmonic amplitudes and the related frequencies. In fact, the frequency harmonics and DC component have a significant effect in grid-tied inverter applications. This factor can be taken into consideration if the harmonic components are weighted by their frequency.

The proposed SVPWM algorithm has been verified through simulation using MATLAB/SIMULINK. The above results show SVPWM to be somewhat superior to SPWM in many aspects. The main conclusion is summarized below:

- 1) The modulation index is higher for SVPWM as compared to SPWM.
- 2) The output voltage is about 1% more in case of SVPWM as compared to SPWM [follows on from (1)].
- 3) The current and voltage harmonics are less in the case of SVPWM which produces a THD lower than that of SPWM by about 10%.

The important difference between SVPWM and other PWM is that the SVPWM scheme uses adjacent vectors and controls the sequence in which the vectors are applied within the switching cycle. Besides the previous conclusions, the SVPWM has other advantages over SPWM in terms of the flexibility of algorithms. With the SVPWM algorithm, the degrees of freedom the designers have are:

- 1) Freedom to choose the vector sequence.

- 2) Freedom to arrange sequencing of the vectors.
- 3) Splitting of the duty cycles of the vectors without introducing additional commutations.

The SVPWM algorithm is intended for use in the grid-tied inverter applications. This algorithm calculates the instantaneous reference voltage vector magnitude in the synchronous rotating frame (d - q) coordinates in 3-phase inverters. The SVPWM is also a suitable technique for generating inverter switching gate signals in a single-phase inverter. However, despite all the above mentioned advantages that SVPWM enjoys over SPWM, the performance of inverter system also depends on the type of current-control technique used. In the current controller, load currents are measured and compared with reference currents, the errors are used as an input to the PWM modulator, which eventually provides inverter switching signals.

Chapter 4

THEORETICAL ASPECTS OF STATIONARY FRAME AND SYNCHRONOUS ROTATING FRAME

4.1 Introduction

This chapter begins with a description of the stationary reference frame, the synchronous rotating reference frame, and the transformations between these frames in a three-phase system. The Clarke transform [90, 91] is used to transform parameters within circuits to a two-dimensional stationary reference frame. The Clarke transformation is often used to translate balanced three-phase quantities into an orthogonal two-dimensional reference space, and is thus sometimes known as a 3-2 transform in that it transforms, for example three measured currents into two internal variables. The Park transform [90] is commonly used in three-phase electric machine models. It allows the elimination of time-variance of the parameter in the two-dimensional static reference frame by introducing a rotating reference frame, and referring the parameter to this. The Park transform is a 2-2 transform that also has a reference angle input. If the reference angle is rotating at the same speed as a frequency component of the two-dimensional input to the Park transform, the output of the latter corresponding to this frequency component will be time invariant.

This chapter evaluate the principles of the application of these transforms within a three-phase system, with a view to how they may be modified to apply to a single-phase system. Currently the transformation theories applications require a minimum of two independent phases in the system. As a result, the single-phase system suffers from a difficulty in application of the transformation from stationary to rotating reference frame (the Park transform).

The end of this chapter provides an overview of the relevant published work for single-phase inverters. It discusses the single-phase inverters that currently employ the synchronous rotating frame controller, drawing on studies and previous research. This is aimed at understanding the limitations of such existing systems and identifying the direction the proposed development should take.

4.2 Synchronous and Reference Frames in Literature

In the 1920's, R. H. Park [90] revolutionized electric machine analysis. He formulated a change of variables; by replacing the variables (currents, voltages, and flux) associated with the stator windings of a synchronous machine with similar variables associated with the rotor. In other words, he used projection and two-axis equations in order to transform the stator variables to a frame of reference fixed in the rotor. Park's transformation has the unique property of eliminating all fundamental frequency components of time-varying parameters from the voltage equations of the synchronous machine that occur due to:

- Electric circuits in relative motion.
- Electric circuits with varying magnetic reluctance.

Rotating induction electrical machines have the same basic principles in operation, but they differ from synchronous machines in the winding arrangement and the excitation method. Park's idea was developed by G. Kron [91] to deal with other types of rotating electrical machines. Consequently, each development in transformation was derived to analyse a type of rotating machine. There are several different forms of transformation depending on the reference frame chosen, such as stationary reference frame, synchronous

reference frame, rotor reference frame, and arbitrary reference frame. However, in each of them, time variance of a synchronous machine is eliminated at the fundamental frequency by using the Park transform in which the reference frame is fixed in the rotor (or in the stator if this desired).

The transformation of the three-phase system from the stationary frame to the synchronous rotating frame can be easily done by the following procedure:

1. Resolving the three-phases into two axes through the Clarke transformation as in (4.1). In other words, the three-phase stationary reference frame components are projected onto two orthogonal axes ($X\alpha$ and $X\beta$) appropriately fixed in the same stationary reference frame, Figure 4.1.

$$\begin{bmatrix} X\alpha \\ X\beta \end{bmatrix} = \begin{bmatrix} 1 & -1/2 & -1/2 \\ 0 & \sqrt{3}/2 & -\sqrt{3}/2 \end{bmatrix} \begin{bmatrix} U \\ V \\ W \end{bmatrix} \quad (4.1)$$

where U , V , and W represent three-phase stationary-frame components, and $X\alpha$ and $X\beta$ represent the components projected onto the two stationary orthogonal axes.

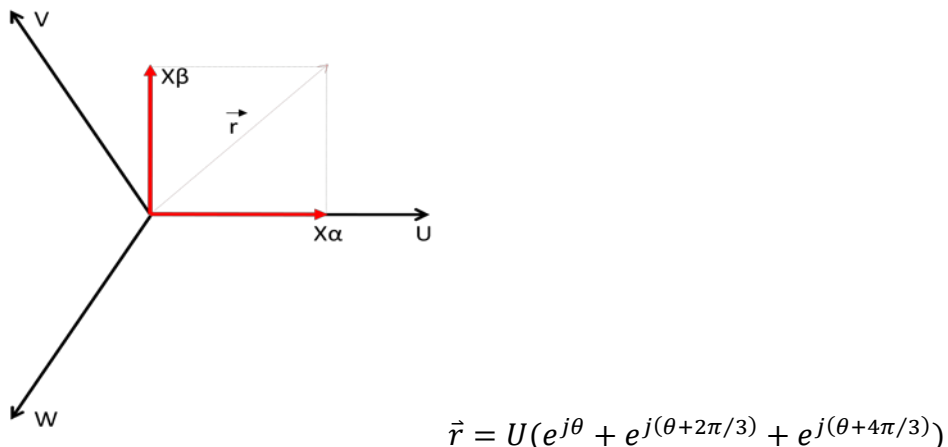


Figure 4.1: Clarke transformation vector.

2. Transforming the two phase quantities ($X\alpha$ and $X\beta$) from the stationary reference frame to the synchronous rotating frame (with the corresponding d and q axes) that rotates with the rotor at an angular velocity (ω) in the synchronous machine. This ensures that the synchronous rotating frame represents the stationary frame relative to the angular velocity of the system. In the case when these transformations apply to synchronous electrical machines, the key AC variables (voltage, current, and flux) become time-invariant at the fundamental frequency in the synchronously rotating reference frame. Equation (4.2) is known as the Park transformation, which performs the transformation from the stationary to the rotating reference frame axes (Xd and Xq), Figure 4.2.

$$\begin{bmatrix} Xd \\ Xq \end{bmatrix} = \begin{bmatrix} \cos \omega t & \sin \omega t \\ -\sin \omega t & \cos \omega t \end{bmatrix} \begin{bmatrix} X\alpha \\ X\beta \end{bmatrix} \quad (4.2)$$

Note that the Park transformation matrix is an orthogonal non-singular matrix ($T \cdot T^{-1} = 1$). It represents the relationship between the stationary and rotating frame components.

These transformations lead to the new frame components becoming time invariant in the rotating reference frame rotating with angular velocity ω , Figure 4.2.

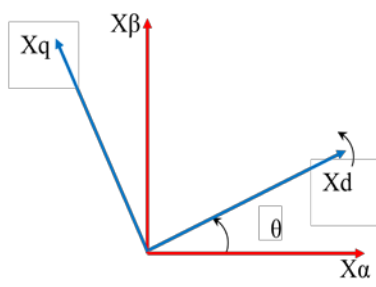


Figure 4.2: Park transformation.

The transformations and reference frame theory topic has recently received renewed interest in control strategies as a result of the following factors [92- 94]:

- The time-invariant quantities (at the fundamental frequency) have advantages over time-variant quantities in the feedback control when compensated by using PI controllers. In other words, PI regulators are conventionally regarded as unsatisfactory for AC systems because of the evidently unavoidable steady-state amplitude and phase errors that they create.
- Use of solid-state inverters for AC machine drives applications, in which transformation theory is already used for their control.
- Digital controllers have become powerful, practical, and their cost has dropped rapidly. They are also popular in industry.
- The design of voltage-source inverter switching strategies is most effectively done by using space vector pulse width modulation (SVPWM) [88].

4.3 Synchronous Frame Transformation in three-phase system:

The rotating vector in the stationary reference frame becomes a constant vector in the rotating reference frame due to the rotation of the reference plane itself. Figure 4.3 shows stationary and rotating reference frame vector representations.

$$\text{The instantaneous angle } \theta \text{ is defined as } \theta = \int \omega(\tau) d\tau + \theta_{int} \quad (4.3)$$

where ω is the angular frequency in rad/sec, θ_{int} is the initial angle of the system, and τ is the time. In Figure 4.3, \vec{X} is an arbitrary phase state variable projected into the stationary

reference frame. It can be decomposed into two component vectors $\vec{X}\alpha$ and $\vec{X}\beta$, as explained by the vector relationship (Figure 4.3):

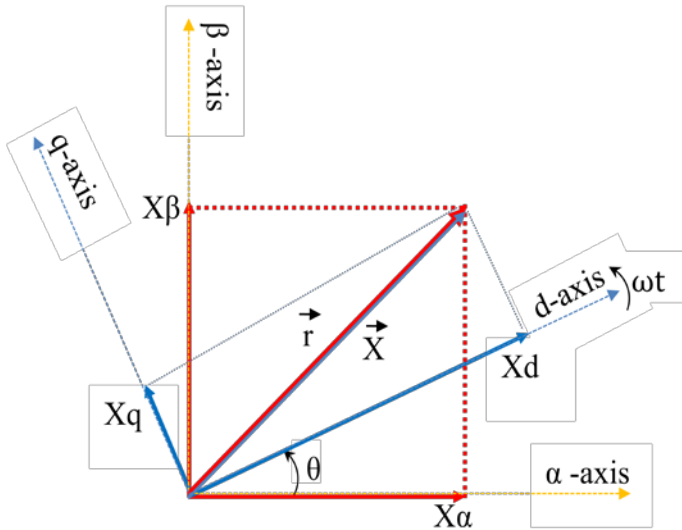


Figure 4.3: The stationary and rotating vector relationship representations.

The rotating frame coordinate $(\vec{X}d, \vec{X}q)$ rotates in the same angular frequency and direction of \vec{X} . This leads to the magnitude of the rotating reference frame components being dependent on the magnitude of \vec{X} only, and not being affected by its instantaneous position in the stationary reference frame.

For more insight, let us consider $X\alpha$ and $X\beta$ representing the stationary reference frame components (of a voltage or current), and apply the Park transformation as in (4.4).

$$\begin{bmatrix} Xd \\ Xq \end{bmatrix} = \begin{bmatrix} \cos \omega t & \sin \omega t \\ -\sin \omega t & \cos \omega t \end{bmatrix} \begin{bmatrix} X\alpha \\ X\beta \end{bmatrix} \quad (4.4)$$

$$\text{where } \begin{cases} X\alpha = X \cos(\omega t + \phi) \\ X\beta = X \sin(\omega t + \phi) \end{cases} \quad (4.5)$$

and where ϕ represents the initial angle, e.g. in an AC electrical circuit the currents (the signal which is need to transformed) can be lag their corresponding voltage by ϕ , while the transformation matrix is synchronous with the voltage waveform.

$$\begin{bmatrix} Xd \\ Xq \end{bmatrix} = \begin{bmatrix} \cos \omega t & \sin \omega t \\ -\sin \omega t & \cos \omega t \end{bmatrix} \begin{bmatrix} X \cos(\omega t + \phi) \\ X \sin(\omega t + \phi) \end{bmatrix}$$

$$Xd = \frac{X}{2} \{ [\cos(\omega t - \omega t - \phi) + \cos(\omega t + \omega t + \phi)] + [\cos(\omega t - \omega t - \phi) - \cos(\omega t + \omega t + \phi)] \}$$

$$Xq = \frac{X}{2} \{ -[\sin(\omega t - \omega t - \phi) + \sin(\omega t + \omega t + \phi)] + [\sin(\omega t - \omega t - \phi) - \sin(\omega t + \omega t + \phi)] \}$$

$$\left. \begin{aligned} Xd &= \frac{X}{2} \{ [\cos(-\phi) + \cos(2\omega t + \phi)] + [\cos(-\phi) - \cos(2\omega t + \phi)] \} \\ Xq &= \frac{X}{2} \{ [\sin(-\phi) - \sin(2\omega t + \phi)] + [\sin(-\phi) + \sin(2\omega t + \phi)] \} \end{aligned} \right\}$$

$$\left. \begin{aligned} Xd &= \frac{X}{2} [2\cos(-\phi)] \\ Xq &= \frac{X}{2} [2\sin(-\phi)] \end{aligned} \right\}$$

$$\left. \begin{aligned} Xd &= X \cos \phi \\ Xq &= X \sin \phi \end{aligned} \right\} \quad (4.6)$$

It is clear from (4.6) that when the AC quantity represented by $(X\alpha, X\beta)$ is at sinusoidal steady-state, the rotating reference frame components Xd and Xq are constants (i.e. DC quantities). The rotating reference frame vector magnitude is dependent on the value of ϕ . When ϕ is equal to zero, Xd has a maximum value equal to X , and Xq is equal to zero.

4.4 Stationary reference frame Controller in Three-Phase Systems

The motor drive applications and their controller have been studied in detail [30, 95]. Subsequently, PWM has been utilized in AC motor drive applications where it is necessary to regulate motor speed.

With the use of a current controller, the three-phase voltage-source inverter controller employs three channels to provide independent three-phase PWM sources (three individual single-phase sources). With the Clarke transformation in the three-phase system, the number of stationary variables is reduced from three individual phase components to two orthogonal stationary-reference-frame components. The latter two components are the primary key in enabling the use of SVPWM. From the Clarke transformation matrix (4.1), it can be noted that the phase angle information is not necessary in this transformation. In a controller operating in the stationary reference frame, the control variables (voltages and currents) are time-variant. Therefore, it is difficult to remove the steady-state error by using a PI controller alone [92, 94]. Some approaches [63, 92, 94, 96] employ a proportional resonant controller (P-R), which has attracted considerable attention during the last decade. The proportional resonant controller transfer function is defined as: [92, 97]

$$G_{P-R}^{\alpha\beta}(s) = \begin{bmatrix} Kp + Ki \frac{s}{s^2 + \omega^2} & 0 \\ 0 & Kp + Ki \frac{s}{s^2 + \omega^2} \end{bmatrix} \quad (4.7)$$

where ω is the resonant frequency of controller, K_p is the proportional gain, and K_i is the integral gain of the controller. The proportional resonant controller is well suited to regulating sinusoidal signals since it has the ability to eliminate the steady-state error

and offers the possibility to compensate low-order harmonics by means of a harmonic-compensator function [97]:

$$G_{HC}(s) = \sum_{h=3,5,7} K_i \frac{s}{s^2 + (\omega \cdot h)^2}$$

where h denotes the harmonic order. The general circuit structure of a controller using proportional resonant control with a harmonic compensator is shown in Figure 4.4.

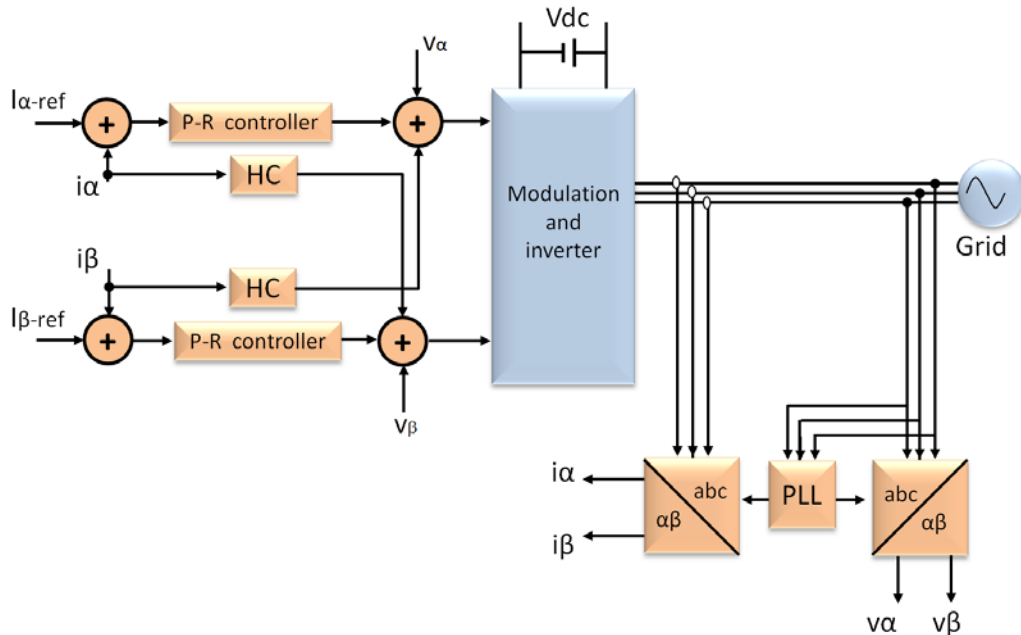


Figure 4.4: General structure of three-phase proportional resonant control strategy.

4.5 Rotating Reference Frame Control Structure in Three-Phase Systems

Another method of structuring the control loop is by using a rotating reference frame. The rotating reference frame method, also called d - q control, is widely used in three-phase systems. Rotating reference frame regulators have become industry standard in the field of high-performance current-control methods [98-100]. This ‘vector control’ can be understood by using space vector theory [101], which can be implemented by using two orthogonal axes. In this case, three-phase quantities (such as voltages, currents, etc.) are

expressed in terms of space vectors. Such a model is valid for any instantaneous variation of voltage and current and adequately describes the system performance under both steady-state and transient operation [97, 102]. In addition, it can offer ease of linking to the SVPWM technique of generating inverter switching states. Vector control is performed entirely in the rotating d - q coordinate system to make the controller side elegant for a wide range of applications, owing to its:

- Suitability for motor drive applications,
- Compatibility with the inverter gate-drive SVPWM technique,
- Flexibility to control grid-tied solid-state distributed generators.

Figure 4.5 shows the general structure of the three-phase rotating reference frame

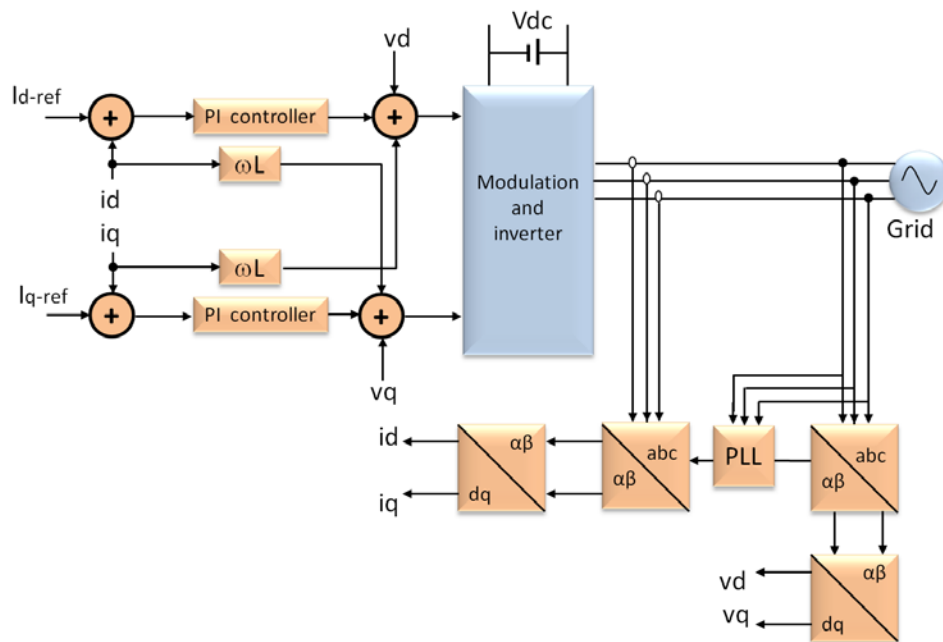


Figure 4.5: General structure of three-phase synchronous rotating reference frame control strategy.

control strategy. In this method (synchronous rotating frame), the measured three-phase stationary current components are transformed to the two components ($\alpha\beta$) by the Clarke transformation, which outputs a two-coordinate time-variant system (stationary system)

through the mathematical representation shown in equation (4.1). In most cases, the three-phase system is symmetrical, which means that the sum of the phase quantities is always zero. Thus, by transforming $\alpha\text{-}\beta$ from the stationary frame to the synchronous rotating frame ($d\text{-}q$) via Park transformation matrices, the $d\text{-}q$ coordinates are arranged to rotate synchronously with the power line frequency (hence the term ‘synchronous’ rotating reference frame).

Some applications require inverters to provide a different or variable voltage and frequency, such as motor speed control. In this case the inverter frequency may be simply defined by a voltage-controlled oscillator. The amplitude of the output wave is determined by the level of the DC supply voltage to the inverter block, but it can be varied by controlling the inverter switching circuit to provide a variable output voltage. In other cases, such as grid-tied inverters for renewable energy applications, inverters are designed to deliver regulated AC mains power from sources which may have a variable input voltage (DC-link). In such cases, they must deliver a fixed output voltage at a fixed frequency to the load since the application requires it and may depend on it. In this case, the output frequency is locked to that of the grid and is not variable by other means, e.g. by the user. In the grid-tied PV system application, the DC-link voltage is set at the DC-to-DC converter stage (PV system front-end stage). This is effected by a PI controller and an error amplifier that compares the actual DC bus voltage to the reference value generated by, for example, a Maximum Power Point Tracking (MPPT) controller. The PI controller’s output provides the active current component of the required current vector. The other component of the current vector represents the reactive current, and it can be fixed at a desired level for power factor or voltage control. If supply of reactive power to the grid is not required, the reactive current component is set to zero. In the case when reactive power

must be supplied (such as in power quality management), a non-zero reactive power reference can be used. The transformed d - q currents are compared with their reference values, and the result is fed to the compensators to generate the feedback voltage references in the synchronous reference frame. The active and reactive power (or voltage) consists of a combination of feed-forward signals and decoupling of the inductive cross-coupling. These cross-coupling terms can be caused by the interaction between the inverter, filter circuit and PWM modulation scheme. The decoupling eliminates this coupling in the feedback controller between the d and q channels and yields two independent current controller channels. The voltage references are added to the feedback reference signal to form the total d and q axis voltage references. In the sinusoidal pulse width modulation (SPWM) technique, it is then necessary to transform from the d - q rotating frame variables to the α - β stationary frame variables. By inverse transformation from rotating synchronous frame to the stationary frame, the modulator can then generate the switching device gate signals.

Given that the controlled current has to be in phase with the grid voltage, the required phase angle has to be extracted from the grid voltage. The synchronous reference frame regulator has many advantages for the three-phase grid-tied inverter:

- Time invariant control variables and fast response in case of load change [98].
- Controller design is similar to that used with a conventional DC-to-DC converter; zero state error at steady-state and easy filtering [94, 100].
- Decoupling of the control of active and reactive power. This leads to the ability to control amplitude and phase separately [100].
- Potentially a high controller gain at the fundamental frequency [100].

- The voltage feed-forward terms allow a wider PI controller gain choice and wider number range for the integrators [94, 99].
- Improvements to the dynamic response [103].
- Improvements to the anti-islanding detection zone [104-106].

The following matrix transfer functions represent the proportional-integral controller in the rotating synchronous reference frame [92].

$$G_{PI}^{dq}(s) = \begin{bmatrix} Kp + \frac{Ki}{s} & 0 \\ 0 & Kp + \frac{Ki}{s} \end{bmatrix} \quad (4.8)$$

The major difference between the stationary-reference-frame current controllers and the synchronous-rotating-reference-frame current controllers is that most stationary-frame current controllers suffer from an inability to eliminate steady-state error. The synchronous rotating frame solves this problem by shifting fundamental power frequency information back to DC, at which point a conventional DC regulator can be used such as the PI controller [94]. However, the synchronous-rotating-reference-frame controller is more complex and requires pathways for each of the orthogonal components in order to apply further transformations (Park transformation), [61, 99].

4.6 Overview of the relevant published work for single-phase inverters employing the synchronous rotating frame controller

The Clarke Transformation in single-phase inverter controller has been attempted and is discussed in [107-118]. The thought is based on the idea that an ordinary single-phase quantity can be complemented by a virtual fictitious phase so that both of them will

together create orthogonal system, as is usual in three-phase systems (Clarke Transformation).

Certain observations can be made from this, including some general observations relating to the transformation stage as well as the controller structure.

1. The methods used are based on creating a virtual two-phase system from the original single-phase system by adding a new fictitious phase. This virtual quantity is obtained either by derivation from the fundamental signal [107] or through a $\frac{1}{4}$ real axis time delay, regarding to its own period [108-112].
2. [107] reviews the problems associated with the Park transformation. The sine and cosine terms in the Park transform are generated from a lookup table or similar depending on voltage phase.
3. [61, 113-115] point to the fact that the synchronous reference frame controller is widely used in three-phase inverters. It theoretically can achieve zero steady-state tracking error by shifting the fundamental power frequency components back to DC. However, its limitation is the inability of direct use in single-phase inverters, requiring additional significant computational burden to make use of it at all.
4. As described in [114, 115], the single-phase system transformation theory is not directly applicable, and additional complexity is needed for $d-q$ transformations in the synchronous rotating reference frame.
5. [61, 113], that it is difficult to implement synchronous rotating reference frame PI control using a low-cost fixed-point digital signal processor (DSP).

6. The theoretical concepts of the single-phase synchronous rotating reference frame are presented and discussed in [61]. It is observed that “The only complication with this equivalent single-phase conversion is that the chosen frequency component not only appears as a DC quantity in the synchronous frame, it also contributes to harmonic terms at a frequency of 2ω (this is unlike three-phase synchronous d–q conversion where the chosen frequency component contributes only towards the DC term)”.
7. The emerging difference between the transformation matrix phase θ_1 and the current feedback phase θ_2 explains the harmonic appears of within the DC components. This causes the transformation to contribute harmonic terms at a frequency of 2ω to the controller stage.
8. The harmonics associated with the transformed current components increase with the inductive load. That is because the phase difference between the current and voltage increases, leading to an increase in the phase difference between the current feedback signal and the transformation matrix phase angle (which tracks the voltage waveform). As a result, the reactive loads contribute to an increase in the harmonic terms at a frequency of 2ω .
9. [116] In the presence of an unbalanced load on a three-phase inverter, the quantities in the rotating reference frame are no longer completely time-invariant and contain a double line frequency component [116].
10. The harmonics associated with transformation stage come from using external sine and cosine functions in the transformation matrix. These functions are usually saved in a lookup table with limited precision [116].
11. The feedback signals are transformed to the rotating frame and fed to the

controller stage in [61, 117, 118, 108, 109, 111]. Then, adding a transformation back to the stationary frame in order to apply PWM causes additional computational burden.

12. In order to reduce the computational burden, the amount of calculation is reduced to the minimum required to yield an optimal trade-off between complexity and performance. Some researchers [108, 117] try to reduce the controller complexity further, this by ignoring the decoupling term in the voltage loop (ωC). This step is not sufficient to reduce the controller complexity when compared with real-time evaluation with transformation function stages.

From the above reasons, use of the synchronous rotating reference frame lost its flavour in the single-phase inverter controller.

The main aim of vector control is to implement control schemes which produce high dynamic performance and are similar to those used to control DC-to-DC converters. It is worth saying that it is too early to incorporate the voltage and current phase difference in the transformation stage. The transformation stages should be used for conditioning the feedback signal from time-variant to time-invariant only. This thesis validates SVPWM in single-phase inverter. Use of this method reduces additional computational burden caused by transformation back to the stationary frame before applying conventional PWM.

In a single-phase system, the harmonic terms at a frequency of 2ω an result from transformation stage itself. The 2ω harmonic term can be result for the following reasons:

- The created component is not orthogonal with the original component.
- The created and original components values are unequal.

- The coupling terms which are result in transformation stage should be decoupled with opposite sign in controller stage.

Therefore, the progress in thesis is to model the power stage of a single-phase inverter based on synchronous rotating reference frame mathematically. Then, solve the 2ω harmonic issue and reduce computational requirements further.

4.7 Summary

The aim of vector control is to implement control schemes which produce high dynamic performance and are similar to those used for controlling DC-to-DC converters. Hence, this chapter started by demonstrating synchronous rotating frame theory.

This chapter provides an overview of the relevant published work for single-phase inverters employing the synchronous rotating frame controller. It discusses the single-phase inverter controller, drawing on studies and previous research. Then, identifies the direction the proposed developments will take.

Chapter 5

SINGLE-PHASE INVERTER POWER STAGE MODELLING BASED ON SYNCHRONOUS ROTATING FRAME

5.1 Introduction

Current application of the transformations requires a minimum of two independent phases in the system. As a result, the single-phase system suffers from a difficulty in applying the transformation from stationary to rotating frame.

This chapter discusses strategies to overcome these difficulties in single-phase systems. One approach is to create an orthogonal stationary component, in a manner equivalent to that of the Clarke transformation in three-phase systems. The system will then be in a position where the Park transformation can be applied in order to transition to a rotating reference frame.

The power stage of a single-phase voltage-source inverter based on the synchronous rotating reference frame is modelled mathematically. The principle of possible solutions is discussed in detail, including the construction of the imaginary orthogonal circuit, transformation from the single-phase real circuit in the stationary reference frame, and transformation of the single-phase stationary reference frame to the d - q rotating frame.

The aim is to build a single-phase inverter controller operating in the synchronous rotating frame which can produce high dynamic performance while being able to minimize error at the fundamental power frequency, and thus to improve the electrical power quality generated by a single-phase PV system.

5.2 Use of the Imaginary Orthogonal Phase in Single-Phase Systems

Due to the limitation of having only one available phase in single-phase converters, the $d-q$ synchronous frame transformation method is not readily adaptable to the single-phase inverter unless a second orthogonal phase is created for every state variable in the circuit.

In order to create the additional orthogonal phase information from the single-phase inverter signal, three approaches can be adopted in order to create the additional phase-shifted state variables. These are:

3. Differentiating the inverter output voltage and inductor current [107]. This is done by differentiating the measured real component to build another stationary orthogonal component. However, this method is very sensitive to noise. The inverter real-phase output waveform contains harmonics in addition to the fundamental component. Differentiation process thus does not yield a purely orthogonal component. The inverter feedback controller is significantly affected by error in the stationary orthogonal phases. At the same time, the differentiation calculations require significant microcontroller processing time.
4. Some work such as [117] proposes using an observer to construct the β -axis component. This approach can achieve a good result, but it is very complex in terms of software and processing requirements to design and implement. Hence, none of these approaches represents a solution that is simple or cheap to implement.

The approach adopted in this research is a technique to create an imaginary orthogonal phase by generating a phase shift of 90° with respect to the real phase [108-112]. Using (5.1), the original phase delay of $1/4$ of the line phase of system can create another component (β) orthogonal with the original signal (α) as shown in Figure 5.1. The imaginary orthogonal component is estimated from the real component, and it introduces the dynamics of a quarter cycle delay in the construction of it.

$$\left. \begin{array}{l} X_\alpha = X \sin \omega t \\ X_\beta = X \sin(\omega t - 90^\circ) \end{array} \right\} \quad (5.1)$$

The orthogonal stationary component (V_β) is created by an integer delay ($k - n$) of the real component. The sampling frequency $f_s = 4nf$, where f is the inverter fundamental frequency and n is an integer equal to the quarter fundamental frequency sampling.

$$n = \frac{1}{4} \left(\frac{T}{T_s} \right), V_\beta = V_{\alpha(k-n)}$$

where T is the fundamental period, T_s is the sampling period, k is the sample number (at time $t = k T_s$), $n = T/4T_s$ is the delay in generating a stationary orthogonal component).

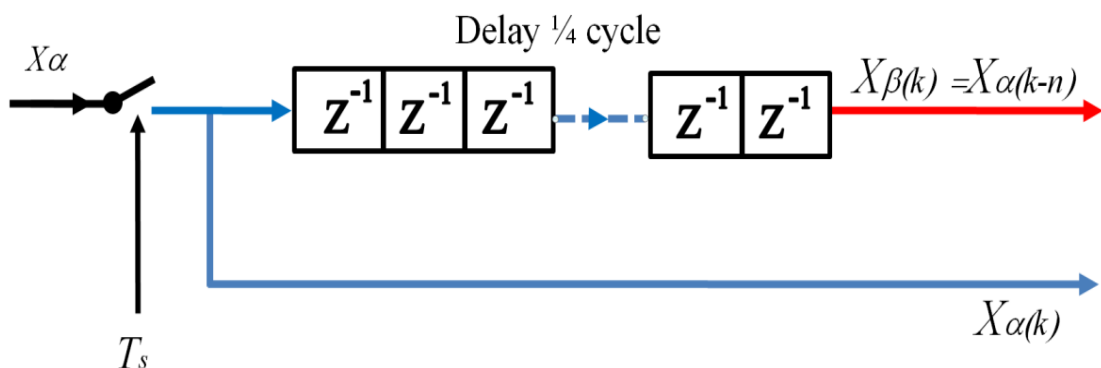


Figure 5.1: Real and imaginary phases.

This system can easily be implemented in a digital controller by a ring buffer storing data for a quarter cycle of the real stationary component. This method is examined using MATLAB/SIMULINK with input voltage $V_\alpha = 311 \sin(50 * 2\pi t)$. Figure 5.2 shows the two orthogonal stationary component waveforms created in the single-phase system.

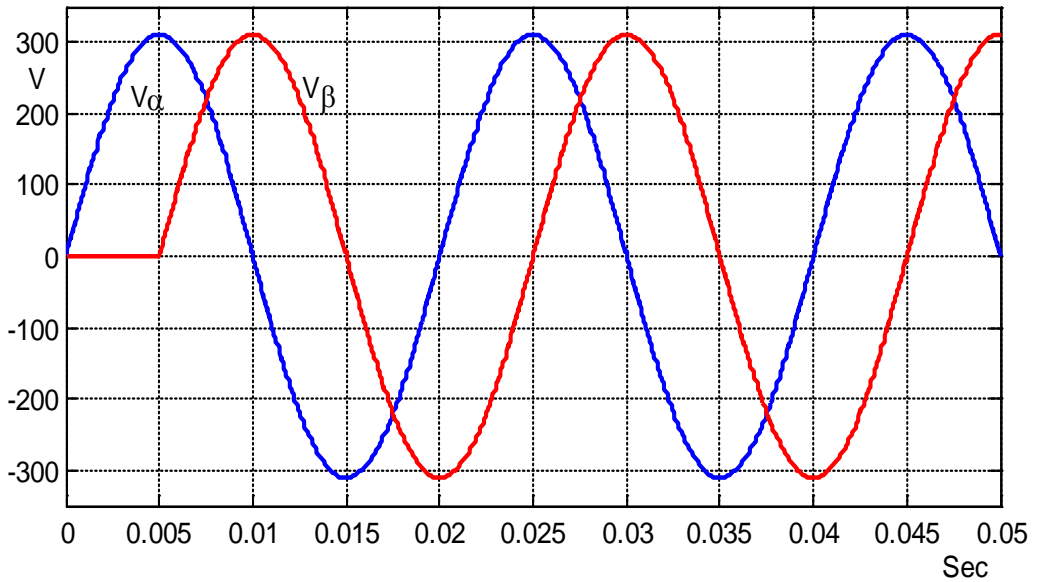
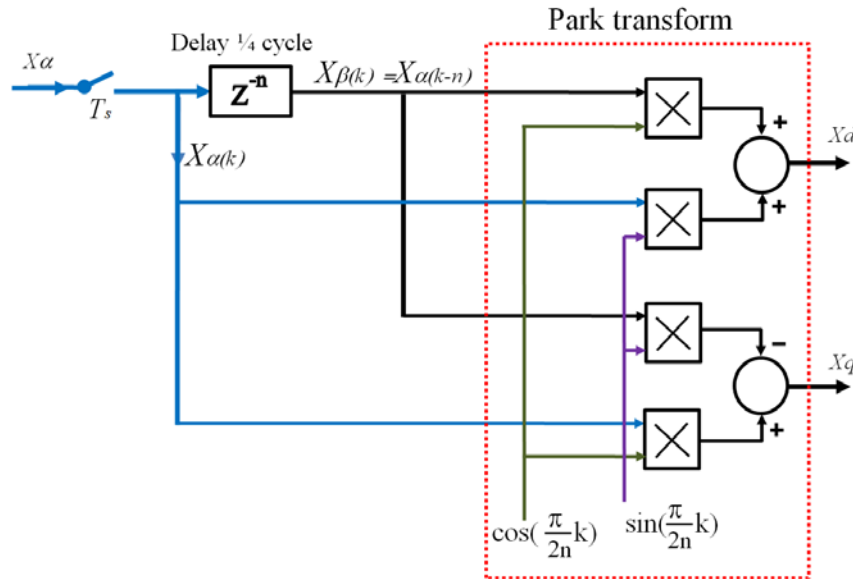


Figure 5.2: MATLAB/SIMULINK results for real and imaginary phase waveforms.

It is evident that V_β is valid after 0.005 sec which represents a quarter-cycle delay from V_α . The process is to generate two stationary frames in a single-phase system in a manner equivalent to the Clarke transformation in a three-phase system. The next step is the transformation from stationary reference frame to the synchronous rotating reference frame by the application of the Park transformation, expressed as:

$$\begin{bmatrix} V_{d_k} \\ V_{q_k} \end{bmatrix} = \begin{bmatrix} \cos\left(\frac{\pi k}{2n}\right) & \sin\left(\frac{\pi k}{2n}\right) \\ -\sin\left(\frac{\pi k}{2n}\right) & \cos\left(\frac{\pi k}{2n}\right) \end{bmatrix} \begin{bmatrix} V_{\alpha(k)} \\ V_{\alpha(k-n)} \end{bmatrix}, \quad \text{where } \begin{cases} t = kT_s \\ n = \text{integer} \end{cases} \quad (5.2)$$


 Figure 5.3: $\frac{1}{4}$ cycle delay with Park transformation scheme.

The Park transformation was implemented using MATLAB/SIMULINK and is connected with the $1/4$ cycle delay as shown in Figure 5.3. Figure 5.4 shows the synchronous rotating reference frame components for a single-phase system. It can be seen that both d and q axis components reach steady-state within a quarter cycle.

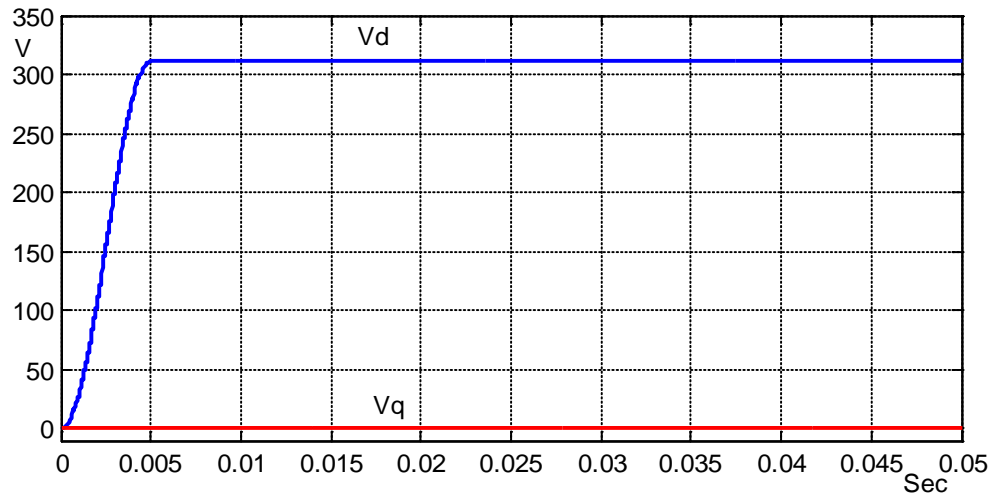


Figure 5.4: MATLAB/SIMULINK synchronous rotating frame components.

5.3 Modelling of the Single-Phase Inverter in Stationary and Rotating Reference Frames

A model for a single-phase inverter controller in the stationary and rotating reference frames was developed.

5.3.1 Single-Phase Inverter Model in Stationary Reference Frame

Figure 5.5 represents a real single-phase inverter scheme. The mathematical description is as follows [108-112],

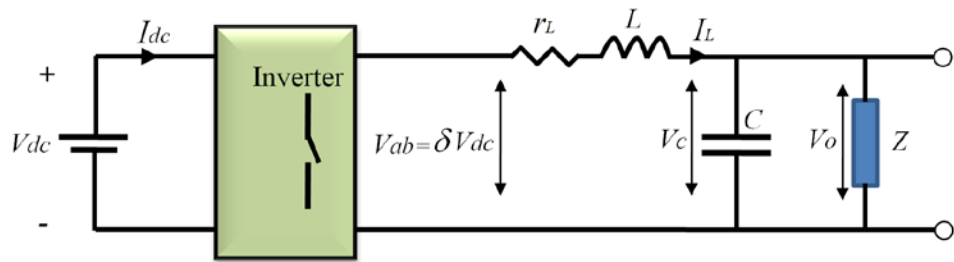


Figure 5.5: Single-phase inverter circuit scheme.

$$L \frac{dI_L}{dt} + r_L I_L = V_{ab} - V_o \quad (5.3)$$

where

$$\delta = \begin{cases} 1 & v_{ab} = v_{dc} \\ 0 & v_{ab} = 0 \\ 1 & v_{ab} = -v_{dc} \end{cases}$$

$$I_L = C \frac{dv_c}{dt} + \frac{V_o}{Z} \quad (5.4)$$

where δ is the duty cycle, Z is the load impedance. A single-phase inverter average circuit model was developed by splitting the inverter model into two ‘virtual’ circuits as shown in

Figure 5.6. The imaginary circuit has a set of ‘virtual’ components with the exact same values as those in the real circuit. The DC-link current (I_{dc}) is equal to I_α as the imaginary circuit does not physically exist; it is derived from the real circuit for the purposes of modelling.

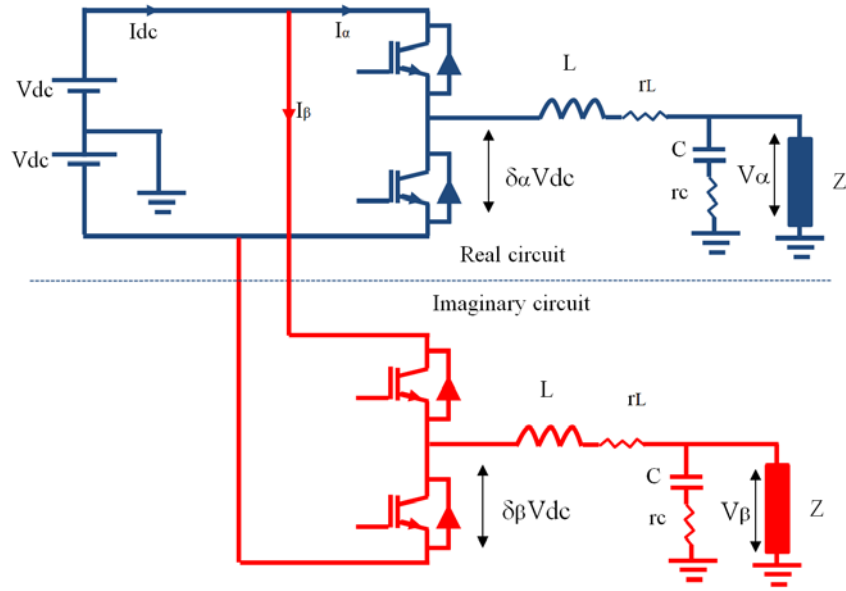


Figure 5.6: Single-phase inverter representation as real and imaginary parts of the circuit.

Rewriting the above equations using the real and imaginary circuits in Figure 5.6, the capacitor voltage and inductor current can be written as below:

$$\left. \begin{aligned} L \frac{d}{dt} I_\alpha + r_L I_\alpha &= V_{dc} \delta_\alpha - V_\alpha \\ L \frac{d}{dt} I_\beta + r_L I_\beta &= V_{dc} \delta_\beta - V_\beta \end{aligned} \right\} \quad (5.5)$$

$$\left. \begin{aligned} I_\alpha &= C \frac{dv_{ac}}{dt} + \frac{V_\alpha}{Z} \\ I_\beta &= C \frac{dv_{\beta c}}{dt} + \frac{V_\beta}{Z} \end{aligned} \right\} \quad (5.6)$$

where V_α is the real output voltage, V_β is the imaginary output voltage, I_α is the real inductor current, I_β is the imaginary inductor current.

The duty cycle (δ) can be averaged over one switching period providing that the highest frequency component in any change in δ does not violate the Nyquist criterion with respect to the switching frequency. Hence the dynamics of the system are constant over one switching period. The average filter voltage is obtained in (5.7).

$$\delta V_{dc} = \frac{1}{T_{sw}} v_{dc} \int_{t-T}^t \delta(\tau) d\tau = u \quad (5.7)$$

where u is the inverter average sinusoidal duty ratio. Applying average state variables to the switching model of the single-phase inverter based on the real and imaginary circuits (Figure 5.6), equations (5.5) and (5.6) are averaged using (5.7).

$$\left. \begin{aligned} L \frac{dI_\alpha}{dt} + r_L I_\alpha &= u_\alpha - V_\alpha \\ L \frac{dI_\beta}{dt} + r_L I_\beta &= u_\beta - V_\beta \end{aligned} \right\} \quad (5.8)$$

$$\left. \begin{aligned} I_\alpha &= C \frac{dv_{\alpha c}}{dt} + \frac{V_\alpha}{Z} \\ I_\beta &= C \frac{dv_{\beta c}}{dt} + \frac{V_\alpha}{Z} \end{aligned} \right\} \quad (5.9)$$

where $V_{\alpha c}$ is the real capacitor voltage, $V_{\beta c}$ is the imaginary capacitor voltage

$$\left. \begin{aligned} V_\alpha &= v_{\alpha c} + C \frac{dv_{\alpha c}}{dt} r_c \\ V_\beta &= v_{\beta c} + C \frac{dv_{\beta c}}{dt} r_c \end{aligned} \right\} \quad (5.10)$$

Using (5.10) in (5.8) and (5.9)

$$\left. \begin{aligned} L \frac{dI_\alpha}{dt} + r_L I_\alpha &= u_\alpha - [v_{\alpha c} + C \frac{dv_{\alpha c}}{dt} r_c] \\ L \frac{dI_\beta}{dt} + r_L I_\beta &= u_\beta - [v_{\beta c} + C \frac{dv_{\beta c}}{dt} r_c] \end{aligned} \right\} \quad (5.11)$$

$$\left. \begin{aligned} I_\alpha &= C \frac{dv_{\alpha c}}{dt} + \frac{1}{Z} [v_{\alpha c} + C \frac{dv_{\alpha c}}{dt} r_c] \\ I_\beta &= C \frac{dv_{\beta c}}{dt} + \frac{1}{Z} [v_{\beta c} + C \frac{dv_{\beta c}}{dt} r_c] \end{aligned} \right\} \quad (5.12)$$

The state-space average model of the single-phase half-bridge inverter in real and imaginary stationary reference frames is given in (5.13) and (5.14), and the circuit model is shown in Figure 5.7.

$$\frac{d}{dt} \begin{bmatrix} I_\alpha \\ I_\beta \end{bmatrix} = \begin{bmatrix} u_\alpha \\ u_\beta \end{bmatrix} \frac{1}{L} - \begin{bmatrix} I_\alpha \\ I_\beta \end{bmatrix} \frac{1}{L} \left(r_L + \frac{Zr_c}{Z+r_c} \right) - \begin{bmatrix} V_\alpha \\ V_\beta \end{bmatrix} \left(\frac{1}{L} - \frac{r_c}{L(Z+r_c)} \right) \quad (5.13)$$

$$\frac{d}{dt} \begin{bmatrix} v_{\alpha c} \\ v_{\beta c} \end{bmatrix} = \begin{bmatrix} I_\alpha \\ I_\beta \end{bmatrix} \frac{Z}{c(Z+r_c)} - \begin{bmatrix} V_\alpha \\ V_\beta \end{bmatrix} \frac{1}{c(Z+r_c)} \quad (5.14)$$

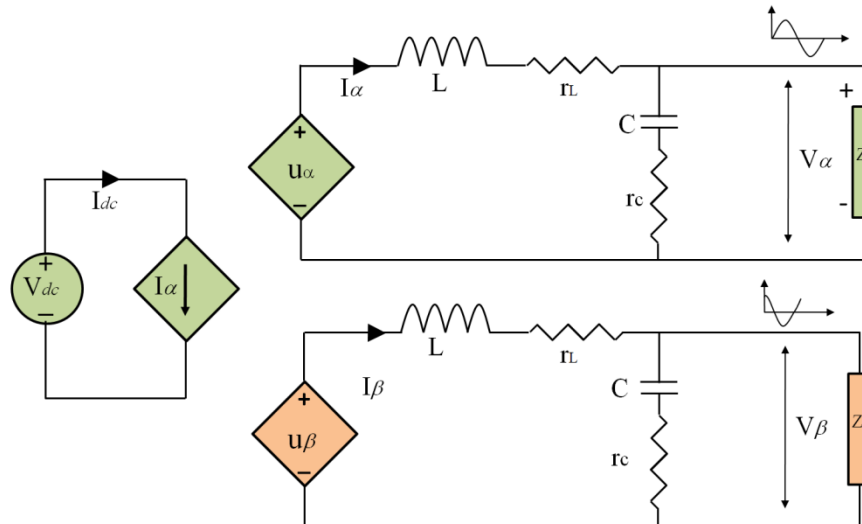


Figure 5.7: Stationary reference frames model of single-phase inverter.

In Figure 5.7, colour-filled component symbols have the following meanings:
 Round symbol with internal +/- signs represents “constant voltage-source”, diamond-shaped symbol with internal +/- signs represents “dependent voltage-source” with the dependency expression shown inside the symbol, diamond-shaped symbol with internal

arrow represents “dependent current source” with the dependency expression shown inside the symbol.

5.3.2 Single-Phase Inverter Model in Rotating Reference Frame

Once the average real and the average imaginary models are obtained (as given in the following equations (5.13) and (5.14)), the d - q model of the inverter can be developed by applying the transformation matrix equation (5.15 and 5.16) to equations (5.13) and (5.14).

$$\begin{bmatrix} X_d \\ X_q \end{bmatrix} = T \begin{bmatrix} X_\alpha \\ X_\beta \end{bmatrix} \quad (5.15)$$

$$\begin{bmatrix} X_\alpha \\ X_\beta \end{bmatrix} = T^{-1} \begin{bmatrix} X_d \\ X_q \end{bmatrix} \quad (5.16)$$

where (T) is transformation matrix

$$T = \begin{bmatrix} \cos \omega t & \sin \omega t \\ -\sin \omega t & \cos \omega t \end{bmatrix} \quad T^{-1} = \begin{bmatrix} \cos \omega t & -\sin \omega t \\ \sin \omega t & \cos \omega t \end{bmatrix} \quad (5.17)$$

This results in (5.18) and (5.19):

$$\begin{aligned} \frac{d}{dt} (T^{-1} \begin{bmatrix} I_d \\ I_q \end{bmatrix}) &= T^{-1} \begin{bmatrix} u_d \\ u_q \end{bmatrix} \frac{1}{L} - T^{-1} \begin{bmatrix} I_d \\ I_q \end{bmatrix} \left(\frac{r_L}{L} + \frac{r_c}{1 + r_c/Z} \right) \\ &\quad - T^{-1} \begin{bmatrix} V_d \\ V_q \end{bmatrix} \left(\frac{1}{L} - \frac{r_c}{L(1 + r_c/Z)} \right) \end{aligned} \quad (5.18)$$

$$\frac{d}{dt} (T^{-1} \begin{bmatrix} v_{dc} \\ v_{qc} \end{bmatrix}) = T^{-1} \begin{bmatrix} I_d \\ I_q \end{bmatrix} \left(\frac{1}{C(1 + r_c/Z)} \right) - T^{-1} \begin{bmatrix} V_{dc} \\ V_{qc} \end{bmatrix} \left(\frac{1}{ZC(1 + r_c/Z)} \right) \quad (5.19)$$

By applying the chain rule to the $\frac{d}{dt}(T^{-1} \begin{bmatrix} X_d \\ X_q \end{bmatrix})$ in equations (5.18) and (5.19), and separating d and q components, the state space model is obtained as given in (5.20) and (5.21), as follows:

$$\frac{d}{dt} T^{-1} = \begin{bmatrix} -\omega \sin \omega t & -\omega \cos \omega t \\ \omega \cos \omega t & -\omega \sin \omega t \end{bmatrix}$$

$$T \frac{d}{dt} T^{-1} = \omega \begin{bmatrix} -\cos \omega t \sin \omega t + \sin \omega t \cos \omega t & -(cos \omega t)^2 - (sin \omega t)^2 \\ (\sin \omega t)^2 + (\cos \omega t)^2 & -\cos \omega t \sin \omega t + \sin \omega t \cos \omega t \end{bmatrix}$$

$$T \frac{d}{dt} T^{-1} = \omega \begin{bmatrix} 0 & -1 \\ 1 & 0 \end{bmatrix} = \begin{bmatrix} 0 & -\omega \\ \omega & 0 \end{bmatrix}$$

$$\frac{d}{dt} \begin{bmatrix} I_d \\ I_q \end{bmatrix} = \begin{bmatrix} u_d \\ u_q \end{bmatrix} \frac{1}{L} + \begin{bmatrix} 0 & -\omega \\ \omega & 0 \end{bmatrix} \begin{bmatrix} I_d \\ I_q \end{bmatrix} - \begin{bmatrix} I_d \\ I_q \end{bmatrix} \left(\frac{r_L}{L} + \frac{r_c}{L(1+r_c/Z)} \right) - \begin{bmatrix} V_d \\ V_q \end{bmatrix} \left(\frac{1}{L} - \frac{r_c}{LZ(1+r_c/Z)} \right) \quad (5.20)$$

$$\frac{d}{dt} \begin{bmatrix} v_{dc} \\ v_{qc} \end{bmatrix} = \begin{bmatrix} I_d \\ I_q \end{bmatrix} \left(\frac{1}{C(1+r_c/Z)} \right) + \begin{bmatrix} 0 & -\omega \\ \omega & 0 \end{bmatrix} \begin{bmatrix} V_{dc} \\ V_{qc} \end{bmatrix} - \begin{bmatrix} V_{dc} \\ V_{qc} \end{bmatrix} \left(\frac{r_c}{CZ(1+r_c/Z)} \right) \quad (5.21)$$

The d-q equations of inverter are simplified in (5.22) and (5.23) by neglecting r_L and r_c as in practice they have very small values. It can be noted that the cross coupling terms occur between d and q components in the following equations.

$$\frac{d}{dt} \begin{bmatrix} I_d \\ I_q \end{bmatrix} = \frac{1}{L} \begin{bmatrix} u_d \\ u_q \end{bmatrix} + \begin{bmatrix} 0 & -\omega \\ \omega & 0 \end{bmatrix} \begin{bmatrix} I_d \\ I_q \end{bmatrix} - \frac{1}{L} \begin{bmatrix} V_d \\ V_q \end{bmatrix} \quad (5.22)$$

$$\frac{d}{dt} \begin{bmatrix} V_d \\ V_q \end{bmatrix} = \frac{1}{C} \begin{bmatrix} I_d \\ I_q \end{bmatrix} + \begin{bmatrix} 0 & -\omega \\ \omega & 0 \end{bmatrix} \begin{bmatrix} V_d \\ V_q \end{bmatrix} - \frac{1}{CZ} \begin{bmatrix} V_d \\ V_q \end{bmatrix} \quad (5.23)$$

Figure 5.8 illustrates equations 5.22 and 5.23 separately, while clearly showing the cross-coupling terms. Figure 5.8(a) describes equation 5.22 showing the inductor cross-coupling terms, whereas Figure 5.8(b) describes equation 5.23 showing the capacitor

cross-coupling terms. Figure 5.9 uses equations 5.22 and 5.23 to illustrate the direct channel (d-channel) inverter model structure.

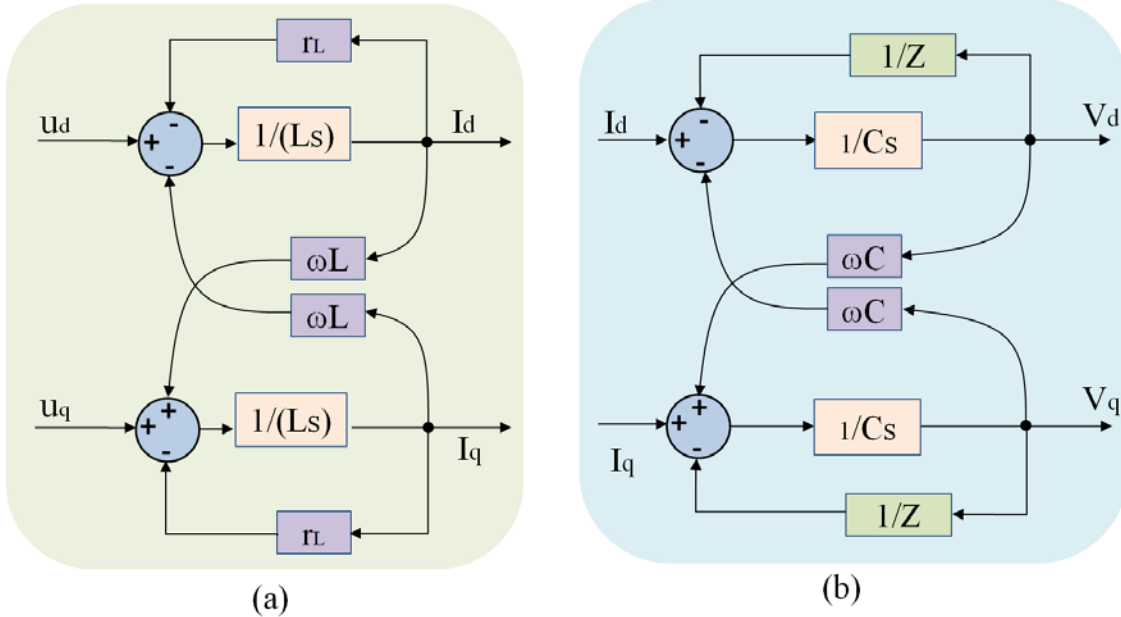


Figure 5.8: Inverter coupling terms associated with filter components.

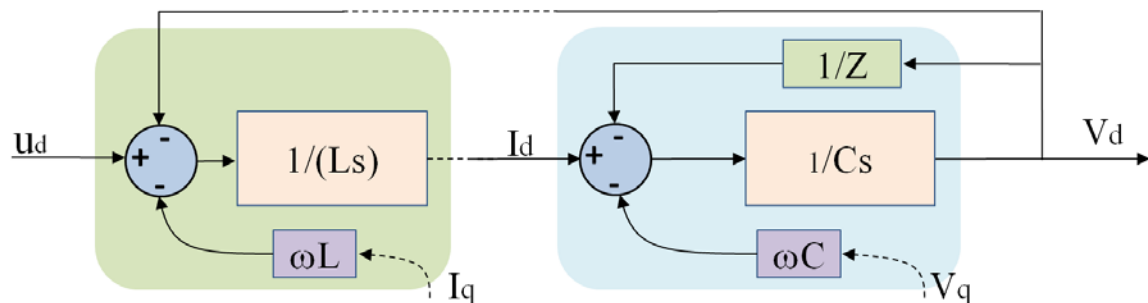
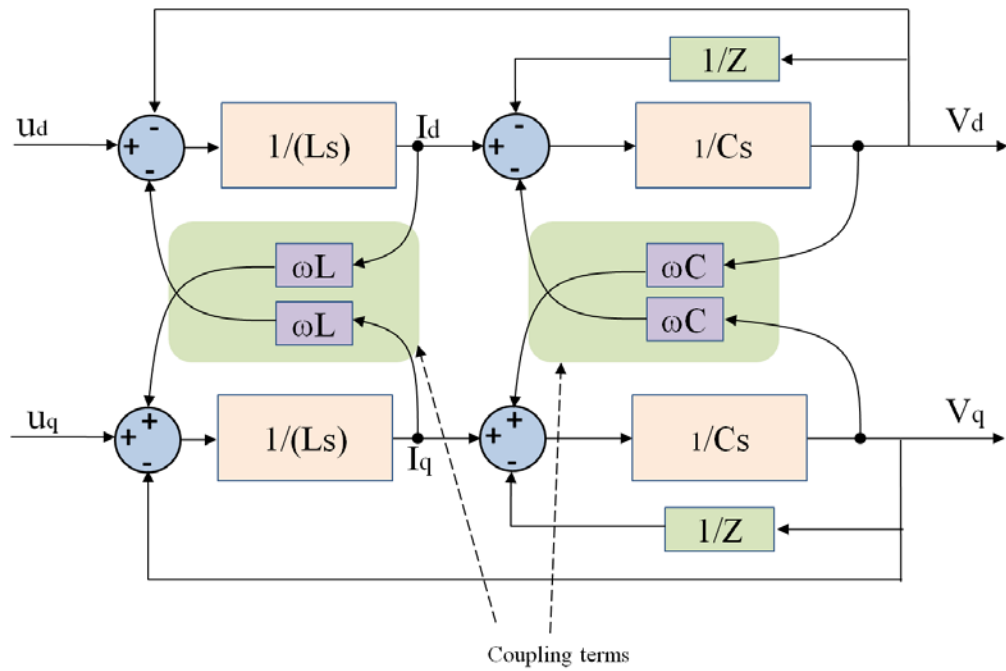


Figure 5.9: Inverter d-channel structure.

Figure 5.10 uses equations (5.22) and (5.23) to illustrate the overall d - q synchronous rotating reference frame inverter modelling structure up to the cross-coupling terms associated with these channels.

As noted previously, the inverter d - q parameters are DC (i.e. constant, time-invariant). Therefore the inverter steady-state operation is also time-invariant.


 Figure 5.10: Single-phase half-bridge inverter circuit d - q model.

5.4 Summary

This chapter shows the possible solutions to the problems of transformation to the synchronous rotating reference frame in a single-phase system. A model of the single-phase inverter in the synchronous rotating reference frame has been accomplished, including:

- Construction of an imaginary orthogonal circuit.
- Transformation from the single-phase real circuit into the stationary reference using real and imaginary orthogonal circuits.
- Transformation of the model in the single-phase stationary reference frame to the d - q rotating reference frame.

The transformation technique in the single-phase system is accomplished by the introduction of a quarter-cycle phase delay to the original phase. This action is adopted in

order to generate two orthogonal components in the stationary reference frame in a manner analogous to the Clarke transformation in a three-phase system. The transformation to the synchronous rotating reference frame is then completed by the application of the Park transformation.

Chapter 6 presents the proposed controller design based on d - q rotating frame, making use of this single-phase inverter modelling.

Chapter 6

TRANSFORMATION STRATEGY AND CONTROLLER DESIGN

6.1 Introduction

As has been described in Chapters 4 and 5, the objective of the proposed modelling strategy for the single-phase inverter is to facilitate the use of the synchronous rotating reference frame in single-phase inverters. This allows the transformation of signal components at the fundamental power frequencies to DC quantities, allowing simple PI controllers to be used in the feedback loops in order to achieve system stability.

This chapter describes the design of the controller including the selection of its parameters. It defines the dynamics of the system. An evaluation of the sensitivity of the proposed method to the variations of system parameters is included. As a consequence, this chapter evaluates some of the guidelines appropriate to the design of the controller. Finally, the controller was implemented and evaluated in MATLAB/SIMULINK in order to verify its performance.

This is followed by a discussion of control strategies for grid-connected power converters. This forms a first step in the considerations for connecting such a system to the grid. The DC-link capacitors are sized such to allow the input DC-link voltage to be considered to be constant over one cycle at fundamental line frequency at maximum load.

6.2 Single-Phase Inverter Controller

The approach to converter control design varies depending on the system requirements in order to achieve the required performance. Using the state space approach,

an overall system model is developed from which system stability and other dynamic characteristics can be determined.

In most cases, the order of the system model may be reduced by assuming that the DC-link voltage is constant within a single switching period. In this study, the inverter modelling dynamics are defined at medium to high frequencies. The DC-link voltage changes very slowly over the time, owing to the action of the DC-link capacitor.

The single-phase half-bridge inverter shown in Figure 6.1 includes an *LC* filter with r_L and r_c parasitics. All the passive components are on the AC side. The switching strategy is derived based on the power stage topology.

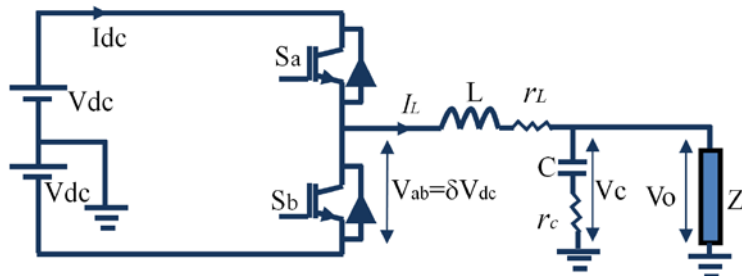


Figure 6.1: Single-phase half-bridge inverter with *LC* filter.

The single-phase inverter transfer function equation (neglecting parasitics) is derived in Appendix B and is given below.

$$G(s) = \frac{V_o}{\delta} = \frac{V_{dc}}{1 + (L/Z)s + (LC)s^2} \quad (6.1)$$

The plant transfer function in (6.1) represents a traditional second-order low-pass filter with the following definitions:

$$\omega_o = 1/\sqrt{LC} \quad (6.2)$$

$$Q = Z\sqrt{C/L} \quad (6.3)$$

$$\xi = 1/2\xi \quad (6.4)$$

$$\xi = \frac{1}{2Z} \sqrt{\frac{L}{C}} \quad (6.5)$$

The system parameters are defined in Table 3-2, Figure 6.2 shows the Bode plot of the open loop control to output transfer function under full-load and no-load condition without parasitics.

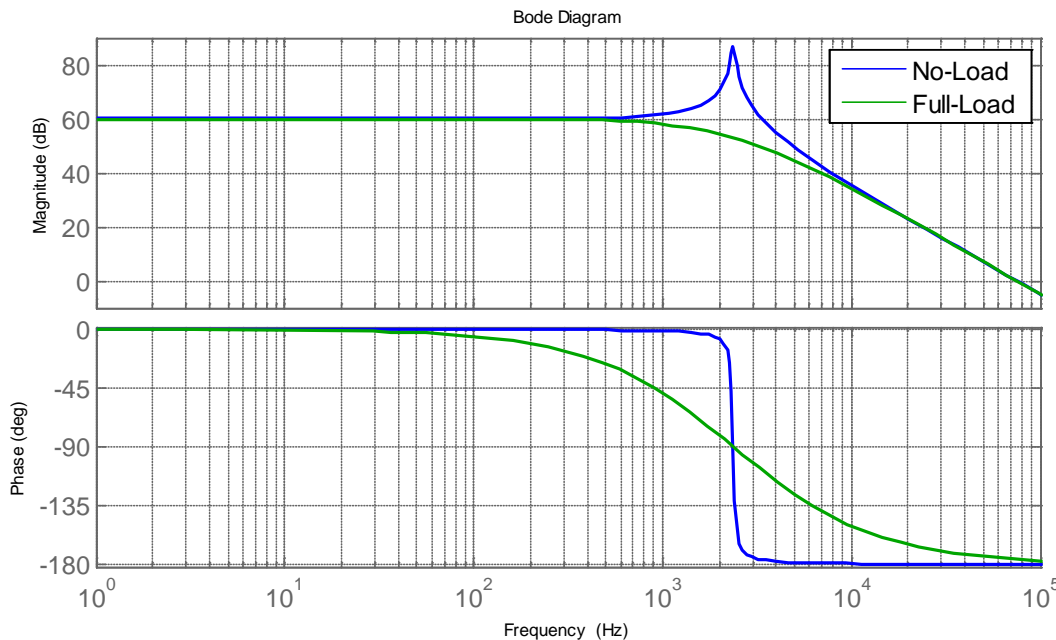


Figure 6.2: Open loop control to output transfer function under full-load and no-load condition without parasitics.

It can be noted that the no-load condition, $Z = \infty$, leads to $Q = \infty$, so the above converter transfer function is undamped. The specific interests in controller design are at no-load and full-load operation; the system can become unstable in the face of changing loads if the controller is designed without considering operation at such conditions. Figure 6.2 shows the difference between no-load and full-load (2500W). The no-load has a large peak at the resonant frequency at which point the phase sharply changes. In the fact, the inverter output filter is lightly damped and has significant peaking at its resonant

frequency. The resonant peak should be considered in controller design, in order not to affect the system stability.

In traditional control design, to avoid the concerns in respect of the resonant frequency, the controller bandwidth should be limited to a level above the resonant frequency of the inverter output filter. If the crossover frequency (the frequency at the point when the gain curve passes through the point 0 dB) is designed below the resonant frequency, the system may become unstable because the peaking can cause gain to rise above 0 dB with the phase-shift greater or equal to -180° . For an appropriate inverter stability margin, the controller is designed at a no-load and, as a result, the controller will perform better under full-load due to higher damping factor, thus worse case operation is at no-load (or a very light-load).

In a practical filter, parasitic resistances provide some damping. Therefore, at the no-load condition, the plant transfer function is, to some degree damped by filter parasitic resistances. The plant state-space equations with added inductor and capacitor parasitic resistances are derived in Appendix B. The open loop inverter transfer function is defined below.

$$G(s) = \frac{\left(s + \frac{1}{C r_c}\right) \frac{Z r_c}{L(Z+r_c)}}{s^2 + s \frac{\omega_o}{Q} + \omega_o^2} \quad (6.6)$$

$$\omega_o = \sqrt{\frac{(r_L + Z)}{L C (Z + r_c)}} \quad (6.7)$$

$$\frac{\omega_o}{Q} = \left(\frac{r_L}{L} + \frac{(Z C r_c + L)}{L C (Z + r_c)} \right) \quad (6.8)$$

$$Q = \frac{\sqrt{(r_L + Z)(L C Z + L C r_c)}}{(Z C r_c + r_c r_L C + Z r_L C + L)} \quad (6.9)$$

The above transfer function indicates that a high frequency zero is added to the plant as a result of capacitor resistance. Furthermore, the combination of parasitic contribution from both the capacitor and the inductor can be providing significant damping to the plant under no-load condition. Figure 6.3 is shows no-load and full-load (2500W).

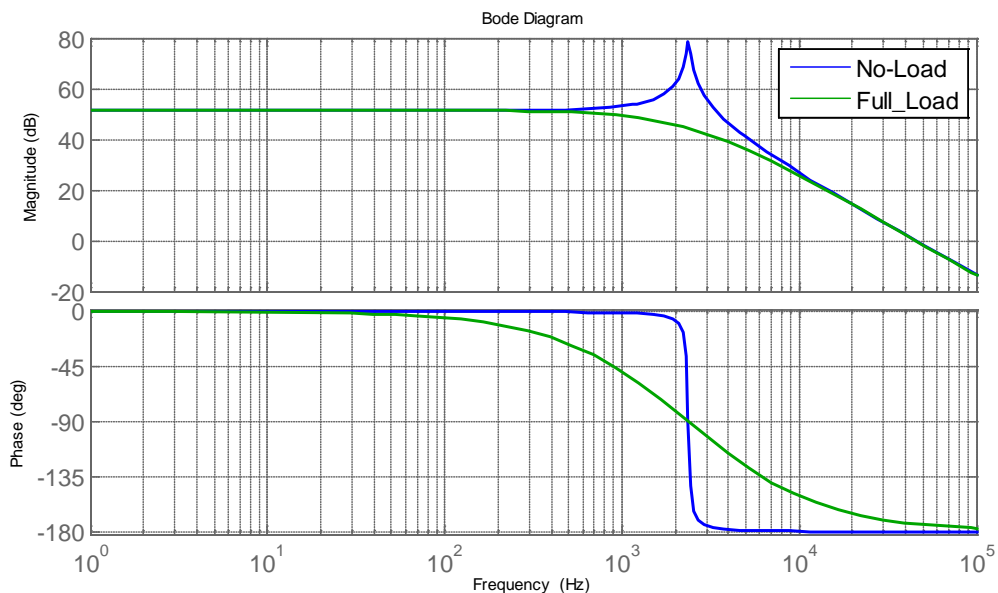


Figure 6.3: Open loop control to output transfer function under full-load and no-load condition with parasitics.

High-order frequency components in the output voltage caused by switching of the inverter are mainly eliminated by the filter, and low-order harmonics of the fundamental power frequency caused either by the inverter itself or by nonlinear loads are suppressed by appropriate control design. The higher the order of harmonics requiring suppression, the higher the control bandwidth of the system must be. The bandwidth of the system is related to the cut-off frequency of filter and control parameters.

Good results with near zero steady-state error at the fundamental frequency can be achieved by applying conventional voltage loop control design. However, slow transient response to load changes can be observed, which is undesirable. In this regard, the design

of multi-loop controllers can be conducted in a way that makes several improvements to the system.

6.3 Double Feedback Loop Control Strategy

The control of inverter is adopts a double feedback loop control strategy including an outer voltage feedback loop and an inner current feedback loop [97,115, 119]. A mathematical representation of both current and voltage loops is derived. Figure 6.4 shows a model of a single-phase voltage-source inverter. The structure of a two-loop controller is illustrated.

The control system block diagram shows:

- The inner loop uses the filter inductor current as a feedback signal, and $H_i(s)$ the inner loop PI controller.
- The outer loop uses the load voltage as a feedback signal, and $H_v(s)$ is the outer loop PI controller.

where $H(s)$ represents the PI controller $H(s) = kp + ki/s$

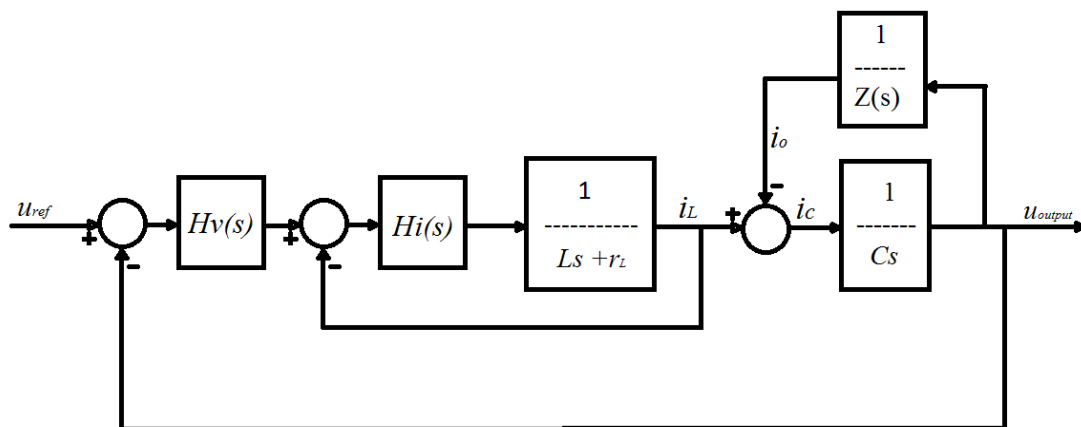


Figure 6.4: Controller structure with inner current loop and outer voltage loop.

It must be noted that if the cross-coupling terms are not insignificant and need to be considered, the plant model order will increase (to 4th-order transfer functions), complicates the design of the controller when a traditional loop controller is used.

6.4 Proposed *d-q* controller structure

The single-phase inverter model in this research developed in the previous chapter is used in developing a suitable controller in the *d-q* reference plane.

The single-phase inverter model was derived in the chapter 5 using a synchronous rotating reference frame. Consequently, the controller should also operate in the *d-q* reference frame. The controller consists of two channels (d-channel and q-channel), and each channel contains two feedback loops (outer voltage loop and inner current loop) as well as dynamic compensators in each loop.

The system is configured as in Figure 6.5. The diagram shows the voltage-source inverter, the orthogonal signal extraction and Park transformation blocks, controller structure and the SVPWM block. The output voltage and current are sampled and two orthogonal stationary reference frames are generated. The transformation into the synchronous rotating reference frame is then applied. The controller tracks active current in channel d, and tracks reactive current in channel q, including the cross-coupling terms. This is followed by the last step in the controller procedure: to produce switching gate signals by transforming the controller output vector into a pulse width pattern in the SVPWM block.

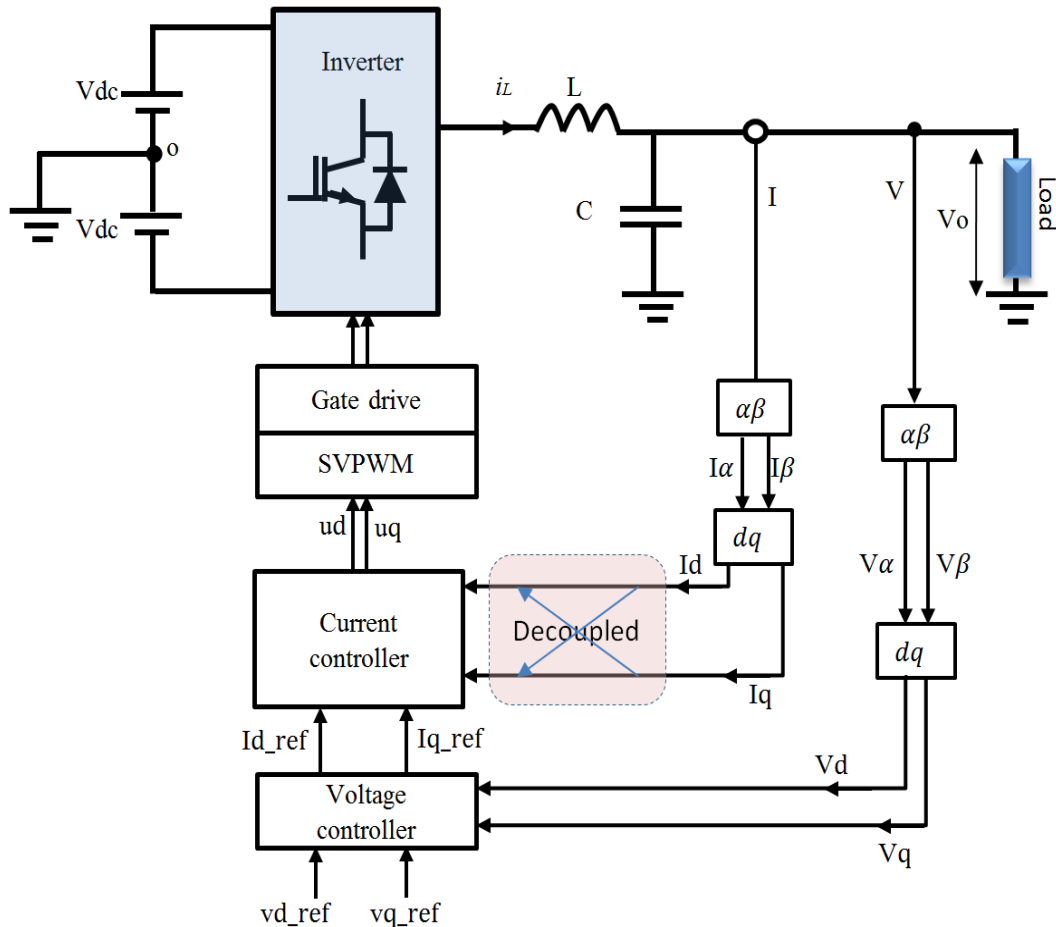


Figure 6.5: The system structure containing transformations, controller structure and decoupled terms between the d and q channel controller.

6.5 The Stand-Alone Closed-loop Model

The single-phase inverter closed-loop models and controller structure have adopted the inverter model in the synchronous rotating reference frame. The continuous-time state equation for the inverter in the d - q coordinate system depends on the inverter model in the synchronous rotating reference frame as arrived at in chapter 4; it is rewritten in (6.10).

$$\left. \begin{aligned} u_d &= L \frac{di_d}{dt} - \omega L i_q + r_L i_d + v_d \\ u_q &= L \frac{di_q}{dt} + \omega L i_d + r_L i_q + v_q \end{aligned} \right\} \quad (6.10)$$

The coupling terms in (6.10) (derived from inverter modelling in the synchronous rotating reference frame) are decoupled in (6.11) for the controller. This is shown in Figures 6.6 and 6.7.

$$\left. \begin{aligned} u_d &= L \frac{di_d}{dt} + \omega L i_q + r_L i_d + v_d \\ u_q &= L \frac{di_q}{dt} - \omega L i_d + r_L i_q + v_q \end{aligned} \right\} \quad (6.11)$$

where u_d and u_q are the control signals. v_d and v_q are the inverter output voltage components in the d - q frame respectively.

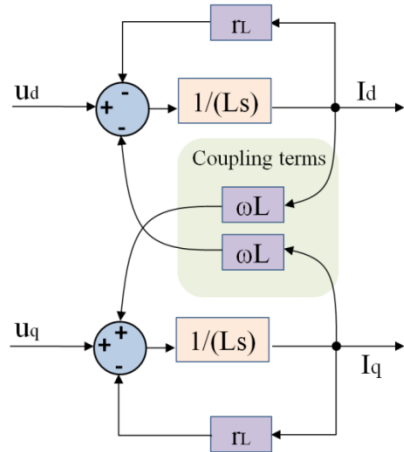


Figure 6.6: The d and q coupling terms on the inverter side.

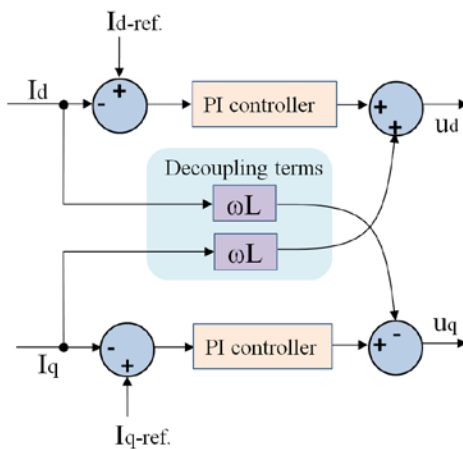


Figure 6.7: The d and q decoupling terms on the controller side.

The controller equations presented here are derived by integrating (6.11). The backward Euler method is adopted over the sample period from $(k - 1)T_s$ to kT_s . The $\frac{di}{dt}$ variation is averaged over one sampling period and dividing by T_s , Therefore:

$$\frac{di_d}{dt} \approx \frac{i_{d,k} - i_{d,k-1}}{T_s} \quad (6.12)$$

$$\frac{di_q}{dt} \approx \frac{i_{q,k} - i_{q,k-1}}{T_s} \quad (6.13)$$

By using the backward Euler approximation method [120], the output current variation between two consecutive samples i_k and i_{k-1} can be approximated to average levels.

$$i_{d,k} \approx \frac{i_{d,k} + i_{d,k-1}}{2} \quad (6.14)$$

$$i_{q,k} \approx \frac{i_{q,k} + i_{q,k-1}}{2} \quad (6.15)$$

where i_k and i_{k-1} are the $d-q$ reference currents at the sampling instants k and $k-1$, respectively.

The above assumption leads to,

$$u_{d,k} = L \frac{i_{d,k} - i_{d,k-1}}{T_s} + \omega L \left(\frac{i_{q,k} + i_{q,k-1}}{2} \right) + r_L \left(\frac{i_{d,k} + i_{d,k-1}}{2} \right) + v_{d,k-1} \quad (6.16)$$

$$u_{q,k} = L \frac{i_{q,k} - i_{q,k-1}}{T_s} - \omega L \left(\frac{i_{d,k} + i_{d,k-1}}{2} \right) + r_L \left(\frac{i_{q,k} + i_{q,k-1}}{2} \right) + v_{q,k-1} \quad (6.17)$$

The current error is eliminated in one sampling interval, the current at instant k equal the current reference at instant k-1 ($i_{d,k-1}^*$). Thus,

$$\begin{cases} i_{d,k} = i_{d,k-1}^* \\ i_{q,k} = i_{q,k-1}^* \end{cases}$$

The fundamental output voltage is assumed to be constant within the one sampling period (sampling frequency usually is several times faster than the highest frequency component in the output voltage), i.e.

$$\begin{cases} v_{d,k} \approx v_{d,k-1} \\ v_{q,k} \approx v_{q,k-1} \end{cases}$$

According to above, the PI control signal used within the *d-q* controller in stand-alone mode is given by (6.18) and (6.19).

$$u_{d,k+1}^* = L \frac{i_{d,k}^* - i_{d,k}}{T_s} + \omega L \left(\frac{i_{q,k}^* + i_{q,k}}{2} \right) + r_L \left(\frac{i_{d,k}^* + i_{d,k}}{2} \right) + v_{d,k} \quad (6.18)$$

$$u_{q,k+1}^* = L \frac{i_{q,k}^* - i_{q,k}}{T_s} - \omega L \left(\frac{i_{d,k}^* + i_{d,k}}{2} \right) + r_L \left(\frac{i_{q,k}^* + i_{q,k}}{2} \right) + v_{q,k} \quad (6.19)$$

The integral term is a multiplication of the integral gain and the sum of the recent errors. The steady-state error can be constructed as sum of previous errors in the integral part of the PI controller, i.e. the steady-state current error can be equal to the sum of the previous current errors, which results in:

$$\left. \begin{aligned} i_{d,k} &= \sum_{m=0}^{k-1} [i_{d,m}^* - i_{d,m}] \\ i_{q,k} &= \sum_{m=0}^{k-1} [i_{q,m}^* - i_{q,m}] \end{aligned} \right\}$$

where m is intermediate discrete samples.

This resulting PI-controller is given by (6.20). The closed loop system configuration is shown in Figure 6.8.

$$\left. \begin{aligned} u_{d,k+1}^* &= k_p \{(i_{d,k}^* - i_{d,k}) + \frac{1}{T_i} \sum_{m=0}^{k-1} [i_d^*(m) - i_d(m)]\} + k_c \left(\frac{i_{q,k}^* + i_{q,k}}{2} \right) + e_{d,k} \\ u_{q,k+1}^* &= k_p \{(i_{q,k}^* - i_{q,k}) + \frac{1}{T_i} \sum_{m=0}^{k-1} [i_q^*(m) - i_q(m)]\} - k_c \left(\frac{i_{d,k}^* + i_{d,k}}{2} \right) + e_{q,k} \end{aligned} \right\} \quad (6.20)$$

where $k_p = \frac{L}{T_s} + \frac{r_L}{2}$, $k_c = \omega L$, $T_i = r_L / \left(\frac{L}{T_s} + \frac{r_L}{2} \right)$

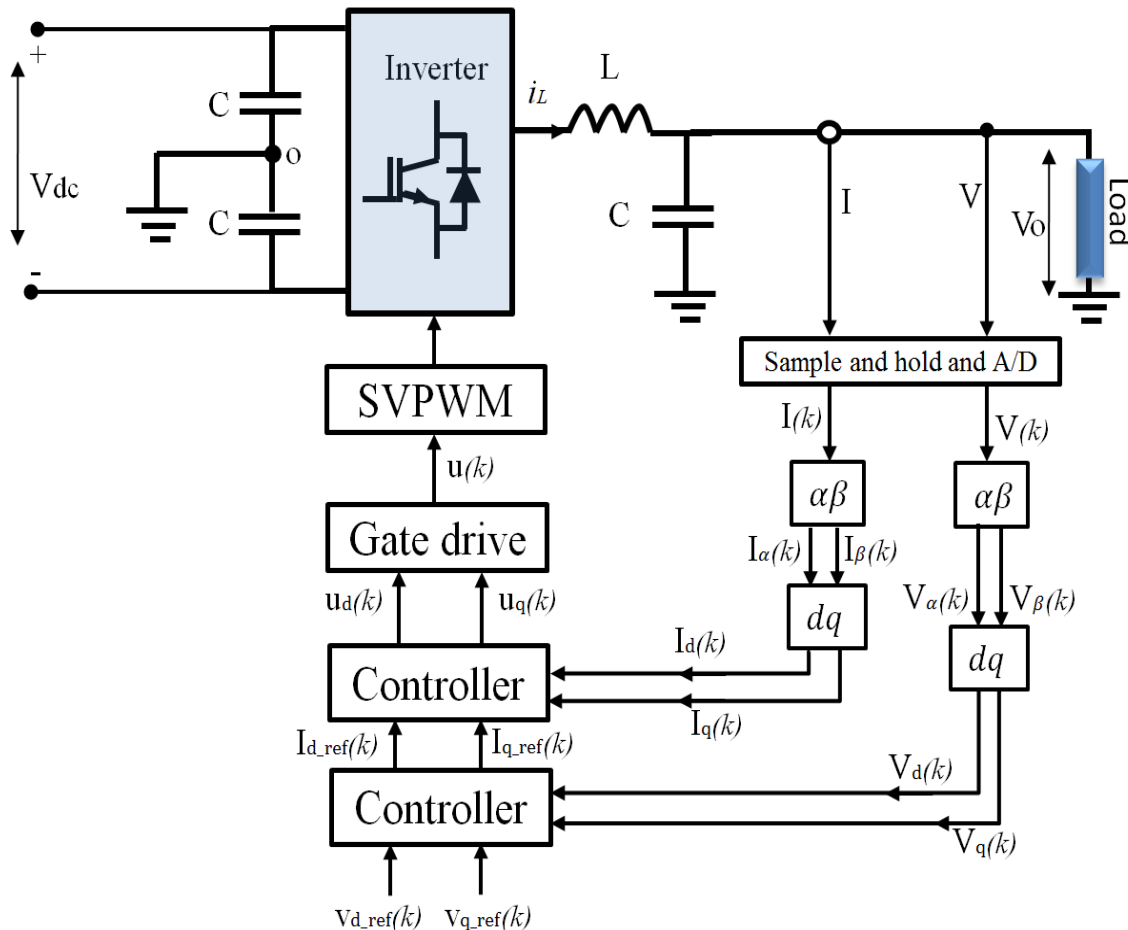


Figure 6.8: The system structure containing the transformations, controller structure and decoupled terms between the d and q channel controller.

6.6 Transformation stage modification

The purpose of $d-q$ transformation in the inverter controller is to reduce compensator complexity by converting the AC voltage and current waveforms to DC values. This can be realised when the transformations achieve the two conditions:

$$A\cos\theta_1 \cos\theta_2 + A\sin\theta_1 \sin\theta_2 = A \quad (6.21)$$

$$A\cos\theta_1 \sin\theta_2 - A\sin\theta_1 \cos\theta_2 = 0 \quad (6.22)$$

where θ_1 is transformation matrix phase angle, θ_2 is the phase angle of the transformed signal (voltage and/or current) waveform, and A represents the peak value of current or voltage waveforms. The d component should be equal to the peak value of the signal waveform after the transformation process. This can be achieved only if $\theta_1 = \theta_2 = \theta$ which leads to:

$$\begin{aligned} A\cos^2\theta + A\sin^2\theta &= A \\ A\cos\theta \sin\theta - A\sin\theta \cos\theta &= 0 \end{aligned} \quad \} \quad (6.23)$$

The proposed transformation approach about to be described provides solutions for some of the drawbacks associated with conventional synchronous reference frame transformations. A new and fast transform strategy is introduced, and a significant reduction of computation in the controller stage is achieved. This is effected by using a transformation matrix to transform voltage and current separately, i.e. using the voltage phase as a reference for the voltage at the Park transformation stages, and the current phase as a reference for the current at the transformation stages from stationary reference frame to the synchronous rotating reference frame. The new transform strategy satisfies the following equations:

$$\begin{aligned} \cos(\theta + \theta) &= \cos\theta \cos\theta - \cos(\theta + 90) \cos(\theta + 90) \\ \sin(\theta + \theta) &= -A \cos\theta A \cos(\theta + 90) - A \cos(\theta + 90) A \cos\theta \end{aligned} \quad \} \quad (6.24)$$

$$\begin{aligned} A \cos\theta A \cos\theta + A \sin\theta A \sin\theta &= A^2 \\ A \cos\theta A \sin\theta - A \sin\theta A \cos\theta &= 0 \end{aligned} \quad } \quad (6.25)$$

By this method, if $|A| > 1$ the stationary waveform will swing in the range $A \geq A \sin\theta$ and $A \cos\theta \geq -A$ resulting in error in the d-component calculation. $|A^2|$ will increase if $|A| > 1$, $|A^2|$ will reduce if $|A| < 1$. This problem can be solved by setting $|A| \leq 1$ to force the multiplication results in one direction only.

Figure 6.9 shows the schematic diagram of new transformation strategy. It is employed to satisfy the following equations:

$$\begin{aligned} V \cos\theta V \cos\theta + V \cos(\theta + 90) V \cos(\theta + 90) &= V^2 \\ V \cos\theta V \cos(\theta + 90) - V \cos(\theta + 90) V \cos\theta &= 0 \end{aligned} \quad } \quad (6.26)$$

$$\begin{aligned} I \cos\theta I \cos\theta + I \cos(\theta + 90) I \cos(\theta + 90) &= I^2 \\ I \cos\theta I \cos(\theta + 90) - I \cos(\theta + 90) I \cos\theta &= 0 \end{aligned} \quad } \quad (6.27)$$

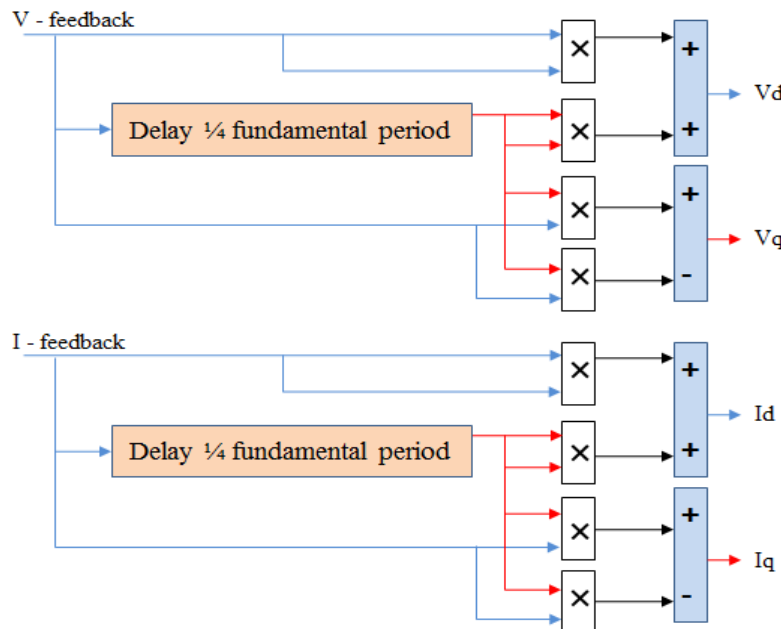


Figure 6.9: New transformation strategy.

The new transformation strategy offers some advantages such as:

1. Fast, simple $d-q$ transformation.
2. Low harmonics associated with the transformed quantities.
3. Fast tracking of sudden frequency changes.
4. The new transformation strategy is followed by a newly developed controller stage, overcoming the computational burden by using low time-cost functions
5. Reduce time-cost of controller calculation thus increasing processor time available for other functions.
6. Thus, it can be implemented with a low-cost fixed-point DSP.

These advantages are validated in the next section.

6.7 Validation and operating principles of feedback path

Before discussing the actual response obtained from the system, the feedback path must first be defined stage by stage. This section describes the requirements and operating principles of each stage in the feedback path. The general system model is made up of several subsystems. The general proposed circuit is divided into the two main elements in stand-alone mode (inverter and load). The feedback loop is divided into several subsystems to facilitate the study of each stage in this loop individually as subsystems connected in cascade (stationary to rotating reference frame transform, Park transformation, controller, and SVPWM). The configuration of the simulation model is depicted in Figure 6.10. It shows the general structure of the proposed system including 4 subsystems in feedback path (stage 1, 2, 3, and 4). The details of the subsystems are shown in Figures 6.12, 6.14, 6.16, 6.18 and the SVPWM program listing is given in Appendix A.

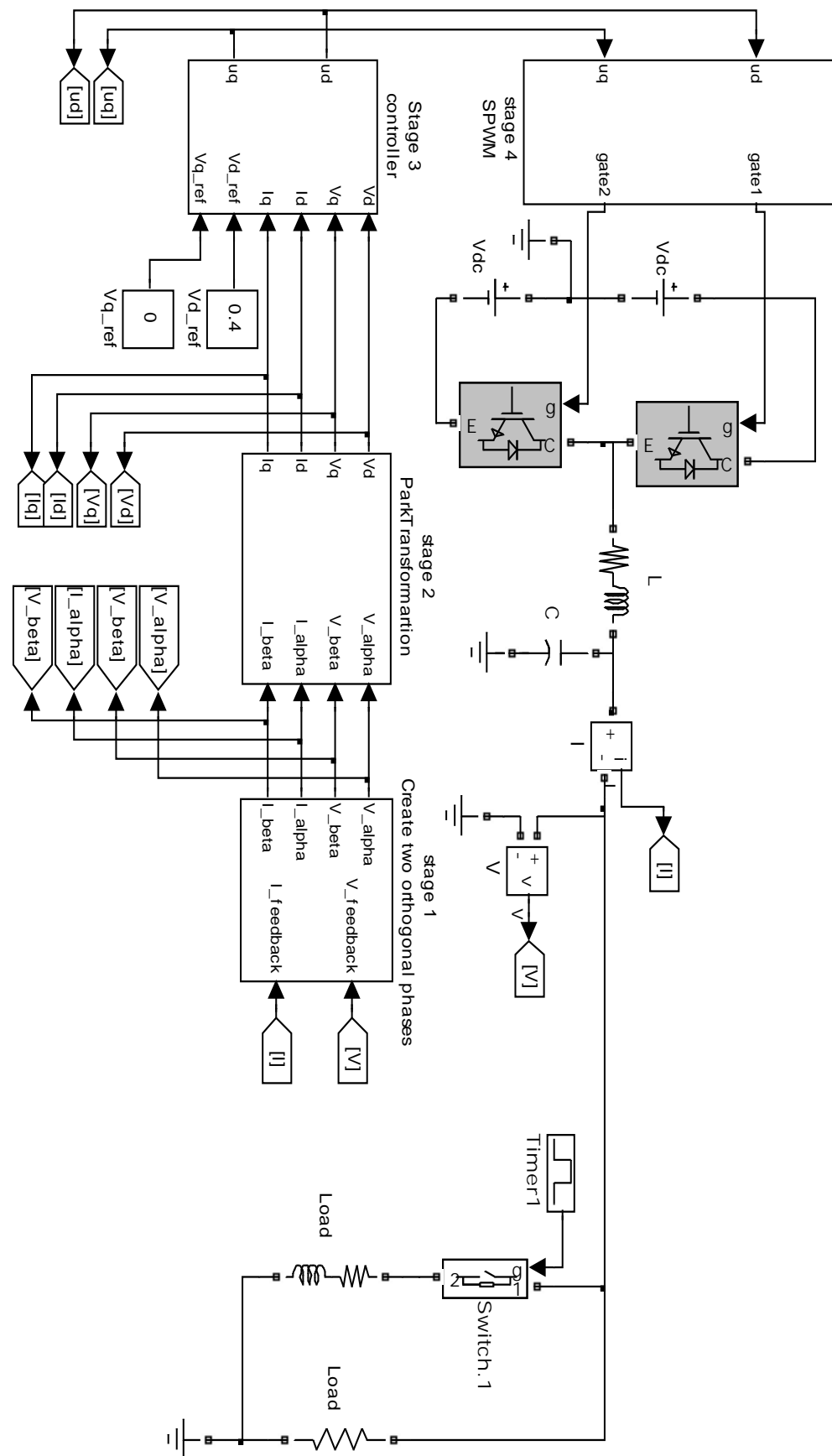


Figure 6.10: Closed loop system with the proposed control scheme.

Below, each subsystem description is followed by the output signal waveform relating to that particular subsystem stage.

The output voltage and current are measured (at different load values 1000W, 1500 W, 2000W+500VAr, 1500W+1000Var) (Figure 6.11) then utilized as a feedback signal.

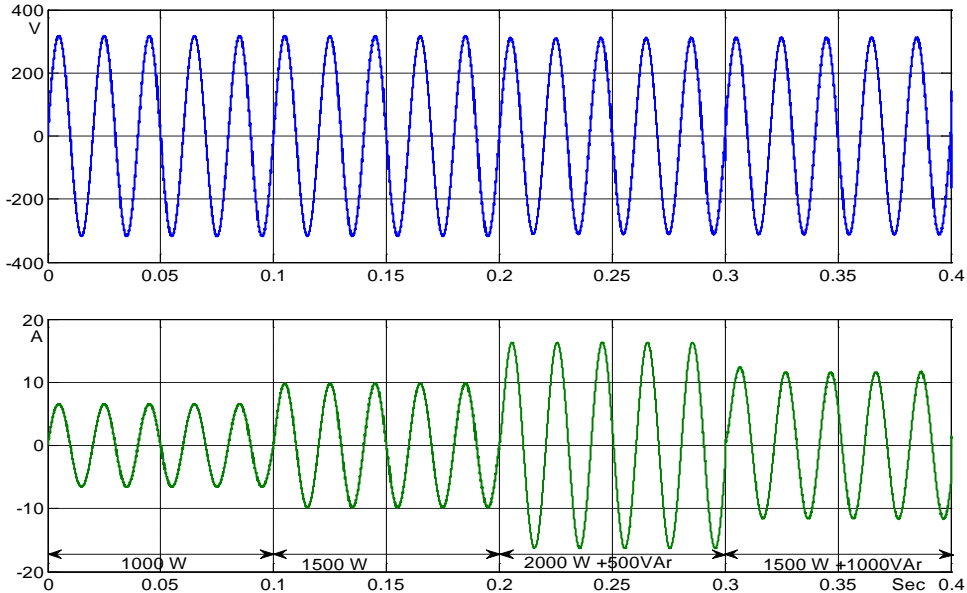


Figure 6.11: Voltage and current measured at the inverter output side.

The first step in the feedback loop is to create an imaginary orthogonal component from the real component (Figure 6.10, Stage 1). Figure 6.12 gives more details about Stage 1. It describes the stationary orthogonal component generation technique (α and β , or alpha and beta as denoted in MATLAB/SIMULINK Figures 6.10, 6.12, 6.13 and 6.14).

When the system does not require high bandwidth control, the sample rate can be reduced to switching frequency($f_s = f_{sw}$) [121]. In Stage 1 (Figure 6.12), the voltage and current feedback signals are scaled by 1/500 and 1/25 respectively before being sampled by Zero-Order Hold 1 and 2. The input for the sample period is specified at a frequency of

20 kHz. Thus, the number of sampling intervals for one cycle at the fundamental frequency (of 50Hz) can be calculated as follows:

$$\text{Sampling number} = \text{sampling frequency} / \text{fundamental frequency}$$

$$\text{Sampling number} = 20000 \text{ Hz} / 50 \text{ Hz} = 400$$

The voltage and current sampled-and-held signals are converted to the digital domain using the analog to digital converter (ADC1 and ADC2). The ‘Integer Delay’ blocks are set to delay their inputs by 100 samples. The 100 samples delay is equal to the quarter of the total sampling number (400) for one cycle at the fundamental frequency of 50 Hz. Thus, it is equivalent to a delay by a quarter cycle of the signals of fundamental frequency. The outputs V_{α} and I_{α} represent the original phase voltage and current signals to be used for feedback. The outputs V_{β} and I_{β} are created from original feedback signals (V_{α} and I_{α}) by means of the quarter-cycle delay method.

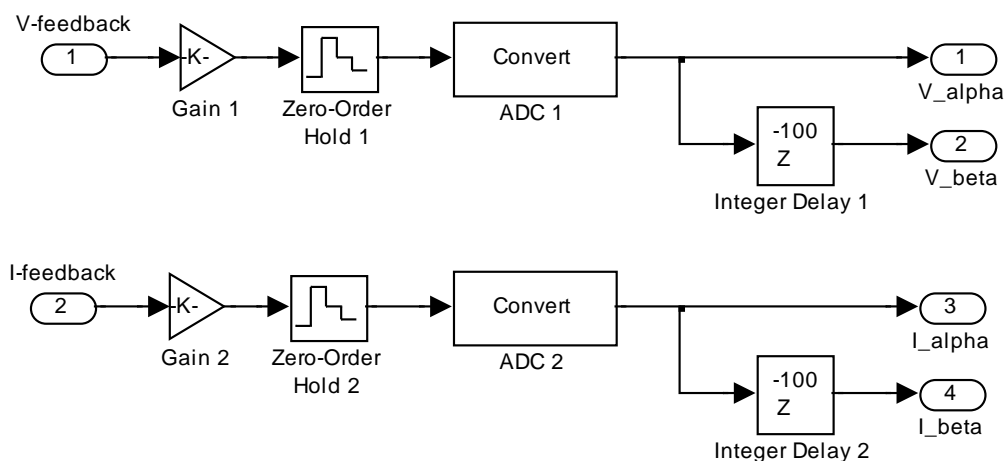


Figure 6.12: Stage 1, stationary orthogonal component generation technique.

The voltage and current stationary reference frame waveforms at the outputs (V_{α} , I_{α} and V_{β} , I_{β}) are presented in Figure 6.13. It can be noted that the

integer delay output signals (V_{beta} and I_{beta}) are orthogonal to the input signals. The voltage and current stationary reference frame waveforms in Figure 6.13 illustrate that the real and created phases remain orthogonal and are not affected by active and reactive load changes. The process in this stage is equivalent to the Clarke transformation in three-phase systems. This technique can be used only in stand-alone mode when the inverter output is set at fixed frequency. This stage is to be modified in section 6.12 to enable use in grid-tied mode.

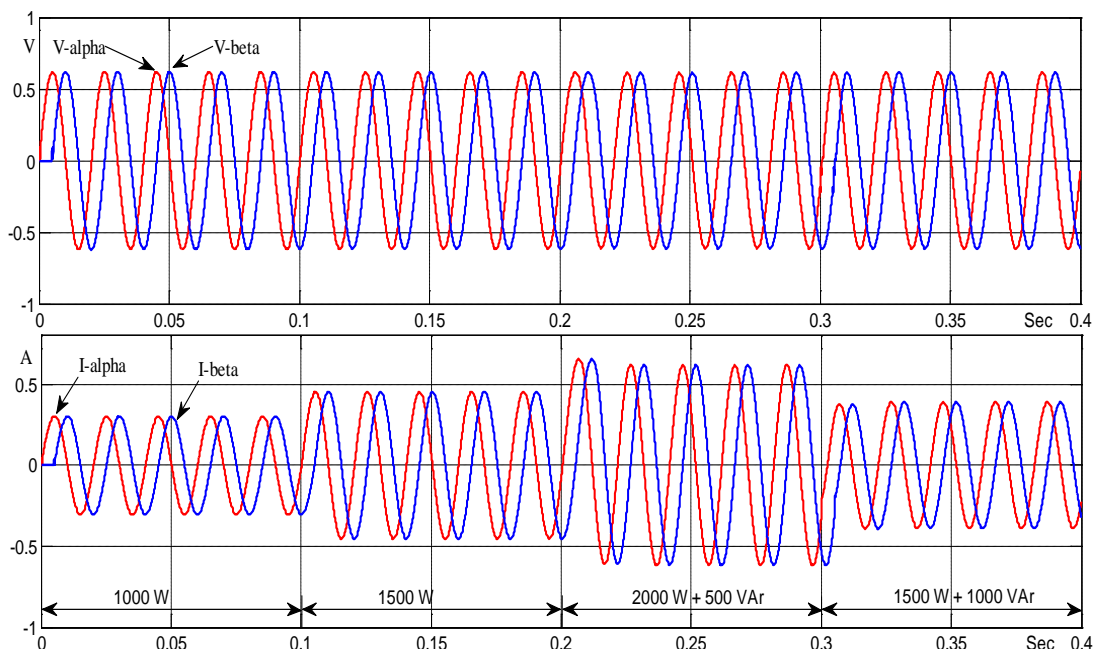


Figure 6.13: Voltage and current stationary frame waveforms.

The voltage and current stationary frame waveforms are fed to the second stage (Stage 2) in the feedback loop path, and the details of this stage is shown in Figure 6.14. The purpose of this stage is to transform stationary AC waveforms to the synchronous rotating reference frame (DC components). This stage is represented by mathematical operations arranged to satisfy equations 6.38, and 6.39.

Figure 6.15 shows the voltage and current components in the synchronous rotating frame. It is clear from this figure that the output voltage and current d - q components are reflected as DC levels. It can also be seen that the V_q and I_q components are zero. This leads to the conclusion that the output stationary-frame waveforms from the previous stage (Stage 1) are exactly orthogonal. By comparing Figures 6.13 and 6.15, it can be noted that voltage and current DC values (V_d and I_d synchronous rotating reference frame components) represent the average values of voltage and current, respectively, in the stationary reference frame. As a result, the feedback signals become time-invariant signals; see Figure 6.15.

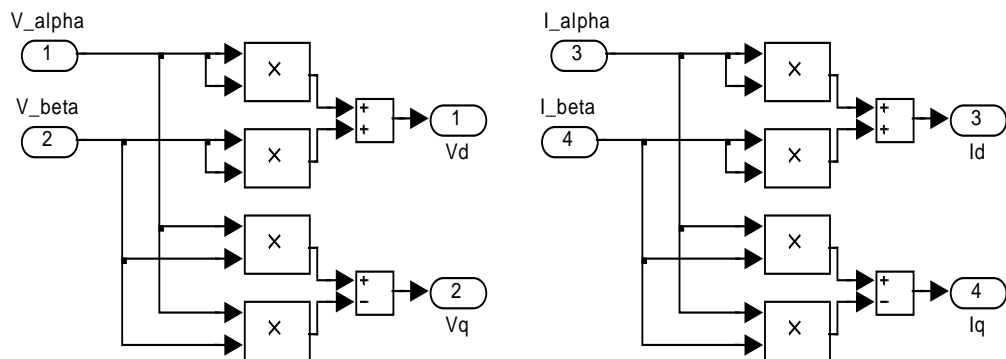


Figure 6.14: Stage 2, transformation to the synchronous rotating reference frame.

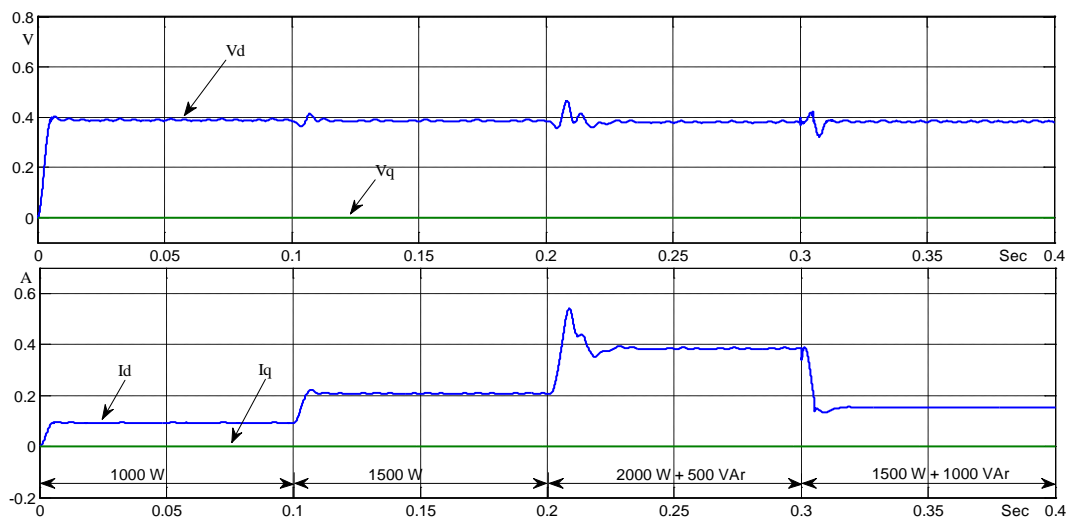
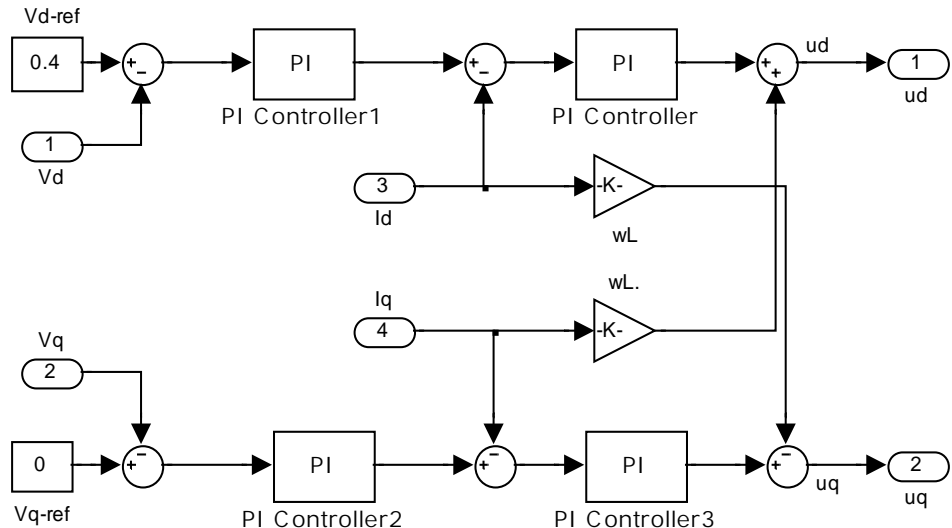
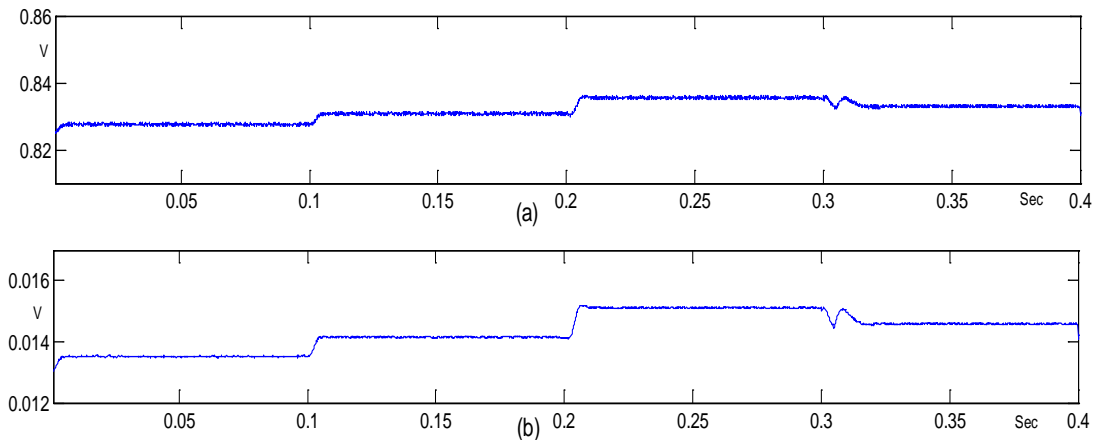


Figure 6.15: Voltage (V_d , V_q) and current (I_d , I_q) components in the synchronous rotating reference frame.

The above-described steps convert the time-variant feedback signals to time-invariant components. This allows control of the inverter in a manner similar to that of a DC-to-DC converter. The controller scheme is shown in Figure 6.16. It is constructed in two channels (d and q channels), with decoupling terms. Each channel is structured from the outer voltage loop and inner current loop (the system structure is shown in Figure 6.8), with the use of PI controllers in the outer voltage loops as well as in the inner current loops. The voltage is controlled relative to the reference, and this reference is pertinent to the case when the inverter works as stand-alone. The voltage feedback signals (V_d and V_q) are compared with the desired values (V_{d_ref} and V_{q_ref}) of the output. The voltage aligned with q-component is set to zero by setting V_{q_ref} to zero to get zero reactive power at the output side. The error of the outer voltage loops is fed as references to the inner current loops in each channel. The current component I_q is based on the coupling term only. In other words, the I_q component is not affected by the load state because:

1. V_q is zero from the last stage (Stage 2 of Figure 6.10)
2. I_q is zero from the last stage (Stage 2 of Figure 6.10)
3. V_{q_ref} is set to zero in this stage (Stage 3 of Figure 6.10)
4. V_{d_ref} is set to 0.4 in this stage (Stage 3 of Figure 6.10)

The purpose of the control stage is to enable the inverter to generate a fixed output voltage of a preset magnitude that remains constant regardless of changes to its input voltage or load conditions. Figure 6.17 shows the controller output signals u_d and u_q under step-wise varying load conditions. The d-channel controller output signal (u_d) is responding well to the load changes. The u_q control signal is affected by the decoupling term.

Figure 6.16: Block diagram (Stage 3) of d - q rotating reference frame controller.Figure 6.17: controller output signals (a) u_d (b) u_q .

The final step in feedback loop is the SVPWM stage (Figure 6.10, Stage 4). The SVPWM stage is shown in Figure 6.18. This stage was developed to utilize the control signal as a reference value (V_{ref}) to generate switching gate drive (PWM). This block has been described earlier in Chapter 3, Section 3.10 and its MATLAB/SIMULINK program listing is given in Appendix A.

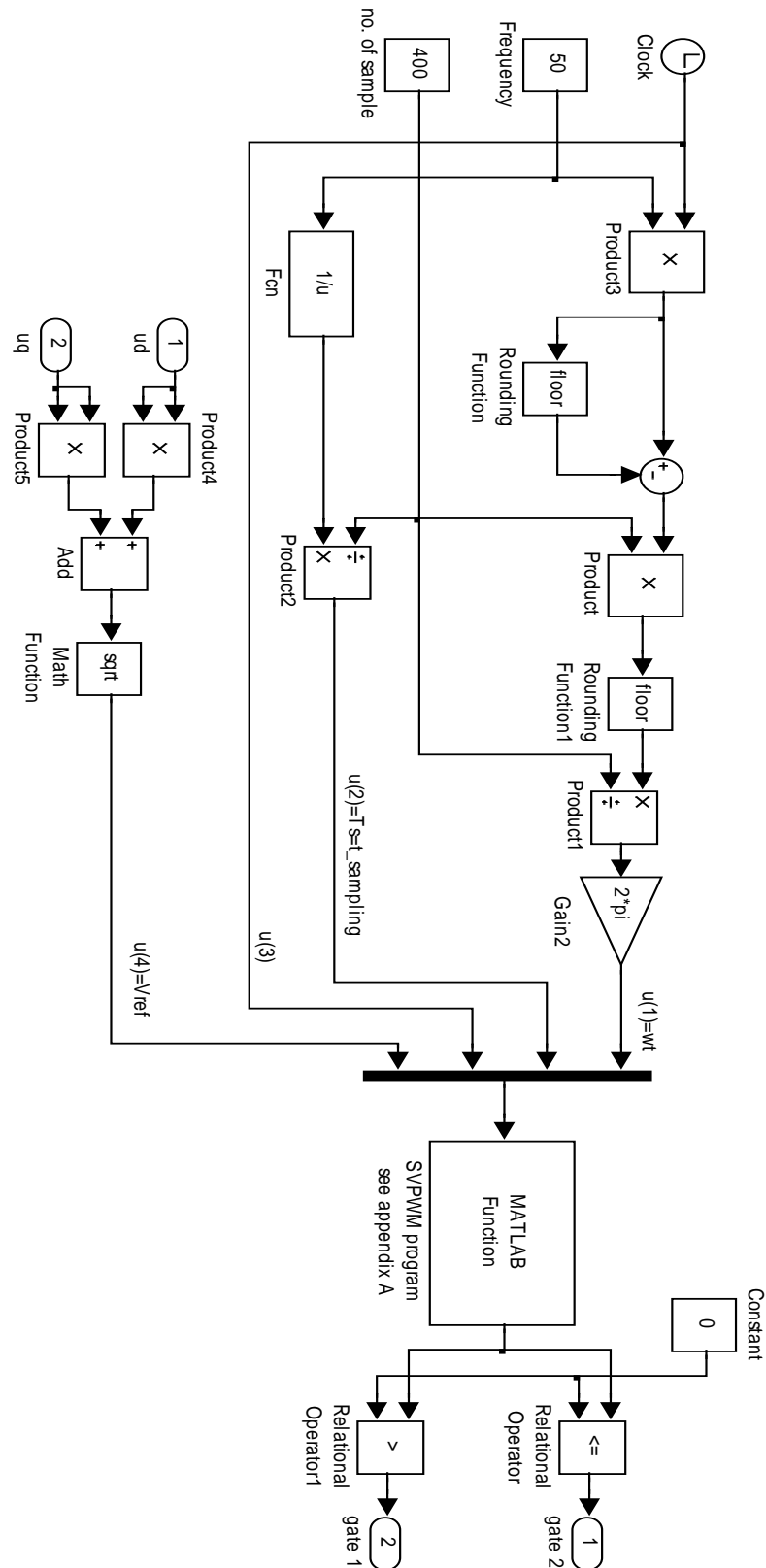


Figure 6.18: SVPWM stage.

The outputs of the SVPWM stage are shown in Figure 6.19. It can be seen that the SVPWM outputs are complementary, and have a pulse width varying with time.

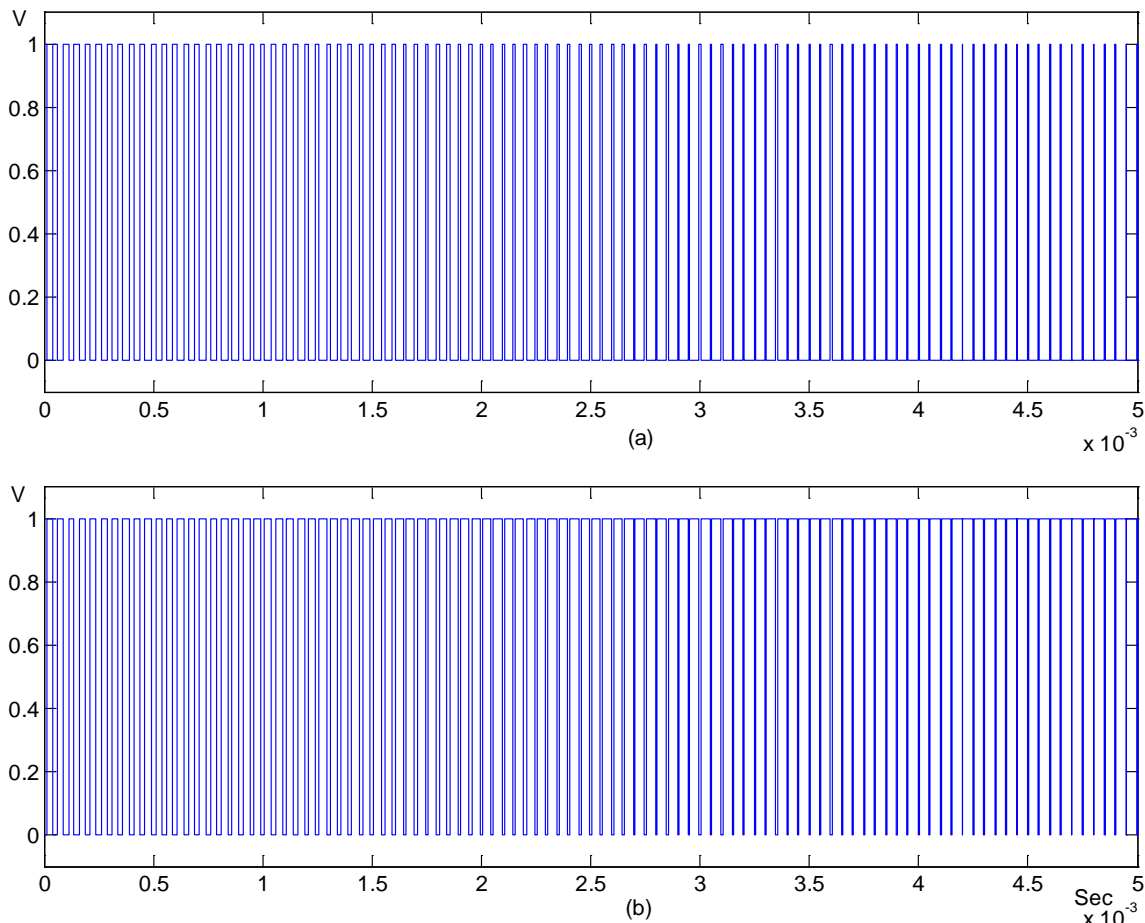


Figure 6.19: SVPWM outputs (a) is gate 1 (b) is gate 2.

6.8 Validation of the proposed strategy in stand-alone mode

The system was simulated with the new controller strategy and the results outlined the system performance at steady-state, sudden load-change, resistive and inductive loads, poor power factor as a result of inductive loads, nonlinear load test, and sudden frequency-change. Furthermore, the step load changes are initiated when the current waveform crosses the zero at first, and then when it crosses the peak points again, as it is indicated in the results. The objective from this approach is to study steady-state and transient system

performance of the new closed loop configuration (transformation and controller stages), and to compare the new system performance with the previous publications (section 4.6 chapter 4) in this area. Table 6-1 provides a summary of test cases. The system parameters are provided in Table 3.2

Note: For the case of study, the feedback signals (V_d , V_q , I_d , I_q) are relative to the output peak values at the point of measurement.

Table 6-1.

Stand-alone mode test using proposed strategy			
Figure no.	Sudden case	Changing values	Step change
Figure 6.21 Figure 6.22	Load-change	500W → 1500W → 500W 50Hz	1000W
Figure 6.24 Figure 6.25	Load-change	500W → 1000W + 500VAr → 500W 50Hz	500W + 500VAr
Figure 6.26 Figure 6.27	Load-change	500W → 800W + 900VAr → 500W 50Hz	300W + 900VAr
Figure 6.28 Figure 6.29 Figure 6.30	Load-change	100W → 300W + 900VAr → 100W 50Hz	300W + 900VAr
Figure 6.31 Figure 6.32	Spectrum	Output voltage FFT spectrum Inverter current FFT spectrum	
Figure 6.33 Figure 6.34	Nonlinear load change	Nonlinear load test	

6.9 Step Load Parameter Variation:

This case is to observe the dynamic response, stability, and performance of the control system in stand-alone mode with respect to changes in the load. The load change is imposed by closing a load switch while the system is under normal operating conditions,

Figure 6.20.

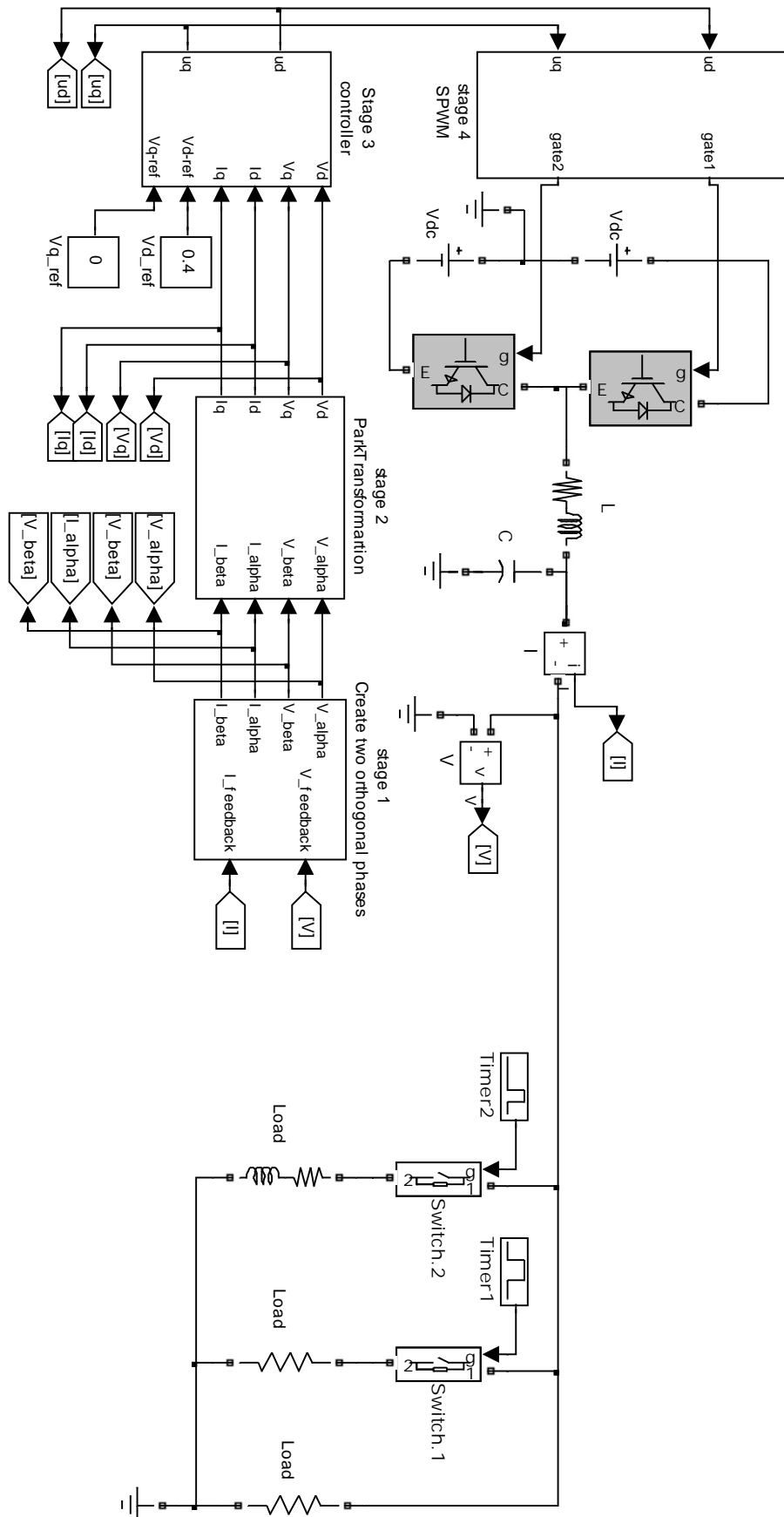


Figure 6.20: General structure of the proposed system in stand-alone mode.

Figure 6.21 shows the load-change transient effect on the inverter output voltage. It depends on the point in the cycle at which the change occurs as well as the step rate of the load change. Therefore, the load change at point 2 causes two voltage spikes associated with the step load change. The first spike represents the rapid changes in real phase from old peak magnitude value ($I_{peak-old}$) to the new peak magnitude value ($I_{peak-new}$), while the second spike represents the rapid change of the imaginary phase after a quarter-cycle delay. The dynamic transformation behaviour associated with the step load transient lies within quarter cycle and is described in equation (6.28).

$$(I_{peak-new})^2 \cos^2 \theta + (I_{peak-old})^2 \sin^2 \theta = I_d \quad (6.28)$$

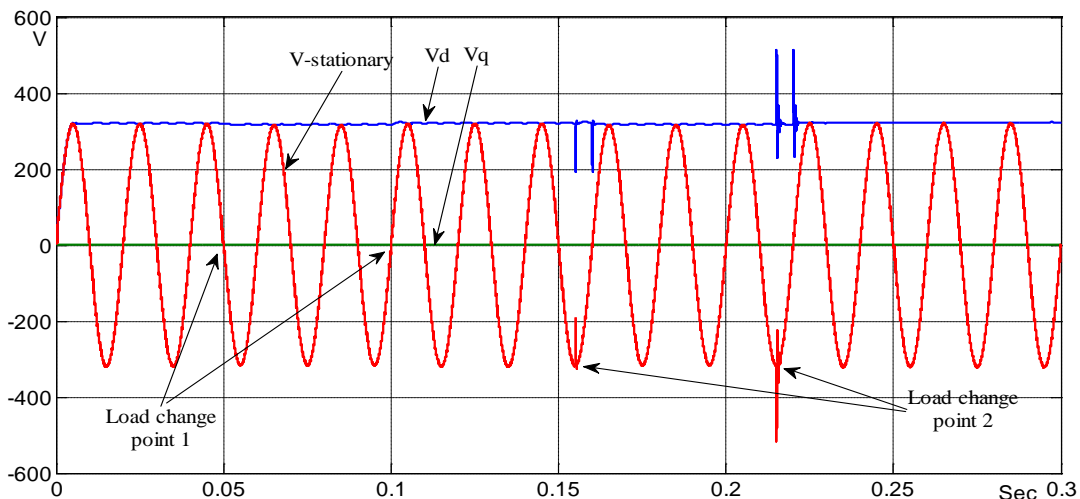


Figure 6.21: Inverter voltages with step load-change from 500 watt to 1500 watt.

Figure 6.22 shows the output current waveform with a 1000 watt step load-change (from 500 watt to 1500 watt) at points 1 and 2. It can be seen that the inverter output current transient at load-change is smoother at point 1 when the load changes at the zero crossing of the waveform. When the same load change takes place at the peak of the

waveform (point 2), the transient takes time equal to $1/4f$, which represents the delay period between real and imaginary phase, and this is clear from the d-component.

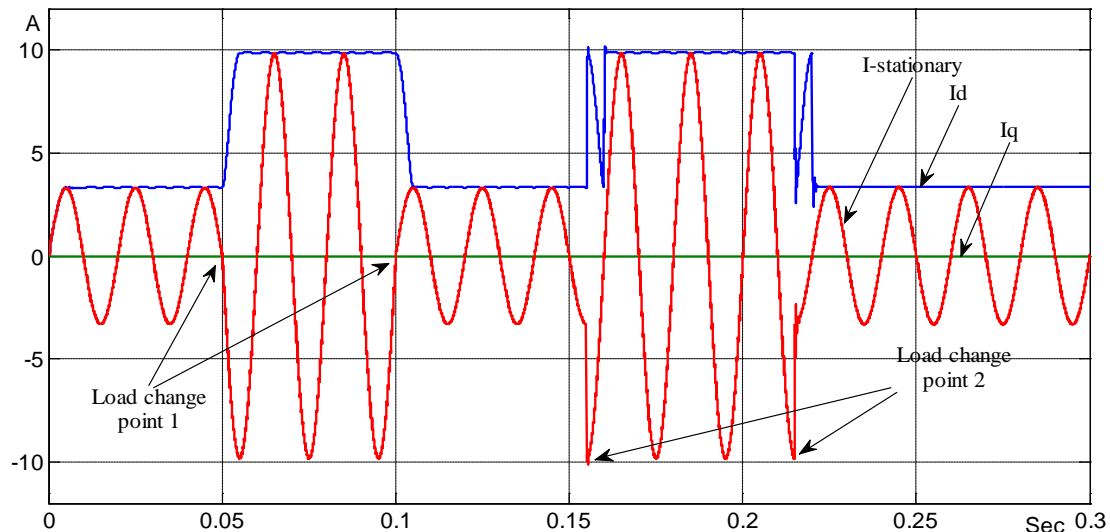


Figure 6.22: Inverter current with step load-change from 500 watt to 1500 watt.

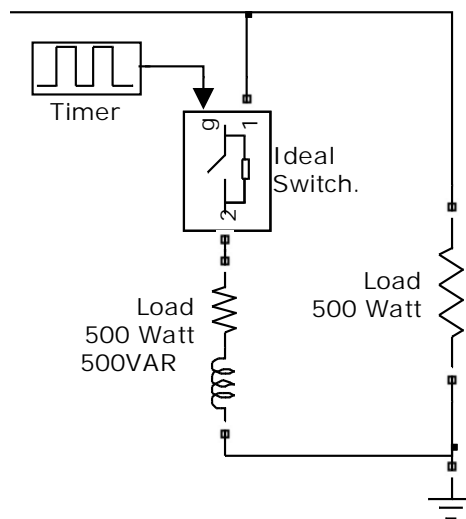


Figure 6.23: 0.5 power factor step load-change.

Figure 6.24 shows the output current waveform with a 0.5 power factor load-change (from 500 watt to 1000 watt + 500 VAr), and the load-change is achieved by the circuit shown in Figure 6.23. The same procedure as above is used to enable the load change at points 1 and 2. The test result in Figure 6.24 shows that the inductive load

damps the transient period at point 2, as a result, the voltage spike is reduced and this is also clear in Figure 6.25.

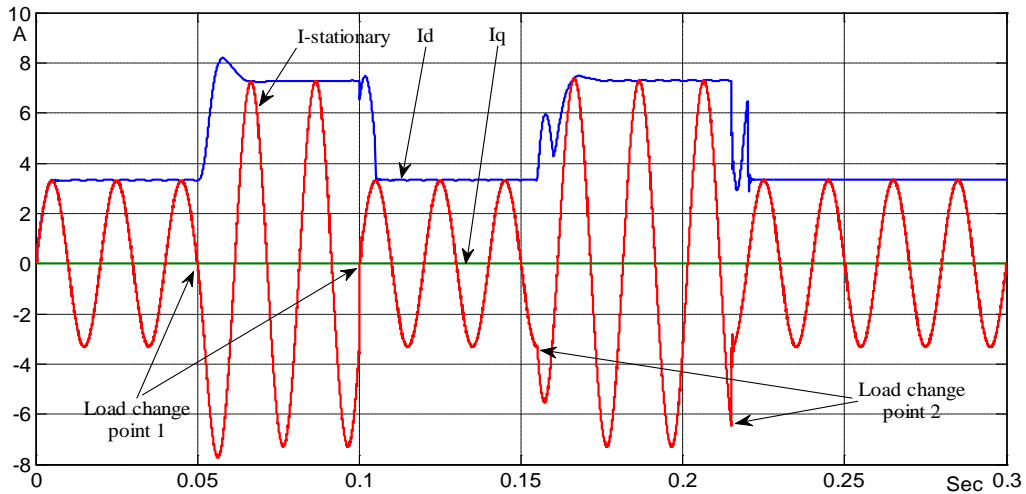


Figure 6.24: Inverter current with step load-change from 500 watt to 1000watt + 500VAr.

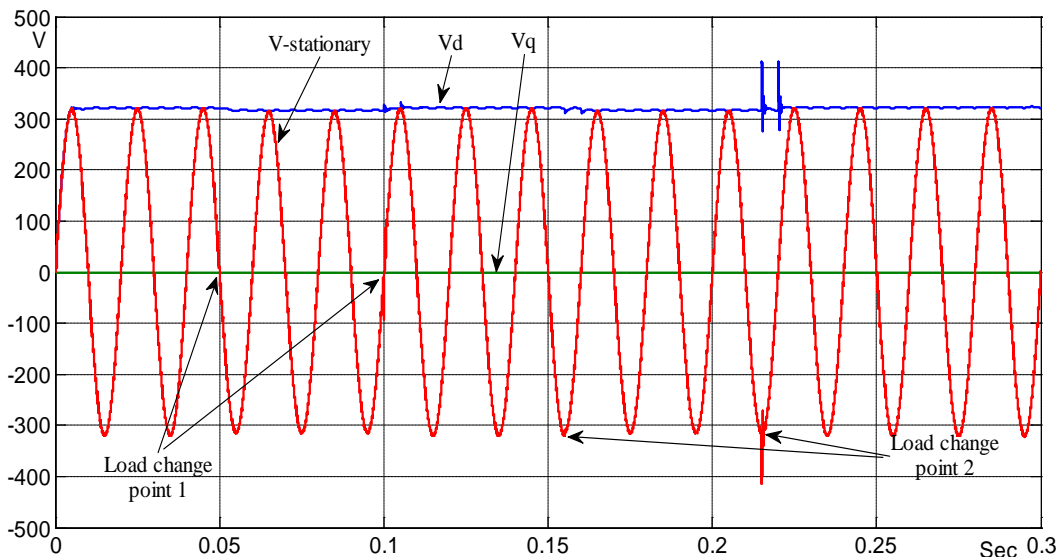


Figure 6.25: Inverter voltages with step load-change from 500 watt to 1000watt + 500VAr.

Figure 6.26 and 6.27 show the output current and voltage waveforms respectively with a 0.3 power factor load-change (from 500 watt to 800 watt +900 VAr) at the zero-crossing and peak points of the waveform. The current waveform (Figure 6.26) is phase shifted with respect to the voltage waveform (Figure 6.27) when the inductive load is switched in. Therefore, the transient is either damped or overshoots based on the point of

the inductive load change within the one fundamental period. When the inductive load is switched out, the active load (500 Watt) is still left in.

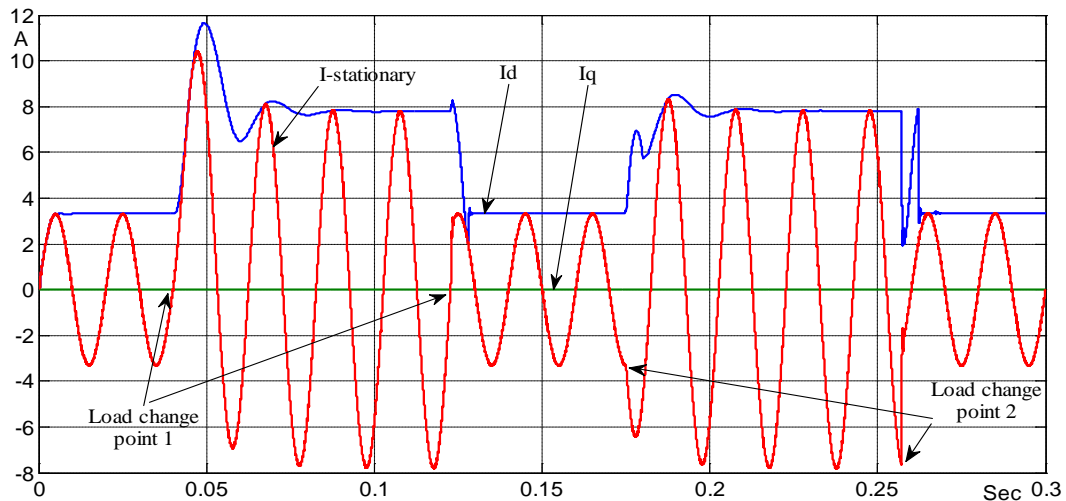


Figure 6.26: Inverter current with step load-change from 500 watt to 800watt+900VAr.

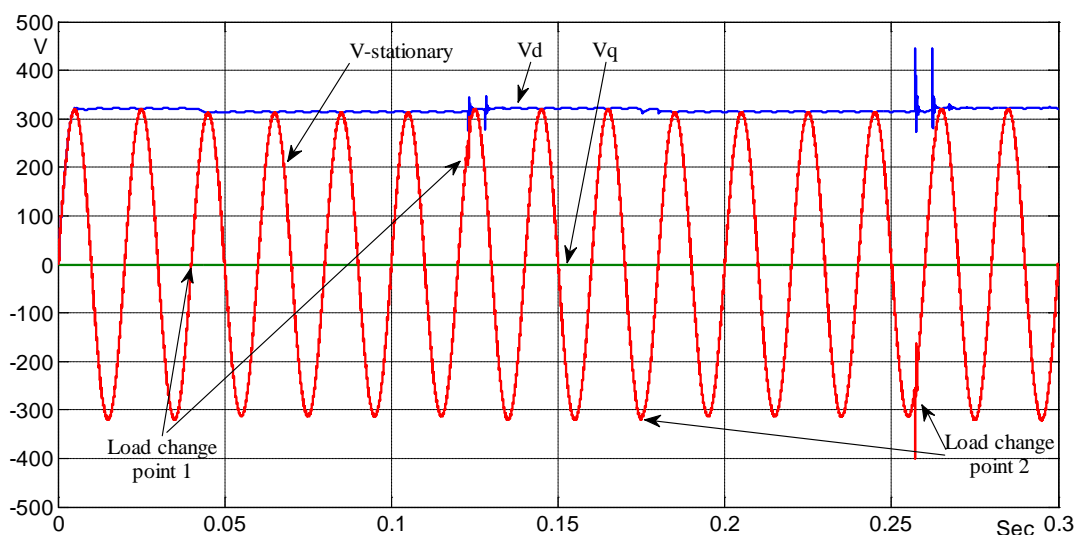


Figure 6.27: Inverter voltages with step load-change from 500 watt to 800watt+900VAr.

For more clarity of system performance, the system was tested under light load (100Watt) as well as under high inductive load (300Watt+900VAr) at 0.3 power factor. The results are shown in Figures 6.28, 6.29 and 6.30. Although this test is done with high inductive load, the transient period does not change significantly. It is clear that the output is damped at the point of the transient.

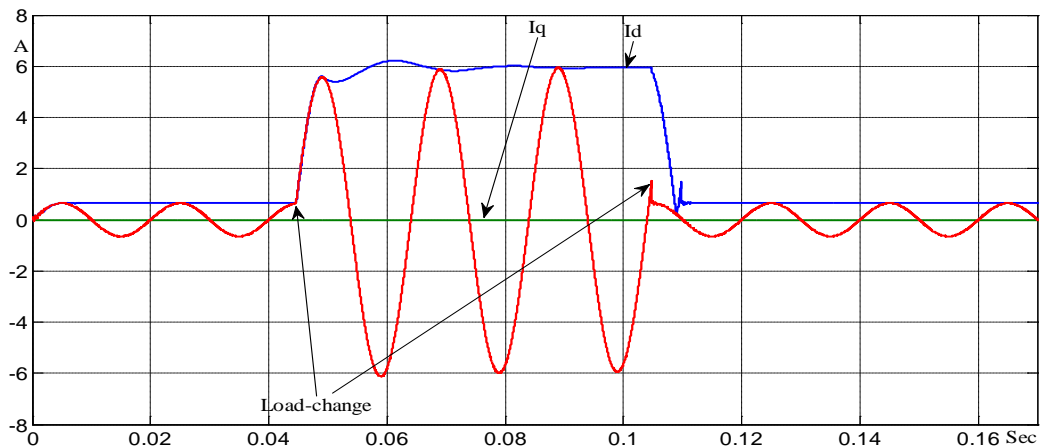


Figure 6.28: Inverter current with step load-change from 100 watt to 300watt+900VAr.

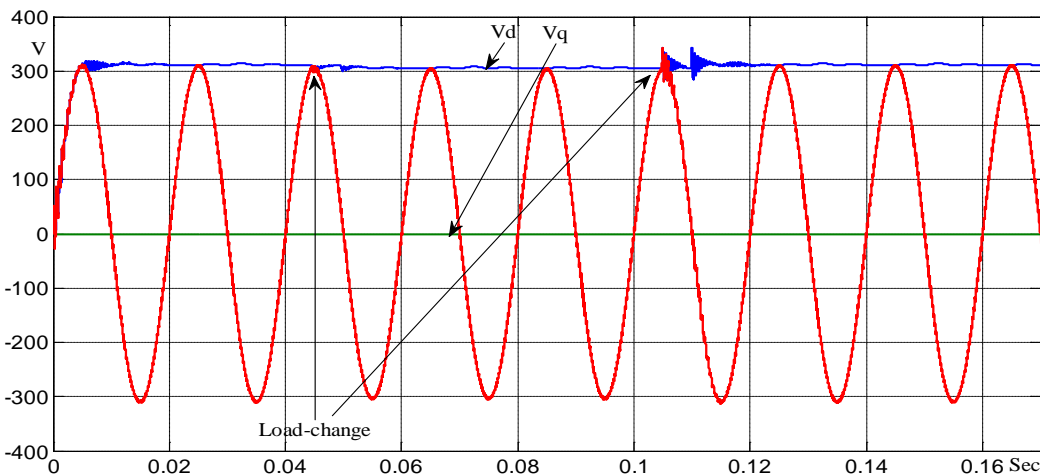


Figure 6.29: Inverter voltage with step load-change from 100 watt to 300watt+900VAr.

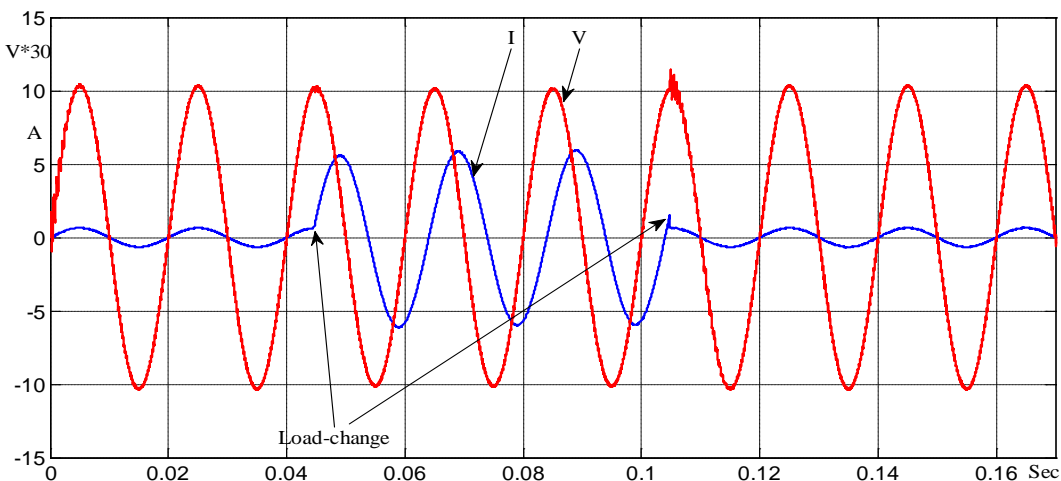


Figure 6.30: Inverter current and voltage waveform with step load-change from 100 watt to 300watt+900VAr.

Generally, all the results show that the sudden load-change transient period lies within a quarter cycle with both the active load-change as well as with the reactive load. This is caused by the quarter cycle delay used for creating the imaginary orthogonal component from the real component. The transient is longer than a quarter-cycle when a reactive load is suddenly connected. This is due to the error across the quarter-cycle delay propagating between the inverter output and the controller as the system returns to the steady-state.

6.10 FFT analysis

The inverter output current and voltage waveform harmonic composition is analysed using an FFT (Fast Fourier Transform). The voltage and current waveforms have harmonic distortion as evident from Figures 6.31 and 6.32. The THD of output voltage is 1.67%, the THD of the output current is 1.23% under a load of 2500W. The results here show a reduction of harmonics when compared with the approach taken in [110, 111]. [110] shows a Table giving the harmonics to the 9th harmonic orders only, the sum of harmonics values presented is equal to 3.38%. [111] shows the THD at 4.80%. Other references such as [107,108,109,117] do not present FFT analysis.

Figures 6.31 and 6.32 show that there is no significant harmonic term of 2ω within the FFT analysis. As a result no significant 2ω harmonics term are associated with the proposed transformation stage.

The IEEE [29] recommends that the PV system output should have low current-distortion levels to ensure that no adverse effects are caused to other equipment connected to the system. Total harmonic current distortion shall be less than 5% of the fundamental

frequency current at rated inverter output [29]. Each individual harmonic shall be limited to the percentages listed in Table 6.2.

Table 6.2: [29] Distortion limits as recommended in IEEE Std 929.

Odd harmonics	Distortion limit
3 rd -9 th	< 4.0%
11 th -15 th	< 2.0%
17 th -21 st	< 1.5%
23 rd -33 rd	< 0.6%
Above the 33 rd	< 0.3%

From the above discussion it can conclude that the objective of proposed system has been achieved when operating in stand-alone mode.

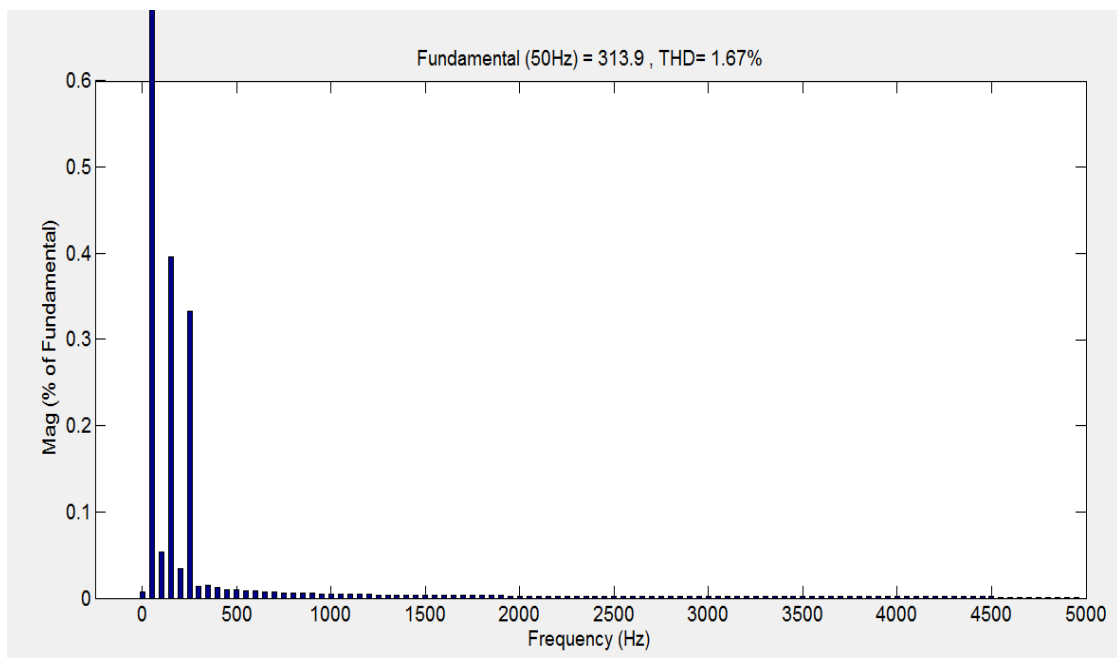


Figure 6.31: Inverter output voltage FFT harmonic analysis at load of 2500Watt.

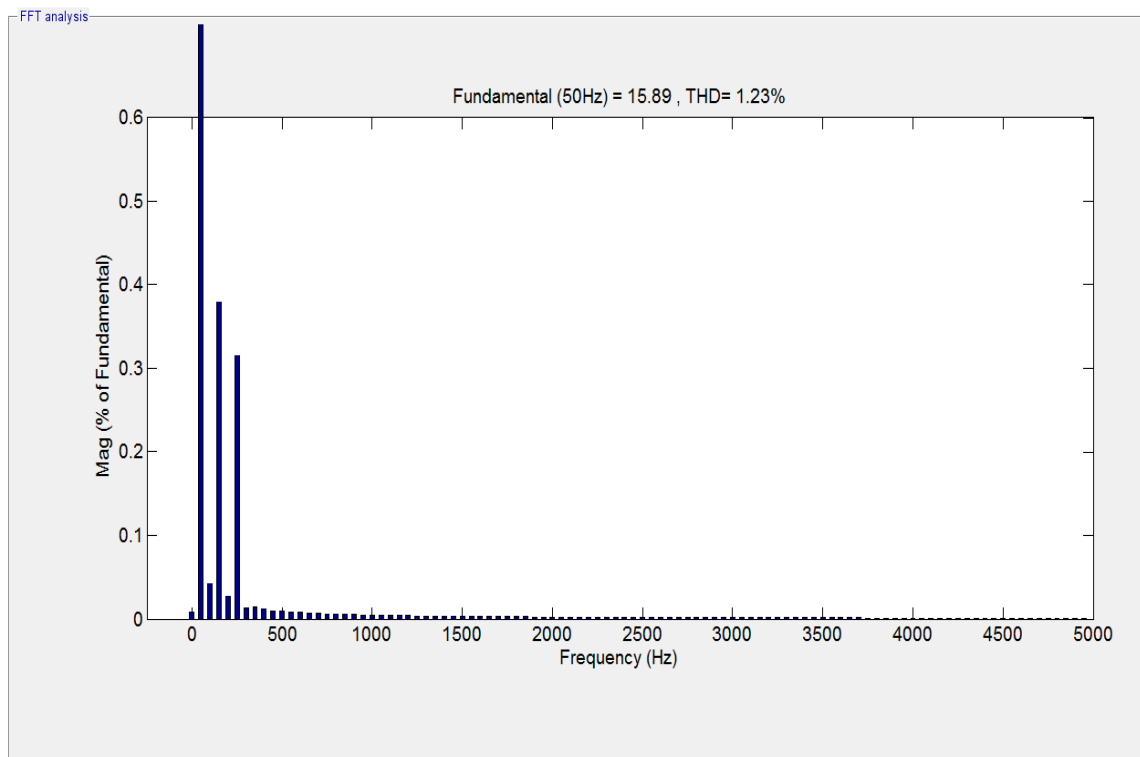


Figure 6.32: Inverter output current FFT harmonic analysis at load of 2500Watt.

6.11 Nonlinear Load Test

The single-phase inverter was simulated operating into a nonlinear load. A single-phase diode bridge rectifier was connected to the output of the single-phase inverter. The rectifier has a 1000uF filter capacitor and a 10mH filter inductor with a resistive load stepped from 250 Watt to 500Watt at 0.2 sec. The results depict the system responses when this common type of non-linear load with a high crest factor is connected. Figure 6.33 shows the inverter output current. Harmonic content analysis of the output voltage is shown in Figure 6.34, where the THD of the output voltage is 3.38%.

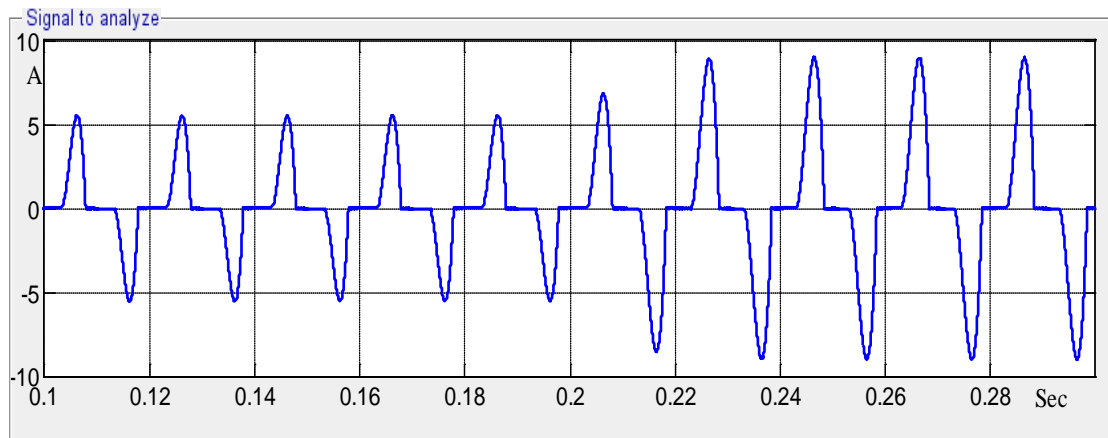


Figure 6.33: Inverter output current powering nonlinear load stepped from 250 Watt to 500Watt at 0.2 sec.

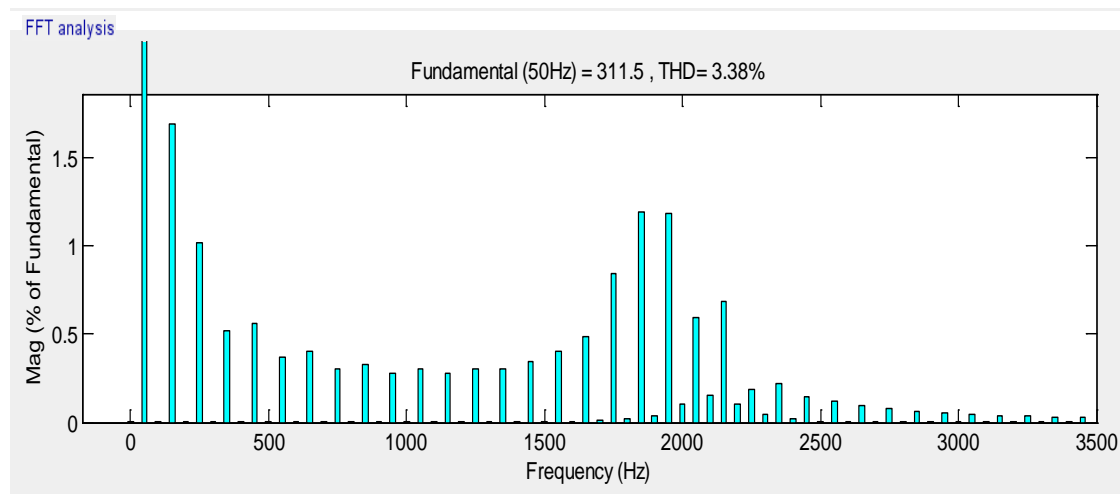


Figure 6.34: Harmonic analysis of inverter output voltage powering nonlinear load of 250 Watt.

6.12 Quarter Cycle Delay Stage Modification

In order to make the system more flexible and able to track the frequency within the limit, the first step in feedback loop (creating an imaginary orthogonal component from the real component, Stage 1. Figure 6.10) is further developed. Figure 6.35 gives the details about this improvement.

The input for the sample period is specified at 20 KHz. The number of samples per cycle for one fundamental frequency (50 Hz) can be calculated as follows:

Sampling number per cycle = sampling frequency / fundamental frequency

The quarter sampling number per cycle = Sampling number per cycle /4

The variable integer delay block (Figure 6.35) delays the discrete-time input at its input by the integer number of sample intervals specified.

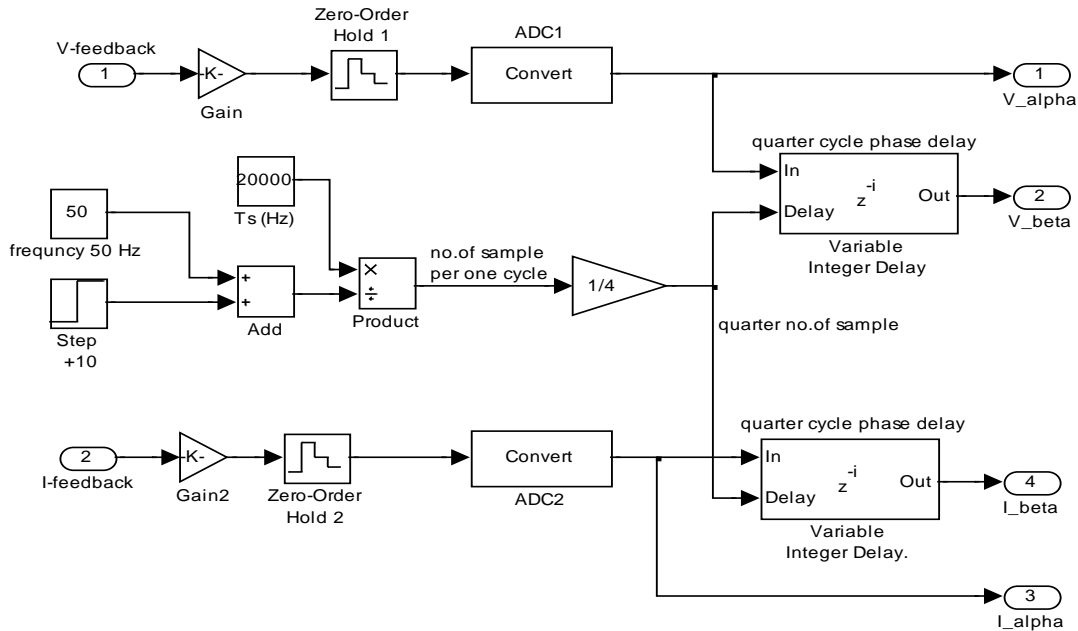


Figure 6.35: Quarter cycle number of samples per cycle delay.

6.13 Grid-tied Inverter mode

While renewable energy systems are capable of powering houses and small businesses without any connection to the electricity grid, many customers prefer the advantages that grid connection offers. A grid-connected system allows customers to power homes with renewable energy during periods when the sun is shining. Any excess electricity produced is fed back into the grid. The electric utilities perform net metering, an arrangement where the excess electricity generated by grid-connected renewable energy systems is metered as it is fed back into the grid. Thus, the consumer will pay only for the

difference between what was used and what was produced, and be reimbursed for any feed-in to the grid. Figure 6.36 shows the grid-tied inverter circuit diagram in which the common coupling point is represented by node A.

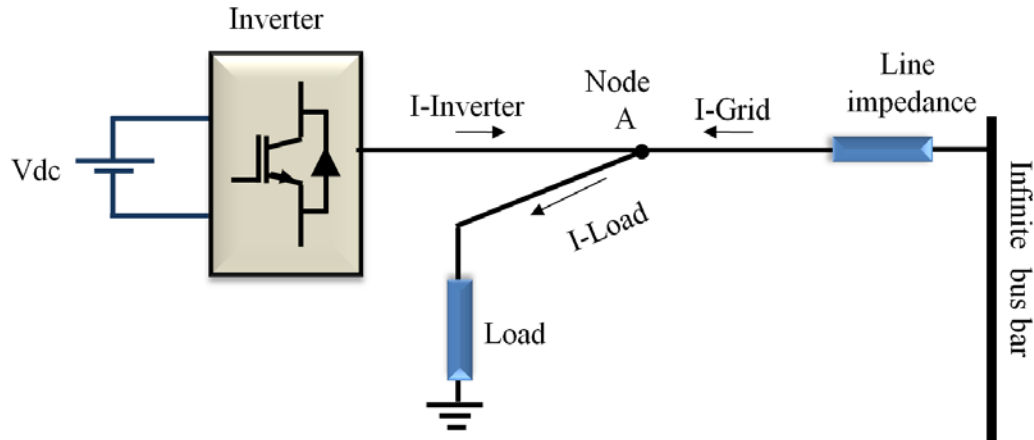


Figure 6.36: Grid-tied inverter circuit diagram.

6.14 The Grid-tied Inverter Model

The single-phase voltage-source inverter and the grid are modelled in the synchronous rotating reference frame as two voltage-sources. The passive filter is placed between them, Figure 6.37. The continuous-time state equation for the grid-tied inverter in the d - q coordinate system is.

$$\begin{cases} u_d(t) = L \frac{di_d(t)}{dt} - \omega L i_q(t) + R i_d(t) + e_d(t) \\ u_q(t) = L \frac{di_q(t)}{dt} + \omega L i_d(t) + R i_q(t) + e_q(t) \end{cases} \quad (6.29)$$

where $u_d(t)$ and $u_q(t)$ are the control signals components in the d - q frame respectively, $e_d(t)$ and $e_q(t)$ are grid voltage in the d - q frame respectively, R is equivalent line resistance, L is equivalent line inductance. To model the closed loop system, the grid-tied model is represented as a state equation.

$$\frac{d}{dt} \begin{bmatrix} i_d(t) \\ i_q(t) \end{bmatrix} = A \begin{bmatrix} i_d(t) \\ i_q(t) \end{bmatrix} + B_u \begin{bmatrix} u_d(t) \\ u_q(t) \end{bmatrix} + B_e \begin{bmatrix} e_d(t) \\ e_q(t) \end{bmatrix}$$

where the matrix definitions are given by

$$A = \begin{bmatrix} -R/L & -\omega \\ \omega & -R/L \end{bmatrix}, \quad B_u = \begin{bmatrix} 1/L & 0 \\ 0 & 1/L \end{bmatrix}, \quad B_e = \begin{bmatrix} -1/L & 0 \\ 0 & -1/L \end{bmatrix}$$

The state-space discrete time model is represented by

$$X(k+1) = FX(k) + G_u(k)$$

where the matrix is represented by

$$F = (SI - A)^{-1} \text{ and } G_u = -G_e = \int_0^{T_s} F d\tau B_u$$

The voltage and current vector controller operates in discrete time. The discrete time state equation of grid-tied model is represented as.

$$\begin{bmatrix} i_d(k+1) \\ i_q(k+1) \end{bmatrix} = F \begin{bmatrix} i_d(k) \\ i_q(k) \end{bmatrix} + G_u \begin{bmatrix} u_d(k) \\ u_q(k) \end{bmatrix} + G_e \begin{bmatrix} v_d(k) \\ v_q(k) \end{bmatrix} \quad (6.30)$$

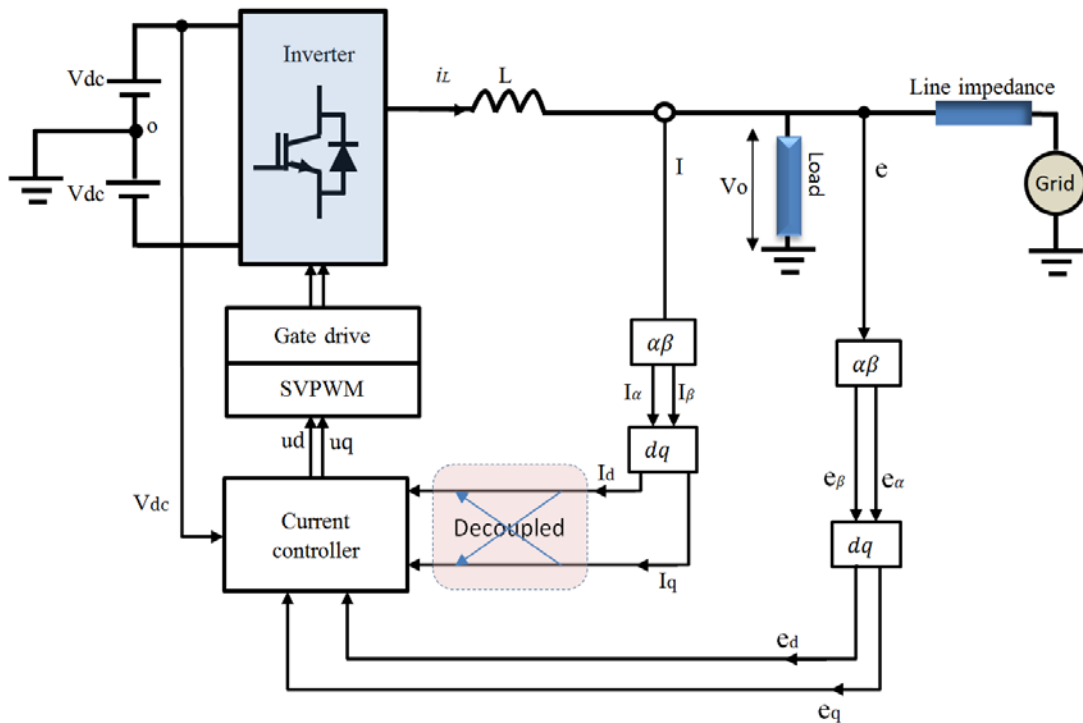


Figure 6.37: Grid-tied inverter circuit diagram.

The sampling frequency is selected so that the grid dynamics are significantly below the Nyquist limit associated with the inverter sampling frequency. So, considering v_d and v_q to be constant during one sample period:

$$\begin{aligned} v_{d,k} &\cong v_{d,k-1} \\ v_{q,k} &\cong v_{q,k-1} \end{aligned} \quad \left. \right\}$$

the above assumption leads to:

$$\begin{aligned} u_{d,k} &= L \frac{i_{d,k} - i_{d,k-1}}{T_s} - \omega L \left(\frac{i_{q,k} + i_{q,k-1}}{2} \right) + R \left(\frac{i_{d,k} + i_{d,k-1}}{2} \right) + e_{d,k-1} \\ u_{q,k} &= L \frac{i_{q,k} - i_{q,k-1}}{T_s} + \omega L \left(\frac{i_{d,k} + i_{d,k-1}}{2} \right) + R \left(\frac{i_{q,k} + i_{q,k-1}}{2} \right) + e_{q,k-1} \end{aligned} \quad \left. \right\} \quad (6.31)$$

In order to achieve high dynamic performance, ‘dead-beat’ gain (the ‘dead beat’ can be achieved when the input signal must be applied to a system in order to bring the output to the steady-state in the smallest number of time steps.) is used in the controller. Within one sampling interval, the current at the sample instant k equals the current at the sample instant $k - 1$ thus:

$$\begin{aligned} i_{d,k} &\cong i^*_{d,k-1} \\ i_{q,k} &\cong i^*_{d,k-1} \end{aligned} \quad \left. \right\}$$

which results in the proportional part of the PI controller given by (6.32), then simplified in (6.33).

$$\begin{aligned} u_{d,k+1} &= L \frac{(i^*_{d,k} - i_{d,k})}{T_s} - \omega L \left(\frac{i^*_{q,k} + i_{q,k}}{2} \right) + R \left(\frac{i^*_{d,k} + i_{d,k}}{2} \right) + e_{d,k} \\ u_{q,k+1} &= L \frac{(i^*_{q,k} - i_{q,k})}{T_s} + \omega L \left(\frac{i^*_{d,k} + i_{d,k}}{2} \right) + R \left(\frac{i^*_{q,k} + i_{q,k}}{2} \right) + e_{q,k} \end{aligned} \quad \left. \right\} \quad (6.32)$$

$$\begin{aligned} u_{d,k+1} &= \left[\frac{L}{T_s} + \frac{R}{2} \right] (i^*_{d,k} - i_{d,k}) - \omega L \left(\frac{i^*_{q,k} + i_{q,k}}{2} \right) + R i_{d,k} + e_{d,k} \\ u_{q,k+1} &= \left[\frac{L}{T_s} + \frac{R}{2} \right] (i^*_{q,k} - i_{q,k}) + \omega L \left(\frac{i^*_{d,k} + i_{d,k}}{2} \right) + R i_{q,k} + e_{q,k} \end{aligned} \quad \left. \right\} \quad (6.33)$$

The steady-state error can be constructed as sum of previous errors in the integral part of the PI controller, i.e. the steady-state current error can be equal to the sum of all the previous current errors, which results in:

$$\left. \begin{aligned} i_{d,k} &= \sum_{m=0}^{k-1} [i_d^*(m) - i_d(m)] \\ i_{q,k} &= \sum_{m=0}^{k-1} [i_q^*(m) - i_q(m)] \end{aligned} \right\}$$

As a result, the PI controller signals are given in (6.34).

$$\left. \begin{aligned} u_{d,k+1} &= k_p \{(i_{d,k}^* - i_{d,k}) + \frac{1}{T_i} \sum_{m=0}^{k-1} [i_{d,k}^*(m) - i_d(m)]\} - k_c \left(\frac{i_{q,k}^* + i_{q,k}}{2} \right) + e_{d,k} \\ u_{q,k+1} &= k_p \{(i_{q,k}^* - i_{q,k}) + \frac{1}{T_i} \sum_{m=0}^{k-1} [i_{q,k}^*(m) - i_q(m)]\} + k_c \left(\frac{i_{d,k}^* + i_{d,k}}{2} \right) + e_{q,k} \end{aligned} \right\} \quad (6.34)$$

$$\text{where } k_p = \frac{L}{T_s} + \frac{R}{2}, \quad k_c = \omega L, \quad T_i = R / \left(\frac{L}{T_s} + \frac{R}{2} \right)$$

6.15 Summary

This chapter focuses on the inverter controller strategy using a synchronous rotating reference frame. In addition this chapter discusses the system performance and the control structure within the stand-alone inverter.

The proposed transformation and control strategy offers certain advantages such as:

- A fast, simple d - q transformation.
- No harmonics term 2ω associated with the transformation stage. This can be concluded from FFT analysis and/or by comparing the voltage and

currents waveforms and d - q components with [110, 111, 112]. The reason which it creates 2ω harmonics term is clear in [116] (Chapter 4, section 4.6).

- The new transformation strategy overcomes the computational burden by using functions that are not computationally intensive. As a result, the system can be implemented with a low-cost fixed-point DSP. The feedback signals are transformed from stationary to rotating reference frames without using trigonometric function computation (in the DSP application the trigonometric function calculation can be time consuming if extreme accuracy is required).
- In [61, 117, 118, 108, 109, 111], the feedback signals are returned to the stationary frame in order to apply PWM. This creates additional computational burden. This study proposes SVPWM to avoid this step.

The proposed control strategy is able to operate with a stand-alone inverter. It assumes the input DC-link to be constant over one fundamental period of the power line frequency. The orthogonal components of current are decoupled as a result of the decoupling terms. For testing, the controller was exposed to transient conditions under a range of operational conditions, e.g. sudden load change, poor power factor load, nonlinear loads, with the load changes occurring under a wide range of resistive and inductive values.

The results are shown as quadrature representations in the rotating reference frame as well as the AC voltage and current waveforms. The dynamics of the system were examined at the instant of sudden load change to determine the transient response. In the steady-state conditions, the contribution to the current THD has been addressed, and low

distortion has been achieved compared to other relevant publications in this area. The results point out the applicability of the proposed control scheme to the stand-alone mode.

Finally, the results suggest further development is required for the grid-tied inverter mode. The single-phase voltage-source inverter and the grid are modelled in the synchronous rotating reference frame as two voltage-sources; the passive filter is placed between them. The closed loop system in grid-tied model is represented as a state equation. This mode has two useful properties to be explored in the context of a grid-tied inverter:

1. Grid parameter estimation, which calculates the amplitude and frequency of the grid voltage at the common coupling point.
2. The droop control scheme, which uses these parameters to inject independently-controlled active and reactive power to the grid. This is to be discussed in the chapter 8.

For the purpose of grid synchronisation, a phase locked loop (or similar) is required. The grid-tied scenario will be developed in chapters 7 and 8.

Chapter 7

INFLUENCE OF PHOTOVOLTAIC POWER SOURCES ON INVERTER

DESIGN

7.1 Introduction

The chapter begins with a review of the processes involved in solar electricity production, and a study of photovoltaic inverter front-end requirements. The effect on inverter performance when sourced from PV renewable energy sources is also considered in this chapter. Inverter performance is examined using a DC source with a variable magnitude and source impedance. The main purpose of this chapter is:

1. To establish the requirements for the selection of DC-link capacitors and to determine the value required
2. To investigate the behaviour of the inverter controller taking into account the characteristics of the PV front-end DC-to-DC converter.
3. To study the inverter controller performance under non-linear DC source voltage fluctuation.
4. To demonstrate how small-scale PV systems behave when integrated with a network and how they make a significant contribution to the total power generated within the network.
5. To aid development of an appropriate controller for such PV systems when connected to the network.

7.2 Environmental Characteristics of PV Module

The solar cell is a passive device. It generates electrical power as a function of solar radiation and ambient temperature. The simple solar cell equivalent circuit is described in Figure 7.1. Figure 7.2 represents a MATLAB/simulation model of a simple photovoltaic cell.

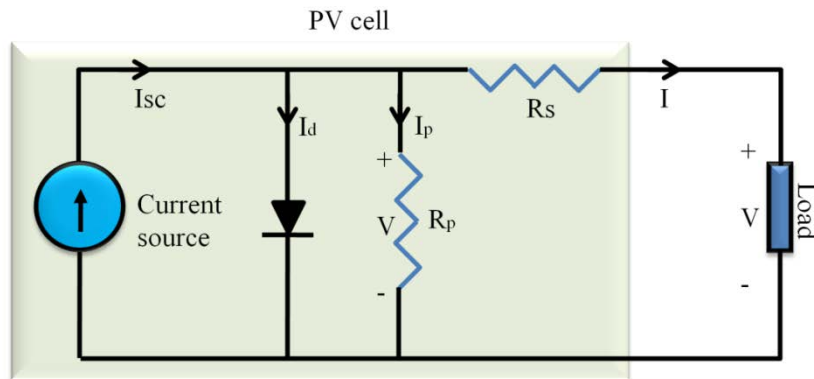


Figure 7.1: Solar cell equivalent circuit.

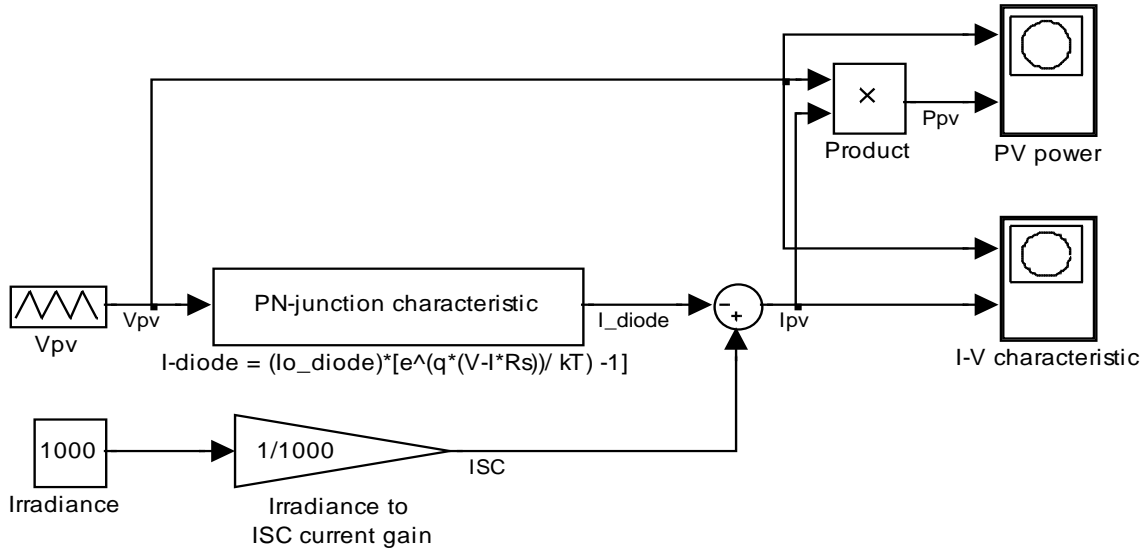


Figure 7.2: MATLAB/SIMULINK model of simple photovoltaic cell.

A MATLAB/SIMULINK model of a PV module is built up as shown in Figure 7.3 by using references [122, 123]. Figure 7.4 shows the details of the PV module model thus obtained. It is configured to provide voltage-current and voltage-power characteristics at

different values of solar irradiance. A module or panel consists of a number of individual cells interconnected and housed in a single package. It is possible to achieve a wide range of voltage and current outputs, depending on how the individual cells are connected together. A single module as used in typical residential applications produces around 200 watts of power [122, 123]. The model parameters were extracted from a cell at standard test conditions (1kW/m^2 , 1.5 AM, 25°C) (see Appendix C). A factor of 36 represents the number of PV cells connected in series in this module. When 36 PV cells producing around 0.6 volts are connected in series, the result is a 22-volt module.

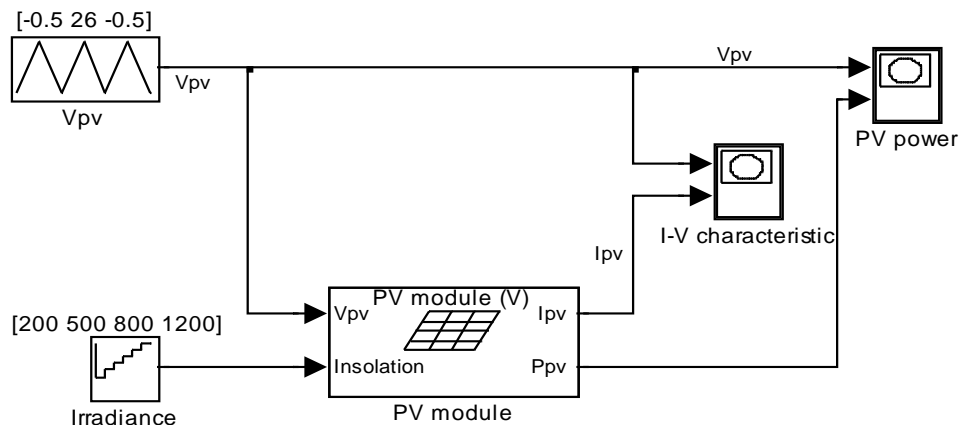


Figure 7.3: PV model with variable irradiance values.

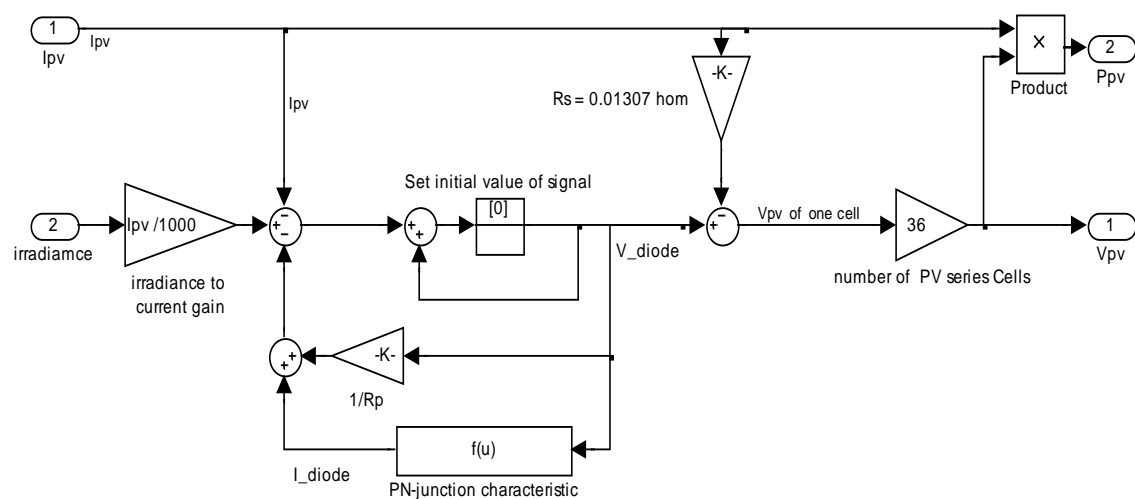


Figure 7.4: MATLAB/SIMULINK Details of PV module model.

Figures 7.5 and 7.6 show the PV module I-V and P-V characteristics at the terminals of the cell at different irradiance levels respectively. Figure 7.5 shows that the I-V curve is non-linear. The I-V curve changes position with the irradiance level. As a result, the power delivered by the PV module varies in value with irradiance, (Figure 7.6).

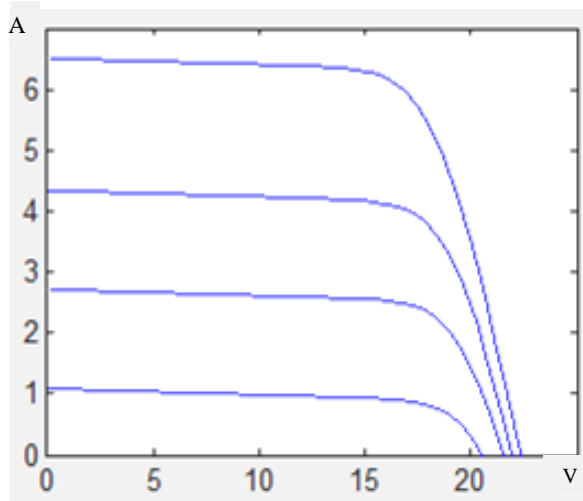


Figure 7.5: PV module I-V characteristics at different irradiance level.

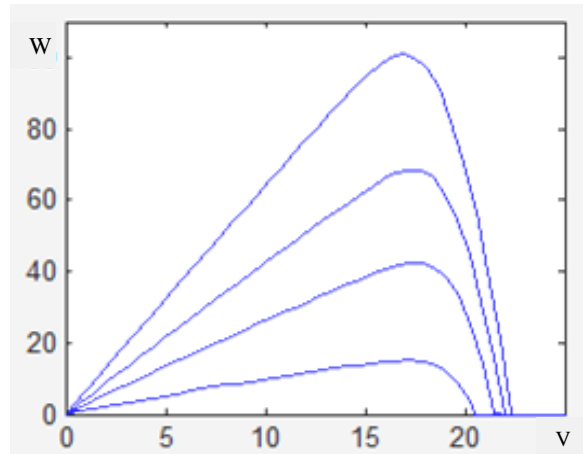


Figure 7.6: PV module P-V characteristics at different irradiance level.

The above figures show that:

1. The PV module is an electrical energy source; used to directly convert sunlight into electrical power. It generates electrical power as a function of irradiation level.

2. The relationship between irradiation (sunlight), voltage, current and output power is non-linear.
3. The maximum power operating point is close to the knee area in the I-V curve.
4. The maximum power output (MPP) from the PV module is not constant and changes with irradiance and temperature. The control system must therefore track the MPP continuously in order to ensure the module always provides maximum power.
5. It must be noted that the converter control system aims to keep PV module output power at the varying maximum power point in real time.

7.3 PV System Structure

As described above, the output characteristic of the PV module depends on irradiance and temperature. This means that further processing must be carried out (Figure 7.7).

The PV array output voltage is not a fixed value. The inverter requires a DC-link voltage value higher than inverter AC peak voltage (i.e. for 220V inverter AC output voltage, the DC-link voltage should be higher than $220 * \sqrt{2} = 311V$). Therefore, the PV array output voltage must be stepped up using some form of boost converter, Figure 7.7.

The boost converter is a step-up converter with an output voltage greater than its input voltage. The boost converter duty cycle is modulated by the maximum power point control algorithm to match the output power at the point $dp/dv = 0$, where p and V are the power and voltage supplies by PV array respectively.

The boost converter diode additionally serves as a blocking diode to avoid reverse current flowing to the source side.

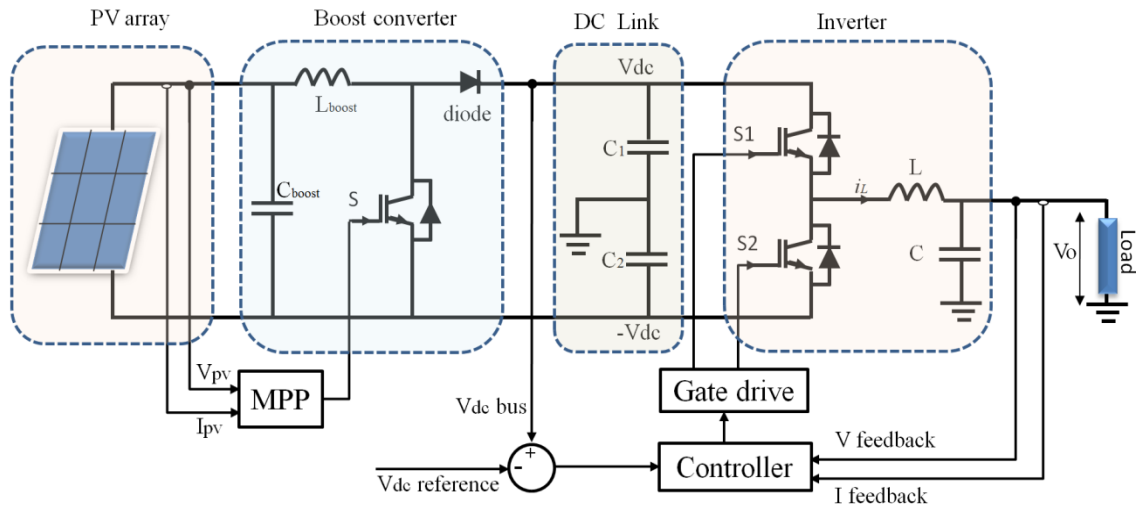


Figure 7.7: PV system scheme.

Since the boost converter is controlled by an MPP algorithm, the PV array and boost converter work together as a time-varying non-linear DC power source. It is necessary to include a DC-link capacitor between the PV system front-end source and the inverter. The capacitor is normally added to the output of the boost converter to limit ripple on the output DC-link voltage, and to support the load when the boost diode is in the OFF state. The larger the capacitor, the lower the output voltage ripple will be. However the system transient response will be slower and the capacitor cost will increase.

The inverter controller is designed to regulate the power supplied by the inverter in order to ensure the DC-link voltage does not drop below the minimum required for the inverter to be able to supply the peak output voltage.

The PV system converter and inverter must guarantee safe and efficient operation. The conversion and regulation elements are sometimes termed ‘power conditioning’ elements.

7.4 Voltage Balancing across Split Capacitors in a half-bridge Inverter

This section discusses the effect of the switching strategy on voltage balancing across split capacitors in a half bridge inverter. The capacitor voltage balance is dependent upon the equilibrium of the volt-second products during the charge and discharge cycles of each capacitor. This minimizes the likelihood of D.C. components being injected into the inverter output.

The single-phase half bridge applications require switching devices rated for the full DC-link voltage. The voltage across the DC-link capacitors can be self-balancing because the average current drawn from the positive and negative DC-link capacitors over a modulation cycle is the same and the neutral point potential remains constant.

Figure 7.8 shows a half-bridge inverter consisting of semiconductor switching devices (S_1 and S_2) with anti-parallel diodes (d_1 and d_2) respectively. This is supplied from a DC voltage-source split by the two DC-link capacitors C_1 and C_2 . The inverter load consists of resistance R and inductance L . Figure 7.9 describes the inverter circuit states within one switching cycle.

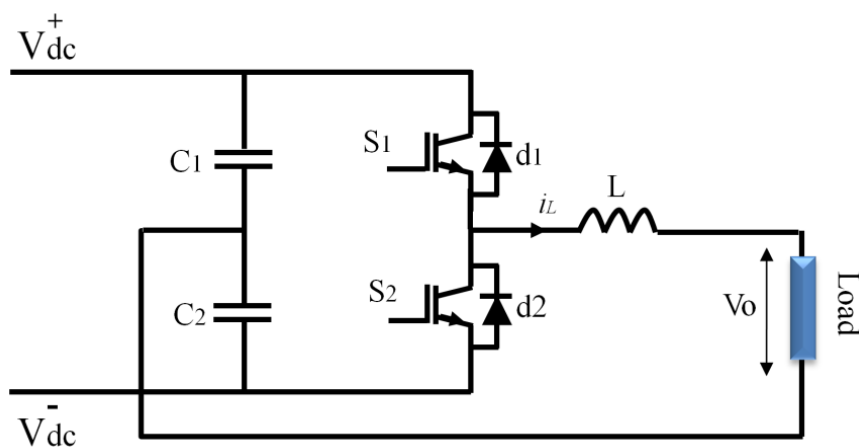


Figure 7.8: DC-link capacitors in the half bridge inverter.

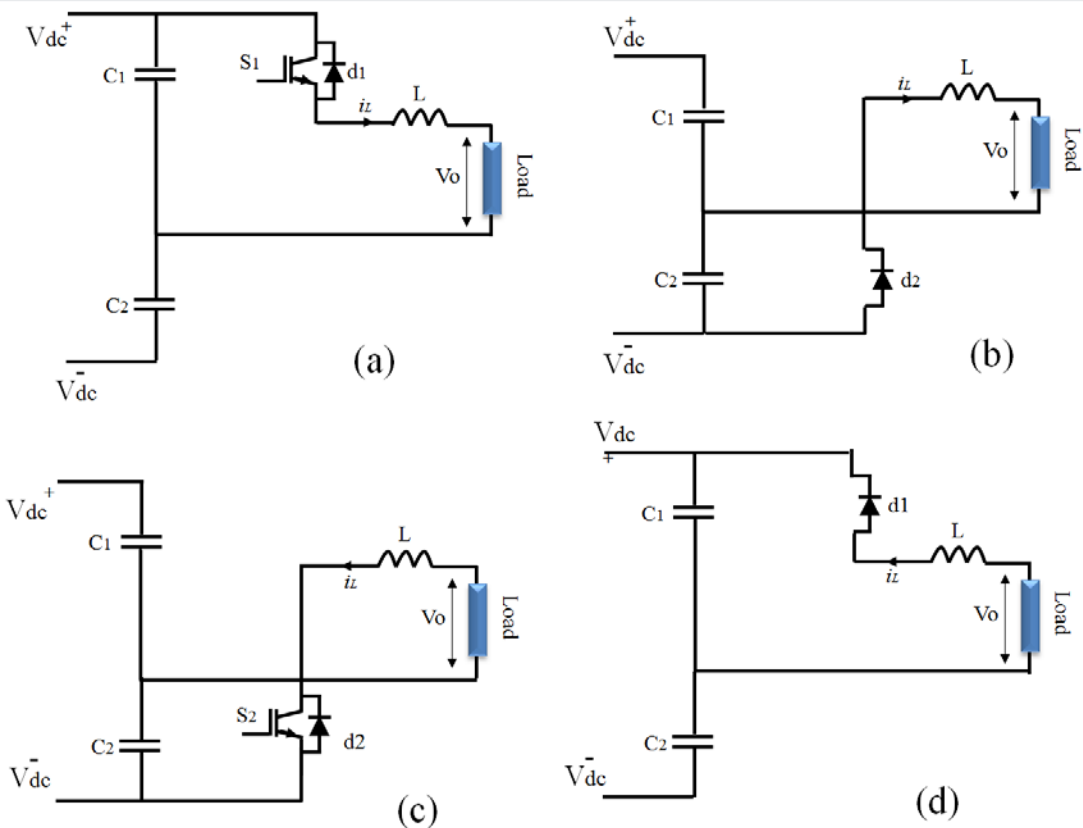


Figure 7.9: Inverter circuit operating sequences within one switching cycle.

7.5 Inverter Input and Output Instantaneous Power

The inverter output voltage, current, and power is shown in Figure 7.10. The instantaneous power oscillates with twice the line frequency.

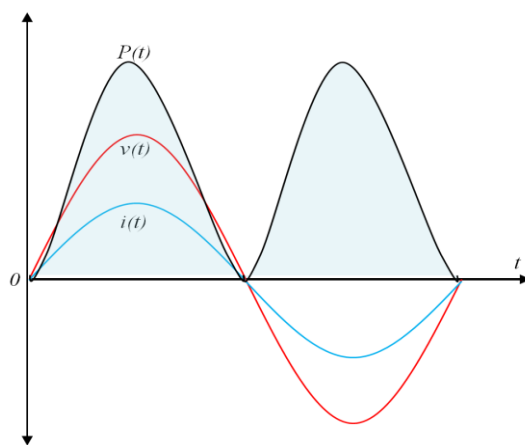


Figure 7.10: The power oscillates with twice line frequency in single-phase systems.

This oscillation in the power on the grid side leads to ripple at twice the line frequency, as follows:

$$P(t) = v(t) \cdot i(t) \quad (7.1)$$

$$P(t) = V \sin(\omega t) \cdot I \sin(\omega t) \quad (7.2)$$

$$P(t) = V \cdot I \sin^2(\omega t) \quad (7.3)$$

$$P(t) = V \cdot I [1 + \sin(2\omega t)] \quad (7.4)$$

As a consequence, in single-phase grid-tied PV systems applications the actual power injected into the grid consists of power pulses of twice of the fundamental frequency. On the other hand, due to the fact that with the exception of the DC-link capacitors the inverter is constructed without energy storage components, the inverter input and output instantaneous power are in equilibrium over a period of time (inverter input power = inverter output power, assuming 100% power conversion efficiency). As a consequence, power pulses at the inverter output side will be reflected at the inverter input side according to 7.5 (neglecting losses).

$$V_{dc} I_{dc} = V_{inv} I_{inv} \quad (7.5)$$

$$I_{dc} = \frac{V_{inv} I_{inv}}{V_{dc}} \quad (7.6)$$

This ripple can affect the single-phase PV system front-end and cause it to deviate from the MPP within a single cycle at the fundamental power frequency. Therefore, the DC-link capacitors must be sized to provide sufficient smoothing of the power flow from PV array front-end to the inverter so as to limit this ripple.

7.6 Utility Interfacing Requirements

The numbers of grid-interactive PV system installations are increasing. Distributed PV systems are making a significant contribution to the power balance in some utility networks.

Grid interactive small-scale PV systems for use in domestic dwelling applications have prescribed specifications [124,125]. The interconnection with the utility involves bidirectional flow of energy. Such PV systems can affect the stability of the utility network and energy distribution systems. Integration issues need to be addressed from two sides, the PV system side and the utility side.

Such PV systems can be connected to the utility only with agreement between the consumer and the utility company, including the maintenance of various safety standards during the connection [124-127]. The general requirements defined by the grid can be summarised as follows [29,124,126, 127]:

1. Inverters are compulsory in grid-connected PV systems.
2. Inverters must be able to detect an islanding situation.
3. Inverters must inject only sinusoidal currents into the grid.
4. Saturation of the distribution transformers must be prevented; by following the standards for allowable amount of injected DC current into the grid.
5. The standard limits of DC current injected into the grid are rather small (e.g. 0.5% and 1.0% of rated output current) [29].
6. Safety of utility workers must be maintained.
7. PV systems should never energize a dead line (or locked out line)

8. A lockable outdoor disconnect switch (accessible to utility personnel) is essential.
9. The systems must essentially operate at unity power factor.
10. An inverter must detect utility fault conditions and disconnect itself within two [126] to five seconds [127].

7.7 The Revenue from Residential Grid-Tied PV Systems

Residential grid-tied PV systems are classified as having a capacity of less than 10 kW, which can meet the load of most consumers. Excess power can be fed back to the grid. The power feed to the grid is metered to monitor the amount of energy transferred. Thus, power drawn from or supplied to the grid will be the balance of electricity generated by PV system and electricity consumed by the loads in the home. A typical case is when the resident moves out of the home on holiday, the power produced by PV system will exceed the demand. The excess generated power can thus yield profit for the consumer as it then can be sold to the grid. [124,125]. Grid-interactive PV systems give users more choice and greater flexibility such as:

- A grid-tied PV system will reduce the energy bill as it is possible to sell excess electricity produced to the local network.
- Grid-tied PV systems do not require a battery and are relatively easy to install.

The cost of PV electricity production is several times more expensive than conventional power. Therefore, the conversion efficiency becomes dominant in the economy of the total PV system.

7.8 Requirements arising from the PV array interface

The operating voltage of the PV array varies as a result of periodic scanning of the I-V curve by the MPPT algorithm. The maximum power point of PV array is determined and the operating voltage is adjusted to the corresponding voltage level. The voltage level is adjusted by the DC-to-DC converter.

There is a relationship between the amplitude of the voltage ripple and the MPPT. Therefore, the DC-link storage capacitors are sized such that the converter can operate around the MPP without excessive fluctuation in the DC-link voltage.

7.9 DC-Link Capacitor Calculation

The DC-link energy storage elements can be used to limit fluctuations in the input power drawn by the inverter by limiting fluctuation of the voltage at the DC side of the inverter. Variations of DC-link capacitor voltage should be minimized to ensure that the inverter can produce a peak AC output voltage without generating undue harmonic distortion due to voltage clipping.

The size of capacitors should be such that the capacitors can store maximum instantaneous power in each switching cycle. The capacitor size determines the voltage ripple. The capacitance value to be designed in depends on the minimum ripple requirement on the output side. The half-bridge single-phase inverter output voltage equations can be derived from the main circuit in Figure 7.11, assuming that the inverter has ideal switches:

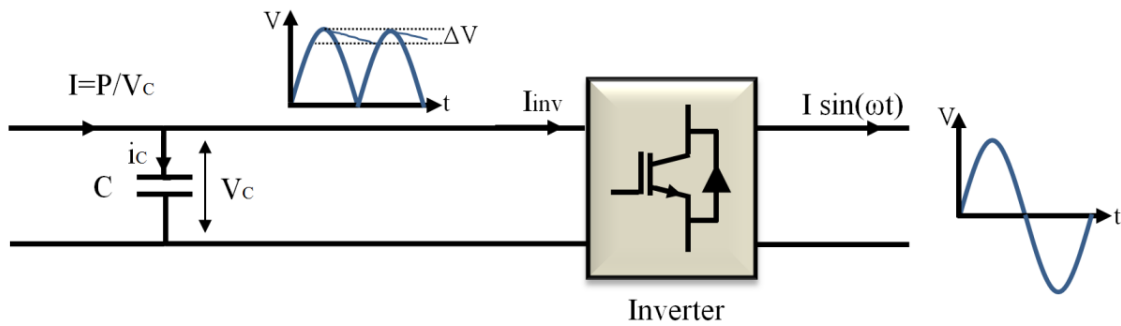


Figure 7.11: Schematic diagram of DC-link capacitor (or DC intermediate circuits are energy storage devices).

$$\Delta V = \frac{1}{C} \int i_c dt \quad (7.7)$$

where ΔV is allowable ripple voltage, i_c is capacitor current and C is the DC-Link capacitance value. The DC-Link capacitor value can be calculated as follows:

$$i_c = \frac{P}{V_c} - I \sin(\omega t) \quad (7.8)$$

$$\Delta V = \frac{1}{C} \int_0^{T/2} \frac{P}{V_c} - I \sin(\omega t) dt \quad (7.9)$$

$$\Delta V = \frac{1}{C} \left[\frac{P}{V_c} t + \omega I \cos(\omega t) \right]_0^{T/2} \quad (7.10)$$

As a result, the inverter DC-link capacitor is given in 7.11

$$C = \frac{1}{\Delta V} \left[\frac{P}{V_c} t + \omega I \cos(\omega t) \right]_0^{T/2} \quad (7.11)$$

$$C = 314 \mu F, \text{ At } P = 2500 W, f = 50 Hz, V_c = 370 V, \Delta V = 10 V.$$

7.10 Non-Linearity Caused By PV Source

This section presents some solutions to deal with the effects of the inverter front-end (DC side) in the PV system. Source non-linearity is an inherent phenomenon in PV systems, in contrast to a traditional solution for energy conversion using conventional generation. The non-linearity arises from the interface of power converters (due to ON/OFF switching actions) and the PV source (which generates variable power based on irradiation and temperature) and/or load. The DC-link voltage should be maintained as constant as possible. The DC-link frontend (PV array and boost converter) is represented as a non-linear power source to allow investigation of the performance of the proposed inverter as the inverter input power is changed in a controlled fashion.

In PV system applications the output power varies continuously due to changing environmental conditions. The boost converter with DC-link capacitors aims to provide a smooth voltage to the inverter. To model the characteristic of the PV array and boost converter, the following approach was adopted. The controlled current source block (CCS) converts the input signal into an equivalent current source. The generated current is driven by the input signal of the block. The controlled current source block is initialized with a specific DC current, Figure 7.12.

In order to address the problems caused by the non-linear PV source, the inverter controller makes use of a PI controller to allow the output of the front-end to be held at a constant DC voltage by regulating power flow between the front-end and the inverter. The inverter controller was developed with the DC input (feed-forward) regulation through the d-channel voltage control loop. The objective of this regulator is to maintain the DC-link

capacitor voltage close to the reference value by regulating the current (and hence power) injected into the mains.

The V_{bus} (or $2V_{dc}$) is scaled by 1/1000 and the reference signal (V_{dc_ref}) is set to 400/500. The inverter feed-forward loop is shown in Figures 7.12 and 7.13. When the PV output power changes, the V_{dc} feed-forward signal does not meet the desired demand voltage. As a result the reference signal (V_d_ref) will reflect the DC-link error and the inverter will alter the power flow into the output.

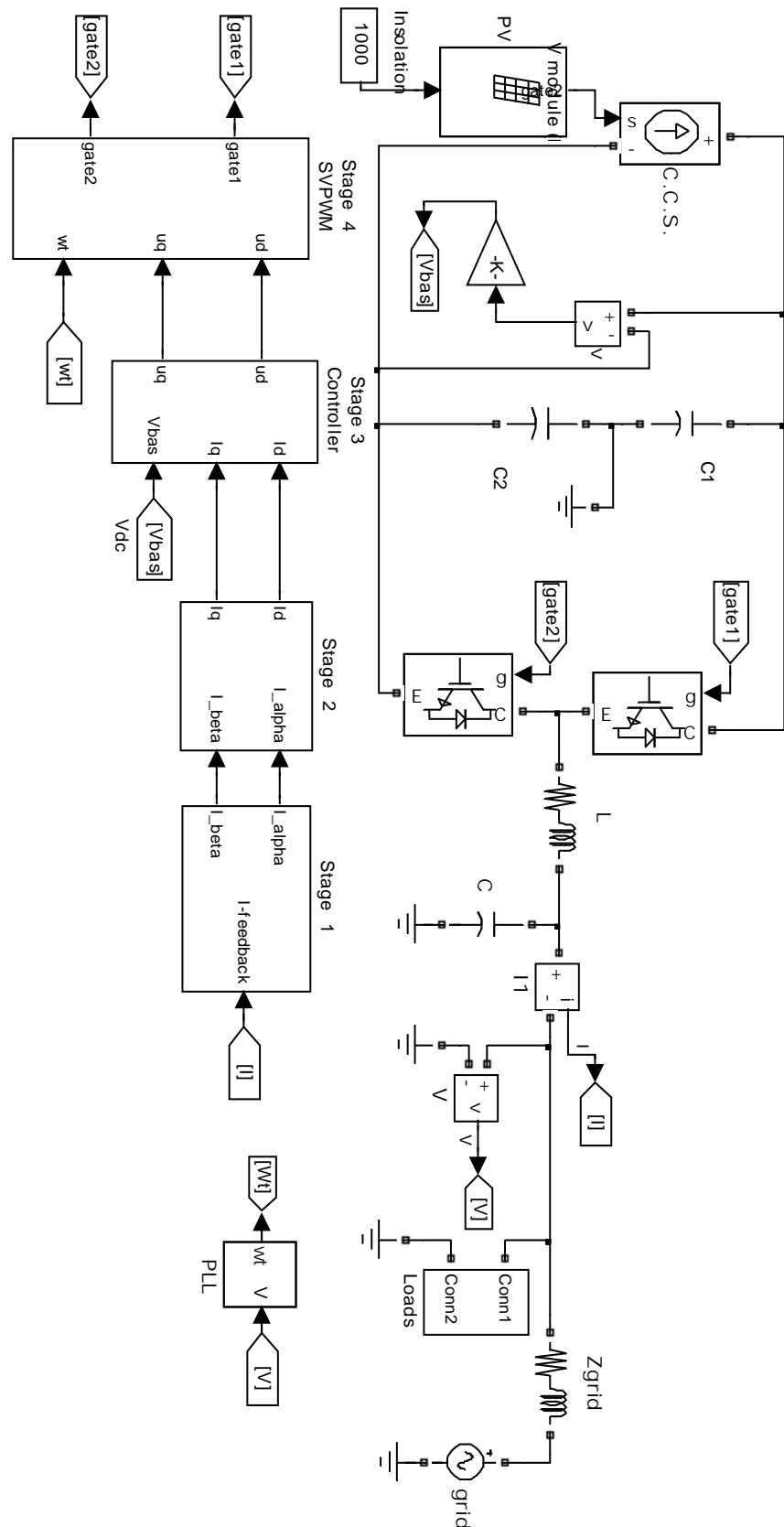


Figure 7.12: MATLAB/SIMULINK scheme of grid-tied PV system.

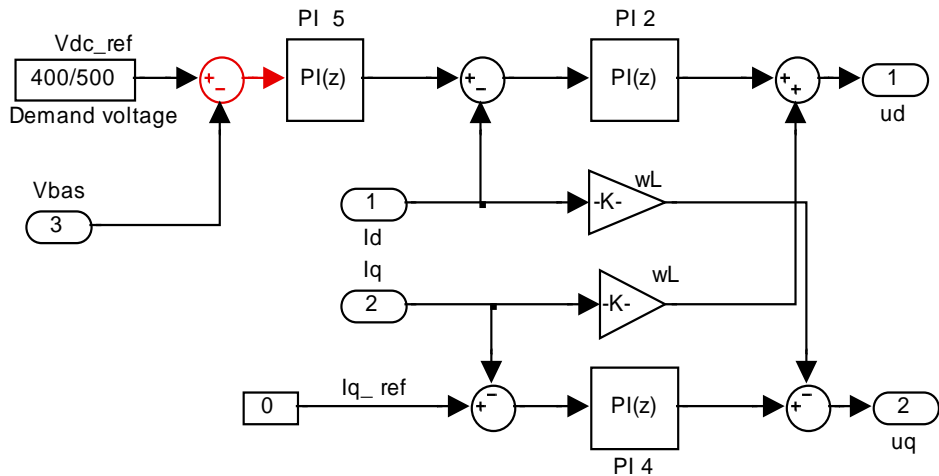


Figure 7.13: Grid-tied inverter controller block scheme with front-end.

Figure 7.13 shows the MATLAB/SIMULINK controller model. The system was developed further by taking into consideration the effect of a variable input power. If there is a considerable difference between the reference DC voltage and the measured DC voltage, this can result in an unacceptably high reference current being calculated by the controller.

7.11 Validation of the PV System Interactive With Utility Grid

The feedback and feed-forward control are employed to improve control of the AC output current waveform for the voltage-source current controlled inverter. The controlled variables are the system output voltage and current. The feed-forward control principle senses the change in input power to the system and compensates for its impact. To maximise the output power the front-end must be able to vary the PV array output voltage while the inverter maintains a fixed AC output voltage. Feed-forward control is introduced into the inverter to control the power flow.

The inverter current should be in phase with the grid voltage, which means that the power factor is unity. Accordingly, a phase-locked loop (PLL, Appendix C) is used to lock

to the phase and frequency of the grid voltage. The PLL is a critical function in grid-tied mode. It synchronizes the system output AC voltage to the grid voltage. Further information about the AC voltage (such as the peak magnitude and RMS values) must be determined by direct measurement of the instantaneous values, such as by sampling with an ADC. The proposed control strategy is intended to improve the power transfer and maintenance of array maximum power flow between inverter front-end and the inverter supplying the grid – to achieve this a feed-forward controller is used to regulate the DC-link voltage by generating an appropriate value for the reference current $I_{d\text{-ref}}$. Current supplied to the grid via the inverter tracks the reference current $I_{d\text{-ref}}$. The reference current is determined by the feed-forward controller, which is a PI controller acting on the DC-link voltage error, i.e. the difference between the DC-link voltage reference V_{dc_ref} and the measured DC-link voltage V_{bus} . The feed-forward controller is evident in the following blocks diagram of Figure 7.14.

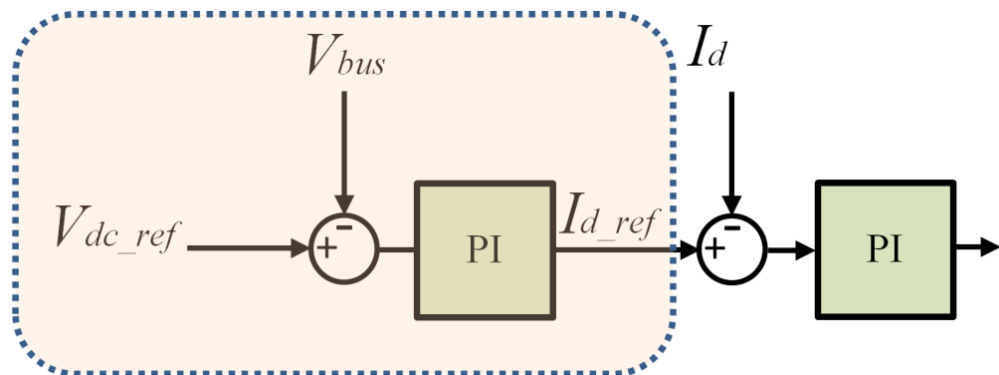


Figure 7.14: Feed-forward controller.

The feed-forward voltage loop PI-controller is designed so that the voltage rise time is 2ms: 10 times faster than the grid frequency. The desired phase margin φ is 45° .

The time constant ($T_{i,dc}$) of the voltage controller is calculated:

$$T_{i.dc} = \sqrt{\frac{1 + \sin \varphi}{\cos \varphi}} T_\alpha$$

$$kp = \frac{2 CV_{dc}}{\omega \sqrt{T_\alpha T_{i.dc}}}$$

where T_α is the design parameter time constant and C is the DC-link capacitor.

$$G_{PI,dc}(s) = k_{P,dc} \left(1 + \frac{1}{s T_{I,dc}} \right) = k_{P,dc} + \frac{k_{I,dc}}{s} \quad (7.12)$$

The DC feed-forward voltage controller is implemented using the backward difference discretization method, the discrete-time representation of the DC voltage controller can be written as:

$$u_{dc} = u_{bus}(k - 1) + k_{i,dc} T_s (u_{dc-ref}(k) - u_{bus}(k)) \quad (7.13)$$

The circuit parameters are summarized in table 7-1. The MATLAB/SIMULINK scheme of the grid tied PV system is shown in Figures 7.12 and 7.13

Table 7-1: Circuit Parameters.

Rated power	2.5kW
Nominal input voltage (V_{dc})	370V
Nominal output voltage (V_{ac})	220V RMS
Switching frequency (f_{sw})	20kHz
Fundamental frequency (f)	50Hz
Filter inductance (L)	3mH
Inductance resistance (r_L)	0.01 ohm
Filter capacitor (C)	1.5uF
Line impedance at grid side	0.64 ohm, 0.25mH
DC link capacitor (C_1 and C_2)	330uF
The switching elements are ideal IGBT antiparallel diode with internal resistance $R_{on}=1e-3$ ohms, and Snubber resistance $R_s=1e5$ Ohms	

7.11.1 Grid-Tied Inverter Load Sharing with Constant PV Power

The system was examined initially for its operating with a resistive load. In this case, the PV module maximum power level was fixed (2500W) and the front-end is tracking maximum power. Note that in this test the load is stepped from 500W to 3500W at the instant $t=0.1$ seconds. Figure 7.15 shows that the inverter current is in phase with common coupling point voltage. This means that the inverter is delivering active power all the time.

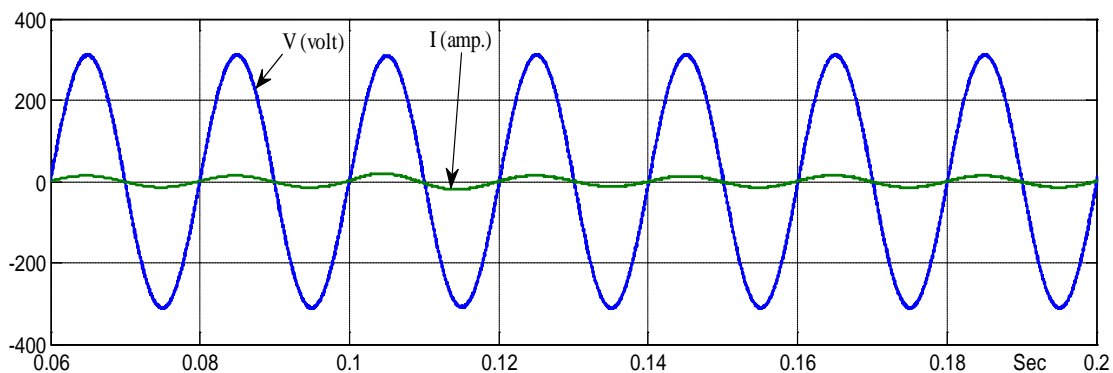


Figure 7.15: Inverter current against the common coupling point voltage.

Figure 7.16 shows the load, inverter, and grid currents distribution at the common coupling point. By comparing the current waveforms at common coupling point, the following observations can be made.

The inverter current waveforms show that the inverter active power delivery is greater than the load demand when the load is 500W (during the period from 0.06 seconds to 0.1 seconds). Therefore, the inverter not only provides power to the local loads but also feeds the remaining power to the grid. The grid input current waveform is sinusoidal and is 180° out of phase with the inverter and load currents (during the period from 0.06 second to 0.1 second). This situation means that the grid is receiving active power during this period.

At the instant $t=0.1$ seconds, the load is stepped from 500W to 3500W. The inverter active power delivery is now less than the load demand during the earlier period from 0.06 seconds to 0.1 seconds.

In this period, the grid current waveform is in phase with the inverter and load current waveforms. This situation means that the grid is now delivering active power to meet the remaining power requirements of the load that the inverter is unable to supply.

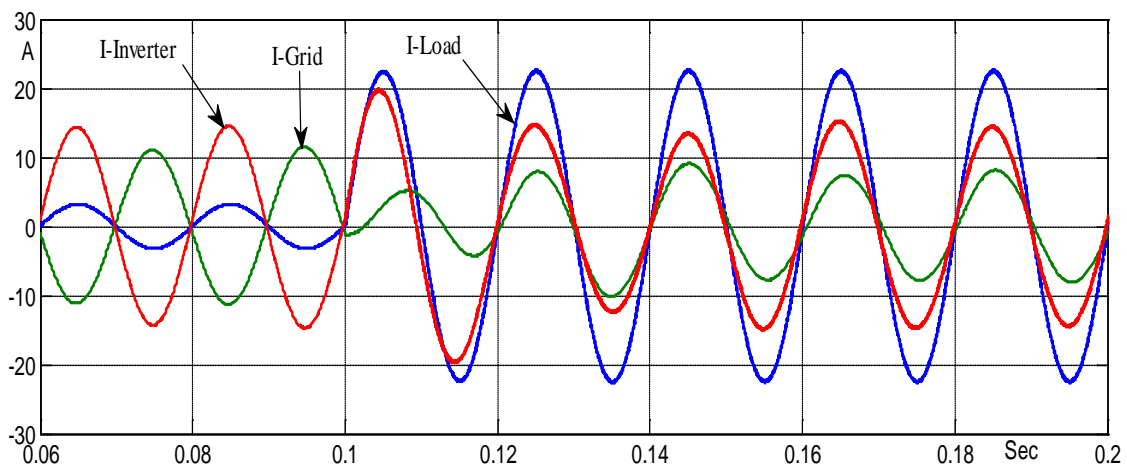


Figure 7.16: Inverter, load, and grid current waveforms at common coupling point when the load is stepped from 500W to 3500W at the instant $t=0.1\text{Sec}$.

In the second test, the load is then stepped to $1500 \text{ W} + 1000 \text{ VAr}$ at the instant $t=0.2$ seconds. Figure 7.17 shows that the inverter current is in phase with common coupling point voltage. Accordingly, the inverter continues to deliver continuous active power at an unchanged level at this time.

Figure 7.18 shows the load, inverter, and grid current distributions at the common coupling point. It can be noted that the load reactive power demands are imported from the grid. Figure 7.18 shows the reactive power implications on the grid current phase at the instant $t=0.1$ seconds, and this effect increases with the increasing reactive power demand by the local loads at $t=0.2$ seconds.

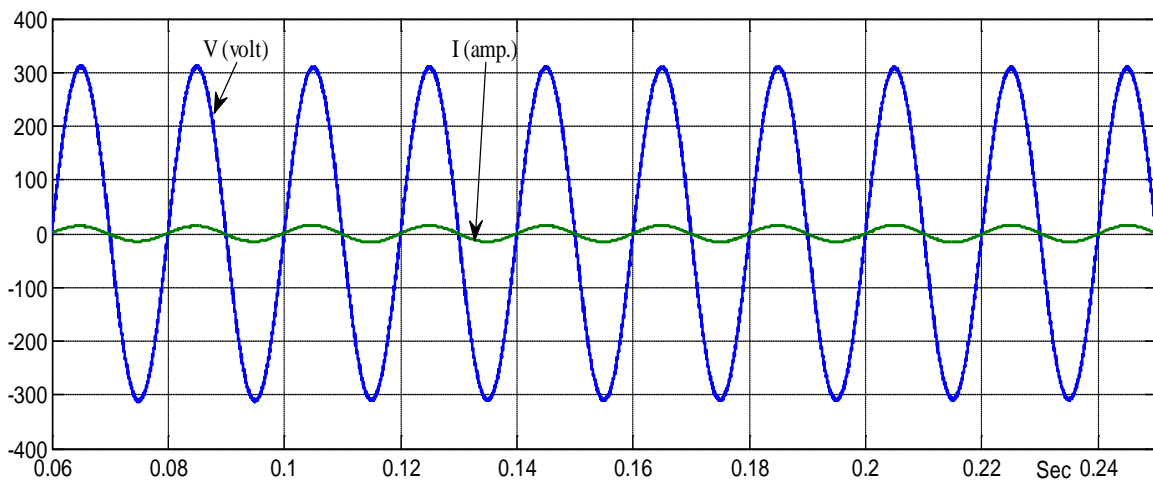


Figure 7.17: The common coupling point voltage and inverter current.

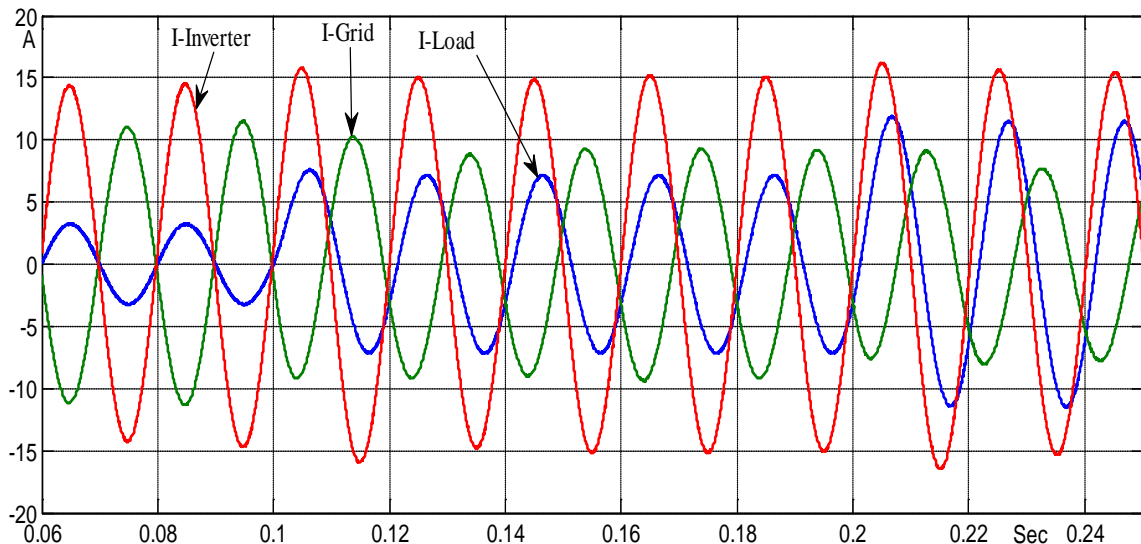


Figure 7.18: Inverter, load and grid current waveforms at the common coupling point when the load is stepped from 500W to the 1000 W + 500 VAr at t=0.1Sec., and then stepped to 1500 W + 1000 VAr at t=0.2 Sec.

Figure 7.19 shows the typical case when the building is unoccupied (for example when the resident moves out on holiday). The load power demanded by the home is at a much lower value (set at 50W in the simulation). The power produced by PV system is very much greater than the demand from the local loads and hence the bulk of the power produced is exported to the grid.

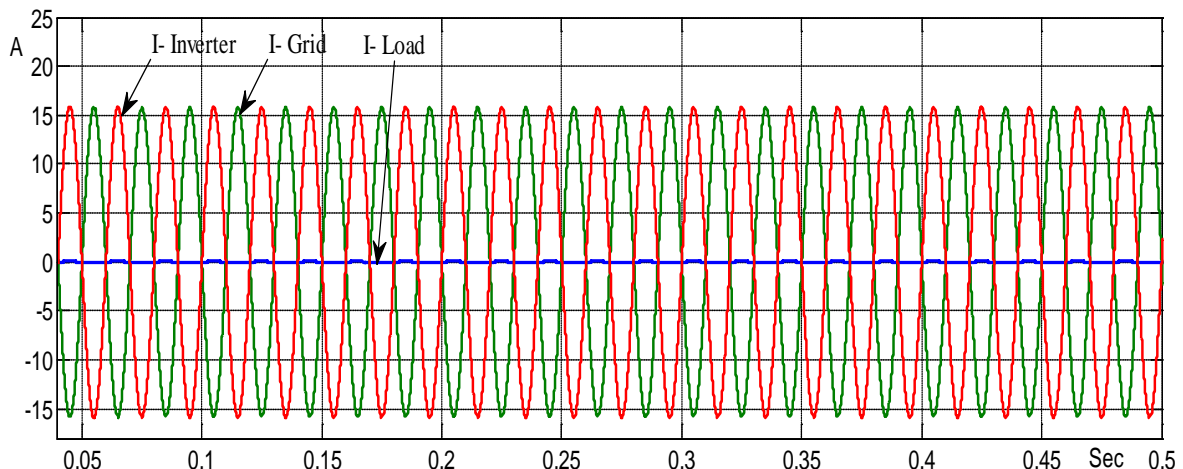


Figure 7.19: Inverter, load and grid current waveforms at common coupling point when the load is at a low value (50 Watt).

7.12 Grid-Tied Inverter Load Sharing with Input Power Dip

The controller has been validated in presence of a power dip (that would typically be caused by irradiation variations). The system was examined with a 2000Watt + 500VAr load and an input power dip. The inverter system as a power quality conditioner is thus tested with the input power dip (Figure 7.20).

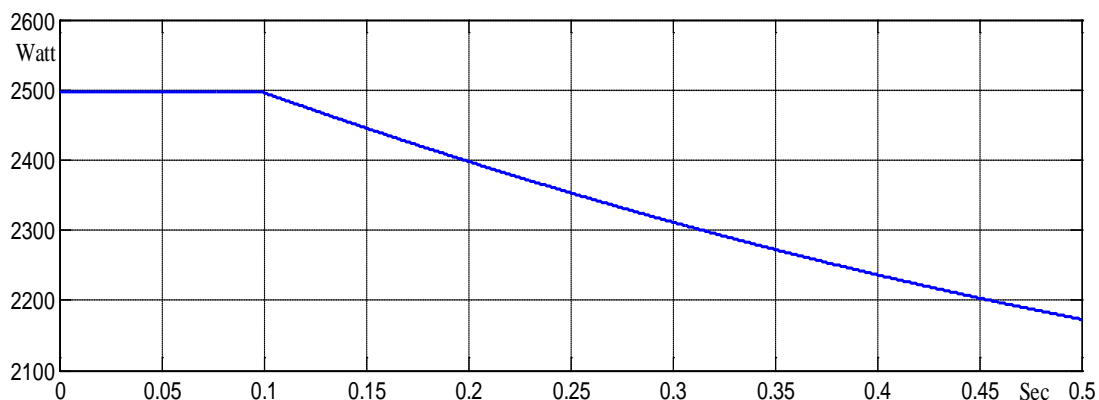


Figure 7.20: input power dip.

Figure 7.21 shows that the common coupling point voltage waveform is kept constant. The voltage feedback signal reflects the common coupling point voltage. Figure

7.22 shows that (except for the starting transient) the Vd and Vq voltage feedback signals are constant in value.

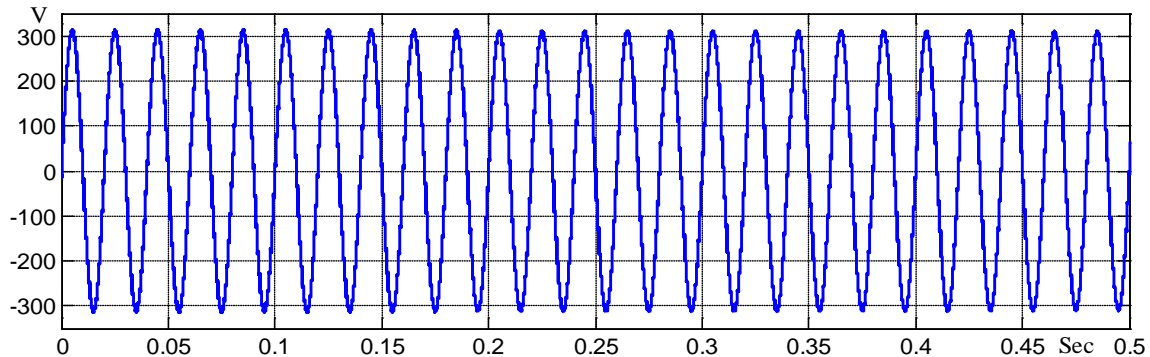


Figure 7.21: common coupling point voltage.

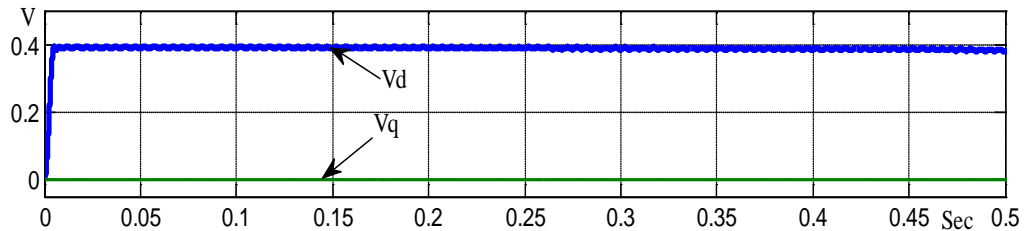


Figure 7.22: voltage feedback signal (Vd and Vq).

The load, inverter, and grid current divider at the common coupling point are shown in Figures 7.23 and 7.24. It can be noted that the inverter current is in phase with the common coupling point voltage, while its amplitude is proportional to the PV power.

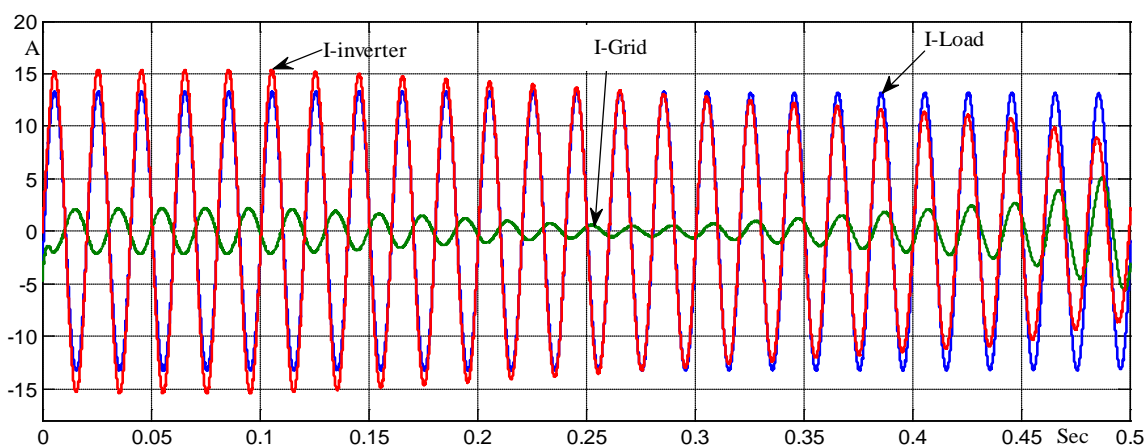
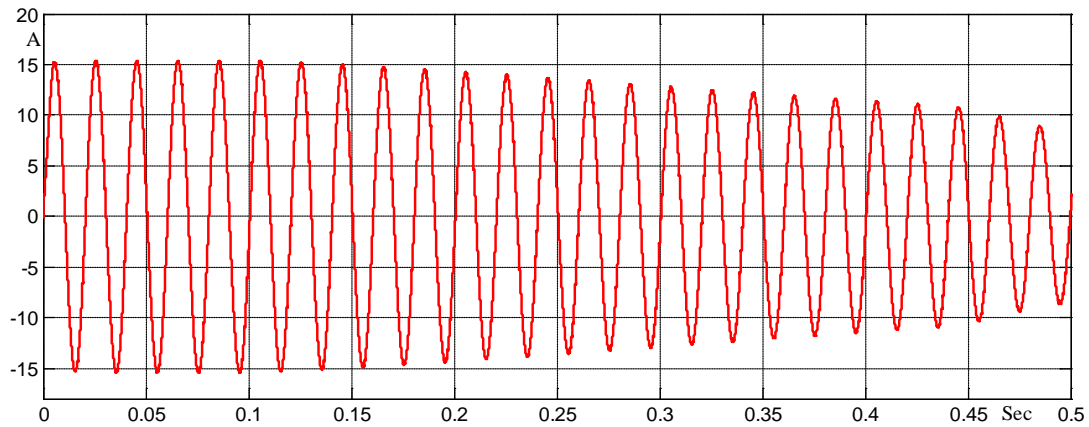
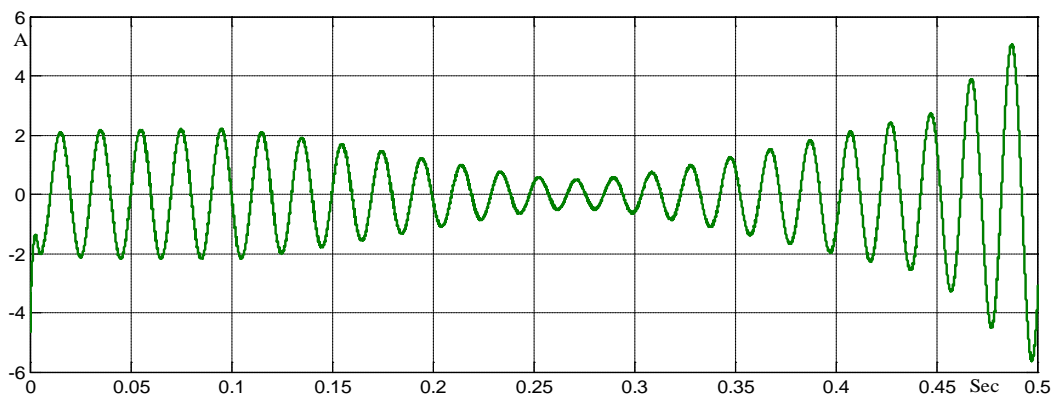


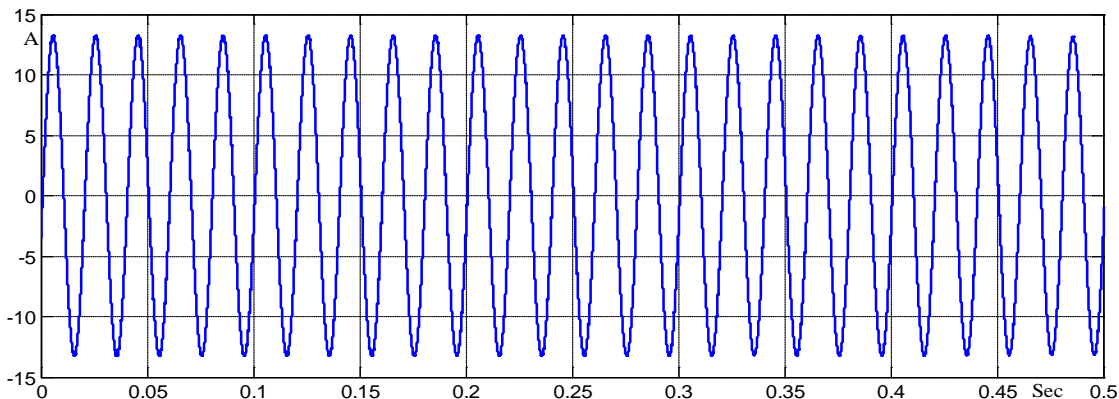
Figure 7.23: Load, inverter and grid currents distribution at the common coupling point.



(a)



(b)



(c)

Figure 7.24: Common coupling point currents
 (a) inverter current (b) grid current
 (c) load current.

The current feedback signals I_d and I_q are shown in Figure 7.25. The control signals u_d and u_q are shown in Figure 7.26. The u_d value is increased to hold the voltage constant. The u_q value decreases proportionally with the inverter current feedback signal.

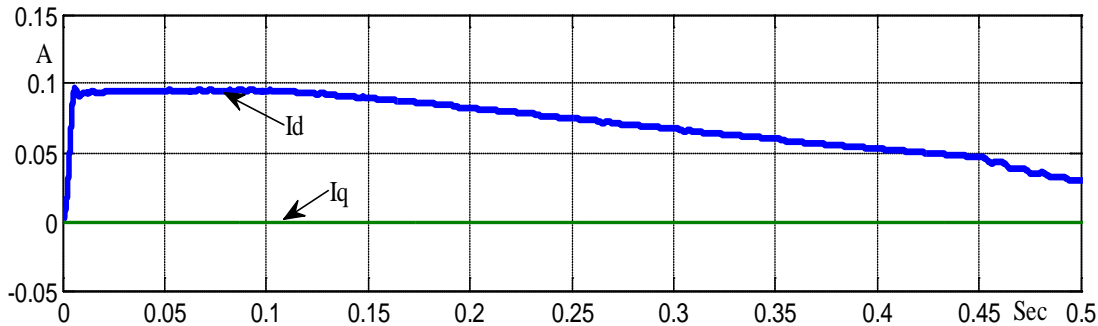
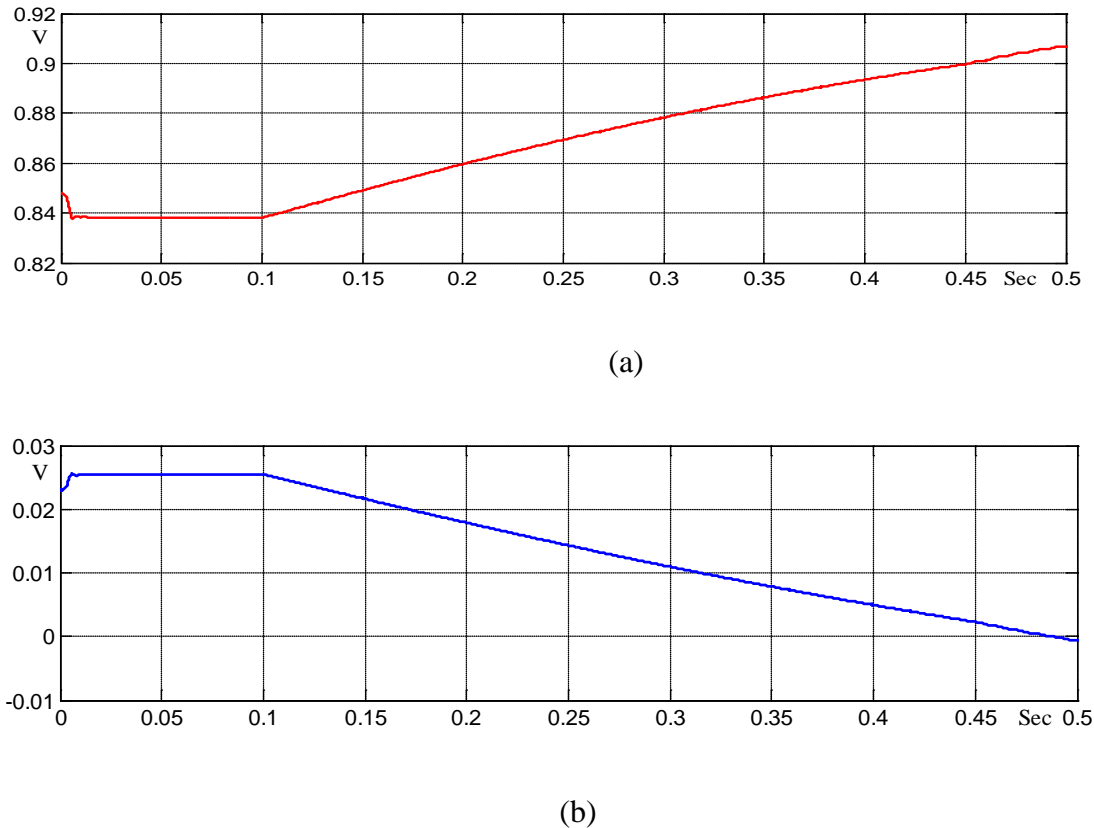


Figure 7.25: Current feedback signals I_d and I_q .

By comparing the inverter and grid current distribution at the common coupling point with the load demand (using Figures 7.23, 7.24 and 7.25) it can be concluded that:

1. In the case when the PV generated power is more than the load demand, the inverter supplies active power to the load and exports the excess power to the grid.
2. The inverter current, and hence power supplied (as the voltage is constant) drops proportionally to the PV power dip.
3. The grid provides the balance of the power demand to the load when the PV power dips.

Figure 7.26: Control signals (a) u_d and (b) u_q .

7.13 Summary

Voltage quality improvement in a PV system through feed-forward control compensation has been investigated. The PV system power source can fluctuate as a result of solar irradiance variation. The PV system output voltage quality is maintained constant in the presence of such fluctuations. This is done through an appropriate choice of value for DC-link capacitors together with feed-forward compensation (in the inverter controller stage). The PV system was tested with a fluctuating non-linear source, and validation of the proposed system is verified through MATLAB/SIMULINK.

A grid-tied PV system has been examined. The selection of the simulation model has been made on the basis of load sharing. The feed-forward controller is set to keep the DC-link voltage constant. The system has been tested with a fixed DC-link voltage. The

controller has been validated in the presence of changes in PV power caused by irradiation variations. The controller was made to operate at the MPP of the PV system to ensure maximum power was drawn from the PV system.

Simulation results based on the MATLAB/SIMULINK model have been presented to validate the effectiveness of the proposed control against PV power variations. It is evident from the results that the controller maintains power injections at unity power factor.

Chapter 8

SYNCHRONOUS SOLID-STATE CONVERTER

8.1 Introduction

Fundamentally, the individual PV system should track the maximum power available from the PV array. With a grid-tied PV system, when the demand from local loads exceeds the PV power generation the difference can be supplied from the grid. When PV power generation is greater than the local load power requirements, the excess power can be exported to the utility grid.

Small-scale individual power production from renewable energy is increasing day after day, leading to the decentralization of power generation. The power utilities now permit the placing of micro-generators on the customer side and the interfacing of them to the utility grid. Hence, the future of power network systems may largely be composed of a significant quantity of low-voltage renewable distributed generators interconnected through the distribution and transmission systems.

To achieve efficient and safe operation of these systems, it is necessary to understand the interaction between the generator and the utility. Therefore, this chapter offers a new approach to the implementation of decentralized embedded generators using synchronous solid-state inverters. Solutions are proposed for certain problems relating to the power management of single-phase solid-state power supplies as distributed generators using synchronous reference frame inverter control systems.

To prevent a generator from overloading when connected to the network, it is essential to ensure that the generator will share the load at a level proportional to its

nominal power rating. This is achieved by adding extra control functions into the controller stage on the basis of voltage magnitude and frequency of each generator, known as droop control [128,129].

Accordingly, an appropriate load sharing function was derived in order to enable this new type of generator to contribute to the management of both active and reactive power within the network. Since the controller in the last chapter was designed in the rotating d - q reference frame and decouples active and reactive power into separate channels, the load sharing function is designed in a way consistent with this approach.

8.2 Power Network Description

A traditional electrical power system is mainly composed of three separate parts [130-131].

1. Generation.
2. Transmission.
3. Distribution.

The generation stage is the first step in the power system, represented by a synchronous generator. The synchronous generator terminal voltage is normally kept constant by field current regulation. The frequency is kept synchronous with the network frequency by regulating rotor speed. The equivalent circuit is represented by a voltage-source in series with a reactance. Larger power networks have smaller external impedances.

Traditional power systems adopt centralized management concepts for distribution, demand and supply in a conventional top-down manner. At the production side the electrical energy is generated at a high voltage level and before reaching the consumer side, it is transformed down and distributed through several layers [130-132]. This results in a rising cost associated with traditional centralized power systems in the production side as well as in the distribution and consumer side [130, 131].

Most of the overhead distribution networks are low-voltage three-phase 4 wire systems. A distribution network has a number of low-voltage transformers with an output voltage (on the consumer side) of 230V or 400V that provide an acceptable level of losses. To maintain quality of the low-voltage network, the voltage magnitude and frequency must be compliant with the statutory limits.

The statutory limits are recommended within most national standards. For example, in the international voltage standard for 3-phase 4-wire LV systems it is recommended by the International Electrotechnical Commission (IEC60038) that the LV appliances must be designed to perform satisfactorily within the limits of $\pm 10\%$ of nominal voltage. This leaves a margin, under the worst conditions (of $\pm 5\%$ at the service position, for example) and -5% allowable voltage drops in the installation wiring [133]. [134] summarizes the voltage and frequency statutory limits of LV consumer side recommended by each country.

8.3 Decentralized Power Management Concept

In brief the decentralized power management concept is how to generate a given amount of power distributed over smaller generators in a lot of places rather than a single generator in one place. This leads to the generation of electrical power near the area of

consumption. Consequently this allows more power to travel with less resistance to reach customers in rural as well as urban areas. One of the most valuable options is the theoretical capability to improve the continuity of power supply even with an upstream supply outage [135].

Where decentralized power supplies are permitted, the utilities allow the placing of numerous micro-sources interconnected with the distribution and transportation systems. In this case, as the number of micro-sources grows the power network will contain an increasing number of interdependent technologies and strategies, thus becoming more complex [132, 136, 137]. A complex network can also be sparse over a large area. Therefore, many researchers [132, 135] have envisioned decentralized power supplies that do not require extensive communication with the central power stations.

Implementation of small-scale individual power production by renewable energy is increasing day after day. Thus, it is important to link these types of power production with the national power network. The network can then make optimal use of small-scale energy generation, as well as allowing the use of renewable energy sources and facilitating operation in an autonomous grid-tied mode. Hence, the future power network systems could be composed of a large quantity of low-voltage renewable distributed generators.

On the other hand, there is a concern on the recent increase in the deployment of individual renewable energy generators within the national power network. This deployment represents a new type of distributed generation using power electronic inverters connected with the radial distribution network. Static inverters (i.e. not based upon rotating machines) have different properties when compared with conventional power plants based on rotating electromagnetic generators. To achieve safe and efficient

integration of such inverters, it is necessary to develop decentralized control techniques at different levels for optimizing deployment of these new resources. Therefore, some requirement for regulation is needed for such resources in order that power quality does not worsen.

This research intends to explore the connection of single-phase inverters with a local network, and the solid-state inverter will appear as a distributed generator in this network. Hence, it is imperative to know the issues involved in controlling the inverter for ensuring both quality of supply and adequate supervision of power management.

8.4 Impact of Decentralized Distributed Generation on the Network

In hybrid applications, different types of energy sources (fuel, wind, solar, micro-turbine) work together [138, 139]. Since electricity cannot be stored in real-time in any major quantity, stability problems can be caused by mismatch between the supply and the demand. Network power quality depends on factors such as the types of distributed generators, capacity of distributed generators and the respective output power fluctuations, and the percentage of distributed generator types connected in this grid. The load is to be shared uniformly according to each generator's capacity.

PV and wind power generation capability is affected by natural conditions. The output power of PV systems tracks solar radiation intensity, while variable speed wind turbine output power depends on the wind velocity. Solar radiation intensity and wind velocity change randomly. As a result, such systems provide a generally unpredictable level of output power. The fluctuating output power will lead to voltage fluctuations (e.g. sag and swell) [138]. When the local network has heavy load, a small voltage drop may lead to partial voltage instability

Consequently, penetration of small-scale renewable energy distributed generators could have a significant impact on the power networks. To avoid large drops in the output voltage amplitude and frequency caused by load variations (through the grid-tied operation of distributed generators), each distributed generator's voltage amplitude and phase need to be controlled so as to keep the network stable.

When such a distributed generator is grid-tied, the voltage and frequency of the common coupling point are dictated by the grid. Therefore, the distributed generator unit usually uses current control methods to deliver power to the network.

More questions are raised within the environment of decentralized solid-state distributed generators. Within the national network, a significant number of grid-tied small-scale individual renewable energy generators exist as distributed generators working in parallel. Synchronization is an issue that arises in this configuration. Synchronization is required to avoid currents circulating among the power sources and contributing to losses. Network estimators and phase lock loops allow the estimation of the grid frequency and phase at the common coupling point as well as the voltage magnitude. The phase locked loop is a control system that generates an output signal whose phase is related to the phase of an input (reference) signal to keep the phase (and the frequency) matched.

In recent years, for the grid-tied mode, load sharing based on droop methodology has been widely utilized for active and reactive power control of electronically coupled three-phase distributed generator units [140]. Three-phase power supplies were equipped with various droop control methods to provide continuous output average power. Many researchers investigated this topic at different levels [137, 141, 142].

Single-phase systems suffer from a characteristic of fluctuating output power. Thus far, little attention has been pushed to the dynamic properties and robustness of the grid-tied single-phase power supplies as distributed generators.

In the approach proposed in this thesis, a method based on the synchronous rotating frame within the controller stage (which is broadly similar to that used in three-phase inverters) was chosen. Droop control can be effective when used with such a system in grid-tied mode, subject to some means of communication between the converters being available.

8.5 Droop Methodology

In a steady-state network operation the apparent power (S) flowing into network lines is described in Figures 8.1 and 8.2. The active and reactive power exported from the distributed generator to the grid can be expressed as follows:

$$S = P + jQ = E \cdot I^* = E(E - V_g)/Z \quad (8.1)$$

where S , P and Q are apparent, active and reactive power, respectively, injected into the grid, E and V_g are the distributed generator and grid voltage magnitudes respectively, Z and θ are impedance magnitude and impedance angle, ϕ is the voltage phase angle between the distributed generator and grid.

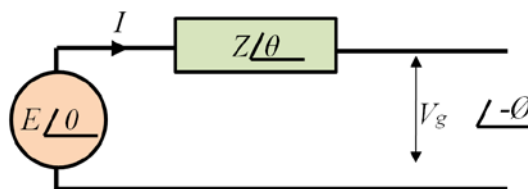


Figure 8.1: Network line power flow.

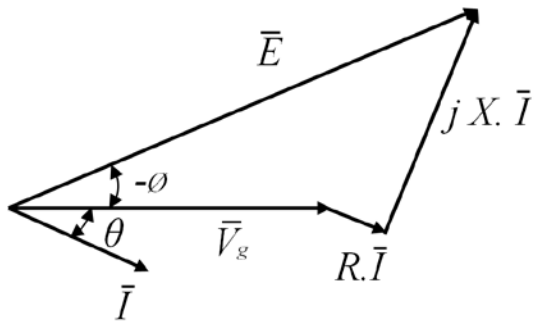


Figure 8.2: line power flow phasor diagram.

$$P = \frac{E^2}{Z} \cos \theta - \frac{EV_g}{Z} \cos(\theta + \phi) \quad (8.2)$$

and

$$Q = \frac{E^2}{Z} \sin \theta - \frac{EV_g}{Z} \sin(\theta + \phi) \quad (8.3)$$

$$Ze^{j\theta} = R + jX \quad (8.4)$$

The equations (8.2) and (8.3) can be rewritten as:

$$P = \frac{E}{R^2 + X^2} [R (E - V_g \cos \phi) + X V_g \sin \phi] \quad (8.5)$$

$$Q = \frac{E}{R^2 + X^2} [-R V_g \sin \phi + X (E - V_g \cos \phi)] \quad (8.6)$$

The simple concept of the droop method can be based on two assumptions:

1. The impedance in the overhead transmission lines is purely inductive, in other words $X \gg R$, and the resistance R can thus be neglected. Consequently $Z = X$ and $\theta = 90^\circ$. This approximation is true if the generator's output impedance is not too large. In the case when a solid-state distributed generator is used the instantaneous real and reactive power is exported to the network through a low

pass filter to obtain the average active and reactive power. Consequently, the converter output impedance plays an important role in power sharing.

$$\sin \phi = \frac{XP}{EV_g} \quad (8.7)$$

$$E - V \cos \phi = \frac{XQ}{V_g} \quad (8.8)$$

2. The power angle ϕ is small, so $\sin \phi \approx \phi$ and $\cos \phi \approx 1$. Thus, equations (8.7) and (8.8) can be approximated as in (8.9) and (8.10).

$$\phi \approx XP/(EV_g) \quad (8.9)$$

$$E - V_g \approx XQ/V_g \quad (8.10)$$

Equations (8.9) and (8.10) show that the voltage difference is proportional to the reactive power (Q), while the power angle is proportional to the active power (P) as expressed in (8.11).

$$\begin{aligned} \Delta P &\propto (\omega_0 - \omega) \\ \Delta Q &\propto n(E_o - E) \end{aligned} \quad (8.11)$$

where ΔP and ΔQ are the generator active power and reactive slope respectively; ω_0 and V_0 are the generator no-load frequency and voltage amplitude respectively; ω and V are the generator output frequency and voltage amplitude respectively. Thus, the active power can be controlled by controlling the frequency, and reactive power by controlling voltage magnitude. The above assumptions lead to two linear droop characteristics (P versus ω) and (Q versus E), the droop functions are expressed in (8.12).

$$\left. \begin{array}{l} \omega = \omega_o - m(\Delta P) \\ E = E_o - n(\Delta Q) \end{array} \right\} \quad (8.12)$$

where m and n are droop slope coefficients (gains) according to their generator nominal power. The droop characteristics $(P - \omega)$ and $(Q - E)$ represent linear equations having fixed no-load values (ω_o) and (E_o) respectively with the negative slopes. The droop characteristics in equation (8.12) are described in Figure 8.3. (see Appendix D for more details).

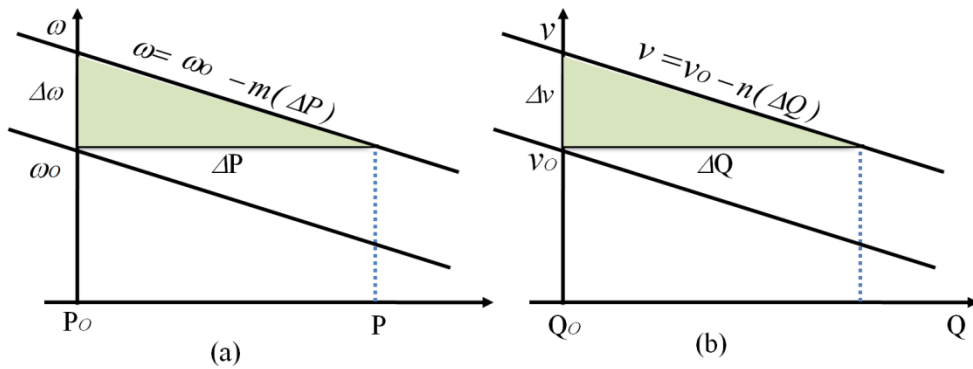


Figure 8.3: Droop characteristics for rotating generators.

It is worth saying that the solid-state distributed generators will have a faster dynamic droop response than the rotating generators. The response of rotating generators is dependent on governor characteristics (e.g. inertia and torque).

8.6 Droop Function Methodology in Literature

In the droop control method, the distributed generator uses only locally-measured quantities at its common coupling point without extensive communications with other sources within the network. It is important to avoid generator overload, so the distributed generator controller must ensure that the component of the load power that is shared is within the normal power limit for the generator.

In this thesis, droop control has been chosen for controlling the inverter voltage magnitude and its fundamental frequency during grid-tied inverter mode. This method is named differently in several papers depending on the approach applied [73, 143-150].

New research uses the droop concept in different ways. Most work deals broadly with the problem [73, 143-145]. [146] shows specifically the technical difficulty of power control when several subsystems work together such as energy sources, stored energy, power electronic inverters, grid and the loads. Other research [147-150] modifies the droop controller based on the line impedance parameters ratio (R/X), where R and X are the transmission line resistance and reactance respectively. This modification is suitable to the situations where the transmission line ratio (R/X) is high, such as in low-voltage rural applications. The line ratio (R/X) differs in each application depending on the line type and length used for connection with distributed generators [147, 148].

The goal of all this work is to achieve a new decentralized distributed generator with the capability of operating in both isolated mode and to seamlessly connect to the utility (grid-tied mode). Important contributions concern the control of power electronic inverters operating as part of the power distribution network, as well as about power management.

It is a normal requirement to control output active and reactive power of these types of distributed generators through inverter control. The inverter can adjust its response to the network and maintain voltage amplitude to meet the load demand.

8.7 Voltage Magnitude and Fundamental System Frequency

In most cases, voltage and frequency controllers for solid-state power converters are designed to follow the load behaviour. Many industrial applications require control of the instantaneous active and reactive power values; in fact, they are used for managing power quality within their system. The Clarke and Park transformations are useful in three-phase solid-state inverter applications to study, analyse and control instantaneous active and reactive powers. Control of the instantaneous active and reactive power increases the stability margin, and improves the voltage regulation in three-phase solid-state inverter applications [151]. The effectiveness of the instantaneous active and reactive power control can be observed in the single-phase inverter application by using rotating reference frame theory [147, 149, 152].

8.8 Solid-State Inverter Droop Behaviours

Before applying the droop control method to the single-phase grid-tied inverter, the inverter voltage magnitude and frequency behaviour requires analysis. The inverter performance is mainly dependent on the control technique employed. The inverter controller is designed to operate with a current reference in the d - q frame. Substantially, the load currents are measured and compared with the reference currents, the result is then used as an input to the PWM modulator to generate inverter switching signals.

In order to obtain correct load sharing between the inverter and the network, it should be determined how the controller controls the inverter output. By using Figure 8.4, the capacitor current is modelled as follows. In the stationary reference frame, the power is averaged over one cycle of the fundamental frequency.

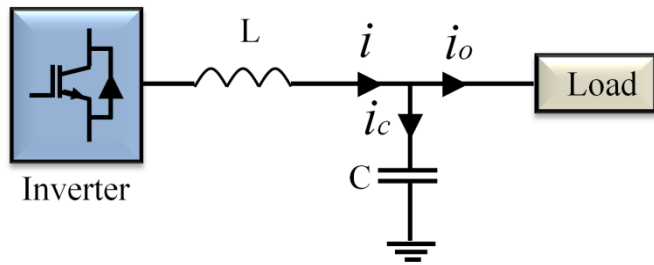


Figure 8.4: Inverter export power to the load.

$$\vec{i}_c = C \frac{d\vec{v}_c}{dt} \quad (8.13)$$

$$\vec{i}_c = C \frac{d\vec{v}_c}{dt} + \omega C \vec{v}_c \quad (8.14)$$

Appling Kirchhoff's current law:

$$\vec{i}_c = \vec{i} - \vec{i}_o \quad (8.15)$$

The components of current in the rotating reference frame are:

$$\begin{cases} \vec{i}_c = i_{cd} + j i_{cq} \\ \vec{i} = i_d + j i_q \\ \vec{i}_o = i_{od} + j i_{oq} \end{cases} \quad (8.16)$$

Hence the capacitor current is:

$$i_{cd} + j i_{cq} = (i_d - i_{od}) + j(i_q - i_{oq}) \quad (8.17)$$

At the same time, the capacitor current in the rotating reference frame is:

$$i_{cd} + j i_{cq} = C \frac{d(v_{cd} + j v_{cq})}{dt} + \omega C(j v_{cd} - v_{cq}) \quad (8.18)$$

The real and imaginary capacitor currents are:

$$i_{cd} = -\omega C v_{cq} + C \frac{d(v_{cd})}{dt} = (i_d - i_{od}) \quad (8.19)$$

$$i_{cq} = \omega C v_{cd} + C d(v_{cd})/dt = (i_q - i_{oq}) \quad (8.20)$$

By the definition given, v_{cq} is zero.

$$i_{cd} = C \frac{d(v_{cd})}{dt} = (v_{cd}/Z - i_{od}) \quad (8.21)$$

$$i_{cq} = \omega C v_{cd} = (i_q - i_{oq}) \quad (8.22)$$

Re-arranging (8.21) and (8.22) as in (8.23)and (8.24)

$$i_{od} = v_{cd}/Z - C \frac{d(v_{cd})}{dt} \quad (8.23)$$

$$i_{oq} = i_q - \omega C v_{cd} \quad (8.24)$$

leads to the active and reactive power of the inverter droop function described by:

$$\left. \begin{array}{l} \Delta Q \propto -(\omega_o - \omega) \\ \Delta P \propto (v_o - v) \end{array} \right\} \quad (8.25)$$

so that:

$$\left. \begin{array}{l} \Delta Q \propto (\omega - \omega_o) \\ \Delta P \propto (v_o - v) \end{array} \right\} \quad (8.26)$$

$$\left. \begin{array}{l} \omega = \omega_o + n(\Delta Q) \\ v = v_o - m(\Delta P) \end{array} \right\} \quad (8.27)$$

where ΔP and ΔQ are the inverter active and reactive power respectively and ω_o and v_o are the inverter no-load frequency and voltage amplitude respectively in the loaded

condition. ω and v are the inverter output frequency and voltage amplitude respectively, n and m are droop slope coefficients.

The inverter droop functions in 8.27 (Figure 8.5) are based on the reactive power frequency controller and active power voltage controller. As such, these droop functions are not appropriate in a network in which rotating generators dominate. Rotating generators have a characteristic based on the speed governors and the voltage regulator, and depend on an active power frequency controller and reactive power voltage controller. Therefore, for grid-tied purpose the inverter controller should be synchronous to the grid.

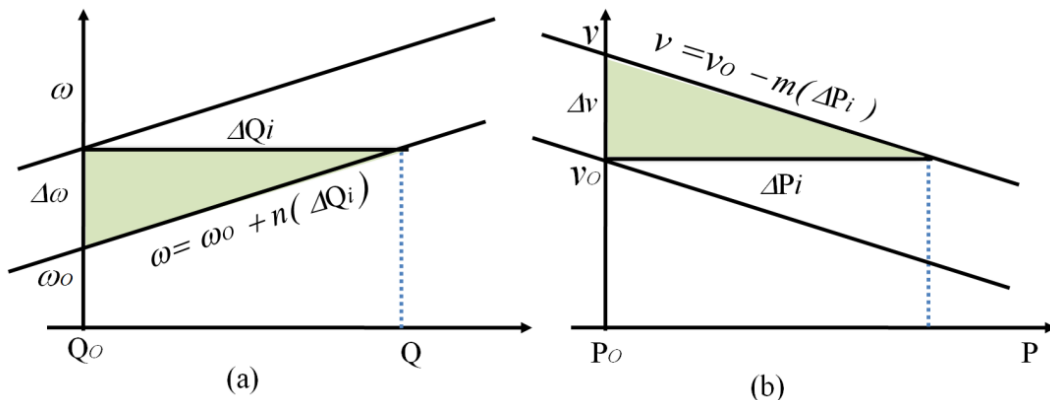


Figure 8.5: Inverter droop characteristics.

8.9 Proposed Inverter Droop Control Method

The dynamic properties of voltage and frequency within the solid-state inverter have been investigated for the proposed PV system. The voltage and frequency controllers are designed so that the performance of the inverter is utilized to achieve load sharing.

These controllers are adapted to mimic the behaviour of rotating generators connected directly to the power system. The inverter droop is preferred to be similar to grid droop behaviour. Thus, making the inverter droop proportional to grid droop, so that:

$$\left. \begin{array}{l} \omega_g = \omega_{og} - m_g(\Delta P) \\ E_g = E_{og} - n_g(\Delta Q) \end{array} \right\} \quad (8.28)$$

$$\left. \begin{array}{l} \omega_i = \omega_{io} + n_i(\Delta Q) \\ E_i = E_{io} - m_i(\Delta P) \end{array} \right\} \quad (8.29)$$

The subscript index (g) denotes a grid droop function parameter, while the subscript index (i) denotes an inverter droop functions parameter.

$$\left. \begin{array}{l} \frac{E_i - E_{oi}}{E_g - E_{og}} = \frac{-m_i(\Delta P)}{-n_g(\Delta Q)} \\ \frac{\omega_i - \omega_{oi}}{\omega_g - \omega_{og}} = \frac{n_i(\Delta Q)}{-m_g(\Delta P)} \end{array} \right\} \quad (8.30)$$

$$\left. \begin{array}{l} E_i - E_{oi} = (E_g - E_{og}) + \frac{m_i(\Delta P)}{n_g(\Delta Q)} \\ \omega_i - \omega_{oi} = (\omega_g - \omega_{og}) - \frac{n_i(\Delta Q)}{m_g(\Delta P)} \end{array} \right\} \quad (8.31)$$

At no-load, ω_{oi} should be equal to ω_{og} ($\omega_{og} = \omega_{oi} = \omega_o$), as well as E_{oi} should be equal to E_{og} ($E_{og} = E_{oi} = E_o$). Thus,

$$\left. \begin{array}{l} E_i = E_g + \frac{m_i(\Delta P)}{n_g(\Delta Q)} \\ \omega_i = \omega_g - \frac{n_i(\Delta Q)}{m_g(\Delta P)} \end{array} \right\} \quad (8.32)$$

The common coupling point is reflected to the grid behaviour; so that E_g will represents the inverter voltage reference E_o within the voltage feedback loop, ω_g represents the angular speed of the inverter frequency reference ω_o .

$$\left. \begin{aligned} E_i &= E_o + \frac{m_i(\Delta P)}{n_g(\Delta Q)} \\ \omega_i &= \omega_o - \frac{n_i(\Delta Q)}{m_g(\Delta P)} \end{aligned} \right\} \quad (8.33)$$

In most cases, distributed generators are synchronised to the network frequency at the point of common coupling. This is often achieved by using a PLL or similar technique. Consequently, equations (8.33) can be modified to use phase angle (\emptyset) instead of frequency, as follows:

$$\left. \begin{aligned} E_i &= E_o + \frac{m_i(\Delta P)}{n_g(\Delta Q)} \\ \emptyset_i &= \emptyset_o - \frac{n_i(\Delta Q)}{m_g(\Delta P)} \end{aligned} \right\} \quad (8.34)$$

The inverter droop coefficients are shown in (8.35), where $\Delta\emptyset$ is maximum permissible variation in frequency and ΔE is maximum permissible voltage variation.

$$\left. \begin{aligned} m_i &= \frac{\Delta\emptyset}{P_{max}} \\ n_i &= -\frac{\Delta E}{Q_{max}} \end{aligned} \right\} \quad (8.35)$$

These coefficients make equation (8.34) to turn into:

$$\left. \begin{aligned} E_i &= E_o - \frac{\Delta\emptyset \frac{\Delta P}{P_{max}}}{n_g(\Delta Q)} \\ \emptyset_i &= \emptyset_o - \frac{\Delta E \frac{\Delta Q}{Q_{max}}}{m_g(\Delta P)} \end{aligned} \right\} \quad (8.36)$$

$$\left. \begin{aligned} E_i &= E_o - \frac{\Delta P}{P_{max}} \frac{\Delta \emptyset}{n_g(\Delta Q)} \\ \emptyset_i &= \emptyset_o - \frac{\Delta Q}{Q_{max}} \frac{\Delta E}{m_g(\Delta P)} \end{aligned} \right\} \quad (8.37)$$

The PV power system supplies maximum PV power with unity power factor, so that $\Delta P \approx P_{max}$, $\Delta Q \approx Q_{max} = 0$. As a result, the inverter droop functions used with the synchronous reference frame controller are given in (8.38). E_o is the inverter reference voltage equivalent to the direct voltage component (v_d) in the synchronous rotating reference frame. \emptyset_o is the inverter reference phase (which is usually set to zero for unity power factor [153] in the inverter applications).

$$\left. \begin{aligned} E_i &= E_o - K_e \frac{\Delta \emptyset}{(\Delta Q)} \\ \emptyset_i &= \emptyset_o - K_\emptyset \frac{\Delta E}{(\Delta P)} \end{aligned} \right\} \quad (8.38)$$

The inverter droop function gain constants K_e and K_\emptyset are chosen depending on the inverter normal power S_i in order to make the droop function solvable.

It is clear that the proposed inverter droop method is coupled in voltage amplitude and phase. The synchronous rotating reference frame controller is decoupled within voltage and current loops in order to eliminate the coupling terms. Thus, the inverter phase and voltage magnitudes at the controller output will respond to the network demand (ΔP and ΔQ). The power angle depends heavily on the real power and the voltage difference depends on the reactive power [131, 132].

8.10 Simulation Result

The control structure in this chapter was developed further to include the droop function. The droop functions adopt the slopes of the ($P - \emptyset$) and ($Q - V$) slopes. The control strategy of the grid voltage amplitude and the grid phase is based on independent adjustment of the reactive and active power. The proposed control strategy was evaluated through MATLAB/SIMULINK in grid-tied mode. In order to test the steady-state and dynamic response during a load change, simulations were carried out. Various operating conditions such as load step, wide range from resistive and inductive loads, poor power factor, and light-load test were explored. The measurement instruments measure the currents and powers (quantities and directions) at node A as denoted in Figures 8.6, 8.9(c), and 8.17. The positive power value reveals the power exported to the node A, and vice versa. The system was tested in three steps as follows:

Case 1: The droop characteristics were set so that the inverter has priority to supply constant maximum active power, Figure 8.7. Thus, the inverter can supply reactive power after it satisfies the active power demand. The general circuit is divided to the three elements: inverter, grid, and load, Figure 8.6. The system was tested with steady-state load sharing and sudden load change. The load was changed in steps in the sequence from 3700W+1000VAr to 1700W+1000VAr to 700W+1000VAr and to 200W. The results were measured at node A representing the point of common coupling between the inverter, grid, and load.

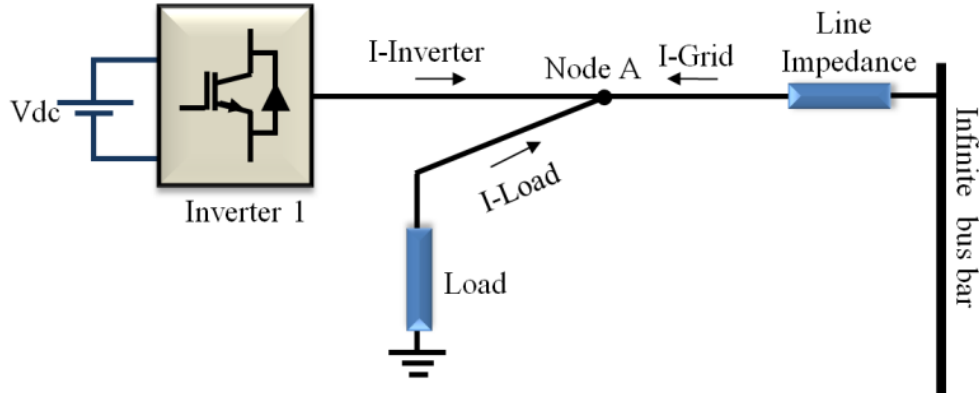


Figure 8.6: The inverter set to have priority to supply constant active power.

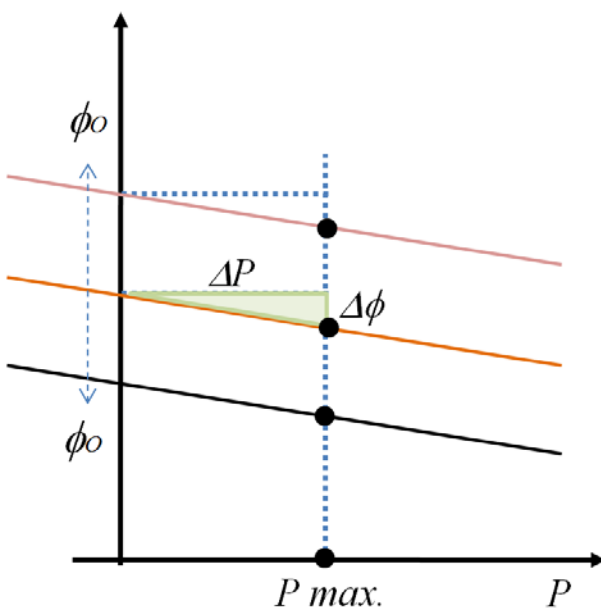


Figure 8.7: The inverter droop set to supply constant active power.

Figure 8.8 shows the inverter, load, and grid current waveforms, and active and reactive power contributions at node A. To demonstrate the phase current waveforms with respect to the voltage at common coupling point, the scale of the y-axis of the common coupling point voltage is reduced and depicted in the same figure. Figure 8.8 additionally illustrates the export and import active and reactive power at node A. Positive value of power denotes power exported to node A. A further evaluation of these results is made after the presentation of Case 2 below.

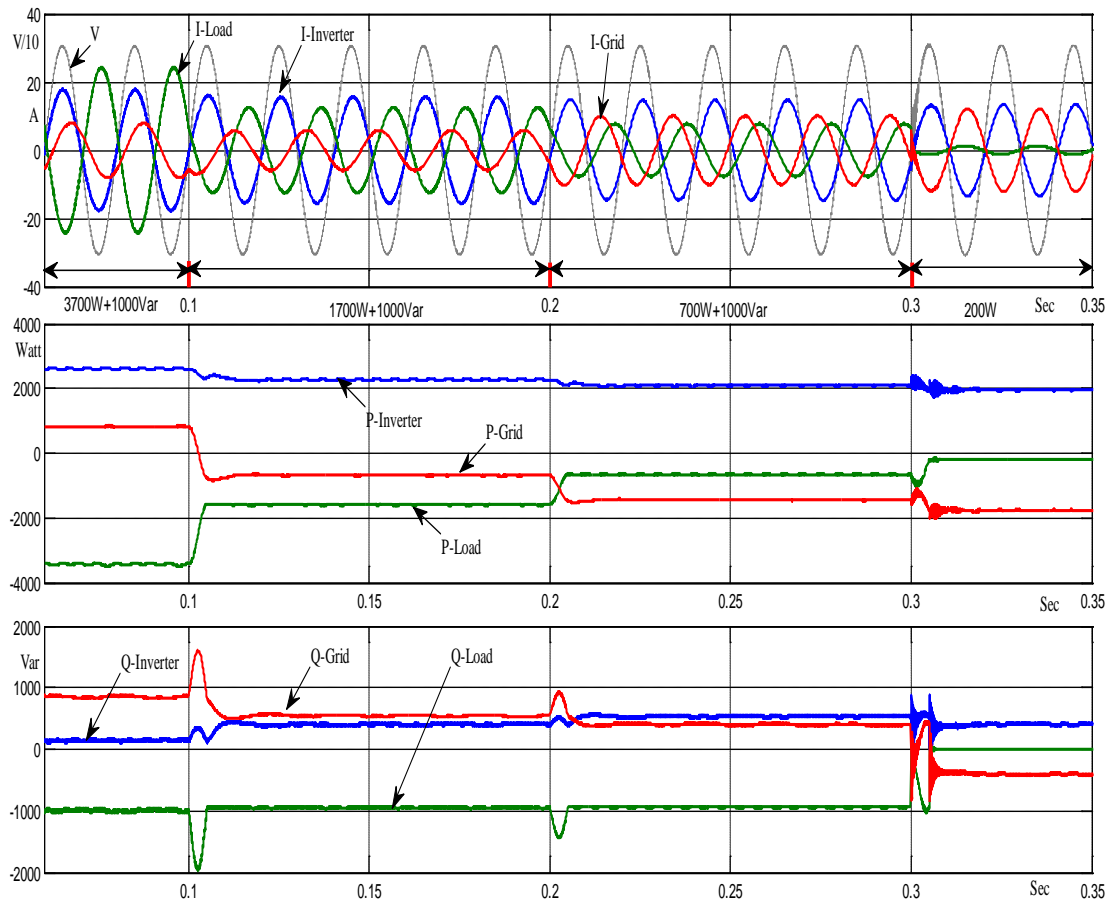


Figure 8.8: Inverter, load, and grid current waveforms and power contributions at node A.

Case 2: The droop characteristics were set so that the inverter has priority to supply constant apparent power ($S=P+Q$), Figure 8.9 (a). The purpose of this test is to clarify the droop controller's effectiveness as part of the inverter output power management. The simulation results measured at node A (inverter, grid and load currents and active/reactive powers) are given in Figure 8.10.

In order to demonstrate the current phase with respect to the voltage at common coupling point, the common coupling point voltage scale is reduced and depicted in the same figure. The load was stepped in the sequence from 3200W+1200VAr to 700W+1000VAr to 200W to 200W. Figure 8.10 illustrates the export and import of active and reactive power at node A. A positive power value denotes power export to the node A.

The results show that, in addition to the active power supplied by the inverter, the droop controller setting enables the inverter to export reactive power to the grid.

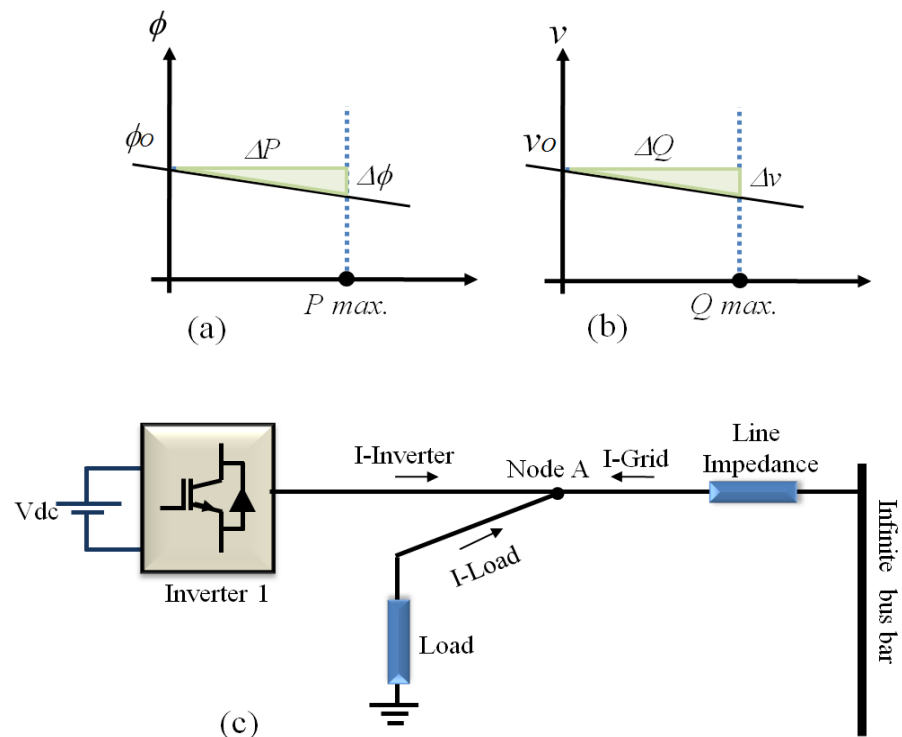


Figure 8.9: The inverter set to supply constant apparent power ($S=P+Q$).

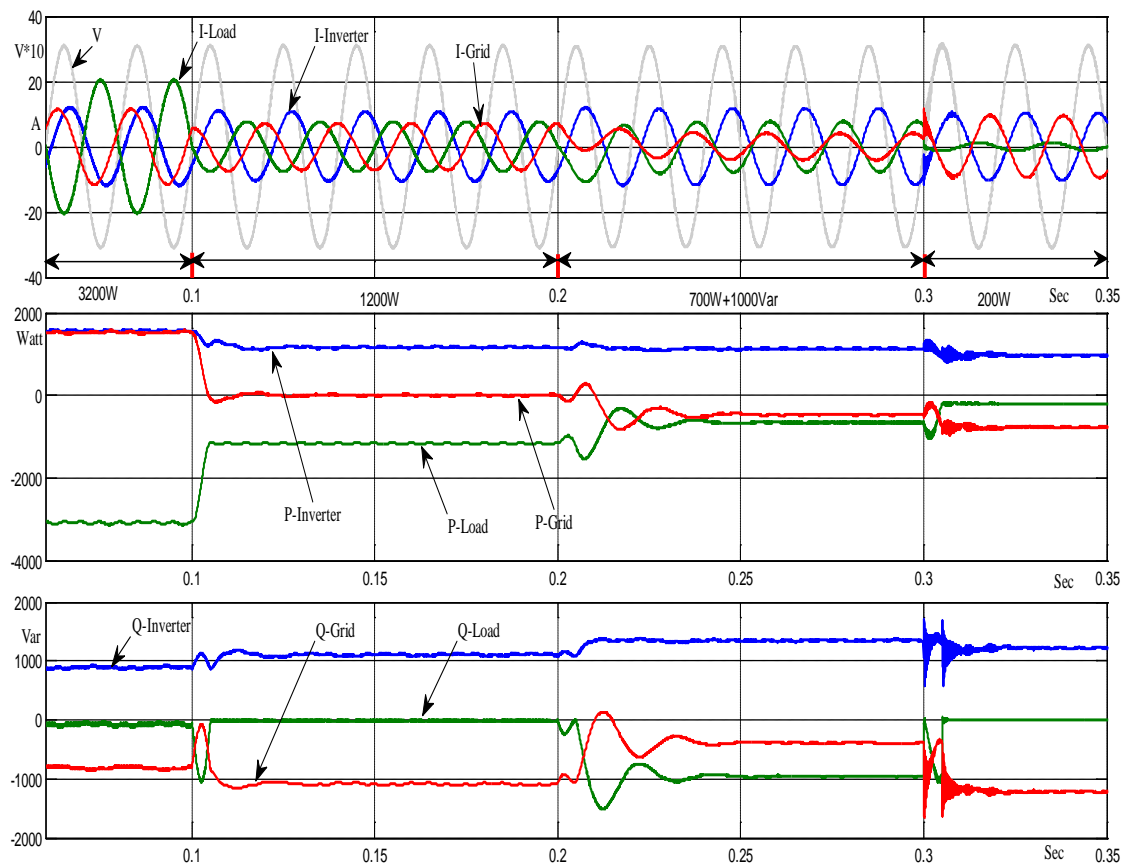


Figure 8.10: Inverter, load and grid current waveforms and power contributions at node A.

From the above results (Case 1 and Case 2), it can be concluded that:

1. The inverter prioritizes the supply of active power over reactive power in Case 1. In Case 2 the droop controller setting enables the inverter to export both reactive power and active power to the grid.
2. During the periods when the load active power demand is greater than the inverter power capacity, the power difference is supplied by the grid.
3. When the load active power demand is less than the inverter power capacity, the inverter exports active power to the grid.
4. In Case 2, when the load reactive power demand is less than inverter power capacity, the inverter exports reactive power to the grid.

5. The above results (Cases 1 and 2) illustrate various cases of inverter power contribution associated with power sharing between solid-state synchronous converters and the network at node A. For generalisation, Figures 8.11, 8.12, 8.13, 8.14, 8.15 and 8.16 summarize these cases of power sharing.

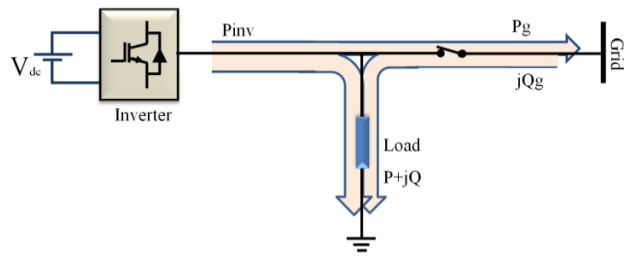


Figure 8.11: The inverter exports active power to the load and grid; the load imports reactive power from grid.

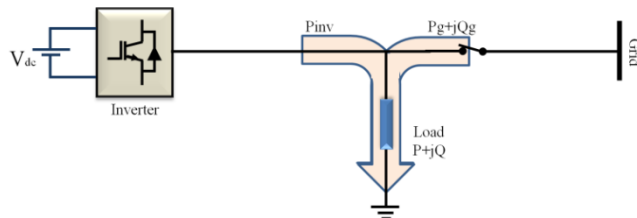


Figure 8.12: The load imports active power from inverter and grid, and imports reactive power from grid.

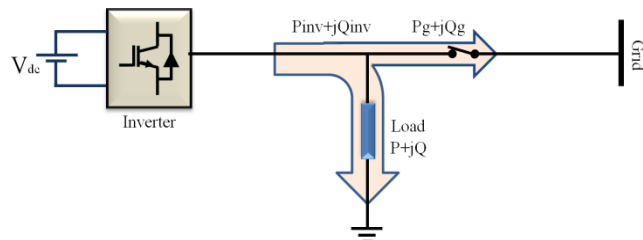


Figure 8.13: The inverter exports active and reactive power to the load and grid.

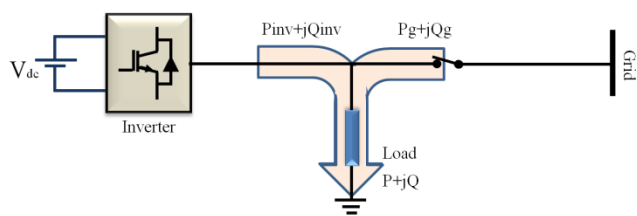


Figure 8.14: The load imports active and reactive power from grid and inverter.

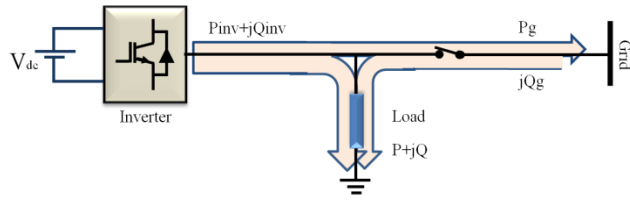


Figure 8.15: The inverter exports active power to the load and the grid; the load imports reactive power from inverter and grid.

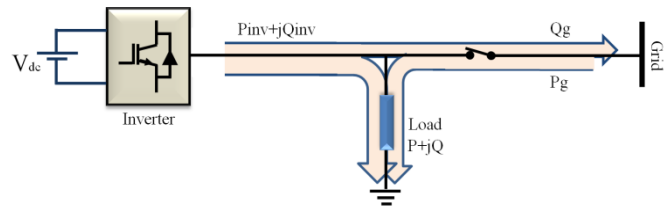


Figure 8.16: The load imports active power from the inverter and grid; the inverter exports reactive power to the load and grid.

8.11 FFT Analysis

The harmonic composition of the voltage and currents at the common coupling point is analysed using an FFT for the case when the converter is supplying a 1500W resistive load. The load active power demand is less than the inverter power capacity. Thus, the inverter exports active power to the grid. The results in Figures 8.17, 8.18, and 8.19, show a reduction in the THD when operating in grid-tied mode compared to the stand-alone mode (Section 6.10), the utility being able to reduce the THD as the voltage at the common coupling point is defined by the utility. The inverter, grid, and load currents THD are 0.54%, 0.51, and 0.52 respectively. The source current THD sufficiently below 5%, it is satisfy the IEEE standard [29].

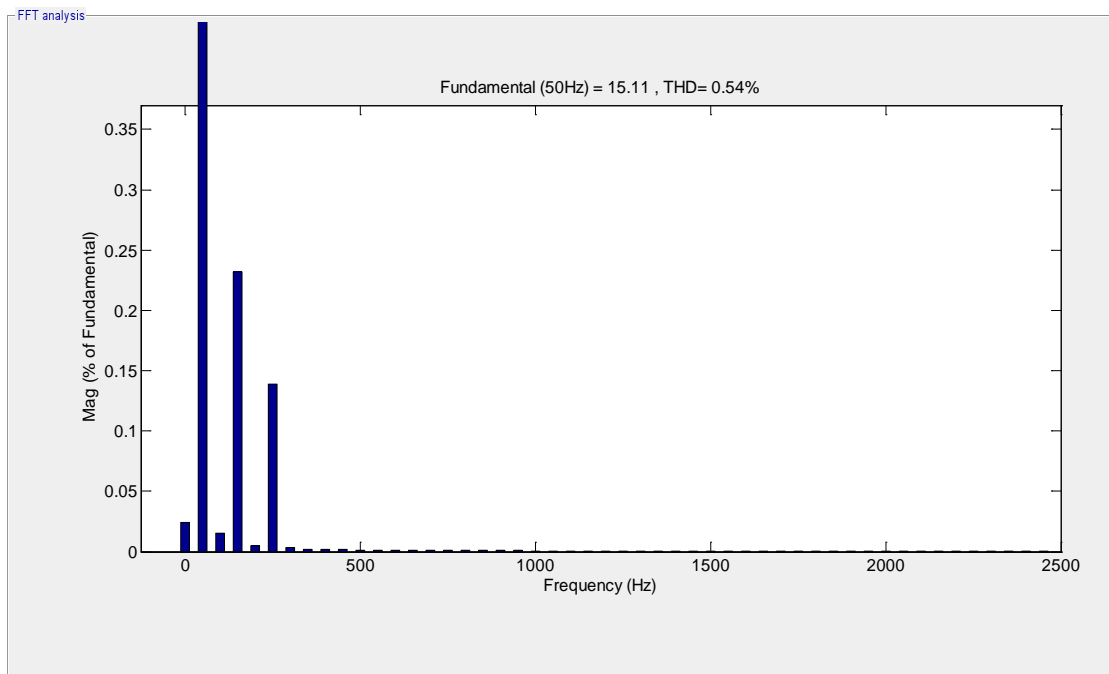


Figure 8.17: Inverter current FFT spectrum.

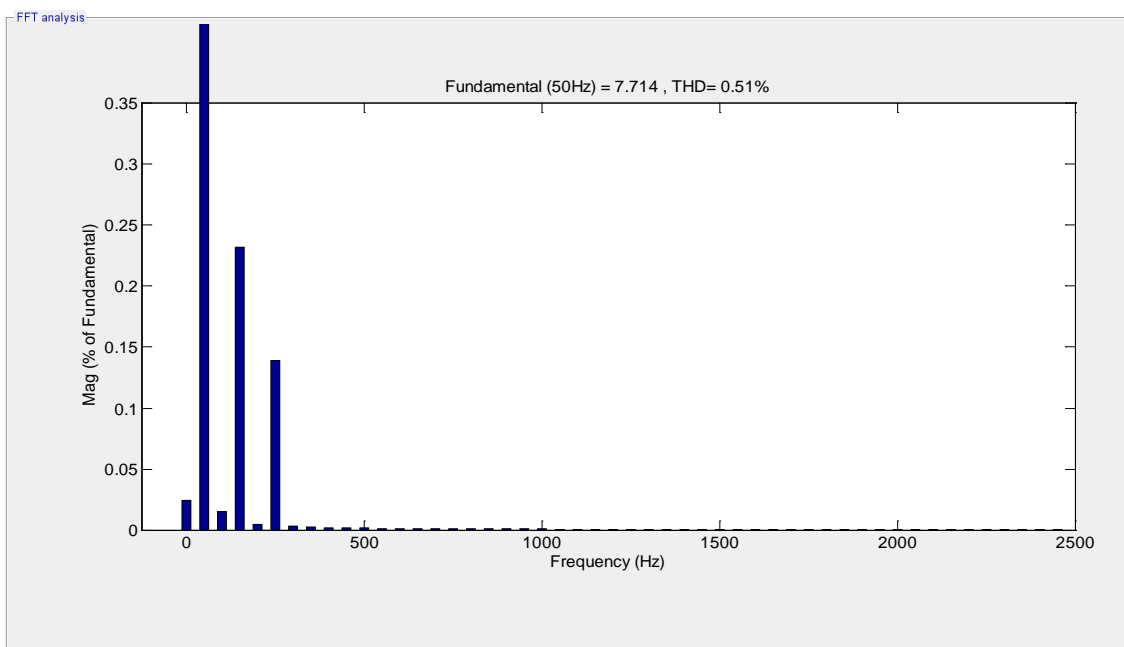


Figure 8.18: Grid current FFT spectrum.

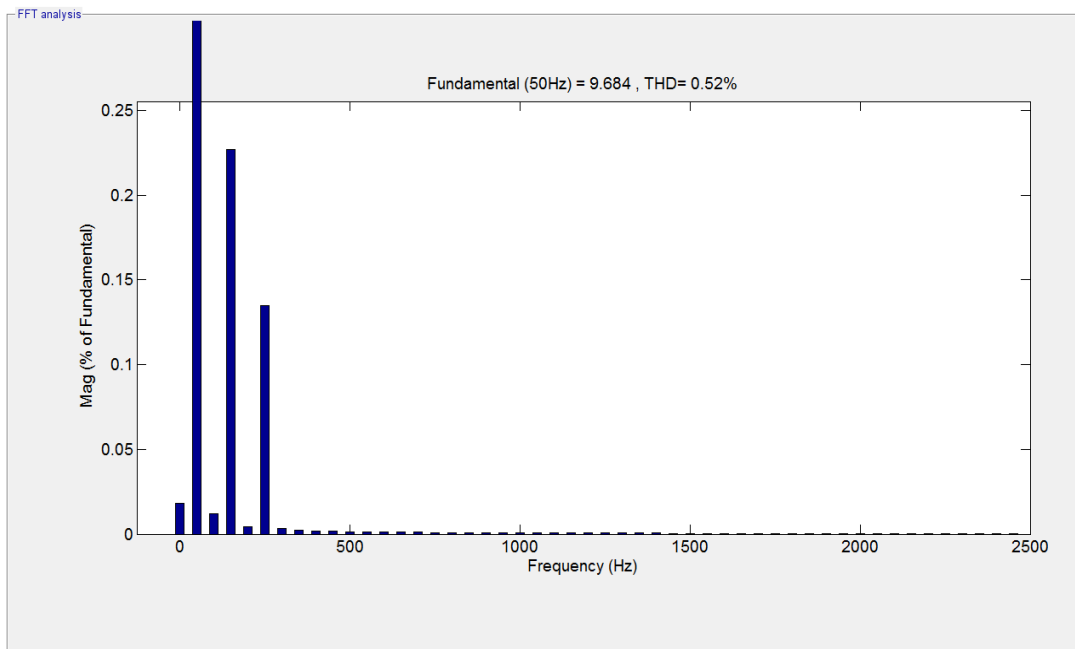


Figure 8.19: Load current FFT spectrum.

8.12 Summary

This chapter begins with a description of the power network, with the aim of decentralized power management, and of the voltage amplitude and phase droop behaviours of rotating generators. It then proposes a small-scale solid-state inverter droop controller for decentralised solid-state synchronous converters. With the achievement of decentralized power management, new power networks will become a reality in a scenario in which small-scale distributed generators can be easily integrated into the grid topology. Decentralized power networks incorporating renewable energy small-scale distributed generators are becoming more important owing to not only environmental aspects, but also economic interests. Thus, such distributed generators should contribute to the reinforcement of the grid and should also maintain an acceptable quality of supply within the limits imposed by the relevant standards [29]. For the consumer, the potential lower cost and energy independence will encourage the use of renewable energy. A network of grid-tied inverters have the ability to reroute power to where it is required, thereby

preventing a potential outage situation. In the future, an increasing number of small-scale solid-state voltage-source distributed generators will feed the utility networks.

This ability is accomplished by using the measured quantities at the common coupling point between the distributed generator and the network without requiring communication either between distributed generators, or between the generators and a control center. Consequently, the proposed control is achieved through the concept of the droop function based in the synchronous rotating reference frame where the active and reactive output power components are regulated according to voltage deviation.

The proposed droop concept is developed from power system theory and is based on active and reactive power, measured in the rotating reference frame. This was investigated for use with an inverter operating in grid-tied mode for synchronization and load sharing. The control scheme was verified by means of using simulation results. The simulation results also demonstrate the validity of the proposed solution in the presence of load changes.

Chapter 9

HARDWARE IMPLEMENTATION

9.1 Introduction

This chapter presents the results of a hardware implementation of the proposed system.

The system has been implemented using a hardware platform based on a generic laboratory power conversion system from Microchip [155]. The system consists of two parts. The power module is the dsPICDEM MC1H 3-Phase High Voltage Power Module [156]. The digital controller module is based around the 16-bit fixed point DSP-based controller dsPIC30F6010A [157]. It lends itself well to the implementation of different inverter digital control algorithms. It includes all the facilities required to implement a multi-loop controller (voltage and current loops) such as:

- An isolated interface between power module and controller module
- All feedback signals are pre-conditioned and scaled within the power module
- Inverter output Hall current sensor.
- Inverter output voltage sensor.
- The DSP has a built-in ADC peripheral.

Experimental results were obtained to validate the simulation. The power stage was configured as a half-bridge inverter implemented using the one-leg SVPWM technique.

The PV system was tested with output voltages of 220V to match those used in the simulation, and the inverter switching frequency was set around 20 kHz. The main aim of the experimental setup was to verify the performance of the control strategy as proposed in this thesis. The quality of the system output power is also considered.

9.2 System Hardware Description

The system has been implemented on a dsPIC30F6010A high-performance digital signal controller from Microchip Technology Inc. In a DSP-based control system, software flexibility facilitates the rapid development of control algorithms. Figure 9.1 shows a photograph of the experimental setup including the DSP board, the inverter and the load. The PWM signals are generated by the dsPIC30F6010A through an on-chip PWM peripheral. The fundamental power frequency is 50 Hz and the switching frequency is 20 kHz. The voltage and current are measured at the point of common coupling with the load.

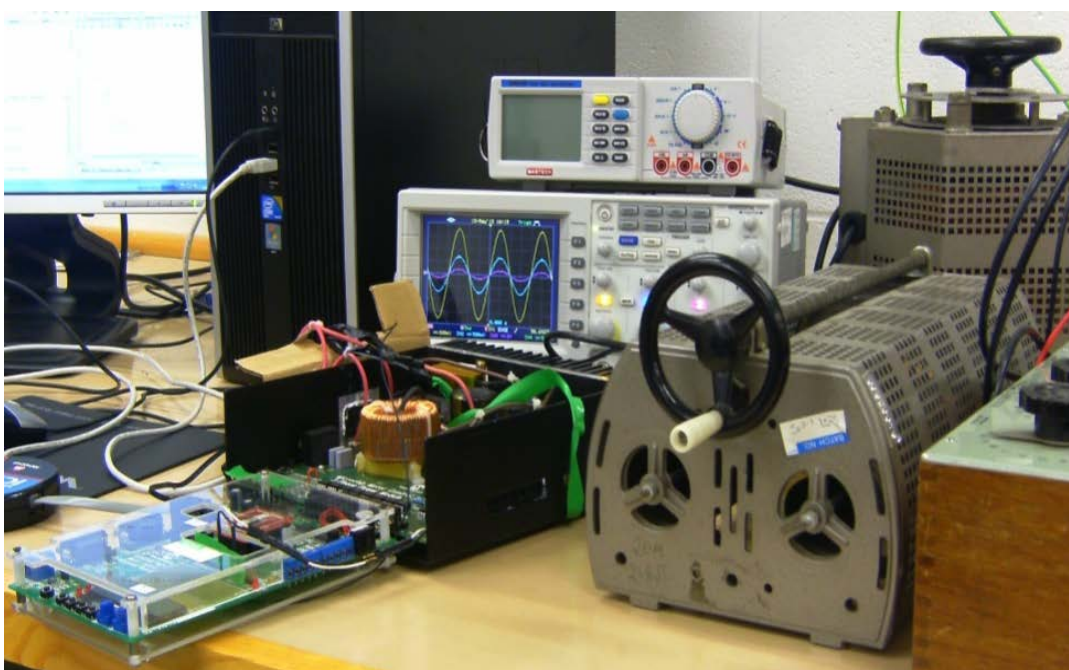


Figure 9.1: General view of the experimental bench.

The system is intended for evaluation purposes in a laboratory environment. The main components of the system are:

1. Power circuit: The Microchip dsPICDEM MC1H 3-Phase High Voltage Power Module was used in this application [156].
2. DSP-based control circuit: The power module includes several components to provide isolated voltage and current feedback to the MC1 DSP module [157].

9.3 Power Circuit Devices

The main components of the gate drive circuits together with one inverter leg are shown in the circuit diagram of Figure 9.2. The inverter consists of Q3 and Q4 n-Channel IGBT transistors with co-packaged anti-parallel 600V diodes in the industry standard TO220 package, and can operate at switching frequencies up to 20 kHz.

A gate drive IC (IR 2112) with an integrated high-side drive provides the drive to the gates of the IGBTs.

The power module derives its low-voltage power supplies from the associated control PCB. The supplies on the isolated supply are taken directly from the control PCB via the 37-pin connector [156].

Within the power module, Hall-effect current transducers (LTS 6-NP) devices are installed in series with the inverter output connection to provide isolated current feedback [156]. Similarly, the inverter output voltage feedback signal is measured by a voltage divider and isolation is provided by a linear optocoupler IL300. A signal conditioning

stage provides gain and offset to yield signals in the 0-5V range with 1.55 V dc offset, thus matching the requirement of the analog to digital conversion of the DSP chip. The gate drive signals are similarly isolated to prevent damage to the DSP from potential faults in the power stage.

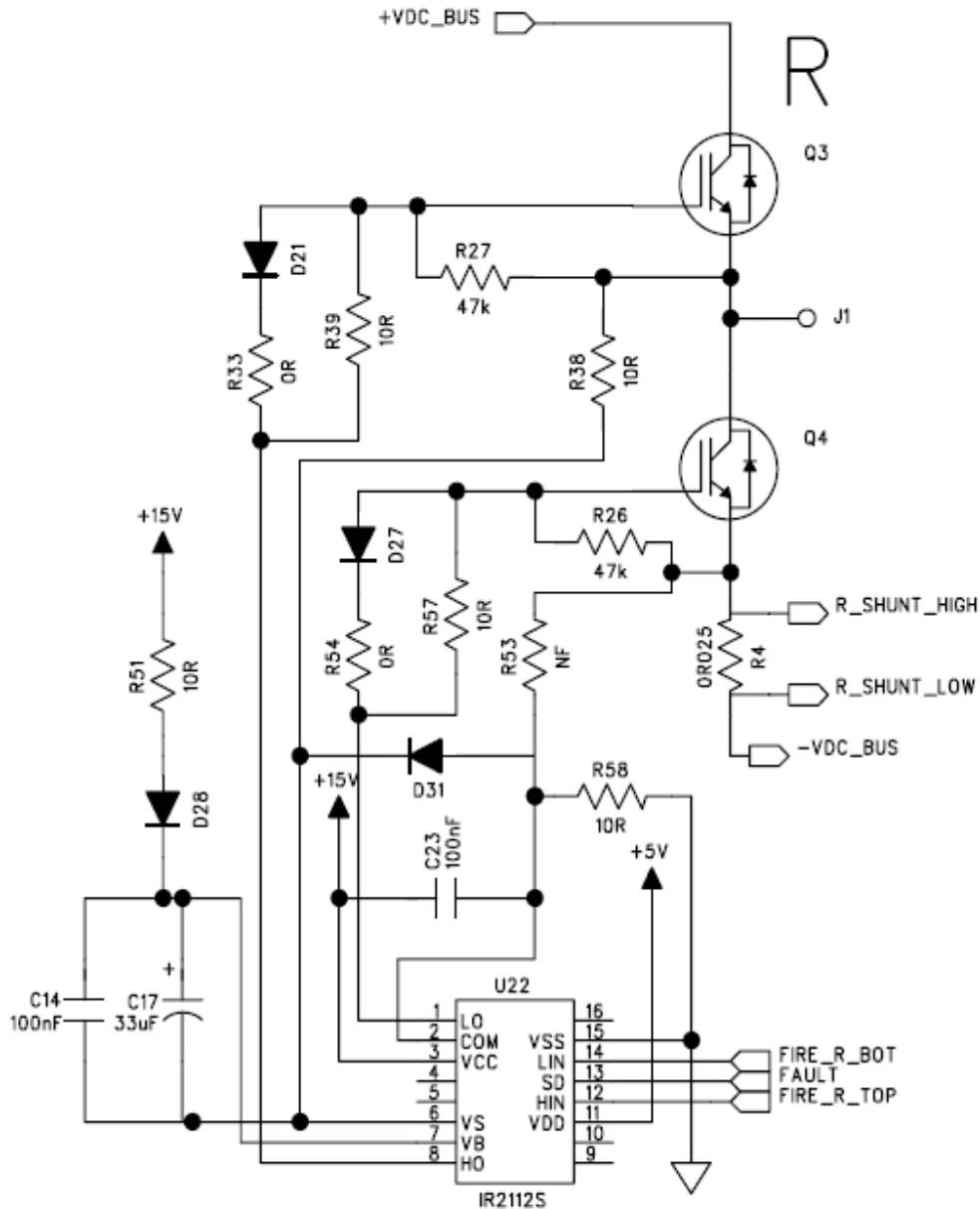


Figure 9.2: The main components of the power inverter [156].

The analog to digital converter module located within the PIC microcontroller has a 10-bit word length [157, 158]. Therefore, analog input voltages between 0v and 5v are

sampled at 2^{10} (1024) levels. The result of A/D conversion is then loaded in a read-only RAM buffer, 16-words deep and 10-bits wide.

Figure 9.3 outlines the main program in flowchart form. Further detail is provided in Appendix D. The feedback current and voltage signals are stored in memory and the quadrature component is obtained by accessing the data history with a delay of 1/4 of fundamental cycle (Figure 9.4).

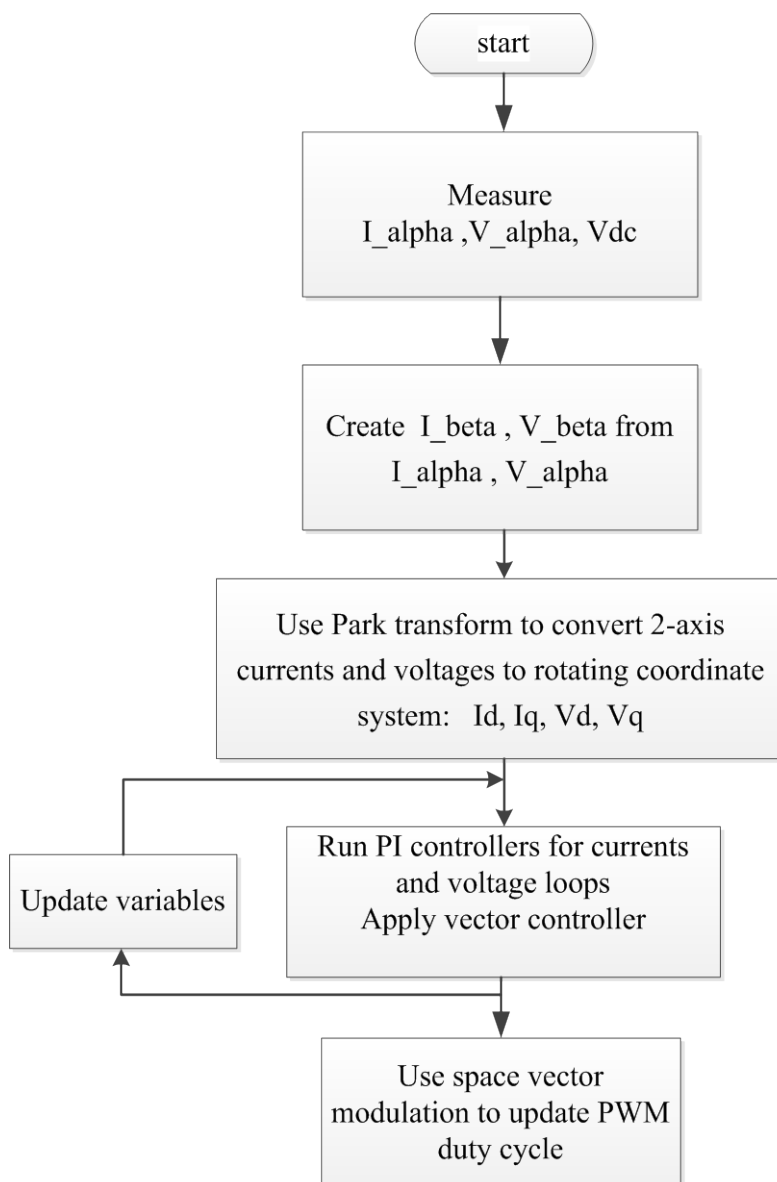


Figure 9.3: Main program flowchart.

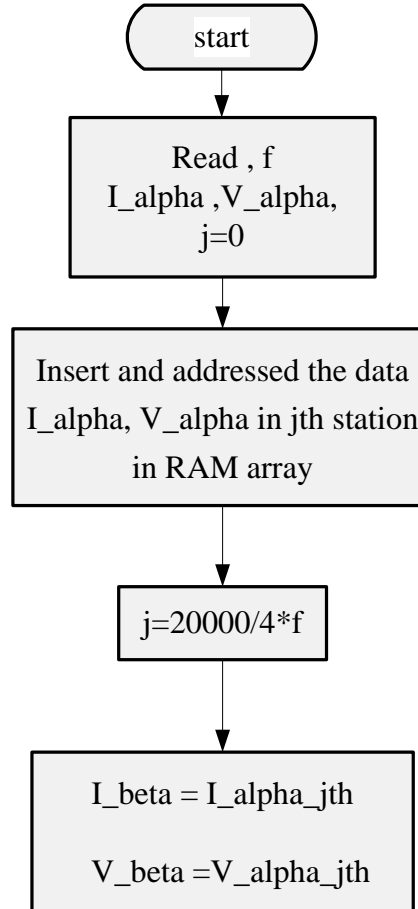


Figure 9.4: Creation of I_{β} , V_{β} from I_{α} , V_{α} .

9.4 The Experimental Setup

The main aim of the present experimental setup is to demonstrate the performance of the proposed inverter. Two different modes of operation of the inverter (stand-alone and utility interactive) were evaluated. Further tests were conducted in order to measure the THD of voltage and current injected into the grid when operating in the grid-tied mode. The current waveforms are measured using an oscilloscope with the inclusion of a small non-significant series resistance.

Experimental tests of the proposed control technique have been performed using a 1KVA single-phase inverter. The DC voltage is set at a constant value of 400V. $L = 3 \text{ mH}$

are used to provide strong suppression of switching frequency ripples. The filter capacitance $C = 1.5\mu F$.

9.5 Stand-Alone Inverter Experimental Setup

Figure 9.5 presents the experimental setup scheme in stand-alone mode. The inverter waveforms during operation in stand-alone mode are presented in Figures 9.6 to 9.9.

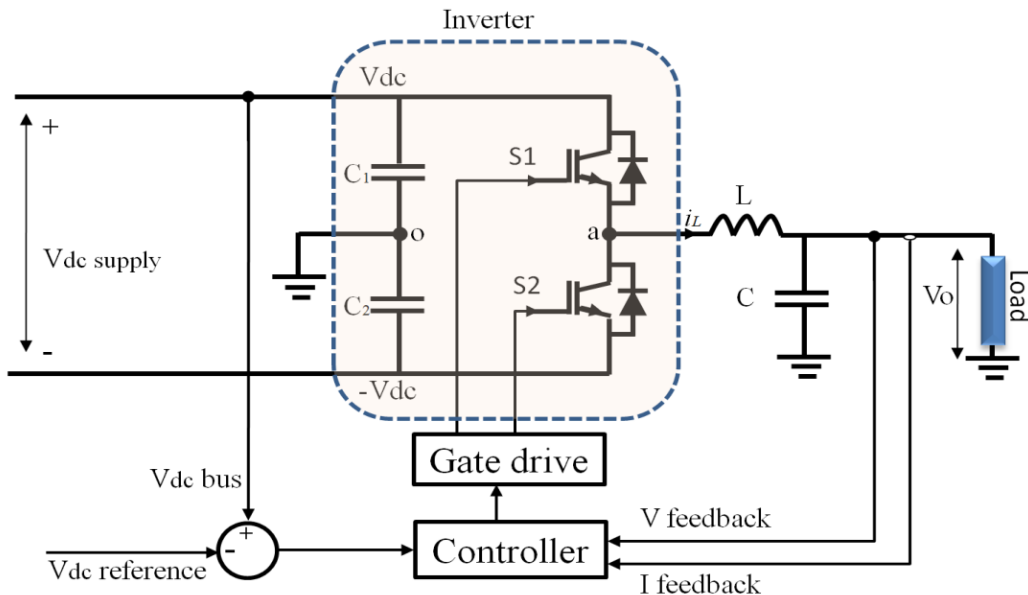


Figure 9.5: Experimental setup scheme at stand-alone mode.

The inverter leg center-point voltage is shown in Figure 9.6. This consists of a train of high frequency pulses of varying width that alternate between positive and negative voltage. The pulse width periods are proportional to the PWM duty ratio. The complementary gate signals drive two complementary IGBTs, thus achieving two complementary IGBT voltages at 20KHz switching frequency between an output node (node a in Figure 9.5) and a neutral point.

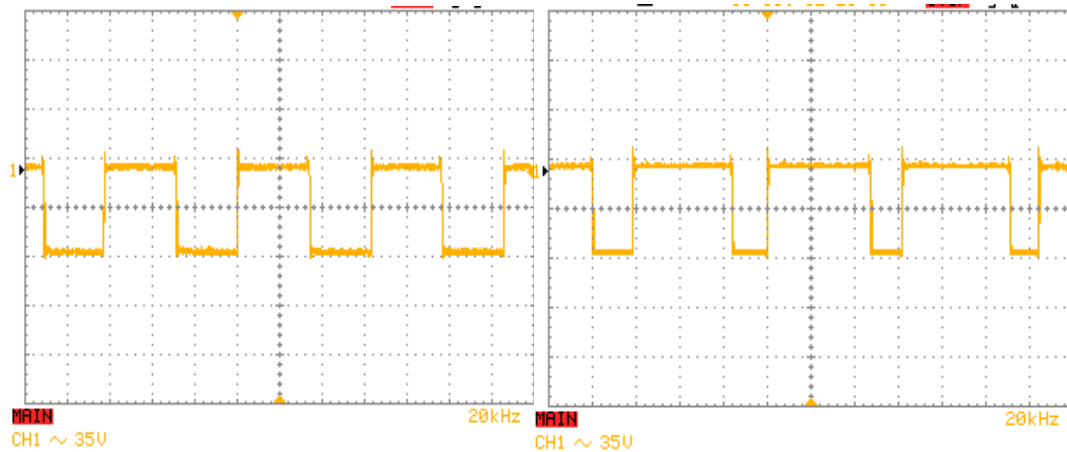


Figure 9.6: The inverter leg output voltage (MOSFETs voltage).

Figure 9.7 shows the experimental output voltage and current waveforms operating into a 310 ohm resistive load. The same tests were also run with a 60 ohm resistive load. The output waveforms for which are shown in Figure 9.8.

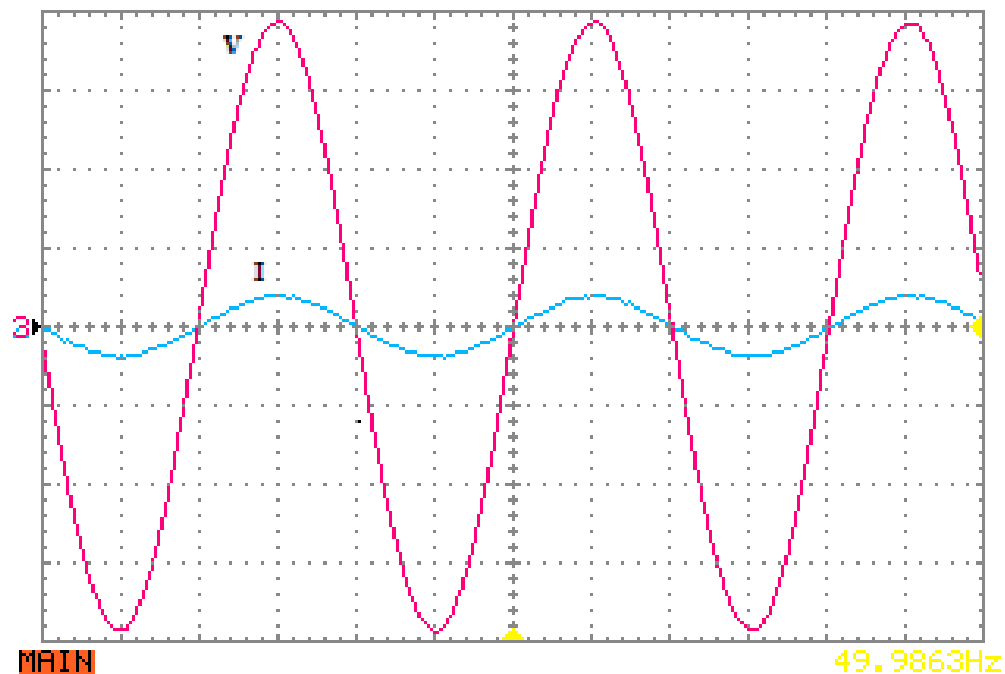


Figure 9.7: Experimental result of load voltage (80V/div) and current (2.5A/div) waveform with 310 ohm resistive load.

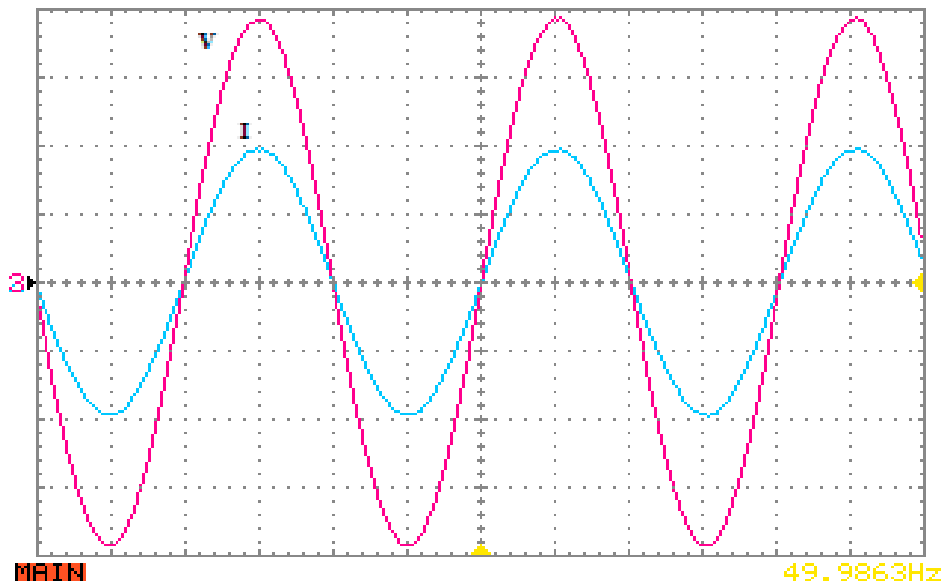


Figure 9.8: Experimental result of load voltage (80V/div) and current (2.5A/div) waveform under 60 ohm resistive load.

Figure 9.9 shows the experimental output waveforms driving (Power Factor: 0.45) inductive load. The corresponding phase angle between the current and voltage waveforms is evident in the figure.

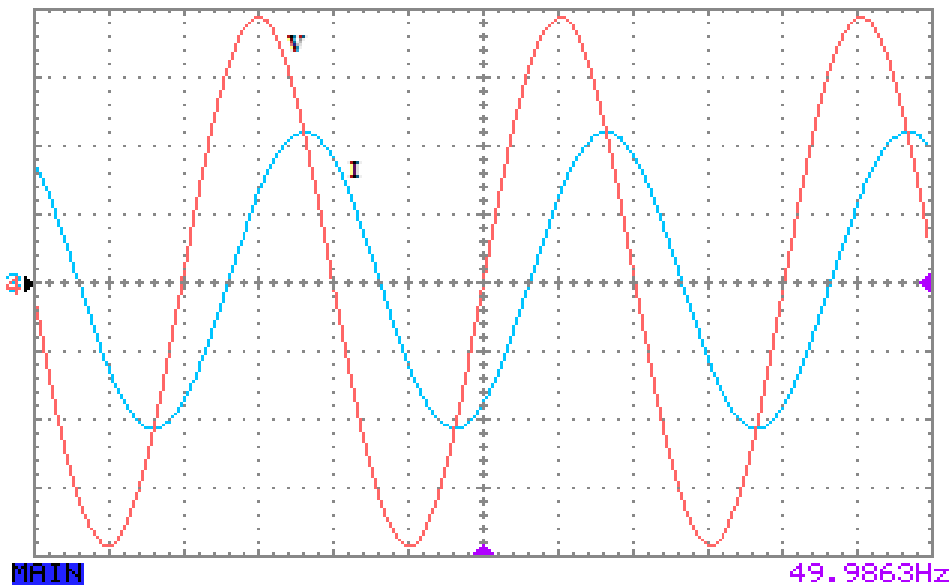


Figure 9.9: Voltage (80V/div) and current (2.5A/div) waveforms under 27 ohm+172mH, 0.45Pf.

It can be concluded from the above results (Figures 9.7 to 9.9) that the voltage and current waveform have periodically constant peak to peak values voltage and the power factor is unity. For purely resistive loads the output current does not affect the output voltage of the inverter. It is thus possible to maintain the AC output voltage within the specifications.

9.6 Experimental Setup in Grid-Tied Mode

In this section the inverter is tested in grid-tied mode. The grid-tied inverter operation was implemented using a variable autotransformer (variac) to match the grid voltage and inverter output voltage (220 V RMS, 311 V peak). The vast majority of the Europe, Asia, Africa, Middle East, and South America are using 220V RMS 50 Hz. The autotransformer will, to some degree, provide a small amount of inductance that will tend to augment the filter inductance.

Initially, some tests were carried out to insure that the PLL and inverter control circuit lock to the transformed grid voltage in phase and magnitude. The grid was tied to the inverter after verification that the voltages at either side of the autotransformer were equal in magnitude and there was zero phase offset between them. This test was performed with the intermediate grid-inverter common coupling point having parallel connection with the load. The controller was configured to export active power to the grid. Figure 9.10 shows the experimental setup scheme in grid-tied mode.

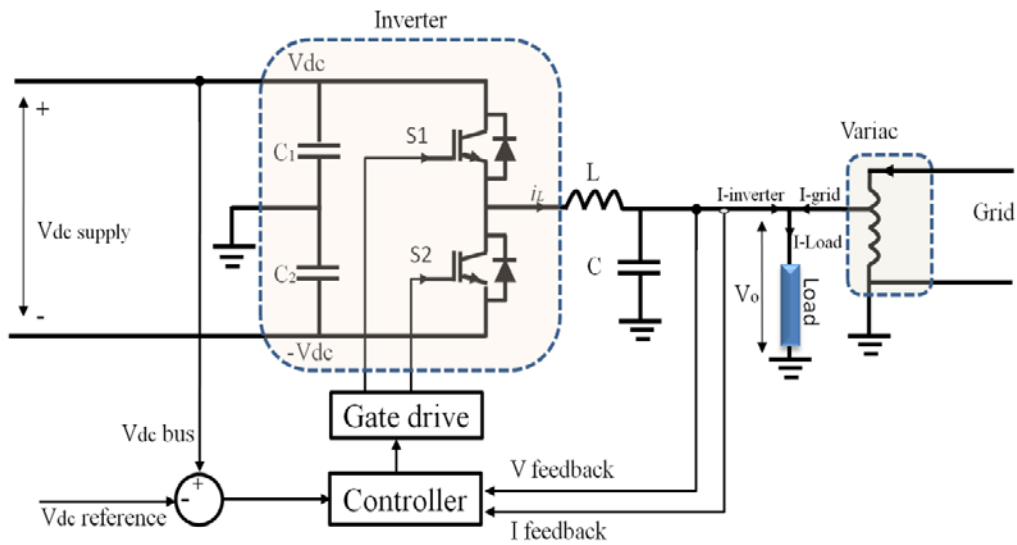


Figure 9.10: Experimental setup scheme in grid-tied mode.

The common coupling point is connected to a 36 ohm resistive load. The inverter exports active power to the load. Figure 9.11 shows that the load demand exceeds the power supplied by the inverter. Therefore, the grid provides active power to complement the load demand. It is clear that the grid and inverter output current waveforms are in phase.

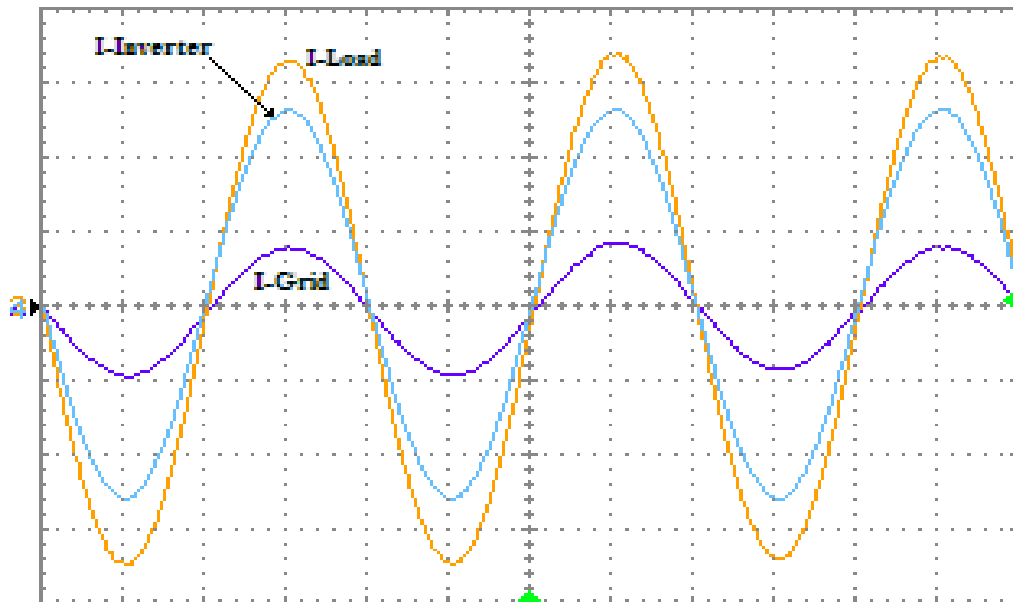


Figure 9.11: Experimental current waveforms at grid-connected common coupling point with a 36 ohm resistive load, (2.5A/div).

Figure 9.12 shows current waveforms at the common coupling point under 44.5 ohm resistive load. The load demand is approximately equivalent to the inverter rated power in this test, therefore the grid current is close to zero.

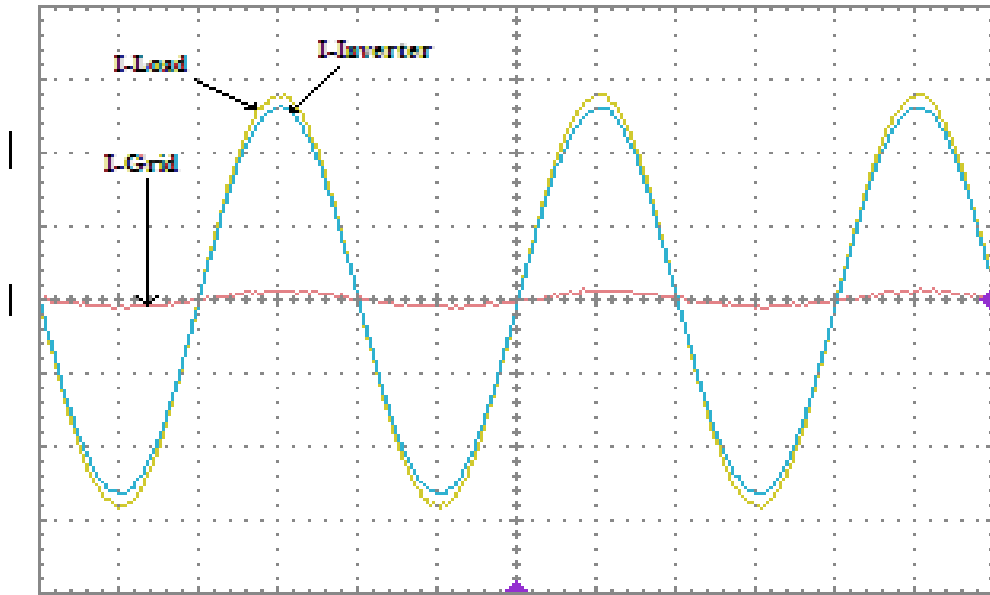


Figure 9.12: Experimental currents waveforms at grid-connected common coupling point under 44.5 ohm resistive load, (2.5A/div).

The system was then tested with a dominating inductive reactance on the load; 23 ohm+100mH, 0.6p.f. The current waveforms are shown in Figure 9.13. The inverter supplies available active power to the load, while the grid supplies the reactive power and the remainder of the active power demanded by the load. It is noted that the grid and load currents are in phase and the inverter current lags the grid current (Figure 9.14). The load reactive power component is being supplied from the grid side in addition to the part of the active component of power being provided by the inverter.

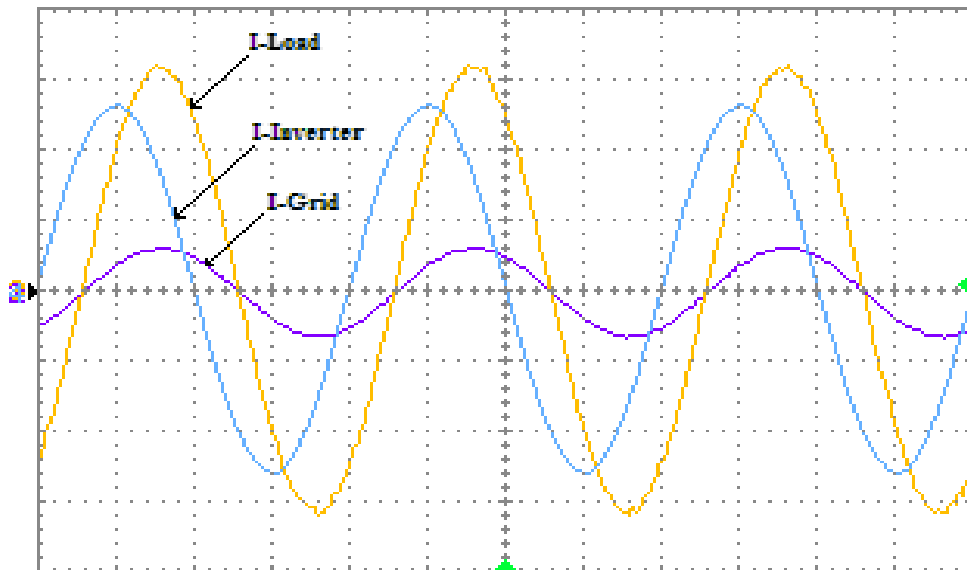


Figure 9.13: Current waveforms at the common coupling point under $23 \text{ ohm} + 100\text{mH}$, 0.6 p.f., (2.5A/div).

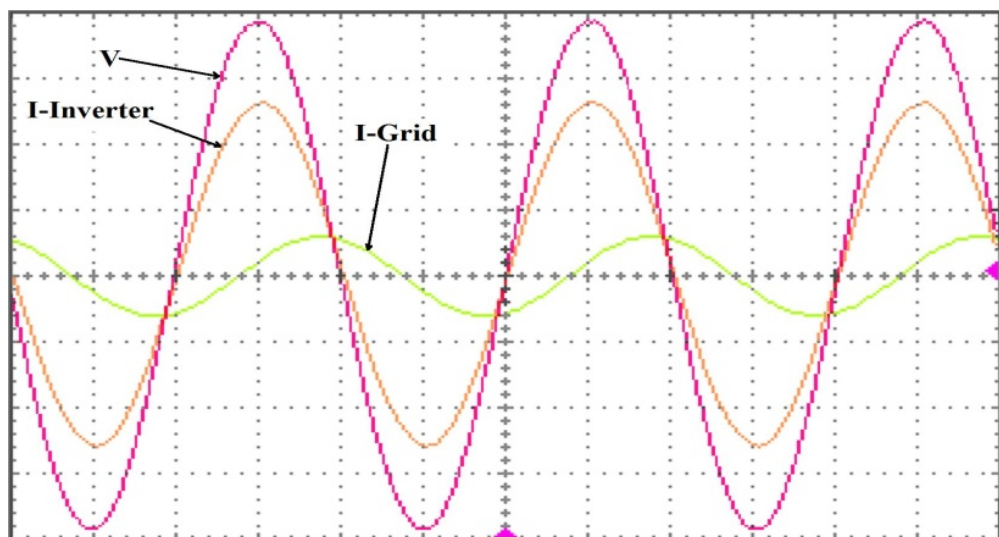


Figure 9.14: Inverter current, grid current (2.5A/div) and voltage (80V/div) waveforms at common coupling point under $23 \text{ ohm} + 100\text{mH}$, 0.6 p.f.

The inverter connected to a grid should allow power flow to or from the grid to the load depending on load power requirements. Therefore, the system was tested with a load power demand lower than the inverter generation capacity. In other words, the inverter generated power exceeds the load demand. As a result, the inverter should export the surplus power to the grid. Figure 9.15 shows that the inverter and load currents waveforms are in phase, while the grid current waveform is 180° out of phase. This case was presented

in simulation in Chapter 7 (using MATLAB/SIMULINK, see Figures 7.16 and 7.18, section 7.11.1).

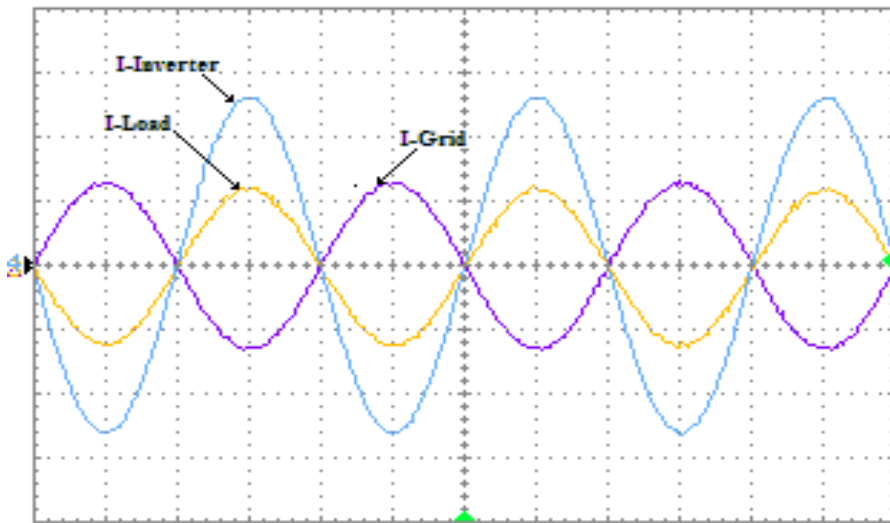


Figure 9.15: Current waveforms at the common coupling point under 105 ohm resistive load, (2.5A/div).

Figure 9.16 shows that the inverter current waveform is out of phase with grid current. The load current is close to zero. As a result the inverter output power is fully exported to the grid side. The same case is presented in Chapter 7 (Figure 7.19, section 7.11.1).

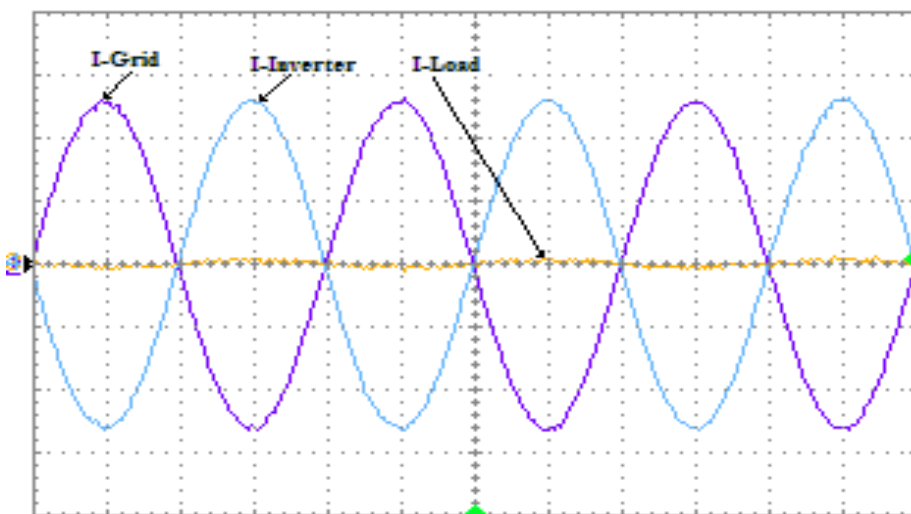


Figure 9.16: Current waveforms at common coupling point under load of 2500 ohm (2.5A/div).

In general, the experimental results indicate the effectiveness of the proposed control strategy. The experimental results validate the results obtained by simulation in sections 6.9 and 7.11.1. It is evident that the controller injects power at unity power factor. The power contributions of the inverter are not enough to give a statement about the performance of inverter without observation of the fundamental and harmonic spectra.

9.7 Inverter Harmonic Spectrum Analysis

The total harmonic distortion (THD) of the experimental inverter waveforms (output voltage and current waveforms) was measured. THD is the most common measurement for the relation between the fundamental and harmonic components of a waveform. The FFT is one method to determine the THD contained within a current or voltage waveform. The harmonic number that specifies a harmonic component is the ratio of the component's frequency to the fundamental frequency. The THD is mathematically given by:

$$THD = \frac{\sqrt{\sum_{n=2}^{\infty} H_n^2}}{H_1}$$

where H_1 is the magnitude of the fundamental component, H_n are the magnitudes of harmonic components, n is an integer. One purpose of the LC filter between source and load is to modify the spectral components of the source voltage appearing at the load.

The FFT of the output waveform is obtained using the digital oscilloscope. The harmonics of the inverter output voltage and current waveforms in stand-alone mode are shown in Figures 9.17 and 9.18, respectively. The tall bar represents the fundamental component, while the low-order harmonics and sideband components appear near the

fundamental component and are attenuated at higher frequencies. The harmonics and sideband spectra appear near to the cut off frequency region.

The voltage and current harmonic spectra should conform to standards [29]. Generally, the FFT analysis in stand-alone mode shows good correlation between the simulation and measurement results (Figures 6.31 and 6.32 sections 6.10). In most cases, the main sources of harmonics in static power converters are related to the PWM technique and filter design.

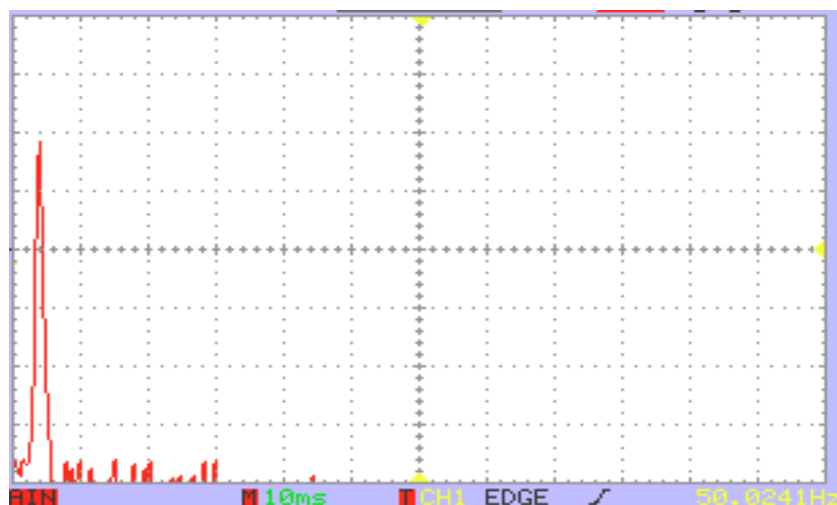


Figure 9.17: Inverter voltage harmonic spectrum in stand-alone mode (50V/div).



Figure 9.18: Inverter current harmonic spectrum in stand-alone mode (3A/div).

The harmonics of the inverter voltage and current output waveforms are also analysed in grid-tied inverter mode; the results being shown in Figures 9.19 and 9.20. It can be seen that the grid voltage causes the output current THD to increase. It is well known that the whole system performance is affected by grid voltage and PLL performance especially when the grid voltage contains harmonics. The voltage harmonics are likely caused by other devices connected to the grid side.

The harmonics of the inverter output voltage and current are also analysed in grid-tied inverter mode; the results being shown in Figures 9.19 and 9.20. It can be seen that the grid voltage causes the inverter output current THD to increase. It is well known [158] that the whole system performance is affected by grid voltage and the PLL performance especially when the grid voltage contains harmonics. The extra harmonics may be arising from the effects of all other devices connected to the grid side.

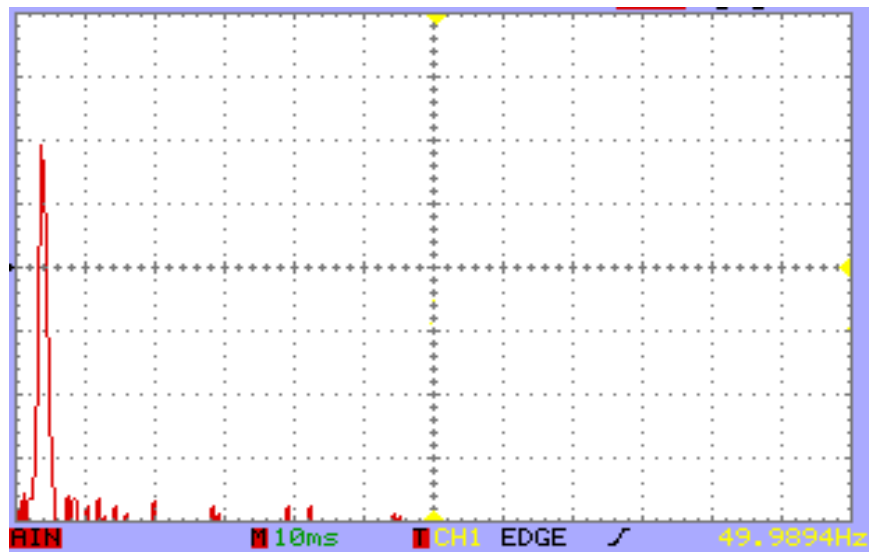


Figure 9.19: Inverter voltage harmonic spectrum in grid-tied mode (50V/div).

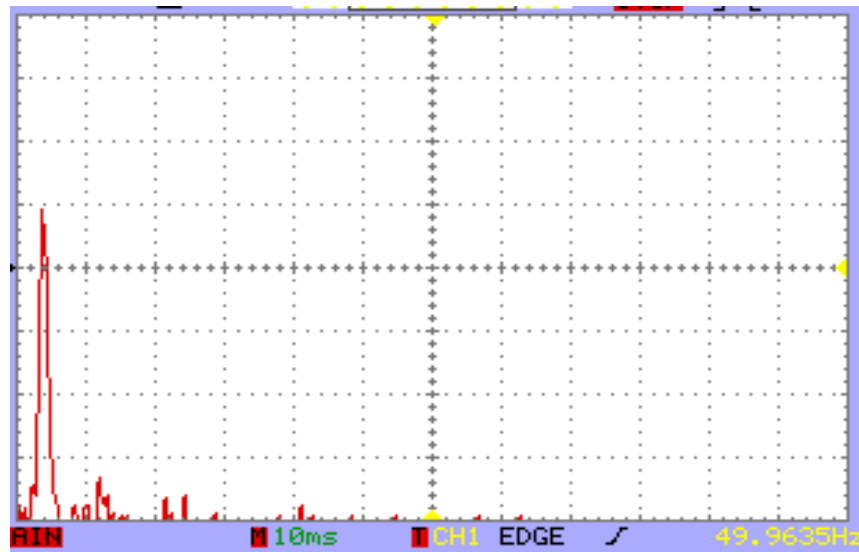


Figure 9.20: Inverter current harmonic spectrum in grid-tied mode (3A/div).

9.8 Summary

This chapter presents experimental verification of the proposed system. The proposed system power production capacity is 2500W. However, in practice, power was limited to 1kW by the available equipment. Nevertheless, in practice it assumes that system performance (data quality) is the target. The experimental system is based on a DSP-controlled inverter. The experimental work carried out employs the single-phase control strategy developed earlier in this thesis (Chapters 6 and 7). A comparison between the experimental and simulation results demonstrates the viability of the proposed control technique.

Regardless of the difference between the proposed system power production capacity (2500W) and practical prototype (1kW); the experimentally-obtained results have been confirmed with reference to the simulation results in stand-alone mode and also in grid-tied mode. The experimental results show good system performance and match the simulation results well in both modes.

There are minor differences between the experimental and simulation results of the FFT analysis. These could occur as a result of the real-world environment in the experimental prototype test, such as electromagnetic interference and, particularly in the case of the line voltage, of the presence of other non-linear loads connected to the same distribution system. Low frequency harmonic distortion in the grid voltage waveform most clearly affects grid-tied mode. The most common sources of harmonics are other high crest factor loads operating within that facility served by the same low-voltage grid/network.

In general, the experimental results show good agreement with the simulation results. The system achieves acceptable levels of harmonic performance. The experimental results enhance the simulation and show that the proposed control method has acceptable performance.

Chapter 10

CONCLUSIONS AND FUTURE WORK

10.1 Conclusions

This chapter summarizes and discusses the contributions made by this thesis and provides some suggestions for further research relating to the various topics considered. Techniques to develop novel and useful solutions for better interconnection of distributed power generation systems with the utility network are considered. At the end, this chapter points out potential future work.

10.2 Summary

PV inverters and their controllers are still undergoing development due to the fact that the requirements for inverter applications increase year upon year. Previous studies present many strategies of controller design that bring some advantages. With the advent of readily available high-speed embedded microprocessors and digital signal processors, the controller operating in the synchronous rotating reference frame has become the preferred solution for three-phase inverter applications in which high accuracy is required. However, a single-phase inverter controller design based on rotating reference frame theory has significant inherent complexity.

The transformation of AC waveforms to DC quantities through the use of a synchronous rotating reference frame is found to be a very useful tool for evaluating and designing controllers for three-phase inverters. The synchronous rotating reference frame controller has been proposed previously for high performance three-phase inverter applications. This is due to the fact that time-invariant systems are easier to control than

time-variant systems. After the transformation using the synchronous rotating reference frame, the internal representation of key signals becomes time-invariant. This:

- Provides a frequency transform such that the fundamental component of voltages at the power frequency is ‘seen’ as a time-invariant quantity, allowing the use of integral-term compensators (for example PI controllers) to achieve zero steady-state error;
- Segregates the control of the phase offset and the amplitude into two separate channels.

In many cases, developments in single-phase systems have followed the developments in three-phase systems. Accordingly, this thesis proposes a type of synchronous rotating reference frame method for controlling single-phase inverters for use in small-scale individual PV systems. Particular attention has been paid to the issues below:

1. Inverter modelling: Single-phase inverter modelling is based on the synchronous rotating reference frame. As a result, the single-phase inverter model is represented as two parallel channels (Phase and Amplitude channels). Thus, the inverter model exposes coupling terms between the phase and the amplitude channels.
2. Feedback signal transformation (Clarke and Park transformations): Special attention was paid to achieve a transformation stage requiring limited computational complexity as well as resulting in harmonics sufficiently below 5%, it is satisfy the IEEE stranded.
3. Controller structure: After the transformation step, the current and voltage feedback signals become time-invariant components separated in the ‘phase’ and the

'amplitude' channels (including coupling terms). Each channel consists of a current loop and an outer voltage loop. The coupling terms between the phase and the amplitude channels are decoupled within the controller. This allows for an alternative implementation of a *d-q* controller. The proposed synchronous rotating frame controller yields enhancements in the applications of low-cost and high-performance single-phase inverters.

4. Photovoltaic inverter front-end requirements: These requirements and the inverter controller performance under non-linear DC source voltage fluctuations were studied. This has led to improvements in the PV system output voltage quality. These improvements were achieved through appropriate choice of values for the DC-link capacitor, together with feed-forward compensation in the inverter controller stage. Subsequently, the inverter performance was examined using a DC source with a variable magnitude and source impedance.

5. Grid synchronization: This is based on a droop control technique. The sunlight changes randomly and hence the PV system can supply power that is not constant with time (sag and swell). As a result, this static, solid-state type of generator differs in its properties to conventional rotating generators. The inclusion of this type of energy sources within the power distribution network will also promote the following two interests:

- Power quality improvement: the potential improvement in achievable power quality in terms of the total harmonic distortion, transient case at rapid load change, and transient case at sudden frequency change.
- Network enhancement: The overall security of the power network is enhanced by generating smaller amounts of power in a lot of places rather than a lot of power in one single place.

The converter presented in this thesis can operate in a ‘flexible’ grid-tied mode. This flexibility is achieved by managing the active and reactive power injected to the grid at the common coupling point without requiring extensive communications between converters or the use of a centralized management service. The synchronous rotating frame technique for the single-phase inverter controller was developed in such a manner as to mimic synchronous rotating generators. The control structure was based on the droop method in order to achieve autonomous operation of PV systems as distributed generators. The proposed control strategy allows for achieving P and Q regulation performance based on *d-q* rotating frame controller. The results have been presented in order to validate the proposed control approach, and they demonstrate acceptable steady-state regulation and transient response.

6. Inverter switching gate-drive PWM technique: A part of the thesis has dealt with inverter switching gate drives by investigating the SVPWM algorithm for single-phase inverters. The newly developed SVPWM algorithm proposed herein is applicable to both single-phase half- and full-bridge inverters. The proposed SVPWM algorithm has been tested and the results compared with SPWM.

10.3 General Contributions of the Thesis

This thesis has presented analysis, simulation and experimental results focusing on modelling, control, and analysis of DG units, according to the following steps:

1. Modelling and analysis of single-phase inverter circuits by using a technique based on the synchronous rotating reference frame.
2. Reduction in the harmonic distortion associated with the transformation process (transforming AC control signal to DC components).

3. Enhancement of the PI controller performance by controlling the single-phase inverters based on the synchronous rotating reference frame.
4. Achievement of a controller structure for the single-phase inverter (based on the synchronous rotating reference frame) that imposes a lower computational burden on the control operations compared to previous work.
5. Several other advantages offered by the new transformation approach, such as:
 - Being fast and easy to implement.
 - Being more suitable and convenient with low-cost (rather than complex and expensive) DSP chips.
6. Improvements in the steady-state and transient response.
7. Capability to enhance the power networks by incorporating individual single-phase PV systems within the network as decentralized / distributed generators.
8. Analysis of the solid-state inverter droop function via synchronous rotating reference frame method.
9. Augmentation of the single-phase inverter control design with droop functions to mimic the rotating generators behaviour.
10. In grid-tied mode, grid-synchronisation of the inverter output via droop control functions without requiring extensive communications. As a result it has additional features such as facilitating a simple connection to the grid at the low-voltage consumer side of the network, and allows variable power flow to or from the grid and the local load.
11. Droop controller allowing active and/or reactive power to be imported and exported from the grid.
12. Control of the inverter output phase and amplitude separately.
13. The effectiveness of the proposed system has been verified by simulation.

14. A practical, experimental setup was implemented by using DSP and a suitable inverter bridge. The experimental prototype was tested under various conditions. The practical test results confirm and verify the performance obtained from simulations.

10.4 Future Work

The power conditioning unit proposed in this study is a part of a small-scale PV system. Although a significant amount of research has been carried out in order to come up with the above-mentioned achievements and solutions, there is still place for more improvements.

1. This thesis proposes a low-cost controller strategy based on using a synchronous rotating reference frame that is capable of being implemented on platforms where computation speed is limited. This opens the door to enhance much previous work that is based on the synchronous rotating reference frame, for example multilevel converters and controlled rectifiers.
2. Further work to explore control of parallel-connected inverters can make use of the new transformation strategy. For instance, a peak current and/or average current controller could conceivably achieve good results when applied together with the new transformation strategy.
3. Paralleling of single-phase converters within a hybrid network is a good way to improve the power rating and system reliability.
4. The droop function used by the proposed controller can handle different transmission line R/X ratios and this subject can be studied further.

References

- [1] Eldiclau,"Energy – Second generation technologies", Designed by Elegant WordPress Themes, Powered by WordPress, <http://www.eldiclau.ro/?p=445>
- [2] F. Sick and T. Erge, "Photovoltaics in Buildings", A Design Handbook for Architects and Engineers. Earthscan/James & James, 1996.
- [3] J. Nelson, "The Physics of Solar Cells", Imperial College Press London, 2003.
<http://www.worldscibooks.com/physics/p276.html>
http://www.icpress.co.uk/etextbook/p276/p276_chap1.pdf
- [4] http://www1.eere.energy.gov/solar/pdfs/solar_timeline.pdf
- [5] <http://www.missolar.com/faq.php>
- [6] <http://micro.magnet.fsu.edu/primer/java/solarcell/>
- [7] R. Kadri, J. P. Gaubert and G. Champenois, "An improved maximum power point tracking for photovoltaic grid-connected inverter based on voltage-oriented control", IEEE Transactions on Industrial Electronics, 2011, vol. 58, pp. 66-75.
- [8] M. Salhi, "Maximum Power Point Tracking controller for PV systems using a PI regulator with boost DC/DC converter," ICGSTACSE Journal, 2009, vol. 8, pp. 21-27.
- [9] M. L. Chiang, C. C. Hua and J. R. Lin, "Direct power control for distributed PV power system", Conference on Power Conversion (PCC).Proceedings of the Osaka 2002, vol. 1, pp. 311-315.
- [10] B. Alajmi, K. Ahmed, S. Finney and B. Williams, "Fuzzy Logic Controlled Approach of a Modified Hill Climbing Method for Maximum Power Point in Microgrid Stand-alone Photovoltaic System", IEEE Transactions on Power Electronics, 2011, pp. 1-1.

- [11] Q. Mei, M. Shan, L. Liu and J. M. Guerrero, "A novel improved variable step-size incremental-resistance MPPT method for PV systems", IEEE Transactions on Industrial Electronics, 2011, vol. 58, pp. 2427-2434.
- [12] F. Liu, S. Duan, F. Liu, B. Liu and Y. Kang, "A variable step size INC MPPT method for PV systems", IEEE Transactions on Industrial Electronics, 2008, vol. 55, pp. 2622-2628.
- [13] B. M. T. Ho, H. S. H. Chung and W. Lo, "Use of system oscillation to locate the MPP of PV panels", IEEE Power Electronics Letters, 2004, vol. 2, pp. 1-5.
- [14] J. Kimman, E. Ter Horst and E. Lysen, "PV in the Netherlands, learning while growing", IEEE First World Conference on Photovoltaic Specialists, Record of the Twenty Fourth, 1994.
- [15] J. Chadjivassiliadis, "Solar photovoltaic and wind power in Greece", Physical Science, Measurement and Instrumentation, Management and Education-Reviews, IEE Proceedings, 1987, vol. 134, pp. 457-463.
- [16] F. Juquois, P. Boulanger and P. Malbranche, "French guidelines for PV grid connection", Conversionon Photovoltaic Energy. Proceedings of 3rd World Conference, 2003, Vol. 3, pp. 2648-2651.
- [17] D. Picault, B. Raison and S. Bacha, "Guidelines for evaluating grid connected PV system topologies", IEEE International Conference on Industrial Technology(ICIT), 2009, pp. 1-5.
- [18] E. Spooner, "A new Australian standard for small grid-connected renewable generation systems connected via inverters", Australasian Universities Conference on Power Engineering (AUPE), Proceedings, 2001, pp. 23-26.
- [19] "Australian Guidelines for grid connection of energy systems via inverters"
<http://www.powerwater.com.au/?a=9812>
-

- [20] K. Khouzam and J. Yu, "Economic Assessment of Utility Connected Photovoltaic Systems for Residential and Commercial Use", 2004.
- [21] M. Watt, R. Morgan and R. Passey, "Experiences with residential grid-connected photovoltaic systems in Australia", Paper from ANZSES, Http://www.Ceem.Unsw.Edu.au/content/userDocs/WattMorganPasseySolar06_000.Pdf, 2006.
- [22] H. Wang, X. Yue, X. Pei and Y. Kang, "A novel dynamic strategy for the combined inverters based on feed-forward compensation", Conference on Telecommunications Energy (INTELEC). 31st International, 2009, pp. 1-5.
- [23] A. Zulu, B. Mecrow and M. Armstrong, "Prediction of performance of a wound-field segmented-rotor flux-switching synchronous motor using a dq-equivalent model", International Conference on Electrical Machines (ICEM), 2010 XIX, pp. 1-6.
- [24] N. R. Zargari and G. Joos, "Performance investigation of a current-controlled voltage-regulated PWM rectifier in rotating and stationary frames", IEEE Transactions on Industrial Electronics, 1995, vol. 42, pp. 396-401.
- [25] J. A. Gow, "Modeling, simulation and control of photovoltaic converter systems", A doctor of Philosophy of Loughborough University, 1998.
- [26] J. H. So, Y. S. Jung, B. G. Yu, H. M. Hwang, G. J. Yu and J. Y. Choi, "Performance results and analysis of large scale PV system", IEEE Conversion on Photovoltaic Energy, Conference Record of the 2006 4th World, pp. 2375-2378.
- [27] G. F. Reed, L. Solomon and B. M. Grainger, "Prototype development of a full-bridge isolated boost converter for solar photovoltaic systems integration", IEEE PES Conference Europe on Innovative Smart Grid Technologies (ISGT Europe), 2010, pp. 1-6.

- [28] S. Wakao, H. Takano, N. Nakada and T. Motegi, "Small-scale distributed PV power generation system of networked composition", Conference in Photovoltaic Energy Conversion, Proceedings of 3rd World, 2003, Vol. 3, pp. 2298-2301.
- [29] Anonymous "IEEE Recommended Practice for Utility Interface of Photovoltaic (PV) Systems," IEEE Standards Coordinating Committee 21 on Fuel Cells, Photovoltaics, Dispersed Generation, and Energy Storage Approved 30 January 2000 IEEE-SA Standards Board
- [30] B. K. Bose, "Modern Power Electronics and AC Drives", 2001.
- [31] E.Monmasson, "Power electronic converters; PWM strategies and current control", techniques.John Wiley & Sons. Copyright. Edited by Eric Monmasson, SATIE, University of Cergy-Pontoise, Publication Date: March 2011.
- [32] IEC 61727, "Characteristics of the utility interface for photovoltaic (PV) systems", International Electrotechnical Commission, IEC 61727, 2002.
- [33] S. B. Kjaer, J. K. Pedersen and F. Blaabjerg, "A review of single-phase grid-connected inverters for photovoltaic modules", IEEE Transactions on Industry Applications, 2005, vol. 41, pp. 1292-1306.
- [34] S. V. Araújo, P. Zacharias and R. Mallwitz, "Highly efficient single-phase transformerless inverters for grid-connected photovoltaic systems", IEEE Transactions on Industrial Electronics, 2010, vol. 57, pp. 3118-3128.
- [35] R. González, E. Gubía, J. López and L. Marroyo, "Transformerless single-phase multilevel-based photovoltaic inverter", IEEE Transactions on Industrial Electronics, 2008, vol. 55,pp. 2694-2702.
- [36] G. Spagnuolo, G. Petrone, S. V. Araujo, C. Cecati, E. Friis-Madsen, E. Gubia, D. Hissel, M. Jasinski, W. Knapp and M. Liserre, "Renewable energy operation and
-

- conversion schemes: A summary of discussions during the seminar on renewable energy systems", IEEE Industrial Electronics Magazine, 2010, vol. 4, pp. 38-51.
- [37] N. Mohan and T. M. Undeland, Power Electronics: Converters, Applications, and Design. Wiley-India, 2007.
- [38] M. H. Rashid, "Power electronics: Circuits, devices & applications, International ed." Recherche, 2003.vol. 67, pp. 02.
- [39] A. M. Hava, R. J. Kerkman and T. A. Lipo, "Carrier-based PWM-VSI overmodulation strategies: analysis, comparison, and design", IEEE Transactions on Power Electronics, 1998, vol. 13, pp. 674-689.
- [40] A. Yazdian-Varjani, S. Perera and J. F. Chicharo, "A centroid-based PWM switching technique for full-bridge inverter applications", IEEE Transactions on Power Electronics, 1998, vol. 13, pp. 115-124.,
- [41] R. S. Lai and K. D. T. Ngo, "A PWM method for reduction of switching loss in a full-bridge inverter", IEEE Transactions on Power Electronics, vol. 10, 1995, pp. 326-332.
- [42] T. H. Ai, J. F. Chen and T. J. Liang, "A random switching method for HPWM full-bridge inverter", IEEE Transactions on Industrial Electronics, 2002, vol. 49, pp. 595-597.
- [43] C. Cecati, A. Dell'Aquila, M. Liserre and V. G. Monopoli, "Design of H-bridge multilevel active rectifier for traction systems", IEEE Transactions on Industry Applications, 2003, vol. 39, pp. 1541-1550.
- [44] S. Fukuda and T. Yoda, "A novel current-tracking method for active filters based on a sinusoidal internal model [for PWM invertors]", IEEE Transactions on Industry Applications, 2001, vol. 37, pp. 888-895.

- [45] S. Fukuda and R. Imamura, "Application of a sinusoidal internal model to current control of three-phase utility-interface-converter", IEEE Specialist Conference on Power Electronics (PESC), IEEE 34th Annual, 2003, vol. 3, pp. 1301-1306.
- [46] M. Miloševic, "Hysteresis Current Control in Three-Phase Voltage Source Inverter".
- [47] B. K. Bose, "An adaptive hysteresis-band current control technique of a voltage-fed PWM inverter for machine drive system", IEEE Transactions on Industrial Electronics, 1990, vol. 37, pp. 402-408.
- [48] R. Teodorescu, F. Blaabjerg, U. Borup and M. Liserre, "A new control structure for grid-connected LCL PV inverters with zero steady-state error and selective harmonic compensation", IEEE Conference and Exposition on Applied Power Electronics (APEC).2004, Vol. 1, pp. 580-586.
- [49] B. Fernandes, S. Pillai and V. Subbarao, "Performance of an adaptive hysteresis band current controlled induction motor drive", International Conference on Industrial Electronics, Control, Instrumentation, and Automation, Power Electronics and Motion Control, Proceedings, 1992, vol. 1, pp. 447-452.
- [50] B. R. Lin, "Analysis and implementation of a three-level PWM rectifier/inverter", IEEE Transactions on Aerospace and Electronic Systems, 2000, vol. 36, pp. 948-956.
- [51] G. Bode and D. Holmes, "Implementation of three level hysteresis current control for a single phase voltage source inverter", IEEE 31st Annual Conference on Power Electronics Specialists (PESC), 2000, vol. 1, pp. 33-38.
- [52] L. Dixon, "Average current mode control of switching power supplies", Power Supply Design Seminar Manual in Unitrode (SEM700), 1990.
- [53] A. Davoudi, J. Jatskevich and P. L. Chapman, "Numerical Dynamic Characterization of Peak Current-Mode-Controlled DC-DC Converters", IEEE Transactions on Circuits and Systems II: Express Briefs, 2009, vol. 56, pp. 906-910.
-

- [54] R. Poley and A. Shiravar, "Digital Peak Current Mode Control with Slope Compensation using the TMS320F2803x", Texas Instruments, Application Report SPRABE7A–April 2012.
- [55] F. D. Tan and R. Middlebrook, "A unified model for current-programmed converters", IEEE Transactions on Power Electronics, 1995, vol. 10, pp. 397-408.
- [56] G. K. Andersen and F. Blaabjerg, "Current programmed control of a single-phase two-switch buck-boost power factor correction circuit", IEEE Transactions on Industrial Electronics, 2006, vol. 53, pp. 263-271.
- [57] T. Grote, F. Schafmeister, H. Figge, N. Frohleke, P. Ide and J. Bocker, "Adaptive digital slope compensation for peak current mode control", IEEE Energy Conversion Congress and Exposition (ECCE), 2009, pp. 3523-3529.
- [58] M. Aime, G. Gateau and T. A. Meynard, "Implementation of a peak-current-control algorithm within a field-programmable gate array", IEEE Transactions on Industrial Electronics, 2007, vol. 54, pp. 406-418.
- [59] D. Sera, T. Kerekes, M. Lungeanu, P. Nakhost, R. Teodorescu, G. K. Andersen and M. Liserre, "Low-cost digital implementation of proportional-resonant current controllers for PV inverter applications using delta operator", IEEE Annual Conference on Industrial Electronics Society(IECON). 31st 2005, pp. 6.
- [60] G. Xiaoqiang, Z. Qinglin and W. Weiyang, "A single-phase grid-connected inverter system with zero steady-state error", CES/IEEE 5th International Conference on Power Electronics and Motion Control (IPEMC). 2006, pp. 1-5.
- [61] R. Teodorescu, F. Blåbjer, M. Liserre and P. C. Loh, "Proportional-resonant controllers and filters for grid-connected voltage-source converters", IEE Proceedings on Electric Power Applications, 2006, pp. 750-762.

- [62] A. Kahrobaeian and S. Farhangi, "Stationary frame current control of single phase grid connected PV inverters", Conference on Power Electronic & Drive Systems & Technologies (PEDSTC), 1st, 2010, pp. 435-438.
- [63] A. Maknouninejad, M. G. Simoes and M. Zolot, "Single phase and three phase P resonant based grid connected inverters with reactive power and harmonic compensation capabilities", IEEE International Conference on Electric Machines and Drives (IEMDC'09), pp. 385-391.
- [64] M. Prodanovic and T. C. Green, "Control and filter design of three-phase inverters for high power quality grid connection", IEEE Transactions on Power Electronics, 2003, vol. 18, pp. 373-380.
- [65] H. Zhang, H. Zhou, J. Ren, W. Liu, S. Ruan and Y. Gao, "Three-phase grid-connected photovoltaic system with SVPWM current controller", IEEE 6th International Conference on Power Electronics and Motion Control (IPEMC'09), 2009, pp. 2161-2164.
- [66] S. A. Khajehhoddin, M. Karimi Ghartemani, P. Jain and A. Bakhshai, "A Control Design Approach for Three-Phase Grid-Connected Renewable Energy Resources", IEEE Transactions on Sustainable Energy, 2011, pp. 1-1.
- [67] Q. Zeng and L. Chang, "Study of advanced current control strategies for three-phase grid-connected pwm inverters for distributed generation", Conference on Control Applications(CCA), Proceedings of IEEE 2005, pp. 1311-1316.
- [68] R. Zhang, "High Performance Power Converter Systems for Nonlinear and Unbalanced load/source", A doctor of Philosophy of Virginia Polytechnic Institute and State University, 17-Nov. 1998.

- [69] N. Wohlgemuth and R. Madlener, "Financial support of renewable energy systems: Investment vs. operating cost subsidies", Conference on Towards an Integrated European Energy Market in NAEE, Bergen, Norway, 2000.
- [70] Intelligent energy "Small scale renewable applications", Projects supported by the IEE Programme, 15 innovative projects for an energy-intelligent Europe. Dec. 2006
- [71] IEEE Application Guide for IEEE Std 1547™, "IEEE Standard for Interconnecting Distributed Resources with Electric Power Systems", The published standard is available from the IEEE Std 1547-2003 Web page.
- [72] T. L.Vandoorn, B. Renders, L. Degroote, B. Meersman and L. Vandevelde, "Active load control in islanded microgrids based on the grid voltage", IEEE Transactions on Smart Grid, 2011, vol. 2, pp. 139-151.
- [73] R. Majumder, G. Ledwich, A. Ghosh, S. Chakrabarti and F. Zare, "Droop control of converter-interfaced microsources in rural distributed generation", IEEE Transactions on Power Delivery, 2010, vol. 25, pp. 2768-2778.
- [74] I. Y. Chung, W. Liu, D. A. Cartes, E. G. Collins and S. I. Moon, "Control methods of inverter-interfaced distributed generators in a microgrid system", IEEE Transactions on Industry Applications, 2010, vol. 46, pp. 1078-1088.
- [75] H. Avelar, W. Parreira, J. Vieira Jr, L. Gomes de Freitas and E. Coelho, "A State Equation Model of a Single Phase Grid Connected Inverter Using Droop Control Scheme Including an Extra Phase Shift Control Action", IEEE Transactions on Industrial Electronics, 2011, pp. 1-1.
- [76] R. Majumder, A. Ghosh, G. Ledwich and F. Zare, "Load sharing and power quality enhanced operation of a distributed microgrid", IET Renewable Power Generation, 2009, vol. 3, pp. 109-119.

- [77] K. H. Ahmed, S. J. Finney and B. W. Williams, "Passive filter design for three-phase inverter interfacing in distributed generation", *Compatibility in Power Electronics*, (CPE'07), 2007, pp. 1-9.
- [78] P. Khamphakdi and W. Khan-ngern, "The analysis of output filter for grid connected single phase full bridge inverter based PSpice simulation technique", in *Conf. Rec. of ICEMC-Phuket*, 2005.
- [79] J. Holtz, "Pulse width modulation-a survey", *IEEE Transactions on Industrial Electronics*, 1992, vol. 39, pp. 410-420.
- [80] Ó. López, J. Álvarez, J. Doval-Gandoy and F. D. Freijedo, "Multilevel multiphase space vector PWM algorithm", *IEEE Transactions on Industrial Electronics*, 2008, vol. 55, pp. 1933-1942.,
- [81] K. Rahman, M. R. Khan, M. Choudhury and M. Rahman, "Variable-band hysteresis current controllers for PWM voltage-source inverters", *IEEE Transactions on Power Electronics*, 1997, vol. 12, pp. 964-970.
- [82] K. D. Belloum and A. Moussi, "A Fixed Band Hysteresis Current Controller for Voltage Source AC Chopper", *World Academy of Science, Engineering and Technology* 45 2008.
- [83] K. V.Kumar, P. A. Michael, J.P. John and S. S. Kumar "simulation and comparison of spwm and svpwm control for three phase inverter", *journal of engineering and applied sciences (ARPN)*, no. 7, July 2010 vol. 5, pp61-74.
- [84] T. Sutikno, A. Jidin and M. F. Basar, "Simple Realization of 5-Segment Discontinuous SVPWM Based on FPGA", *International Journal of Computer and Electrical Engineering*, February, 2010, Vol. 2, No. 1, pp148-157

- [85] P.Tripura1, Y.S.Kishore Babu2, Y.R.Tagore2, "Space Vector Pulse Width Modulation Schemes for Two-Level Voltage Source Inverter", ACEEE Int. J. on Control System and Instrumentation, October 2011, Vol. 02, No. 03.
- [86] J. Chelladurai, G. S. Ilango, C. Nagamani and S. S. Kumar, "Investigation of various PWM techniques for shunt active filter", International Journal of Electrical Systems Science and Engineering, 2008, vol. 1, pp. 87-93.
- [87] D. Yuan, G. Xu, B. Hu, A. Xiang and J. Kang, "Research on a novel SVPWM for three-phase VSI", IEEE Conference on Vehicle Power and Propulsion (VPPC'08), 2008, pp. 1-5.
- [88] D. H. Jang and D. Y. Yoon, "Space-vector PWM technique for two-phase inverter-fed two-phase induction motors", IEEE Transactions on Industry Applications, 2003, vol. 39, pp. 542-549.
- [89] B. Hariram and N. Marimuthu, "Space vector switching patterns for different applications-a comparative analysis", IEEE International Conference on Industrial Technology (ICIT) 2005, pp. 1444-1449.
- [90] P. C. Krause, O. Wasynczuk, and S. D. Sudhoff, "Analysis of Electric Machinery" Volume 3 of IEEE Press Series on Power Engineering, Publisher IEEE Press, 1995. Original from the University of Michigan
- [91] G. Kron "Equivalen circuits of electric machinery", John Wiley and Sons, Inc., New York, NY., 1951.
- [92] D. N. Zmood, D. G. Holmes and G. H. Bode, "Frequency-domain analysis of three-phase linear current regulators", IEEE Transactions on Industry Applications, 2001, vol. 37, pp. 601-610.
- [93] P. Mattavelli, "Synchronous-frame harmonic control for high-performance AC power supplies", IEEE Transactions on Industry Applications, 2001, vol. 37, pp. 864-872.
-

- [94] D. N. Zmood and D. G. Holmes, "Stationary frame current regulation of PWM inverters with zero steady-state error", IEEE Transactions on Power Electronics, 2003, vol. 18, pp. 814-822.
- [95] L. Prokop and P. Grasblum, "3-Phase PM Synchronous Motor Vector Control Using a 56F80x, 56F8100, or 56F8300 Device", Freescale Semi—conductor Application Note, 2005.
- [96] H. Cha, T. K. Vu and J. E. Kim, "Design and control of proportional-resonant controller based photovoltaic power conditioning system", IEEE Energy Conversion Congress and Exposition (ECCE), 2009, pp. 2198-2205.
- [97] S. Buso, and P. Mattavelli, "Digital Control in Power Electronics", First Edition, Printed in the United States of America.
- [98] J. W. Choi and S. K. Sul, "Fast current controller in three-phase AC/DC boost converter using dq axis cross coupling", IEEE Transactions on Power Electronics, 1998, vol. 13, pp. 179-185.
- [99] F. Briz, M. W. Degner and R. D. Lorenz, "Analysis and design of current regulators using complex vectors", IEEE Transactions on Industry Applications, 2000, vol. 36, pp. 817-825.
- [100] M. Cichowlas and M. Kamierkowski, "Comparison of current control techniques for PWM rectifiers", IEEE International Symposium on Industrial Electronics (ISIE) Proceedings of the 2002, vol. 4, pp. 1259-1263.
- [101] I. Boldea, and S. A. Nasar, "Vector Control of Ac Drives", 1992
- [102] K. Dai, P. Liu, J. Xiong, and J. Chen, "Comparative study on current control for three-phase SVPWM voltage-source converter in synchronous rotating frame using

- complex vector method", IEEE 34th Annual Conference Power Electronics Specialist (PESC '03), 2003 , vol.2, pp 695 – 700.
- [103] Z. Lixia, K. Wei, J. Li, Z. Min and X. Ronggen, "Control of bidirectional current source SVPWM converter in the power accumulator battery testing system", Conference on Power and Energy Engineering (APPEEC), 2010 Asia-Pacific, 2010, pp. 1-4.
- [104] X. Wang, W. Freitas, W. Xu and V. Dinavahi, "Impact of interface controls on the steady-state stability of inverter-based distributed generators", IEEE Meetingin Power Engineering Society General, 2007, pp. 1-4.
- [105] H. Zeineldin and S. Kennedy, "Sandia frequency-shift parameter selection to eliminate nondetection zones", IEEE Transactions on Power Delivery, 2009, vol. 24, pp. 486-487.
- [106] S. K. Kim, J. H. Jeon and H. K. Choi, "Design of dq-based voltage positive feedback for anti-islanding of a DG inverter", Conference & Exposition on Transmission & Distribution: Asia and Pacific, 2009, pp. 1-4.
- [107] R. Carnieletto, D. B. Ramos, M. G. Simões and F. A. Farret, "Simulation and analysis ofDQ frame and P resonant controls for voltage source inverter to distributed generation", Conference on Power Electronics (COBEP'09). Brazilian, pp. 104-109.
- [108] B. Crowhurst, E. El-Saadany, L. El Chaar and L. Lamont, "Single-phase grid-tie inverter control using DQ transform for active and reactive load power compensation", IEEE International Conference on Power and Energy (PECon), 2010, pp. 489-494.

- [109] G. Franceschini, E. Lorenzani, C. Tassoni and A. Bellini, "Synchronous reference frame grid current control for single-phase photovoltaic converters", IEEE Annual Meeting on Industry Applications Society (IAS'08), 2008, pp. 1-7.
- [110] N. A. Ninad, L. A. C. Lopes and A. Rufer, "A vector controlled single-phase voltage source inverter with enhanced dynamic response", IEEE International Symposium on Industrial Electronics (ISIE), 2010, pp. 2891-2896.
- [111] S. Samerchur, S. Premrudeepreechacharn, Y. Kumsuwun and K. Higuchi, "Power control of single-phase voltage source inverter for grid-connected photovoltaic systems", IEEE/PES Conference and Exposition on Power Systems (PSCE), 2011, pp. 1-6.
- [112] J. Farhood and J. A. Gow, "Single Phase SVPWM for Grid-Tied Inverter Based on d-q Synchronous Reference Frame Controller", MESM'2010 - GAMEON-ARABIA'2010, December 1-3.
- [113] S. Yang, Q. Lei, F. Z. Peng and Z. Qian, "A robust control scheme for grid-connected voltage-source inverters", IEEE Transactions on Industrial Electronics, 2011, vol. 58, pp. 202-212.
- [114] G. Shen, X. Zhu, J. Zhang and D. Xu, "A new feedback method for PR current control of LCL-filter-based grid-connected inverter", IEEE Transactions on Industrial Electronics, 2010, vol. 57, pp. 2033-2041.
- [115] C. Liu, C. Sun and W. Hu, "Proportional-resonant controller of high power 400Hz inverter in stationary frame", International Conference on Electrical Machines and Systems (ICEMS), 2008, pp. 1772-1777.
- [116] N. A. Ninad and L. A. C. Lopes, "Per-phase DQ control of a three-phase battery inverter in a diesel hybrid mini-grid supplying single-phase loads", IEEE International Conference on Industrial Technology (ICIT), 2011, pp. 204-209.
-

- [117] B. Saritha and P. Jankiraman, "Observer based current control of single-phase inverter in DQ rotating frame", International Conference on Power Electronics, Drives and Energy Systems (PEDES'06), 2006, pp. 1-5.
- [118] S. WenSheng , Y.F. Xiao and X. Chenglin,"A Neutral Point Voltage Regulation Method With SVPWM Control For Single-phase Three-level NPC Converters",IEEE Vehicle Power and Propulsion Conference (VPPC), 2008, pp.1-4
- [119] N. Mohan, "first course on power electronics and drives", copyright© 2003 by Ned Mohan Printed in the United States of America
- [120] F. Haugen, "Discrete-time signals and systems", 2005.
- [121] A.Kulka, "Sensorless digital control of grid connected three phase converters for renewable sources", A doctoral thesis Trondheim, Norwegian University of Science and Technology, March 2009.
- [122] MATLAB/Simulink tutorial, ECEN 2060, Spring 2008.
http://ecee.colorado.edu/~ecen2060/materials/simulink/tutorial/MATLAB_Simulink_tutorial.pdf
- [123] PV Module Simulink models, ECEN 2060, Spring 2008.
http://ecee.colorado.edu/~ecen2060/materials/simulink/PV/PV_module_model.pdf
- [124] International Energy Agency (IEA), "Building Integrated Photovoltaic Power Systems" Guidelines for economic evaluation of building integrated PV, Report IEA PVPS T7-05: 2002
- [125] Economics of Solar Electric Systems 2009, Andy Black. All rights reserved. 19 of July 2009.

- [126] M.H. Coddington, R.M. Margolis, and J. Aabakken, Utility-Interconnected Photovoltaic Systems: Evaluating the Rationale for the Utility-Accessible External Disconnect Switch, Operated for the U.S. Department of Energy, Office of Energy Efficiency and Renewable Energy, Technical Report NREL/TP-581-42675 January 2008
- [127] IEA PVPS, "Risk analysis of islanding of photovoltaic power systems within low-voltage distribution networks", International Energy Agency, Implementing Agreement on Photovoltaic Power Systems, TASK V, Grid Interconnection of Building Integrated and Other Dispersed Photovoltaic Power Systems. Report IEA PVPS T5-08: 2002
- [128] R. Teodorescu, M. Liserre, P. Rodriguez "Grid Converters for Photovoltaic and Wind Power Systems" first published 2011 john Wiley
- [129] S. J. Chiang and J. M. Chang, "Parallel control of the UPS inverters with frequency-dependent droop scheme", IEEE Conference on Power Electronics Specialists (PESC'01), June 17-21, June 2001.
- [130] H. L. Willis and W. G. Scott, Distributed Power Generation: Planning and Evaluation. CRC Press, 2000.
- [131] K. E. Knapp, J. Martin, S. Price and F. M. Gordon, "Costing methodology for electric distribution system planning", Prepared for the Energy Foundation, 2000.
- [132] H. F. Wedde, S. Lehnhoff, C. Rehtanz and O. Krause, "Bottom-up self-organization of unpredictable demand and supply under decentralized power management",

Second IEEE International Conference on Self-Adaptive and Self-Organizing Systems (SASO'08). 2008, pp. 74-83.

[133] IEC standard voltages, INTERNATIONAL STANDARD (IEC 60038), Edition 6.2 2002,

[134] Wiki Electrical Installation Guide (WIKI-EIG), "Low voltage utility distribution networks, Low-voltage consumers", http://www.electrical-installation.org/enwiki/Low-voltage_consumers

[135] S. Barsali, M. Ceraolo, P. Pelacchi and D. Poli, "Control techniques of dispersed generators to improve the continuity of electricity supply", IEEE Winter Meeting in Power Engineering Society, 2002, vol. 2, pp. 789-794.

[136] I. Zabet and M. Montazeri, "Decentralized control and management systems for power industry via multi-agent systems technology," in Power Engineering and Optimization Conference (PEOCO), 2010 4th International, 2010, pp. 549-556.

[137] M. Kandil, M. El-Saadawi, A. Hassan and K. Abo-Al-Ez, "A proposed reactive power controller for DG grid connected systems," IEEE International Conference in Energy and Exhibition (Energy Con.), 2010, pp. 446-451.

[138] W. Deng, W. Pei and Z. Qi, "Impact and improvement of distributed generation on voltage quality in micro-grid," Third International Conference on Electric Utility Deregulation and Restructuring and Power Technologies (DRPT), 2008, pp. 1737-1741.

- [139] C. K. Sao and P. W. Lehn, "Control and power management of converter fed microgrids", IEEE Transactions on Power Systems, 2008, vol. 23, pp. 1088-1098.
- [140] J. M. Guerrero, L. G. De Vicuna, J. Matas, M. Castilla and J. Miret, "A wireless controller to enhance dynamic performance of parallel inverters in distributed generation systems", IEEE Transactions on Power Electronics, 2004, vol. 19, pp. 1205-1213.
- [141] M. Dai, M. N. Marwali, J. W. Jung and A. Keyhani, "Power flow control of a single distributed generation unit with nonlinear local load", IEEE Conference and Expositionin Power Systems, 2004, vol. 1pp. 398-403.
- [142] M. Reza, D. Sudarmadi, F. Viawan, W. Kling and L. Van Der Sluis, "Dynamic stability of power systems with power electronic interfaced DG," IEEE Conference and Expositionin Power Systems, 2006. pp. 1423-1428.
- [143] R. Majumder, B. Chaudhuri, A. Ghosh, G. Ledwich and F. Zare, "Improvement of stability and load sharing in an autonomous microgrid using supplementary droop control loop," IEEE Transactions on Power Systems, 2010, vol. 25, pp. 796-808.,
- [144] M. N. Marwali, J. W. Jung and A. Keyhani, "Stability analysis of load sharing control for distributed generation systems," IEEE Transactions on Energy Conversion, 2007, vol. 22, pp. 737-745.
- [145] H. Karimi, A. Yazdani and R. Iravani, "Robust Control of an Autonomous Four-Wire Electronically-Coupled Distributed Generation Unit," IEEE Transactions on Power Delivery, 2011, vol. 26, pp. 455-466.

- [146] T. Goya, E. Omine, Y. Kinjyo, T. Senju, A. Yona, N. Urasaki and T. Funabashi, "Frequency control in isolated island by using parallel operated battery systems applying $H\infty$ control theory based on droop characteristics," Renewable Power Generation, IET, 2011, vol. 5, pp. 160-166.
- [147] J. J. Seo, H. J. Lee, W. W. Jung and D. J. Won, "Voltage control method using modified voltage droop control in LV distribution system," Conference & Expositionin Transmission & Distribution: Asia and Pacific, 2009, 2009, pp. 1-4.
- [148] A. Engler and N. Soultanis, "Droop control in LV-grids," International Conference on Future Power Systems, 2005, pp.-6.
- [149] K. De Brabandere, B. Bolsens, J. Van den Keybus, A. Woyte, J. Driesen and R. Belmans, "A voltage and frequency droop control method for parallel inverters" , IEEE Transactions on Power Electronics, 2007, vol. 22, pp. 1107-1115.
- [150] J. Au-Yeung, G. M. A. Vanalme, J. M. A. Myrzik, P. Karaliolios, M. Bongaerts, J. Bozelie and W. L. Kling, "Development of a voltage and frequency control strategy for an autonomous LV network with distributed generators," Engineering Conference in Universities Power (UPEC), 2009 Proceedings of the 44th International, 2009, pp. 1-5.
- [151] L. Harnefors and H. P. Nee, "A general algorithm for speed and position estimation of AC motors," IEEE Transactions on Industrial Electronics, 2000, vol. 47, pp. 77-83.

- [152] Y. Li and Y. W. Li, "Decoupled power control for an inverter based low voltage microgrid in autonomous operation," IEEE 6th International Conference in Power Electronics and Motion Control (IPEMC'09), 2009. pp. 2490-2496.
- [153] V. R. Bathula and B. Chitti Babu, "Power Quality Improvement by Using Synchronous Virtual Grid Flux Oriented Control of Grid Side Converter, "<http://cdn.intechweb.org/pdfs/23861.pdf>
- [154] S. Jena, B. C. Babu and A. Naik, "Experimental study on reactive power management in inverter-interfaced distributed generation system," International Conference on Sustainable Energy and Intelligent Systems (SEISCON 2011), 2011, pp. 80-85.
- [155] Microchip website "<http://www.microchip.com/>"
- [156] dsPICDEM™ MC1H 3-Phase High Voltage Power Module User's Guide, (DS70096A).<http://ww1.microchip.com/downloads/en/DeviceDoc/70096A.pdf>
- [157] dsPICDEM™ MC1L 3-Phase Low Voltage Power Module User's Guide, (DS70097A).<http://ww1.microchip.com/downloads/en/devicedoc/70097A.pdf>
- [158] O. Krievs, I. Steiks and L. Ribickis "A PLL Scheme for Synchronization with Grid Voltage Phasor in Active Power Filter Systems" Scientific Journal of Riga Technical University, Power and Electrical Engineering, 2010, Vol. 27.

Appendix A:

MATLAB/SIMULINK SVPWM Program

```
function y=SVPWM(u)
clock=u(3);
t_sampling=u(2); t_sampling = 1/(frequency*number of sampling)
Vref=u(4);
if u(1)>= pi/2
ta=Vref*sin(u(1))*t_sampling;
sector=1;
elseif u(1)>= pi
ta=Vref*sin(pi-u(1))*t_sampling;
sector=1;
elseif u(1)>=3*pi/2
ta=Vref*sin(u(1)-pi)*t_sampling;
sector=2;
else ta=Vref*sin(2*pi-u(1))*t_sampling;
sector=2;
end
ta=ta+t_sampling/2;
tb=t_sampling-ta;
t_count = fix(clock/t_sampling)*t_sampling;
if sector ==1
if (clock < (ta+t_count));
    OUTPUT = 1;
else OUTPUT = 0;
end;
else
if (clock < (tb+t_count));
    OUTPUT = 1;
else OUTPUT =0;
end;
end
y=OUTPUT;
```

Appendix B:

State-Space Equations of Half-Bridge Inverter with an LC Output Filter

The single-phase half-bridge inverter shown in Figure B.1 includes $L\ C$ filter with r_L and r_c parasitics. All the passive components are on the AC side. The switching model is calculated based on the power stage topology.

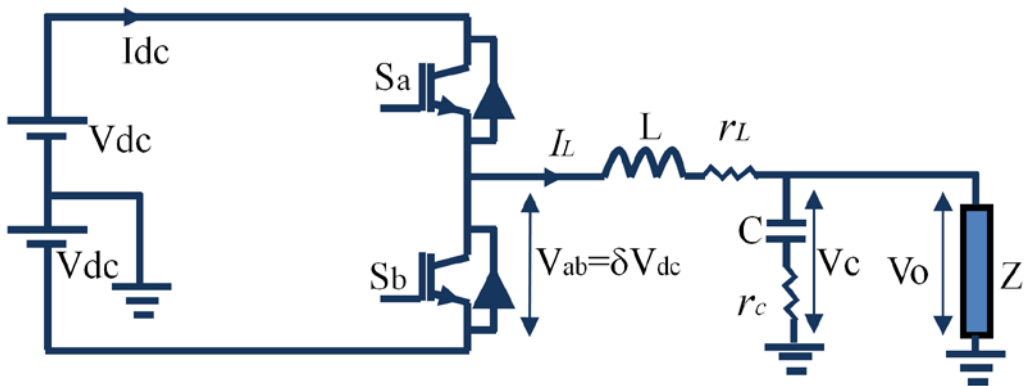


Figure B.1: Single-phase half-bridge inverter with $L\ C$ filter.

The switching function can be concluded in accordance with the inverter operation principle, which can be deduced from:

$$\delta(t) = \begin{cases} 1 \\ 0 \\ -1 \end{cases} \quad (B-1)$$

The control variable V_x takes the values depending on the switching state in the half-bridge inverter, where $V_{ab} = V_{dc}\delta$. Thus:

$$V_{ab} = \begin{cases} V_{dc} \\ 0 \\ -V_{dc} \end{cases} \quad (B-2)$$

The state space equations of the single phase half-bridge inverter are given below:

$$C \frac{dv_c}{dt} = I_L - \frac{V_o}{Z} \quad (B-3)$$

$$L \frac{dI_L}{dt} + r_L I_L = V_x - V_o \quad (B-4)$$

where V_o is defined as:

$$V_o = V_c + C \frac{dv_c}{dt} r_c \quad (B-5)$$

Substituting (B-5) into (B-3) gives:

$$C \frac{dv_c}{dt} = I_L - \frac{1}{Z} (V_c + C \frac{dv_c}{dt} r_c) \quad (B-6)$$

Simplify (B-6) step by step as follow

$$\begin{aligned} C \frac{dv_c}{dt} &= I_L - \frac{1}{Z} V_c - \frac{1}{Z} C \frac{dv_c}{dt} r_c \\ C \frac{dv_c}{dt} + \frac{1}{Z} C \frac{dv_c}{dt} r_c &= I_L - \frac{1}{Z} V_c \\ \frac{dv_c}{dt} \left(C + \frac{C r_c}{Z} \right) &= I_L - \frac{1}{Z} V_c \\ C \frac{dv_c}{dt} &= \left(I_L - \frac{1}{Z} V_c \right) \left(\frac{Z}{Z + r_c} \right) \end{aligned} \quad (B-7)$$

$$\frac{dv_c}{dt} = \left(I_L - \frac{1}{Z} V_c \right) \left(\frac{Z}{C Z + C r_c} \right) \quad (B-8)$$

Substituting (B-5) into (B-4) gives:

$$L \frac{dI_L}{dt} + r_L I_L = V_x - \left(V_c + C \frac{dv_c}{dt} r_c \right) \quad (B-9)$$

$$L \frac{dI_L}{dt} + r_L I_L = V_x - V_c - C \frac{dv_c}{dt} r_c$$

Substituting (B-7) into (B-4) gives:

$$L \frac{dI_L}{dt} + r_L I_L(t) = V_x - V_c - \left[\left(I_L - \frac{1}{Z} V_c \right) \left(\frac{Z}{Z + r_c} \right) r_c \right] \quad (B-10)$$

Simplify (B-10) step by step as follow

$$\begin{aligned} L \frac{dI_L}{dt} + r_L I_L &= V_x - V_c - I_L \left(\frac{Z r_c}{Z + r_c} \right) + V_c \left(\frac{r_c}{Z + r_c} \right) \\ L \frac{dI_L}{dt} &= V_x - r_L I_L - I_L \left(\frac{Z r_c}{Z + r_c} \right) - V_c + V_c \left(\frac{r_c}{Z + r_c} \right) \\ L \frac{dI_L}{dt} &= I_L \left[-r_L - \left(\frac{Z r_c}{Z + r_c} \right) \right] + V_c \left[-1 + \left(\frac{r_c}{Z + r_c} \right) \right] + V_{ab} \\ L \frac{dI_L}{dt} &= I_L \left[-r_L - \left(\frac{Z r_c}{Z + r_c} \right) \right] + V_c \left[-1 + \left(\frac{r_c}{Z + r_c} \right) \right] + V_{ab} \\ \frac{dI_L}{dt} &= \frac{I_L}{L} \left[-r_L - \left(\frac{Z r_c}{Z + r_c} \right) \right] + V_c \frac{1}{L} \left[-1 + \left(\frac{r_c}{Z + r_c} \right) \right] + \frac{1}{L} V_{ab} \end{aligned} \quad (B-11)$$

The state space equations of the single phase inverter are derived by (B-8) and (B-11), are given below

$$\begin{aligned} \frac{dI_L}{dt} &= \frac{I_L}{L} \left[-r_L - \left(\frac{Z r_c}{Z + r_c} \right) \right] + V_c \frac{1}{L} \left[-1 + \left(\frac{r_c}{Z + r_c} \right) \right] + \frac{1}{L} V_{ab} \\ \frac{dv_c}{dt} &= I_L \left(\frac{Z}{C Z + C r_c} \right) - V_c \left(\frac{1}{C Z + C r_c} \right) \end{aligned} \quad (B-12)$$

$$\dot{X} = A X + B U$$

$$\begin{bmatrix} \dot{i}_L \\ \dot{v}_c \end{bmatrix} = \begin{bmatrix} \frac{1}{L} \left[-r_L - \left(\frac{Z r_c}{Z + r_c} \right) \right] & \frac{1}{L} \left[-1 + \left(\frac{r_c}{Z + r_c} \right) \right] \\ \left(\frac{Z}{C Z + C r_c} \right) & \left(\frac{-1}{C Z + C r_c} \right) \end{bmatrix} \cdot \begin{bmatrix} I_L \\ V_c \end{bmatrix} + \begin{bmatrix} \frac{1}{L} \\ 0 \end{bmatrix} \delta V_{dc} \quad (B-13)$$

$$Y = C X + D U$$

$$V_o = \begin{bmatrix} Z r_c \\ Z + r_c \end{bmatrix} \cdot \begin{bmatrix} I_L \\ V_c \end{bmatrix} \quad (B-14)$$

The state variables, i_L and v_c represent the first time derivatives of the inductor current and the capacitor voltage, respectively. The above state-space model describes a simple model with linear differential equations.

The above state-space model is used to derive the inverter transfer function.

$$X(s) = (sI - A)^{-1} B U(s)$$

$$Y(s) = [C(sI - A)^{-1} B + D]U(s)$$

$$A = \begin{bmatrix} \left[-\frac{r_L}{L} - \left(\frac{Z r_c}{Z + r_c} \right) \frac{1}{L} \right] & \left[-\frac{1}{L} + \left(\frac{r_c}{Z + r_c} \right) \frac{1}{L} \right] \\ \left(\frac{Z}{C Z + C r_c} \right) & \left(\frac{-1}{C Z + C r_c} \right) \end{bmatrix}$$

$$A = \begin{bmatrix} a_{11} & a_{12} \\ a_{21} & a_{22} \end{bmatrix}$$

$$(sI - A) = \begin{bmatrix} s - a_{11} & -a_{12} \\ -a_{21} & s - a_{22} \end{bmatrix}$$

$$(sI - A)^{-1} = \frac{1}{(s - a_{11})(s - a_{22}) - a_{12} a_{21}} \begin{bmatrix} s - a_{22} & a_{21} \\ a_{12} & s - a_{11} \end{bmatrix}^T$$

$$(sI - A)^{-1} = \frac{1}{(s - a_{11})(s - a_{22}) - a_{12} a_{21}} \begin{bmatrix} s - a_{22} & a_{12} \\ a_{21} & s - a_{11} \end{bmatrix}$$

$$(sI - A)^{-1} = \frac{1}{\left(s - \left[-\frac{r_L}{L} - \left(\frac{Z r_c}{Z + r_c} \right) \frac{1}{L} \right] \right) \left(s - \left(\frac{-1}{C Z + C r_c} \right) \right) - \left[-\frac{1}{L} + \left(\frac{r_c}{Z + r_c} \right) \frac{1}{L} \right] \left(\frac{Z}{C Z + C r_c} \right)} \begin{bmatrix} s - \left(\frac{-1}{C Z + C r_c} \right) & \left[-\frac{1}{L} + \left(\frac{r_c}{Z + r_c} \right) \frac{1}{L} \right] \\ \left(\frac{Z}{C Z + C r_c} \right) & s - \left[-\frac{r_L}{L} - \left(\frac{Z r_c}{Z + r_c} \right) \frac{1}{L} \right] \end{bmatrix}$$

$$\frac{Y(s)}{U(s)} = [C(sI - A)^{-1} B + D]$$

$$C = \begin{bmatrix} \frac{Z r_c}{Z + r_c} & \frac{Z}{Z + r_c} \end{bmatrix} = [c_{11} \quad c_{12}], \quad B = \begin{bmatrix} 1 \\ 0 \end{bmatrix} = \begin{bmatrix} b_{11} \\ 0 \end{bmatrix}$$

$$\frac{Y(s)}{U(s)} = [C(sI - A)^{-1} B + D]$$

$$\frac{Y(s)}{U(s)} = \frac{1}{(s - a_{11})(s - a_{22}) - a_{12} a_{21}} [c_{11}(s - a_{22}) + c_{12} a_{21}] b_{11}$$

$$\frac{Y(s)}{U(s)} = G(s) = \frac{V_o}{\delta} = \frac{\left[\frac{Zr_c}{Z+r_c} \left(s - \left(\frac{-1}{C Z + C r_c} \right) \right) + \frac{Z}{Z+r_c} \left(\frac{Z}{C Z + C r_c} \right) \right] \frac{1}{L} V_{dc}}{\left(s - \left[-\frac{r_L}{L} - \left(\frac{Z r_c}{Z+r_c} \right) \frac{1}{L} \right] \right) \left(s - \left(\frac{-1}{C Z + C r_c} \right) \right) - \left[-\frac{1}{L} + \left(\frac{r_c}{Z+r_c} \right) \frac{1}{L} \right] \left(\frac{Z}{C Z + C r_c} \right)} \quad (B-15)$$

$$numerator = \left[\frac{Zr_c}{Z+r_c} \left(s - \left(\frac{-1}{C Z + C r_c} \right) \right) + \frac{Z}{Z+r_c} \left(\frac{Z}{C Z + C r_c} \right) \right] \frac{1}{L}$$

$$numerator = \frac{Z}{Z+r_c} \left[\left(sr_c + \frac{r_c}{C Z + C r_c} \right) + \left(\frac{Z}{C Z + C r_c} \right) \right] \frac{1}{L}$$

$$numerator = \frac{Z}{Z+r_c} \left[sr_c + \frac{r_c}{C Z + C r_c} + \frac{Z}{C Z + C r_c} \right] \frac{1}{L}$$

$$numerator = \frac{Z}{Z+r_c} \left[sr_c + \frac{r_c + Z}{C Z + C r_c} \right] \frac{1}{L}$$

$$numerator = \frac{Z}{Z+r_c} \left[sr_c + \frac{1}{C} \right] \frac{1}{L} \quad (B-16)$$

$$denominator = \left(s - \left[-\frac{r_L}{L} - \left(\frac{Z r_c}{Z+r_c} \right) \frac{1}{L} \right] \right) \left(s - \left(\frac{-1}{C Z + C r_c} \right) \right) - \left[-\frac{1}{L} + \left(\frac{r_c}{Z+r_c} \right) \frac{1}{L} \right] \left(\frac{Z}{C Z + C r_c} \right)$$

$$denominator = \left(s + \frac{r_L}{L} + \frac{Z r_c / L}{Z+r_c} \right) \left(s + \frac{1/C}{Z+r_c} \right) + \frac{Z/LC}{Z+r_c} - \left(\frac{r_c / L}{Z+r_c} \right) \frac{Z/C}{Z+r_c}$$

$$denominator = \left(s + \frac{r_L}{L} + \frac{Z r_c / L}{Z+r_c} \right) \left(s + \frac{1/C}{Z+r_c} \right) + \frac{Z/LC}{Z+r_c} - \frac{Z r_c / L C}{(Z+r_c)^2}$$

$$denominator = s^2 + s \frac{r_L}{L} + s \frac{Z r_c / L}{(Z+r_c)} + s \frac{1/C}{(Z+r_c)} + \frac{r_L / LC}{(Z+r_c)} + \frac{Z r_c / LC}{(Z+r_c)^2} + \frac{Z / LC}{(Z+r_c)} - \frac{Z r_c / L C}{(Z+r_c)^2}$$

$$denominator = s^2 + s \left(\frac{r_L}{L} + \frac{Z r_c / L + 1/C}{(Z+r_c)} \right) + \left(\frac{r_L / LC + Z / LC}{(Z+r_c)} \right)$$

$$denominator = s^2 + s \left(\frac{r_L}{L} + \frac{Z r_c / L + 1/C}{(Z+r_c)} \right) + \left(\frac{r_L / LC + Z / LC}{(Z+r_c)} \right)$$

$$denominator = s^2 + s \left(\frac{r_L}{L} + \frac{(Z C r_c + L)}{LC(Z+r_c)} \right) + \left(\frac{(r_L + Z)}{LC(Z+r_c)} \right) \quad (B-17)$$

$$G(s) = \frac{V_o}{\delta} = \frac{\left(s + \frac{1}{C r_c} \right) \left(\frac{Zr_c}{Z+r_c} \right) \frac{1}{L} V_{dc}}{s^2 + s \left(\frac{r_L}{L} + \frac{(Z C r_c + L)}{LC(Z+r_c)} \right) + \left(\frac{(r_L + Z)}{LC(Z+r_c)} \right)} \quad (B-18)$$

$$G(s) = \frac{\left(s + \frac{1}{Cr_c}\right) \frac{Zr_c}{L(Z+r_c)} V_{dc}}{s^2 + s \left(\frac{r_L}{L} + \frac{(ZCr_c+L)}{LC(Z+r_c)}\right) + \left(\frac{(r_L+Z)}{LC(Z+r_c)}\right)} \quad (\text{B}-19)$$

$$\omega_o = \sqrt{\frac{(r_L+Z)}{LC(Z+r_c)}}$$

$$\frac{\omega_o}{Q} = \left(\frac{r_L}{L} + \frac{(ZCr_c+L)}{LC(Z+r_c)} \right)$$

$$\frac{\omega_o}{Q} = \left(\frac{r_L C (Z+r_c) + (ZCr_c+L)}{L C (Z+r_c)} \right)$$

$$\frac{\omega_o}{Q} = \left(\frac{ZCr_c + r_c r_L C + Zr_L C + L}{L C (Z+r_c)} \right)$$

$$Q = \frac{\sqrt{(r_L+Z)(L C Z + L C r_c)}}{(ZCr_c + r_c r_L C + Zr_L C + L)}$$

$$G(s) = \frac{\left(s + \frac{1}{Cr_c}\right) \frac{Zr_c}{L(Z+r_c)} V_{dc}}{s^2 + s \left(\frac{\omega}{Q}\right) + \omega^2} \quad (\text{B}-20)$$

$$x = \frac{-b \pm \sqrt{b^2 - 4ac}}{2a}$$

$$x = \frac{-\left(\frac{\omega}{Q}\right) \pm \sqrt{\left(\frac{\omega}{Q}\right)^2 - 4\omega^2}}{2}, \quad x = \frac{-\left(\frac{\omega}{Q}\right) \pm \omega \sqrt{\left(\frac{1}{Q}\right)^2 - 4}}{2}, \quad x = \frac{\omega}{2} \left(-\frac{1}{Q} \pm \sqrt{\left(\frac{1}{Q}\right)^2 - 4} \right)$$

$$G(s) = \frac{V_o}{\delta} = \frac{\left(s + \frac{1}{Cr_c}\right) \frac{Zr_c}{L(Z+r_c)} V_{dc}}{\left(s + \frac{\omega}{2} \left(-\frac{1}{Q} + \sqrt{\left(\frac{1}{Q}\right)^2 - 4} \right)\right) \left(s - \frac{\omega}{2} \left(\frac{1}{Q} + \sqrt{\left(\frac{1}{Q}\right)^2 - 4} \right)\right)}$$

The state-space equations of the single-phase inverter neglecting parasitics are given below.

$$\begin{bmatrix} \dot{i}_L \\ \dot{v}_c \end{bmatrix} = \begin{bmatrix} 0 & -1 \\ \frac{1}{C} & \frac{-1}{ZC} \end{bmatrix} \cdot \begin{bmatrix} I_L \\ V_c \end{bmatrix} + \begin{bmatrix} 1 \\ \frac{1}{L} \end{bmatrix} V_{ab} \quad (\text{B}-21)$$

$$V_o = [0 \quad 1] \cdot \begin{bmatrix} I_L \\ V_c \end{bmatrix} \quad (\text{B}-22)$$

$$G(s) = \frac{V_o}{\delta} = \frac{V_{dc}}{1 + (L/Z)s + (LC)s^2} \quad (\text{B}-23)$$

Appendix C:

MATLAB code of PV module and Phase Locked Loop (PLL)

C.1: PV module MATLAB code

Model parameters under standard test conditions (1kW/m², 1.5 AM, 25°C). A bypass diode (a single diode across the entire module) can be included. Temperature effects are not modeled. The standard PV module data-sheet parameters:

- Short-circuit current I_{sc}
- Open-circuit voltage V_{oc}
- Rated current I_R at maximum power point (MPP)
- Rated voltage V_R at MPP

```
% calculation of PV module parameters
% limitation: constant temperature
Ns = round(Voc/0.61); % default number of cells in series
Vt = 26e-3; % thermal voltage
G = Isc/1000; % irradiation to short-circuit current gain
Vmpc = Vr/Ns; % cell voltage at rated Pmax
Vocc = Voc/Ns; % cell open-circuit voltage
Rmpp = Vmpc/Ir; % cell load resistance at Pmax
%
Rp = 100*Vocc/Isc; % initial value for Rp
Vdm = Vocc; % initial value for Vdm
%
% iterative solution for model parameters: Io, Rs, Rp
for i=1:10
%
Idm = Isc - Ir - Vdm/Rp; % pn-junction (diode) current at MPP
Io = (Isc-Vocc/Rp)/(exp(Vocc/Vt)-1); % pn-junction reverse saturation current
Vdm = Vt*log(Idm/Io+1); % pn-junction (diode) voltage at MPP
Rs = (Vdm-Vmpc)/Ir; % cell series resistance
Rd = (Rmpp - Rs)*Rp/(Rp-Rmpp+Rs); % diode incremental resistance at MPP
Idm = Vt/Rd; % diode current at MPP based on incremental resistance
Rp = Vdm/(Isc-Ir-Idm); % cell parallel resistance
%
end
%
```

C.2: Phase Locked Loop MATLAB code

This Phase Locked Loop (PLL) is used to synchronize on a variable frequency sinusoidal signal. If the Automatic Gain Control is enabled, the input (phase error) of the PLL regulator is scaled according to the input signal magnitude. For optimal performance, the following settings are recommended:

$[K_p \ K_i \ K_d] = [180 \ 3200 \ 1]$, Enable Automatic Gain Control

Input : Normalized input signal $V(\text{pu})$

Output : Ramp $\omega \cdot t$ varying between 0 and 2π , synchronized on the zero-crossing (rising) of the fundamental of input signal

```
% Initialization
Kp=ParK(1);
Ki=ParK(2);
if length(ParK)==2
Kd=0;
else
Kd=ParK(3);
end
Phase_Init=Par_Init(1);
Finit=Par_Init(2);
power_initmask();
%Plotting the FFT of the input signal and the output signal of the PLL
%The input should be in the simin = [t,Va] and the
%the output in simout = [out1, out2]
closeall
%Frequency vector
f = (0:length(t)-1)/(ts*length(t));

%Input and rescaling
Va = simin(:,2);
Va = Va/(max(Va));
amp = max(Va);
figure
subplot(2,1,1)
plot(t,Va)
title('Input Va')
axis([0, t(end), -amp, amp])
ylabel('Va')
xlabel('Time [s]')
%Calculating FFT from 0.1 to 0.2s.
tnewin = t(round(length(t)/2):end);
Vanew = Va(round(length(t)/2):end);
```

```
%Frequency vector
f = (0:length(tnewin)-1)/(ts*length(tnewin));
subplot(2,1,2)
Fa = abs(fft(Vanew));
plot(f, Fa)
axis([0 500 0 max(Fa)])
xlabel('Frequency [Hz]')
ylabel('FFT magnitude')
%Output
Vout = simout(:,1);
amp = max(Vout);
figure
subplot(2,1,1)
plot(tout, Vout)
title('Output Vout')
ylabel('Vout')
xlabel('Time [s]')
axis([0, tout(end), -amp, amp])
%Calculating the FFT after tracking
tnew = tout(round(length(tout)/2):end);
Voutnew = Vout(round(length(tout)/2):end);
f = (0:length(tnew)-1)/(ts*length(tnew));
subplot(2,1,2)
Fout = abs(fft(Voutnew));
plot(f, Fout)
axis([0 500 0 max(Fout)])
xlabel('Frequency [Hz]')
ylabel('FFT magnitude')
hold off
figure
plot(t,(10/Vm)*Va);
hold on
plot(tout, simout(:,2), 'g');
title('Input Va, output sine wave and corresponding phase angle
output from PLL')
h=plot(tout, Vout, 'r--')
set(h, 'LineWidth', 0.8)
axis([0, t(end), -10, 10])
xlabel('Time [s]')
legend('Va', 'Phase angle', 'Vout')
```

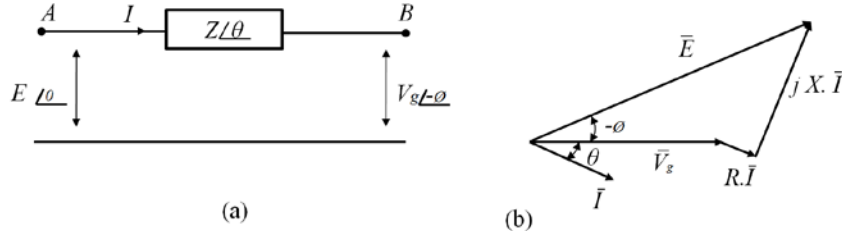
Appendix D:
Droop Characteristics Equations


Figure D.1: (a) power flow through the transmission line, (b) phasor diagram.

Consider the single-phase grid voltage signal as $v_g(t) = V_g(t) \cos(\omega t - \phi(t))$, the generator voltage as $e(t) = E(t) \cos(\omega t)$, which is taken as the phase reference, and the transmission line impedance as $Z = (R + j\omega L)$.

The time-varying dynamic phasor representation $\bar{V}_g(t)$ of $v_g(t)$ is set as in (D-1).

$$\bar{V}_g(t) = V_g(t) \cos \phi + jV_g(t) \sin \phi \quad (\text{D} - 1)$$

The voltage across the power line is

$$\bar{E}(t) - \bar{V}_g(t) = R\bar{I}(t) + L \frac{d\bar{I}(t)}{dt} \quad (\text{D} - 2)$$

Then, making use of the dynamic phasor representation is:

$$\bar{E}(t) - \bar{V}_g(t) = (R + j\omega L) \bar{I}(t) + L \frac{d\bar{I}(t)}{dt} \quad (\text{D} - 3)$$

and thus

$$\bar{I}(t) = \frac{1}{Ls + R + j\omega L} (\bar{E}(t) - \bar{V}_g(t)) \quad (\text{D} - 4)$$

$$\bar{S}(t) = \bar{V}_g(t) \bar{I}^*(t)$$

The subscript (*) denoted for conjugate value. The power flow into the line at point A, shown in Figure D.1, is then

$$\bar{I}^*(t) = \frac{1}{Ls + R - j\omega L} (\bar{E}^*(t) - \bar{V}_g^*(t)) \quad (D-5)$$

$$\bar{S}(t) = \bar{E}(t) \frac{1}{Ls + R - j\omega L} (\bar{E}^*(t) - \bar{V}_g^*(t)) \quad (D-6)$$

$$\bar{S}(t) = \frac{1}{Ls + R - j\omega L} (\bar{E}(t)\bar{E}^*(t) - \bar{E}(t)\bar{V}_g^*(t)) \quad (D-7)$$

$$\bar{S}(t) = \frac{1}{Ls + R - j\omega L} (\bar{E}(t)\bar{E}^*(t) - \bar{E}(t)(V_g(t) \cos \phi - jV_g(t) \sin \phi)) \quad (D-8)$$

$$\bar{S}(t) = P(t) + jQ(t)$$

The power triangle is equivalent to impedance triangle. Using impedance triangle with (D-1) results in (D-9) and (D-10):

$$P(t) = \frac{Ls + R}{(Ls + R)^2 + (\omega L)^2} (E^2 - EV_g \cos \phi) + \frac{\omega L}{(Ls + R)^2 + (\omega L)^2} (EV_g \sin \phi) \quad (D-9)$$

$$Q(t) = \frac{\omega L}{(Ls + R)^2 + (\omega L)^2} (E^2 - EV_g \cos \phi) - \frac{Ls + R}{(Ls + R)^2 + (\omega L)^2} (EV_g \sin \phi) \quad (D-10)$$

Taking into account small disturbances around the state of equilibrium (E, V_g, ϕ), equations (D-9) and (D-10) can be linearized. When $X \gg R$ and both ϕ and $E - V_g$ are small, the cross-coupling terms $\frac{\partial P}{\partial V}$ and $\frac{\partial Q}{\partial \phi}$ can be neglected, yielding two decoupled systems for P and Q :

$$dP \frac{\partial P}{\partial \phi} d\phi = \frac{\omega L E^2}{(Ls + R)^2 + (\omega L)^2} d\phi \quad (D - 11)$$

$$dQ \frac{\partial Q}{\partial E} dE = \frac{\omega L E}{(Ls + R)^2 + (\omega L)^2} dE \quad (D - 12)$$

The small-signal transfer functions are given by:

$$dP = \frac{XE^2}{Z^2} d\phi \quad (D - 13)$$

$$dQ = \frac{XE}{Z^2} dV_g \quad (D - 14)$$

with $Z^2 = R^2 + X^2$ and $X = \omega L$.

The AC network system is considered to have a stiff voltage and frequency characteristics and no harmonics, and the single phase voltage source inverter with passive-element PWM output filter is connected to this network as a distributed generator. The network frequency can be extracted from the network by using a PLL that synchronise the inverter output waveform with the network. The phase angle and voltage amplitude of the generator are controlled by the droop characteristics as a function of active and reactive power.

When considering fast acting inverters connected to network, time derivative becomes significant for ensuring that the system will go through a sequence of states that are infinitesimally close to equilibrium. Thus, the dynamic phasor transfer functions are calculated for the power flow into a power line as a function of the power angle ϕ and the voltage (Figure D.2) by using the functions (D-15) and (D-16) which are called droop functions.

$$\omega - \omega_o = m(P - P_o) \quad (D - 15)$$

$$E - E_o = n(Q - Q_o) \quad (D - 16)$$

which can be written as in (D-17) and (D-18) according to its application in the controller units.

$$\emptyset = \emptyset_o - m(P - P_o) \quad (D - 17)$$

$$E = E_o - n(Q - Q_o) \quad (D - 18)$$

where \emptyset_o and E_o are rated frequency and voltage, respectively. P_o is the offset values for active power and Q_o is the offset values for reactive power. Usually, P_o is set to the desired output power capacity of distributed generators, while the Q_o value is set to zero (or very small value) generally in the solid-state distributed generators.

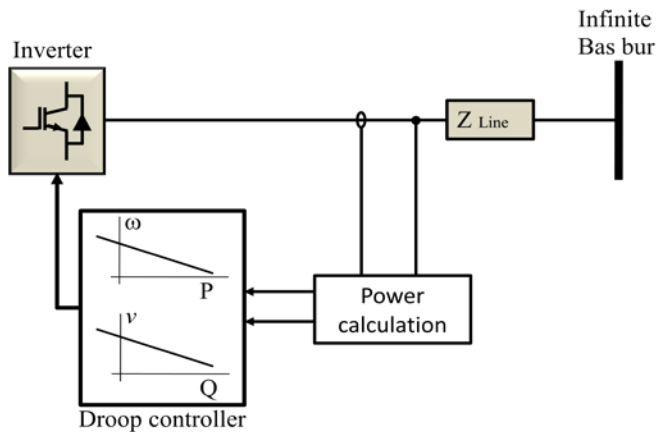


Figure D.2: Solid-state distributed generators based on droop controller.

Appendix E:

C-code

E.1: Circular Buffer

The orthogonal voltage and current components (I_{beta} and V_{beta}) are created from the input_sample (I_{alpha} V_{alpha} components) by using a circular buffer.

An array data structure or simply array is a data structure consisting of a collection of elements (input_sample values), each identified by integer indices, stored so that the address of each element can be computed from its index. Arrays are useful because the element indices can be computed at run time. This feature allows a single iterative statement to process many elements of an array. The set of valid index and the addresses of the elements are usually fixed while the array is in use.



Figure E.1: Circular Buffer array data structure.

In the code below, it can be seen how to add and remove elements from the queue, which are the only two required operations on the buffer.

```
/*** circular buffer ***/
#include<stdio.h>
intmain()
{
intI_alpha []={input_sample}; //input_sample is the variable that
contains the newest input sample//
inti,a,b;
i = 0;
```

```

while ( i < 100 ) //the circular
bufferfirststartsemptyandofsomepredefinedlength
{
printf( "i=%d I_alpha =[%d]\n",i, I_alpha [i]);
i++;
a=i;
b=0;
}
//A consequence
ofthecircularbufferisthatwhenitisfullandasubsequentwriteisperformed, then
itstartsoverwritingtheoldestdata//
while ( a < 101 )
{
// read Ia and Ib from the array//
printf("a=%d I_alpha =[%d], b=%d I_beta =[%d]\n",a, I_alpha [a],b,
I_alpha [b]);
b++;
if ( b == 101)
b=0;
a++;
if ( a == 101)
a=0;
continue;
}
}

```

E.2: Controller C-code

```

*****controller C-code ****
#define PI3.141592654
#define Ts0.5e-4;
#define R0.05;
#define L3.4e-3;
#define C2e-6;
#define S2500;
#define E380;
#define fc0.5;
#define f50;
#define K_adj0.2;

/*----- Constants -----*/
W = 2*pi*f;
Wc = 2*pi*fc;
K = (L/Ts)-(R/2);
Ti = (L/R)-(Ts/2);
Kc = w*L;
imax = 1.2*(S/E);

/*----- initial values -----*/
I_alpha=0;
I_beta=0;
V_alpha=0;
V_beta=0;
Id=0;
Iq=0;
Vd=0;
Vq=0;
Vdf=0

```

```

Vdf_old =E;
Vqf=0;
Vqf_old =0;
enable=0; //When the faultoccursenableissettozero//
error_type=0; // the error_typeindicatesthefaultkind// 
vmax=400;
vmin=311;
Id_ref =imax;
Iq_ref =0;
ud_I_temp=0;
uq_I_temp=0;
ud_I=0;
uq_I=0;
ud_ref=0;
uq_ref=0;
umax=0.9*Vdc;
umim=0.8*Vdc;
Id_ref=8;
Iq_ref=0;

```

/*---- Calculation of alpha beta components---*/

The read feedback voltage and current signals are represents voltage and current alpha signals only. The voltage and current beta signals are created from feedback voltage and current signals using previous samples of alpha signals using circular buffer.

```

I_alpha;
V_alpha;
I_beta;
V_beta;

//--- Transformation from alpha beta to d-q components---// 
Transform voltage and current to the d-q axis using proposed
transformation strategy.
Id = I_alpha*I_alpha + I_beta* I_beta;
Iq = I_alpha* I_beta - I_alpha* I_beta;
Vd = V_alpha*V_alpha + V_beta* V_beta;
Vq = V_alpha* V_beta - V_alpha* V_beta;

//--- filtering ---//
Vdf=(vd-Vdf_old)*wc*Ts)+ Vdf_old; //LP filter
Vqf=(vq-Vqf_old)*wc*Ts)+ Vqf_old; //LP filter
//--- protection ---//

```

To maintain reliable operation of inverter systems associated with power network systems protection is required. In this context, safe protection and minimal outage intervals are key issues. Also needed effort and life-cycle costs also have to be considered. Power-

electronic assets very vulnerable to over-currents and often only few milliseconds are available for protective action to complete a shutdown of the power electronic system.

The inverter system will be connected in parallel with the utility grid. The protection of both the network and the system is an important requirement of policies for promoting grid-tied inverter mode. Therefore, the following kinds of protection are used:

- It is important to have protection for this case, such as the switching does not start without DC-link voltage (U_{dc}).
- The over voltage protection must be able to trip fast in the presence of an over volt.
- Under voltage protection is not so critical and is therefore operating only when the converter is running, otherwise it would be impossible to start the converter.

The statement `error_typ` indicates the fault kind when a fault occurs. Immediately after a fault occurs, the ‘enable’ signal is set to zero and then the inverter switching stops.

```

//-- Over current protection---/
If(Id>imax || Iq>imax)
{
enable=0;
error_type=1;
}
//-- Over voltage protection---/
if(vd>vmax)
{
enable=0;
error_type=2;
}
//-- Under voltage protection---/
if(Vdf<vmin)
{
enable=0;
error_type=3;
}
//-- Current limitation ---/
If (Id_ref>imax)
Id_ref =imax;
If (Iq_ref>imax)
Iq_ref =imax;

//--Current controller---/
ud_I_temp= k_adj*k*(Ts/Ti)*(Id_ref-Id)+ud_I;

```

```

uq_I_temp= k_adj*k*(Ts/Ti)*(Iq_ref-Iq)+uq_I;
ud_ref=k_adj*k*(Id_ref-Id)+ud_I-(kc*0.5*(Iq_ref+Iq))+vdf;
uq_ref=k_adj*k*(Iq_ref-Iq)+uq_I+(kc*0.5*(Id_ref+Id))+Vqf;

//--- anti-windup ---//
```

If a control error signal remains active for a long time, it is probable that the corresponding control signal saturates (i.e. the integral part grows and becomes too large), which is referred to as “integral windup”. The saturation can be considered as a nonlinear drop in gain.

A solution to the problem of integral windup is to prevent the integral part from growing when the control signal is saturated. For this reason, the integral part of controller is limited in magnitude. The output control signal consists of the integral part subtracted from the proportional part. This can be seen in the following code.

```

If(ud_ref>umax)
{
ud_ref=umax;
ud_I=umax-(K_adj*k*(Id_ref-Id));
}
else If(ud_ref<umin)
{
ud_ref=umin;
ud_I=umin-(K_adj*k*(Id_ref-Id));
}
else
{
Ud_I=ud_I_temp;
}
If(uq_ref>umax)
{
uq_ref=umax;
uq_I=umax-(K_adj*k*(Iq_ref-Iq));
}
else
{
uq_I=uq_I_temp;
}

//--- voltage reference calculation---//
//--- SVPWM duty cycle---//
#include<stdio.h>
#define clock,Vref,t_sampling,frequency,number_of_sampling;
#define pi,ta,tb,OUTPUT,w;
main()
intclock,Vref,t_sampling,frequency,number_of_sampling;
intpi,ta,tb,OUTPUT, w,sector, t_count;
```

```
w=2;
//t_sampling = 1/(frequency*number_of_sampling)//
if (w>= pi/2)
ta=Vref*sin(w)*t_sampling;
sector=1;
else
if w>= pi
ta=Vref*sin(pi-w)*t_sampling;
sector=1;
else
if w>=3*pi/2
ta=Vref*sin(w-pi)*t_sampling;
sector=2;
else ta=Vref*sin(2*pi-w)*t_sampling;
sector=2;
end
ta=ta+t_sampling/2;
tb=t_sampling-ta;
t_count = (clock/t_sampling)*t_sampling;
if sector ==1
if (clock < (ta+t_count));
OUTPUT = 1;
else
OUTPUT = 0;
else
if (clock < (tb+t_count));
OUTPUT = 1;
else
OUTPUT =0;

//---- Update variables ----//
```

At the end of this interval, the values calculated during this sampling interval are set as old values for the next interval. Then, they are used during the next sampling interval after the newly sampled current and voltage values are read from the ADC.

```
Vdf_old = Vdf;
Vqf_old = Vqf;
```

E.3: The Discretization Strategies of PI Controller

$$PI(s) = K_i \frac{1 + s \frac{K_p}{K_i}}{s} \quad (E - 1)$$

The controller discretization makes use of Euler backward integration method. For PI discretisation, the method chosen is backward Euler discretisation. The corresponding controller transfer function is given by

$$PI(z) = Ki \frac{1 + \frac{1-z}{zTs} \frac{Kp}{Ki}}{\frac{1-z}{zTs}} \quad (E - 2)$$

$$PI(z) = ((Kp + Ki \cdot Ts) \cdot z - Kp) / (1 - z) = Kp + Ki \cdot Ts (z/1 - z) \quad (E - 3)$$

As can be seen, we have obtained a new rational transfer function that can be simplified to give the discrete time implementation of the PI controller. The block diagram corresponding to the expression in (E-3) is shown in Figure E.2, which represents the parallel realization of the discrete time regulator.

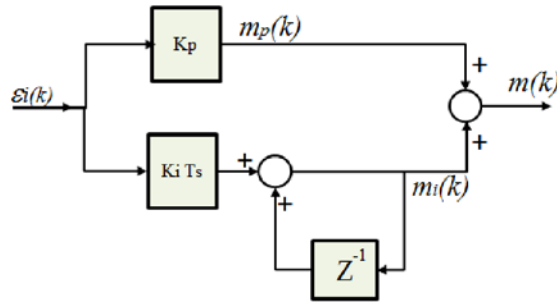


Figure E.2: Block diagram representation of the digital PI controller.

Recalling the basic Z -transform properties, we can immediately write down the control algorithm that may be used to implement the PI regulator in our microcontroller or DSP unit. This is as follows,

$$m_i(k) = K_i \cdot T_s \cdot \varepsilon_i(k) + m_i(k - 1) \quad (E - 4)$$

$$m(k) = m_p(k) + m_i(k) = K_p \cdot \varepsilon_i(k) + m_i(k) \quad (E - 5)$$

where $\varepsilon_i(k)$ represents the current error at instant $k \cdot T_s$. m is intermediate discrete samples.